UNIVERSITY OF SHEFFIELD

DEPARTMENT OF CIVIL AND STRUCTURAL ENGINEERING

YIELDING OF UNSATURATED SOIL

BY :

IDERIS ZAKARIA

Adv. Dip. (Civ. Eng.), M.Sc (Glasgow)

Thesis submitted to the University of Sheffield for the award of the degree of Doctor of Philosophy in Civil Engineering

October 1994

ACKNOWLEDGEMENTS

The author acknowledges Prof. T.H. Hanna the former Head of the Department of Civil and Structural Engineering, University of Sheffield, for providing the opportunity to carry out the research work described in this thesis.

The author is greatly indebted to his supervisors, Dr. S.J. Wheeler, Lecturer in the Department of Engineering Science, University of Oxford and Dr. W.F. Anderson, Reader in the Department of Civil and Structural Engineering, University of Sheffield, for their continuing advice, guidance, assistance and interest shown, without which the work might not have been possible to its final stage. Special thanks are due to Dr. S.J. Wheeler for his comments and criticisms.

Thanks are also due to Mr. P.L. Osborne and Mr. M. Foster, Senior Technician and Technician respectively in the Geotechnics Laboratory of the Department of Civil and Structural Engineering, University of Sheffield, who helped in the fabrication and assembly of the various parts of the apparatus during the early stage of experimental work. The author is also thankful to his colleague Dr. V. Sivakumar for his advice and and assistance.

The author is grateful to the Public Services Department, Government of Malaysia, for providing a scholarship and his employer MARA Institute of Technology, Shah Alam, Selangor, Malaysia for granting study leave.

Finally the author would also like to extend his appreciation to his wife Zaini and his family for their encouragement and support throughout the duration of his study in Sheffield. The time that we spent in Sheffield has been very enjoyable and memorable.

SUMMARY

Considerable efforts have been made in recent years to develop a better understanding of the mechanical behaviour of unsaturated soils in terms of elasto-plastic critical state constitutive models. These models are defined in terms of four independent stress state variables : mean net stress, deviator stress, suction and specific volume. An important feature of the models is the suggestion of the existence of a yield surface in mean net stress : deviator stress : suction space.

Suction-controlled triaxial tests were performed to investigate the shape of the yield surface for unsaturated compacted speswhite kaolin with a particular stress history. The tests were conducted in a Bishop-Wesley triaxial cell with suction applied by the axis translation technique. The soil samples were instrumented with local strain gauges for measuring the sample volume change.

Ten samples were tested, and in each test the location of the yield surface was fixed by isotropically consolidating the sample to a mean net stress of 400 kPa and a suction of 100 kPa. This procedure effectively erased the one-dimensional stress history produced by the compaction process. After unloading to stress states inside the yield surface, samples were re-loaded either isotropically or by drained triaxial shearing. Re-loading stages were conducted at three different values of suction.

Yield points in the re-loading stages were most easily identified from plots of specific volume against the logarithm of mean net stress (even for shear tests), whereas it was often difficult to identify a clear yield point from a plot of deviator stress against shear strain. The yield points identified from the re-reloading stages were used to define the shape of the yield surface in a stress space with axes of deviator stress, mean net stress and suction. Constant suction cross-sections of the yield surface were approximately elliptical in shape, with one axis of the ellipse coinciding with the mean net stress axis. As expected, the size of the elliptical constant suction yield curves increased with increasing suction.

Soil elastic indices obtained from swell-back and suction-change stages showed non-conservative behaviour, indicating that the behaviour of the soil was not truly elastic even for stress states inside the yield surface. Plastic strain increment vectors were plotted for the post-yield behaviour, and these were consistent with an associated flow rule.

LIST OF SYMBOLS

A : Cross-sectional area of sample at any stage of test

: Rate of increase of total stress per hour

: Elastic constant relating changes of volumetric water content to changes of net stress in the model of *Fredlund* (1979)

A_o : Cross-sectional area of sample at start of shear test

E : Young's modulus

D : Diameter of soil sample at start of shear test

F : Deviator load

H : Elastic modulus for changes in suction in model of *Fredlund* (1979)

M : Membrane modulus

LC : Loading Collapse

R : Elastic constant relating changes of volumetric water content to changes of suction in model of *Fredlund* (1979)

S_r : Degree of saturation

V : Total volume of sample

V_w : Volume of water in soil sample

V_s : Volume of solids in soil sample

V_o : Volume of soil sample at start of any test stage

V_{wo} : Volume of water in sample at start of any stage

a, b, c, d : Soil constants defining warped surface linking e, s and p' in model of *Lloret and Alonso* (1985)

c_v : Coefficient of consolidation

c' : Effective cohesion

e : Void ratio

h : half sample height

m : parameter defining the increase of p_o^* as suction increases in model of *Josa, Balmaceda, Gens and Alonso* (1992)

p : mean stress ($=\frac{1}{3}(\sigma_1 + 2\sigma_3)$ for axisymmetric case)

p' : Mean net stress ($= p - u_a$)

p_o' : Isotropic yield stress at suction s

$p_o'(o)$: Isotropic yield stress at zero suction

p^c : Reference stress defining the value of p' where p_o' is independent of suction in model of *Alonso, Gens and Josa* (1990)

p_c : Reference stress defining the value of p' where p_o' is independent of suction in model of *Josa, Balmaceda, Gens and Alonso* (1992)

p_{at} : Atmospheric pressure

p_x' : Critical state value of p'

q : Deviator stress ($=\sigma_1 - \sigma_3$)

s : Suction ($= u_a - u_w$)

s_o : Maximum past suction ever experienced by the soil

u : Pore pressure

u_a : Pore air pressure

u_w : Pore water pressure

u_{ex} : Equilibrium value of excess pore water pressure

v : Specific volume ($=1+e$)

v_w : Specific water volume ($= 1+eS_r$)

w : Water content

A(s) : Intercept of normal compression line in v_w : ln (p'/p_{at}) space

A(o) : Value of A(s) at $s = 0$

M : Saturated critical state aspect ratio

M_a, M_w : Critical state ratios with respect to net stress and suction respectively in model of *Toll* (1990)

M(s) : Slope of critical state hyper-line in $q : p'$ space in model of *Wheeler and Sivakumar* (1995)

N(s) : Intercept of normal compression line in v : ln (p'/p_{at}) space

N(o) : Value of N(s) at zero suction

Γ : Saturated critical state parameter

$\Gamma(s)$: Intercept of critical state hyper-line in v : ln (p'/p_{at}) space in model of *Wheeler and Sivakumar* (1995)

$\alpha(s)$: Slope of normal compression line in v_w : ln (p'/p_{at}) space

ε_1 : Axial strain

ε_3 : Radial strain

ε_s : Shear strain

ε_v : Volumetric strain

ϕ' : Effective angle of internal friction with respect to net stress

ϕ^b : Angle of internal friction with respect to suction

χ : Parameter depending on the degree of saturation (*Bishop*, 1959)

κ : Swelling index with respect to changes in p'

κ_s : Swelling index with respect to changes in s

κ_w : Elastic index relating changes of v_w to changes in p'

κ_{sw} : Elastic index relating changes of v_w to changes in s

$\lambda(s)$: Slope of normal compression line in v : ln (p'/p_{at}) space

$\lambda(0)$: Value of $\lambda(s)$ at s = 0

λ_a, λ_w : Slopes of critical state plane with respect to net stress and suction in model of *Toll* (1990)

$\mu(s)$: Intercept of critical state hyper-line in q : p' space in model of *Wheeler and Sivakumar* (1995)

ν : Poisson's ratio

$\psi(s)$: Slope of critical state hyper-line in v : ln (p'/p_{at}) space in model of *Wheeler and Sivakumar* (1995)

θ_w : Volumetric water content in model of *Fredlund* (1979)

σ : Total normal stress

$\sigma_1, \sigma_2, \sigma_3$: Principal stresses

σ' : Effective stress

τ : Shear strength

ς_x : Value of $p_o^{'}(o)$ at maximum inclination of LC yield curve in the $s : p'$ plane in model of *Josa, Balmaceda, Gens and Alonso* (1992)

ς_y : Peak value of m on increasing suction (= 1 when $p_o^{'} = p'$ (o)) in model of *Josa, Balmaceda, Gens and Alonso* (1990)

TABLE OF CONTENTS

CHAPTER 1
INTRODUCTION

This chapter serves as an introduction to the study of mechanical behaviour of unsaturated soil described in this thesis. The occurence and nature of unsaturated soil are initially given in brief. This is followed by a section explaining some of the practical engineering problems posed by unsaturated soil as encountered by engineers in the field. Although considerable efforts have been made over several decades to investigate and explain the stress-strain behaviour of unsaturated soil, there seemed to be no unified approach until the suggestion of elasto-plastic critical state constitutive models for unsaturated soil in the late 1980s. A section dealing specifically with this type of approach is given in brief. Finally a section on the aims of the project is given at the end of the chapter, explaining briefly the aspects of unsaturated soil behaviour that are investigated in this thesis.

A more detailed review of previous work on the stress-strain behaviour of unsaturated soils is given in Chapter 2, and the objectives and methodology of the project described in the thesis are fully explained in Chapter 3.

1.1 Occurrence of unsaturated soil

From the soil mechanics point of view, soils consist of three basic components :soil particles, air and water. For the purposes of analysis the voids can be filled with air (dry soil) or water (saturated soil) or a mixture of air and water (unsaturated soil). Constitutive modelling in soil mechanics has concentrated on soils containing a single pore fluid i.e. saturated clays, saturated sands and dry sands. However there are practical instances where soils can contain both air and water. These situations include :

a) soil above the water table : in arid and semi-arid regions or in tropical regions where evapo-transpiration exceeds rainfall the depth of the unsaturated soil may extend to many metres ;

b) placement and compaction of granular and clay fills in embankments, behind retaining structures or beneath foundations ;

c) biogenic generation of natural gases within a soil stratum or diffusion of gas into the stratum.

The three different types of formation process for unsaturated soils listed above produce different types of soil structure or fabric. The details of these soil fabrics are given in Section 2.1, but the fabric commonly consists of saturated packets of material, separated by large unsaturated inter-packet voids (*Brackley*, 1975). *Gens and Alonso* (1992) sub-divided the structure of unsaturated compacted soils into two levels of fabric : the saturated microstructure of individual packets and the unsaturated macrostructure, with each level behaving differently. *Seed and Chan* (1959) however proposed either a flocculated or dispersed structure for unsaturated compacted soil, depending upon the compaction water content with respect to its optimum water content.

1.2 Pore pressures within unsaturated soil

For unsaturated soil, the pore water pressure u_w is always lower than the pore air pressure u_a, because of the curvature of the menisci separating water and air (and the fact that the contact angle of the menisci with soil grains is zero means that the menisci must be convex on the water side). In many unsaturated soils, the air phase is continuous and connected to the atmosphere, so that u_a is zero. This means that u_w is negative and the soil therefore has the tendency to draw in water if a supply of water at atmosperic pressure is availabe. This led to the use of the term '*suction*' to describe the tendency of the soil to take up water.

Marshall (1959) suggested the division of suction into two components : matrix suction and solute suction. Matrix suction was the physical value of negative pore water pressure, due to capillary forces, which depended on particle configuration and arrangement, while solute suction was due to the ion concentration of the soil water (resulting from the presence of solutes in the soil). The ability of an unsaturated soil to draw in water is dependent not just upon the physical negative value of u_w but also on any difference in osmotic (chemical) potential between the pore water in the soil and any free water that is available. The flow of water into or through an unsaturated soil can therefore be related to the gradient of '*total suction*' which is made up of two components : the '*matrix suction*' representing the negative value of u_w (arising from the curvature of the menisci i.e. capillary effects) and the '*osmotic suction*' or '*solute suction*' representing any negative osmotic potential in the pore water. However *Aitchison* (1961) pointed out that it was the physical pressure of the pore water (matrix suction) which was relevant in the stress-strain behaviour of unsaturated soil. Therefore the term 'suction' is simply taken to mean matrix suction for the rest of the thesis. To generalise the definition to situations where the pore air presure may not be zero, the suction is taken as the difference between the pore air pressure and the pore water pressure $u_a - u_w$.

Fig. 1.1 illustrates a simple mechanism of suction in soil. If a capillary tube is immersed in water in a container, the water would rise to, say, BB inside the tube. The water level AA in the container represents the ground water level where the water is at atmospheric pressure. At any depth z below AA the water pressure u_w relative to atmospheric is given by

$$u_w = \gamma_w \times z \qquad (1.1)$$

where γ_w is the unit weight of water. The water pressure at BB, a height h above AA, is therefore negative (relative to atmospheric) and is given by

$$u_w = -\gamma_w \times h \tag{1.2}$$

However in actual soil the capillary moisture is somewhat different from that shown in Fig. 1.1. Due to the irregular nature of the soil pores the water rises to a higher level in small sized voids than it does in large sized voids, inevitably leading to an unsaturated zone in which the small voids are water-filled but the large voids are not. Fig. 1.2 shows a no-flow condition i.e. under equilibrium for capillary moisture in the soil. AA is the ground water level where the pore water pressure is zero, hence the zone beneath it is saturated. The pore water pressure below the ground water table is positive given by $u_w = \gamma_w \times z$. Zone 1 which is immediately above the ground water level is saturated, because the capillary rise in even the largest pore sizes is sufficient to ensure full saturation over this depth. The pore water pressure in Zone 1 is negative, given by $u_w = \gamma_w \times z$ (with z taking a negative value). In Zone 2 the soil becomes unsaturated. The water phase is continous while the air phase is discontinous (containing discrete bubbles) and u_a is not necessarily equal to atmospheric pressure. The pore water pressure in Zone 2 is negative and is still given by $u_w = \gamma_w \times z$. Going further up to Zone 3 both the water and air phases are continous, with the pore air now at atmospheric pressure and the pore water pressure given by $u_w = \gamma_w \times z$. Finally in Zone 4, where the air is continous but the water phase is discontinous, $u_a = 0$ and u_w is negative but not necessarily equal to $\gamma_w \times z$.

Considerable efforts have been and are being made to measure soil suction in the laboratory and in the field. Table 1.1 summarizes the methods of suction measurement that have been devised in the past decades, including methods for measuring total suction, matrix suction and osmotic suction. Many of the methods of

suction measurement listed in Table 1.1 measure suction indirectly, in that the suction is related to some other property of the soil or a material placed in contact with the soil (such as a filter paper). Some direct methods of suction measurement, for example the tensiometer (*Krahn, Fredlund and Klassen,* 1989) and the suction transducer (*Ridley and Burland,* 1994) are very useful, because they measure the matrix suction directly in the field without the need for an empirical calibration.

1.3 Practical problems associated with unsaturated soils

By virtue of the variability of unsaturated soil properties and the undeveloped state of unsaturated soil mechanics in the past, engineers dealing with civil engineering works involving unsaturated soil have been faced with increasing problems. *Jennings* (1961) summarized the engineering problems associated with unsaturated soils into four main groups, namely :

a) Immediate settlement due to the undrained compressibility. This was due to the compressibility of the pore air or the rapid flow of pore air to the atmosphere or solubility of air in the pore water.

b) Heave due to swelling on wetting. Wetting can occur due to the ingress of water from the surface (from rainfall or run-off) or it can occur if the soil is covered at the top surface, so preventing evaporation of ground water to the atmosphere. Many unsaturated soils, particularly clays, are known to swell (increase in volume) on wetting.

c) Additional settlement due to collapse of the soil on wetting. Some unsaturated soils are known to collapse (reduce in volume) on wetting.

d) Loss of shear strength due to suction decrease (wetting).

The problems caused by the volume change and shear strength behaviour of unsaturated soil can be illustrated by some practical examples. *Holtz and Hilf* (1961) reported a failure of a canal embankment due to wetting (suction reduction) in the

Mid-western USA, where wind-deposited loess soil was predominant. A low embankment for a canal was constructed of loess soil in Nebraska to a height of five feet, as shown in Fig. 1.3. Loess soil possessed high strength when unsaturated and sustained high loading at low water content. Settlement of the embankment took place shortly after water was introduced into the canal. Failure of the embankment was attributed to loss of shear strength as wetting of the embankment occurred.

Perhaps one of the classic examples of a failure of an earth slope due to suction decrease was given by *Krahn, Fredlund and Klassen* (1989). A railway embankment near Notch Hill, British Columbia, Canada, shown in Fig. 1.4, was constructed of local lacustrine silt which consisted of 10% clay, 85% silt and 5% fine sand. The embankment height varied from 2m to over 10m, with side slopes of 34^{o}. Several years after the construction was completed large segments of the embankment began to fail. The typical failure that took place is shown in Fig. 1.4. Instability of the slope was most active in spring and after the ground had thawed but in late spring and late summer when the weather was dry the movement came to a halt. Observations made by *Krahn, Fredlund and Klassen* (1989) showed that during winter and spring the slope was subjected to wetting, resulting in the reduction of suction. This was followed by a loss of shear strength of the soil and hence failure of the slope.

Aitchison and Woodburn (1969) reported that shrinkage (drying) in unsaturated soil caused cracks in the foundation soil without an increase in load. They described the shrinkage process as dessication as the suction was increased. The dessication induced cracks beneath a timber floor in the Adelaide Steamship Building, Adelaide, South Australia as shown in Fig. 1.5.

Thomas and Rees (1994) examined soil heaving due to swelling in unsaturated soil at a site on Kimmeridge clay in Swindon, UK. They carried out some field observations for nearly nine months by monitoring the ground movement at two stations A and B and data from their observations are shown in Fig. 1.6. Large settlement was initially observed between the months of August and September 1988

following a very dry period. After that period there was no significant movement of the ground between October 1988 and mid-February 1989. However there was a period of significant rainfall between mid-February and mid-March 1989 and large heaving of the soil took place during mid-March. *Thomas and Rees* (1994) reported that the suction in the soil was significantly reduced during the rainy season, and this caused heaving of the ground.

1.4 Stress-strain relationships for unsaturated soil

The development of a proper understanding of the stress-strain behaviour of unsaturated soil has been much more difficult than for saturated soils, because of the fact that u_a and u_w have different values. It has also been hampered by the complex fabrics of many unsaturated soils and the diversity of unsaturated soil types, as dictated by mineralogy, origin and environmental conditions. The diversity of unsaturated soils is very large, covering highly expansive clays, residual laterites, a wide range of alluvial soils, different types of cemented soils and compacted fills (*Alonso, Gens and Hight,* 1987). However considerable efforts have been made in the last four decades towards developing an understanding of unsaturated soil behaviour.

The historical development of stress-strain relationships for unsaturated soil, which is described more fully in Chapter 2, can be divided into three phases. In the first phase the development was dominated by attempts to use a single effective stress equation for unsaturated soil, as proposed by *Bishop* (1959). The equation was characterized by a factor χ, the value of which was said to depend on the degree of saturation of the soil, varying from zero (dry soil) to 1 (fully saturated soil). Many authors including *Bishop, Alpan, Blight and Donald* (1960) and *Bishop and Donald* (1961) attempted to show how χ varied with the degree of saturation. However later experimental results showed that the use of a single effective stress equation for

unsaturated soil was invalid (see, for example *Jennings and Burland* (1962) and *Bishop and Blight* (1963)).

The difficulty of using a single effective stress equation for unsaturated soil led to the use of two stress state variables : net stress $(\sigma - u_a)$ and matrix suction $(u_a - u_w)$ (see *Bishop and Blight* (1963) and *Fredlund and Morgenstern* (1977)). This second phase of development took place between the early 1960s and the late 1980s. The concept of two independent stress state variables was used to explain the volume change behaviour of unsaturated soils by authors such as *Matyas and Radhakrishna* (1968), *Fredlund and Morgenstern* (1976) and *Lloret and Alonso* (1985) (see Section 2.4). The shear strength of unsaturated soils was also related to the net stress $(\sigma - u_a)$ and matrix suction $(u_a - u_w)$ by many authors including *Fredlund, Morgenstern and Widger* (1978), *Escario and Saez* (1986) and *Escario and Juca* (1989) (see Section 2.5).

Finally in the third phase of development, beginning in the late 1980s and continuing to the present time, some authors have attempted to represent the stress-strain behaviour of unsaturated soil by means of elasto-plastic critical state constitutive models. This type of work was pioneered by *Alonso, Gens and Hight* (1987), with the presentation of a possible model in a qualitative form.

1.5 Elasto-plastic critical state constitutive models

Alonso, Gens and Hight (1987) reported that the the behaviour of unsaturated soil could be described in terms of an elasto-plastic critical state model, from their investigation of the soil behaviour observed from many published works. This led to the suggestion of the model in a qualitative form. Subsequently *Alonso, Gens and Josa* (1990) proposed a quantitative form of the model, which was meant for non-expansive or moderately expansive soils, including partially saturated sands, silts or low plasticity clays. The model was based on four independent stress state variables :

mean net stress p', deviator stress q, suction s and specific volume v. The model reduced to modified Cam Clay at full saturation. The full treatment of the model is covered in Section 2.6.1.

For isotropic stress states (q=0) *Alonso, Gens and Hight* (1987) introduced the concept of two sections of yield curve, the Loading Collapse (LC) and the Suction Increase (SI) yield curves in the $s : p'$ plane, as shown in Fig. 1.7. $A_1B_1C_1$ is the initial position of yield curve and $A_2B_2C_2$ is the position of the curve after expansion. The behaviour of the soil inside the yield curve was assumed to be elastic. Irreversible (plastic) compressive volumetric strains were predicted for any stress path involving expansion of the yield curve. Yielding on the LC yield curve could be caused by an increment of p' (loading path), a decrement of s (wetting path) or both. The SI yield curve was introduced to represent the irreversible compression that occurred when the suction was increased above the previous maximum value. The model was able to reproduce some of the basic behaviour of unsaturated soil, such as swelling and collapse on wetting.

For anisotropic stress states (q>0) the LC yield curve was extended into q:p':s space to form a yield surface, as shown in Fig. 1.8. Constant suction cross-sections of the surface were assumed to be elliptical in shape, with the plastic components of the shear and volumetric strains governed by a non-associated flow rule. The critical state line for any value of suction, which passed through the the apex of the relevant elliptical yield curve at a given suction, was assumed to have a constant slope M (equal to the saturated critical state value). *Alonso, Gens and Josa* (1990) used their model to predict some of the behaviour of unsaturated soil and compared the results with some published experimental data. Good agreement was achieved between their model predictions and the published data.

Sivakumar (1993) conducted a series of controlled-suction triaxial tests on samples of compacted speswhite kaolin in the laboratory. The samples were normally consolidated to virgin states at various values of p' and s prior to shearing. Various

test paths were employed during the shear stage until the samples reached critical states. The detailed experimental work was given in *Sivakumar* (1993). *Wheeler and Sivakumar* (1995) used the data of *Sivakumar* (1993) to propose an elasto-plastic critical state model for unsaturated soil which was qualitatively very similar to the earlier model of *Alonso, Gens and Josa* (1990), but differed in points of detail in order to fit the experimental data (see Section 2.6.5). Equations were proposed to define isotropic normal compression relationships, critical state relationships and a section of state boundary. The swelling and collapse behaviour observed during wetting, the elasto-plastic compression behaviour during isotropic loading and the increase in shear strength with suction were all related to the shape of the yield surface and the hardening law defined by the state boundary. Constant suction cross-sections of yield surface were taken to be elliptical in shape, with an associated flow rule used to predict the plastic strain increment vectors. Predictions of the test paths for a variety of shear tests showed good agreement with the observed behaviour.

1.6 Aims of the present study

Examination of the models of *Alonso, Gens and Josa* (1990) and *Wheeler and Sivakumar* (1995) showed that there were some aspects of the soil behaviour within the elasto-plastic critical state framework that had not been directly investigated in the laboratory. These included :

(a) The shape of the yield surface in $q:p':s$ space. Both the models of *Alonso, Gens and Josa* (1990) and *Wheeler and Sivakumar* (1995) assumed a form for this shape, but no direct experimental investigation of the yield surface shape had been undertaken.

(b) The 'elastic' behaviour of unsaturated soil inside the yield surface. *Alonso, Gens and Josa* (1990) assumed elastic indices κ, κ_s (defined later) and G to be independent of s and p' while *Sivakumar* (1993) did not measure these

values in his tests because all samples were monotonically loaded to virgin states.

(c) The form of the flow rule. *Alonso, Gens and Josa* (1990) adopted a non-associated flow rule while *Wheeler and Sivakumar* (1995) adopted an associated flow rule in their respective models.

(d) The elasto-plastic variation of water content. Both existing models did not describe this aspect of unsaturated soil behaviour within the elasto-plastic critical state framework.

The aims of the present research project were therefore to investigate some of the behaviour of unsaturated soil not previously observed in the laboratory. This would complement the experimental tests performed by *Sivakumar* (1993) and the existing elasto-pastic critical state framework put forward by *Wheeler and Sivakumar* (1995). An experimental research programme of triaxial tests on samples of compacted speswhite kaolin was conducted at various values of suction after subjecting the samples to various isotropic loading and unloading paths prior to a final re-loading/shear stage. The test programme looked into four main areas of interest, namely :

(a) The shape of yield surface in $q{:}p'{:}s$ space.

(b) The 'elastic' behaviour inside the yield surface. This meant whether the elastic indices κ and κ_s varied with s and p'. The variation of shear modulus G with s and p' was also investigated.

(c) The appropriate form for the flow rule, in particular whether it was associated or non-associated.

(d) The elasto-plastic variation of water content.

It was hoped that at the end of the research project a better understanding of the behaviour of unsaturated soil would be achieved.

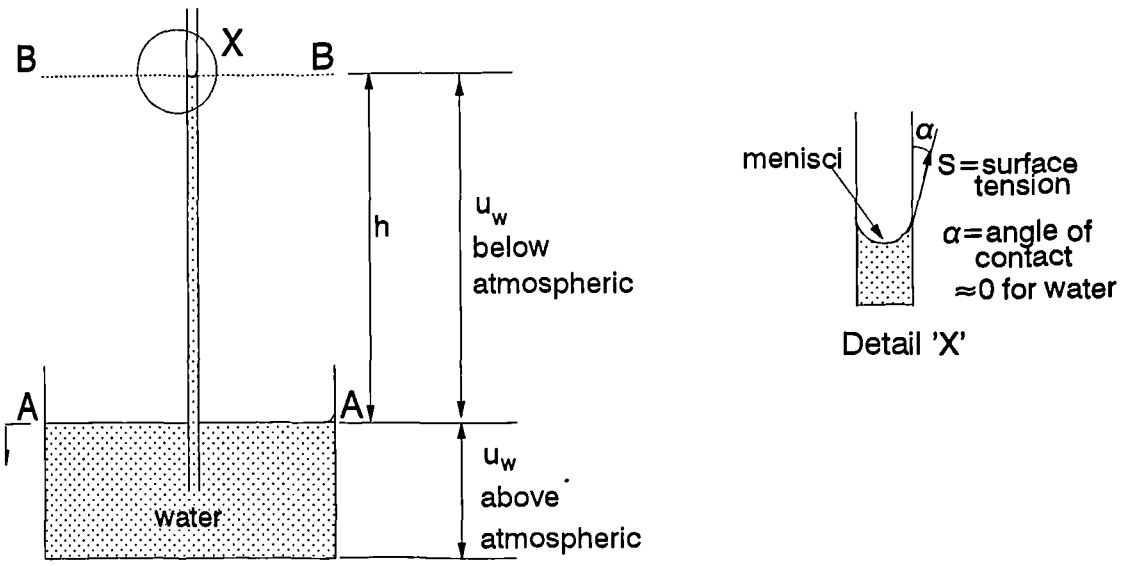

ig.1.1 : Model for negative pore water pressure above the water table

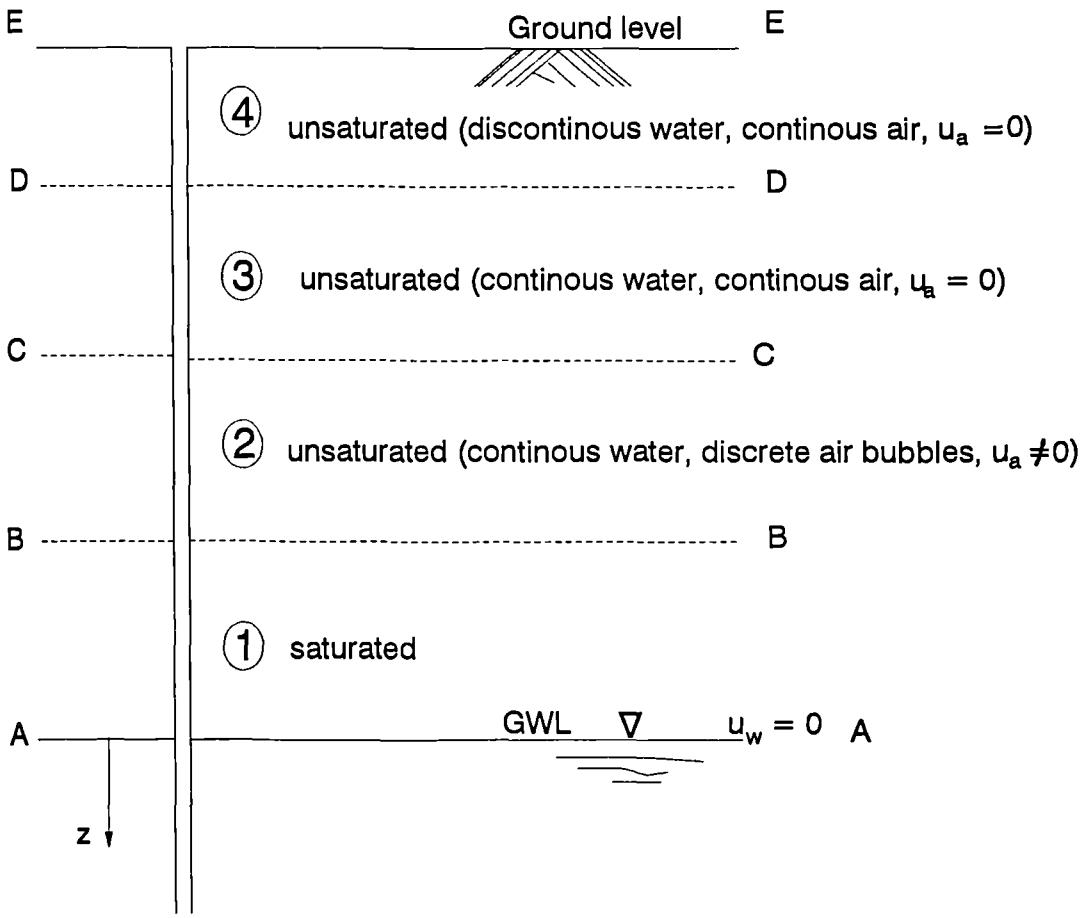

Fig. 1.2 : Capillary moisture at no-flow condition

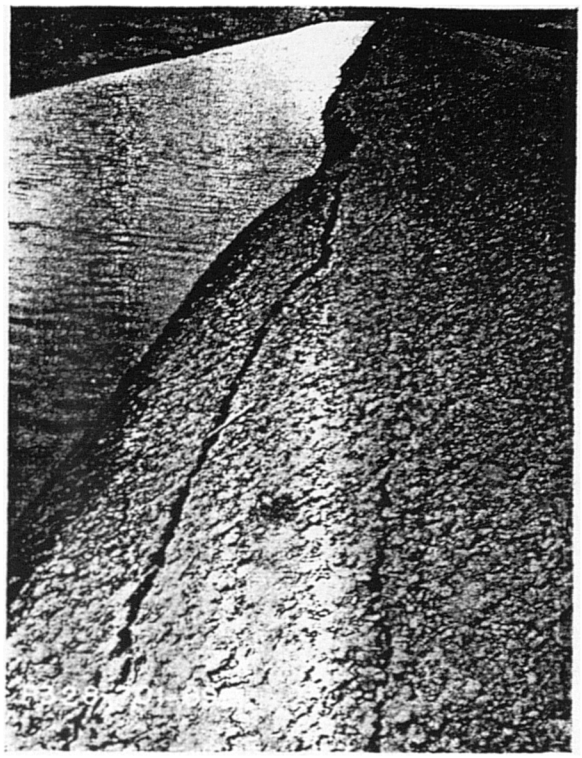

Fig. 1.3 : Cracking of canal embankment in Nebraska, USA on loessal soil due to wetting (Holtz and Hilf, 1961)

Fig. 1.4 : Failure of earth slope at Notch Hill, Canada due to wetting (Krahn, Fredlund and Klassen, 1989)

Fig. 1.5 : Crack pattern at surface beneath timber floor in Adelaide Steamship Building, Australia (Aitchison and Woodburn, 1969)

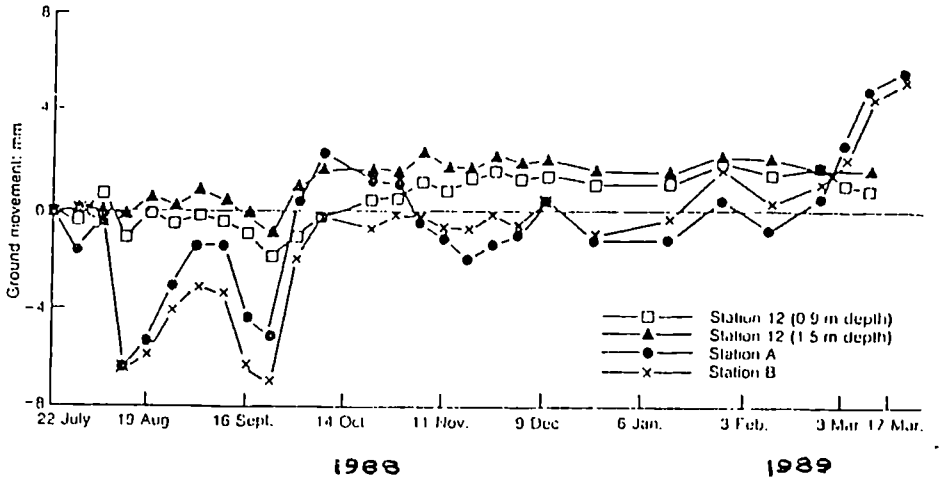

Fig. 1.6 : Field-measured ground movement data (Thomas and Rees, 1994)

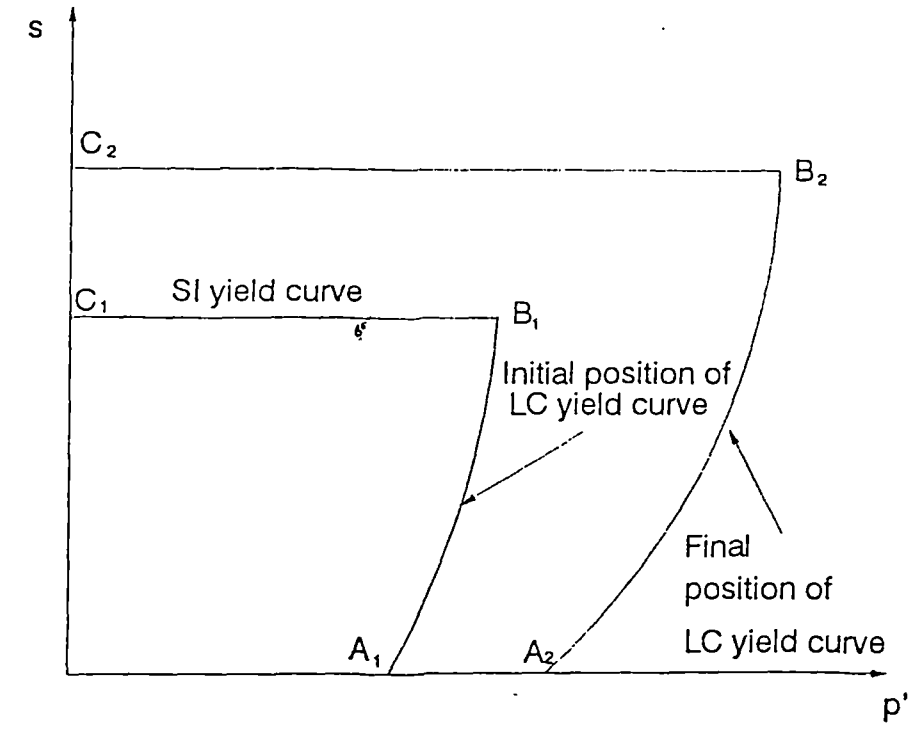

Fig. 1.7 : Loading-Collapse and Suction-Increase yield curves in s : p' plane (Alonso, Gens and Josa, 1990)

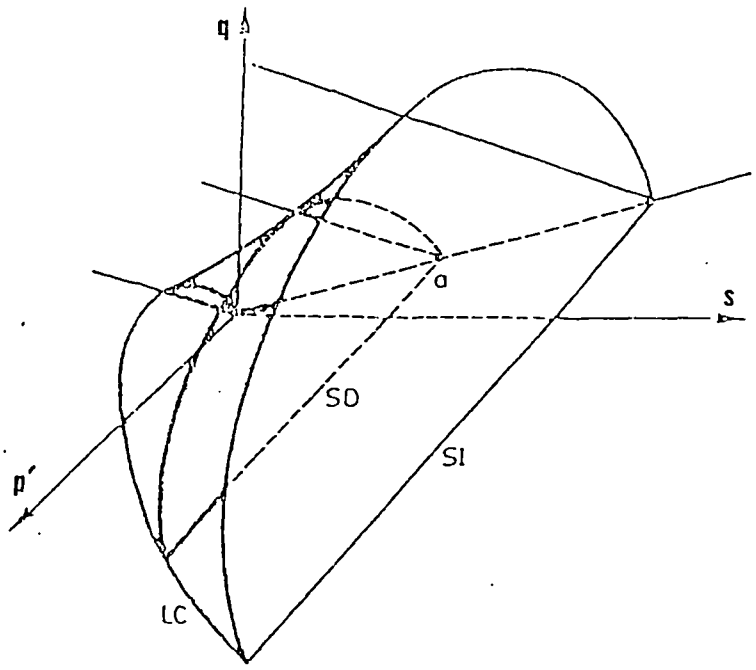

Fig. 1.8 : Yield surface in q:p':s space
(Alonso, Gens and Hight, 1987)

Method of measurement	**Suction component**	**Laboratory / in-situ**	**Direct / indirect**	**Reference**
Filter paper	Matrix	Laboratory / in-situ	Indirect	*Chandler and Gutierrez* (1986)
Filter paper	Total	Laboratory / in-situ	Indirect	*Chandler and Gutierrez* (1986)
Tensiometer	Matrix	In-situ	Direct	*Fredlund and Rahardjo* (1988)
Pressure plate	Matrix	Laboratory	Direct	*Brand* (1988)
Psychrometer	Total	Laboratory / in-situ	Indirect	*Edil, Motan and Toha* (1981)
Suction transducer	Matrix	Laboratory / in-situ	Direct	*Ridley and Burland* (1994)
Thermal conductivity	Matrix	Laboratory / in-situ	Indirect	*Fredlund & Wong* (1989)
Soil-moisture extractor	Matrix	Laboratory	Indirect	*Edil, Motan and Toha* (1981)
Pore-fluid sqeezer	Osmotic	Laboratory	Indirect	*Manheim* (1966)
Pressure membrane	Matrix	Laboratory	Indirect	*Lee* (1993)

Table 1.1 : Methods of suction measurement

CHAPTER 2

REVIEW OF THE STRESS-STRAIN BEHAVIOUR OF UNSATURATED SOIL

This chapter consists of a review of previous work on the mechanical behaviour of unsaturated soils. The chapter begins with a section on the role of soil fabric, because the mechanical behaviour of unsaturated soil is critically affected (even more than saturated soils) by the fabric and structure of the soil. This is followed by a section on the choice of appropriate stress state variables for unsaturated soils. Various aspects of mechanical behaviour are then reviewed (including the volume change behaviour and the shear strength), together with the mathematical equations that have been proposed to represent this behaviour. This leads on naturally to a description of generalised elasto-plastic critical state constitutive models for unsaturated soils, which link together both volumetric and shear behaviour. This type of constitutive model forms the basis for the interpretation of the experimental tests described in later chapters of the thesis. The sections on soil behaviour and constitutive modelling are followed by a section on the experimental methods that have been used for testing unsaturated soils in the laboratory. The chapter concludes with a section on the identification of soil yielding, because this aspect of soil behaviour was of particular concern in the research described in this thesis.

2.1 The role of soil fabric

The study of soil fabric (the arrangement and packing of the soil particles) is particularly important for unsaturated soils, because it has a very large influence on

the behaviour of the soil. The fabric of unsaturated soil depends on several factors, including :

a) The process by which the soil became unsaturated. This means whether the soil was formed by compaction, by de-saturation due to evaporation of water from the ground surface or by de-saturation due to generation of gas within the soil.

b) Size and composition of the soil particles. Differences in the size and composition of soil particles may result in different soil fabrics and thus differences in behaviour.

c) The degree of saturation. Unsaturated soils at high degrees of saturation will often have very different fabrics to those at low degrees of saturation.

Because the process by which the soil became unsaturated is of central importance in dictating the type of soil fabric exhibited by the soil, the following review of soil fabric is sub-divided into unsaturated natural soils (produced by evaporation of water from the ground surface), unsaturated compacted soils and unsaturated gassy soils (produced by gas generation or migration)

2.1.1 Unsaturated natural soils

Natural soils above the water table are normally unsaturated. The pore water pressure above the water table is negative, thus giving the term "suction" (see Section 1.2). Seasonal fluctuations in the level of the water table subject the soil to changes in the value of suction and to cycles of saturation and de-saturation. The maximum value of suction that can be sustained by a soil is dependent on the size of the soil particles, with fine-grained soils able to sustain much larger values of suction than coarse-grained soils.

The types of soil fabric for unsaturated natural soils fall into three main categories, as shown in Fig. 2.1 (*Wroth and Houlsby,* 1985), depending on the continuity of the air and water phases. Fig. 2.1 (a) shows the situation at low degrees of saturation (commonly found in soil near the ground surface) where the water

phase is discontinous while the air phase is continous. In this first category the pore water pressure is strongly negative and the pore air is at atmospheric pressure. Fig. 2.1 (b) shows the situation in the next zone of soil (below the previous zone), where intermediate degrees of saturation occur and both the air and water phases are continous. The pore water pressure will be negative and the pore air pressure is zero as it is connected to the atmosphere. Finally, Fig. 2.1 (c) shows the type of soil found in a narrow transition zone immediately above the saturated soil. The degree of saturation is high and the air phase is discontinous, in the form of occluded bubbles, whereas the water phase is continous. The pore water pressure is negative (because the soil is above the water table) and the pore air pressure is greater than the pore water pressure (because of surface tension effects) but it is not necessarily equal to atmospheric pressure.

For unsaturated natural soils containing widely differing particle sizes, *Burland* (1965) suggested that the type of soil fabric shown in Fig. 2.2 would occur. The large sand or silt grains are bonded together by clay "packets" which are concentrated around the contact points of the larger grains. *Burland* (1965) explained that the volume change that took place on loading / unloading or wetting / drying was not only as a result of grain contact slippage but also by distortion, shrinkage and swelling of the clay "packets".

2.1.2 Unsaturated compacted soils

Unsaturated compacted clays generally consist of saturated "packets", containing small, water-filled intra-packet voids, separated by larger, unsaturated inter-packet voids (see Fig. 2.3). *Brackley* (1975) introduced the concept of "packet void ratio" which was defined as the ratio of the volume of intra-packet voids to the volume of solid particles within the packets. *Gens and Alonso* (1992) refer to the details of soil fabric within the saturated clay packets as the soil "microstructure" and the arrangement of entire packets and the large inter-packet voids as the soil "macrostructure". On wetting (an increase of pore water pressure, corresponding to a

reduction of suction) the saturated microstructure of individual clay packets will swell (increase in volume) but there may also be a tendency for "collapse" (reduction in volume) of the unsaturated macrostructure.

For unsaturated compacted granular fills, the soil fabric is more likely to be as shown in Fig. 2.2, with any small amounts of fine-grained material clustering around the contact points of the larger grains.

The details of soil microfabric in unsaturated soil are very important, because this microfabric controls the condition of the pore water, especially its negative pressure or suction (*Alonso, Gens and Hight,* 1987). The types of soil microfabric for unsaturated compacted soil as proposed by *Alonso, Gens and Hight* (1987), are shown in Fig. 2.4. Within these forms of microfabric there are three levels of particle arrangement : elementary particle arrangements, particle assemblages and pore spaces. *Alonso, Gens and Hight* (1987) pointed out that the microfabric shown in Fig. 2.4 (a) is predominant in expansive soils or clayey soils compacted wet of optimum. Conversely soil compacted at a water content dry of optimum could be viewed as a collection of saturated or nearly saturated aggregations, separated by relatively large pores at low saturation (see Fig. 2.4 (b)).

Seed and Chan (1959) reported that soils compacted dry of optimum had a flocculated structure while soils compacted wet of optimum had a dispersed structure. They showed that the shrinkage on drying of soils compacted dry of optimum was smaller than the shrinkage of soils compacted wet of optimum. This was because soils compacted dry of optimum were much stronger, due to their flocculated fabric, than soils compacted wet of optimum (which had a dispersed fabric resulting in a weaker structure).

Toll (1990) stated that the fabric of unsaturated compacted gravel was influenced by the degree of saturation. This initial fabric was not destroyed even when the soil was sheared to high strains. This agreed with the observations of *Seed and Chan* (1959), who stated that unsaturated soils dry of optimum and wet of

optimum retained different fabrics right up to failure, and this difference in fabric had a profound influence on the shear strength.

2.1.3 Unsaturated gassy soils

Fig. 2.5 shows the structure of gassy soil commonly found in the offshore environment, where gas (typically methane) is formed by bacterial or thermogenic activity. Since the soil is confined within the seabed the pore gas pressure and the pore water pressure are positive. In fine-grained seabed soils the gas bubbles are typically much larger than the normal void spaces (although still a maximum of a few millimetres in diameter) and *Wheeler* (1988a) proposed the structure shown in Fig. 2.5 (a). The gas bubbles form large cavities within an otherwise saturated soil. This structure was idealised by the continuum model shown in Fig. 2.5 (b), with the gas bubbles forming spherical cavities within a continuum of saturated soil.

2.2 Effective stress and stress state variables

In Chapter 1 it was shown how the matrix suction $u_a - u_w$ plays an important role in the behaviour of unsaturated soils. The fact that the pore water pressure u_w and pore air pressure u_a have different values has also made the theoretical analysis in terms of effective stress more difficult. This is why the study of unsaturated soil behaviour has lagged behind that of saturated soil.

2.2.1 Early attempts to use a single effective stress

The principal of effective stress in saturated or dry soil was first put forward by *Terzaghi* (1936), who stated :

"*The stresses at any point of a section through a mass of soil can be computed from the total principal stress* σ_1, σ_2, σ_3 *which act at this point. If the voids of the soil are filled with water under a stress u, the total principal stresses consist of two parts. One part, u acts in the water and in the solid in every direction with equal intensity. It is called the neutral stress (or pore water pressure). The*

balance, $\sigma_1' = \sigma_1 - u$, $\sigma_2' = \sigma_2 - u$ *and* $\sigma_3' = \sigma_3 - u$ *represents an excess over the neutral stress u and it has its seat exclusively in the solid phase of the soil. This fraction of the total principal stresses will be called principal effective stresses"*

"A change in the neutral stress u produces practically no volume change and has practically no influence on the stress conditions for failure. All the measurable effects of a change in stress, such as compression, distortion and a change of shearing resistance are exclusively due to changes in the effective stresses $\sigma_1', \sigma_2', \sigma_3'$.'

In the case of an unsaturated soil, where the pore space contains air and water, an expression for the effective stress was first proposed by *Bishop* (1959), who suggested the following relationship:

$$\sigma' = \sigma - u_a + \chi(u_a - u_w) \tag{2.1}$$

where σ' was the effective stress, σ was the total stress, u_a was the pore air pressure, u_w was the pore water pressure and χ was a parameter depending on the degree of saturation S_r. *Skempton* (1960) stated that the effective stress in an unsaturated soil was that stress controlling the changes in volume or shear strength of the soil and the effective stress could be defined by Bishop's equation (Equation 2.1).

Jennings and Burland (1962) pointed out that , as for saturated soils, the principle of effective stress could take the form of two propositions :

(a) all measurable effects of a change in stress such as compression, distortion and a change of shearing resistance of the soil were exclusively due to changes in effective stress ;

(b) the effective stress σ' in a partially saturated soil was defined as the excess of the total applied stress over the equivalent pore pressure (defined as $\chi u_w + (1-\chi)u_a$ in Equation 2.1).

If the effective stress principle holds for unsaturated soil, then the properties and behaviour of an unsaturated soil sample at a given value of effective stress (as defined

by Equation 2.1) should be identical to those of a saturated sample of the same soil at the same value of effective stress (defined in the conventional way for saturated conditions) and with the same effective stress history. For example, as stated by *Bishop, Alpan. Blight and Donald* (1960), the shear strength τ would be given as

$$\tau = c' + [\sigma - u_a + \chi(u_a - u_w)]\tan\phi' \qquad (2.2)$$

where the friction angle ϕ' and cohesion c' are soil constants whose values are independent of whether the soil is saturated or unsaturated.

To determine the value of χ, *Bishop, Alpan, Blight and Donald* (1960) carried out some drained triaxial tests on normally consolidated Braehead silt. The samples were prepared from slurry and then de-saturated by the application of a suction. The values of cell pressure σ_3, pore air pressure u_a and pore water pressure u_w were controlled. The deviator stress at failure and the average degree of saturation at failure were obtained from observations of load and volume change. The value of χ was back-calculated from Equation (2.2) using values of ϕ' obtained from tests on fully saturated samples. The test results are shown in Fig. 2.6.

The value of χ was also determined by *Bishop, Alpan, Blight and Donald* (1960) from a series of undrained triaxial tests at constant water content on compacted soils having clay fractions of 22%, 18% and 4%. The soils used were a clay shale (22% clay fraction) and two different boulder clays (18% and 4% clay fractions). Both pore water and pore air pressures were measured throughout the tests and values of χ were again back-calculated from Equation (2.2) by using values of ϕ' and c' measured on saturated samples. Results are shown in Fig. 2.7. No unique relationship between χ and the degree of saturation S_r was apparent for the three different soils.

Jennings and Burland (1962) questioned the validity of the effective stress equation proposed by Bishop. They pointed out that the effective stress equation assumed that changes of effective stress caused by changes to the externally applied

total stresses were directly comparable with changes of effective stress caused by changes of suction, and they questioned whether this could be correct. *Jennings and Burland* (1962) also stated that, in order for Bishop's effective stress equation to be valid, the soil behaviour should be unaffected by changes in $(\sigma - u_a)$ and $(u_a - u_w)$ such that σ' as defined by Equation (2.1) remained constant. They carried out three series of oedometer tests on silty soils to check whether this was in fact the case. In one series of tests, on air-dried silts, the specimens were soaked at constant void ratio. If Equation (2.1) was valid it would be expected that soaking at constant volume would require an increase in applied total stress. However the results showed that in order to retain constant volume it was necessary to reduce the applied load during soaking. They concluded that it was not σ' that controlled the behaviour of the majority of unsaturated soils but rather the separate values of $(\sigma - u_a)$ and $(u_a - u_w)$. It was also impossible to model the possibility of collapse on wetting by using Bishop's effective stress equation. *Jennings and Burland* (1962) found no unique relationship between void ratio and effective stress as defined by Equation (2.1).

Burland (1965) pointed out that the stress function controlling shear strength could not be exactly the same as the one controlling volume change. He assumed that the contact area between soil grains was negligible. In unsaturated soil, the pore water pressure only formed as menisci around the grain contact points. This was why a change in all-round applied total stress (which acts on the soil skeleton uniformly throughout the soil) could not be equivalent to any function of a change in pore water pressure (which acts on the soil skeleton only through the grain contact points). Therefore the volume change characteristics could not be related to a unique function of the applied stresses and the pore pressures as was the case for saturated soil. *Burland* (1965) argued that the principle of effective stress could not therefore be used to explain the volume change behaviour of unsaturated soil because the fundamental assumption upon which the principle of effective stress was based was not applicable to unsaturated soil i.e. changes in applied or boundary stresses were

not equivalent to any function of pore water pressure as far as the volumetric behaviour of the soil was concerned.

2.2.2 The use of two independent stress state variables

Having concluded that a single effective stress was unable to describe the stress-strain behaviour of unsaturated soils (particularly the volumetric behaviour), several authors, including *Bishop and Blight* (1963), suggested the use of two independent stress state variables : net stress $\sigma - u_a$ and the suction $u_a - u_w$. In fact it transpired that *Coleman* (1958) had effectively made the suggestion some years earlier, in proposing incremental stress-strain relationships for unsaturated soil (see next section).

Fredlund and Morgenstern (1977) showed from first principles that two independent stress state variables were required to describe the behaviour of unsaturated soil. These stress state variables could be any two chosen from the three stress differences $\sigma - u_a$, $\sigma - u_w$ and $u_a - u_w$. The two normally selected are the net stress $\sigma - u_a$ and suction $u_a - u_w$, because the pore air pressure u_a is commonly zero, and under these conditions, the net stress and suction simplify to the total stress and negative pore water pressure respectively.

At any point within a body of unsaturated soil there will be three principal net stresses $\sigma_1 - u_a$, $\sigma_2 - u_a$ and $\sigma_3 - u_a$. For a three-dimensional problem, a total of four stress parameters are therefore required to define fully the stress state within an element of unsaturated soil : $\sigma_1 - u_a$, $\sigma_2 - u_a$, $\sigma_3 - u_a$ and $u_a - u_w$. For axisymmetric conditions ($\sigma_2 = \sigma_3$) these reduce to a total of three stress parameters, which are most conveniently chosen as the mean net stress p', the deviator stress q and the suction s, defined as follows

$$p' = \frac{\sigma_1 + 2\sigma_3}{3} - u_a \tag{2.3}$$

$$q = \sigma_1 - \sigma_3 \tag{2.4}$$

$$s = u_a - u_w \tag{2.5}$$

2.3 Incremental stress-strain relationships

Coleman (1958) derived incremental stress-strain relationships for an element of unsaturated soil loaded in an axially symmetric manner. Considering only the change dV_w in the volume V_w of water held in the soil, he proposed that:

$$-\frac{dV_w}{V} = C_{11}(du_a - du_w) + C_{12}(dp - du_a) + C_{13}(d\sigma_1 - d\sigma_3) \tag{2.6}$$

Using Equations (2.3) to (2.5) this becomes

$$-\frac{dV_w}{V} = C_{11}ds + C_{12}dp' + C_{13}dq \tag{2.7}$$

Considering the change dV in the overall volume of the soil, Coleman proposed,

$$-\frac{dV}{V} = C_{21}(du_a - du_w) + C_{22}(dp - du_a) + C_{23}(d\sigma_1 - d\sigma_3) \tag{2.8}$$

or

$$-\frac{dV}{V} = C_{21}ds + C_{22}dp' + C_{23}dq \tag{2.9}$$

Finally if ε_1 and ε_3 are the axial and lateral strains of the soil element referred to the current dimensions of the element, the change in shear strain is given by,

$$-(d\varepsilon_1 - d\varepsilon_3) = C_{31}(du_a - du_w) + C_{32}(dp - du_a) + C_{33}(d\sigma_1 - d\sigma_3) \tag{2.10}$$

or

$$(d\varepsilon_1 - d\varepsilon_3) = C_{31}ds + C_{32}dp' + C_{33}dq \tag{2.11}$$

Coleman (1958) stated that the coefficients C_{11} to C_{33} would depend on the current values of all three stress variables and the stress history of the soil. For example, for isotropic elastic behaviour of the soil, *Coleman* (1958) suggested that only coefficients C_{11}, C_{22} and C_{33} would be needed (all other coefficients being zero).

Fredlund (1979) also used the two stress state variables $\sigma - u_a$ and $u_a - u_w$ to define elastic stress-strain relationships for unsaturated soil

$$\varepsilon_x = \frac{\sigma_x - u_a}{E} - \frac{\nu}{E}(\sigma_y + \sigma_z - 2u_a) + \frac{(u_a - u_w)}{H} \tag{2.12}$$

where E was the Young's modulus (which respect to net stress), ν was the Poisson's ratio and H was the elastic modulus for changes of suction. Similar equations were given for ε_y and ε_z. An elasticity form of constitutive relation for the water phase was also given by *Fredlund* (1979)

$$\theta_w = \frac{(\sigma_x + \sigma_y + \sigma_z - 3u_a)}{3A} + \frac{(u_a - u_w)}{R} \tag{2.13}$$

where θ_w was the volumetric water content and A and R were two additional ealstic constants.

2.4 Volume change behaviour

Bishop and Blight (1963) described the volume change behaviour of unsaturated soil by using the two stress state variables : net stress and suction. The behaviour under isotropic loading was expressed as a path in a space with axes of void ratio e, mean net stress $p - u_a$ and suction $u_a - u_w$, as shown in Fig. 2.8. From Fig. 2.8 *Bishop and Blight* (1963) showed that wetting the soil at a low value of $p - u_a$ caused swelling of the soil (path AD) while wetting the soil at a high value of $p - u_a$ caused collapse of the soil (path BE). For an unsaturated soil loaded at constant water content from an initial state A (see Fig. 2.8) the volume decreased and so did the suction (path ABC) until full saturation eventually occurred. If the

sample was saturated at constant volume, it moved from A to A', but in general the increase in $p-u_a$ during wetting was smaller than the decrease in u_a-u_w. *Bishop and Blight* (1963) pointed out that in unsaturated soil the paths of the two components $p-u_a$ and u_a-u_w should be taken into account in describing the volume change.

Matyas and Radhakrishna (1968) stated that the principle of a single effective stress was more difficult to apply to the volume change behaviour than to the shear strength. This was probably due to the fact that the volume change data were normally analysed on an incremental basis in a continous process of deformation, whereas shear strength data were normally analysed only at a failure state. Hence interpretation of the volume change behaviour in terms of a single effective stress required that the behaviour of an unsaturated sample be compared with that of an equivalent saturated sample at every stage of its deformation.

Matyas and Radhakrishna (1968) carried out triaxial tests on a mixture of flint (80%) and kaolin (20%) in all-round compression (Series A) and K_O-compression (Series B). Volume change measurements of pore air, pore water and the specimen were made separately. All samples were statically compacted to the same initial conditions. In Series-A (8 tests) and Series B (5 tests) the suction was either increased (wetting) or reduced (drying) from its initial value at either constant volume or constant mean net stress. The samples were then compressed by the application of a cell pressure (Series A) or by increments of axial load and cell pressure in a stress-controlled machine with no lateral deformation (Series B). The results from both test series were plotted in terms of void ratio e against suction u_a-u_w and mean net stress $p-u_a$, as shown in Figs. 2.9 and 2.10. Each plot shows a warped surface in e, u_a-u_w, $p-u_a$ space, as shown in Fig. 2.9 (c) and 2.10 (c). The results show the possibility of either swelling or collapse taking place when the specimens imbibed water, depending on the magnitude of the mean net stress $p-u_a$. This is illustrated by curves for specimens A2 and A5 in Fig. 2.9 (a). *Matyas and Radhakrishna* (1968) noted that the collapse behaviour caused by decreasing the

suction at high values of $p-u_a$ could not be explained by the principle of effective stress as suggested by *Bishop* (1959)

The pattern of swelling or collapse observed during wetting can be explained by considering the fabric of unsaturated compacted clay soils. The increase of u_w during wetting leads to a decrease in the local value of effective stress within the saturated microstructure of clay packets, and therefore wetting always produces swelling of the individual packets. The softening of these saturated clay packets may however be sufficient to cause slippage at the inter-packet contact points, leading to collapse of the macro-structural arrangement of particles into the large, partially air-filled inter-packet voids. At low values of $p-u_a$, collapse does not occur, because the soil is able to carry the applied load even after softening of the inter-packet contacts. However at high values of $p-u_a$ collapse occurs on wetting, because the macro-structure is unable to carry the high applied load after softening of the inter-packet contacts.

Barden, Madedor and Sides (1969) also examined the volume change in terms of the two stress state variables. They conducted a series of anisotropic consolidation tests in a modified Rowe cell using compacted 6" diameter and 1" thick samples of Westwater and Derwent clays. The samples were divided into 11 groups and were consolidated at given values of suction and mean net stress and then were taken through different stress paths involving wetting at constant mean net stress, consolidation at constant suction and both consolidation and wetting at the same time. The different test paths are shown in Figs. 2.11 (a) and 2.11 (b).

Barden, Madedor and Sides (1969) observed that for samples compacted appreciably dry of optimum, collapse occurred on wetting to zero suction under large p' . The higher the clay content, the smaller was the collapse. This was presumably caused by simultaneous swelling of the clay microstructure taking place. Samples compacted close to optimum showed no collapse. However, regardless of clay content, compressibility on loading decreased with increasing suction for samples compacted dry of optimum. For samples compacted at or wet or optimum the

suction had little effect on compressibility. This was because for samples dry of optimum the soil structure tended to be flocculated which was sensitive to suction, while wet of optimum the structure tended to be more dispersed. A low clay content (presumably less expansive) and a flocculated structure were associated with collapse whereas a high clay content (expansive) and a dispersed structure were associated with swelling behaviour.

Fredlund and Morgenstern (1977) carried out null tests to examine the validity of the stress state variables $p-u_a$ and u_a-u_w. Samples were isotropically consolidated to pre-determined values of $p-u_a$ and u_a-u_w and equal increments of p, u_a and u_w were applied. No overall volume change or water volume change took place during the null tests, confirming the validity of the stress state variables.

Fredlund and Morgenstern (1978) also examined the use of the stress state variables $p-u_a$ and u_a-u_w to investigate the volume change behaviour of unsaturated soils. Like *Matyas and Radhakrishna* (1968), *Fredlund and Morgenstern* (1978) carried out a series of isotropic and K_O- compression tests on three different soils. They calculated the moduli linking changes of e to changes of $p-u_a$ and u_a-u_w from test data for two different stress paths, and then compared the predicted behaviour for a third stress path with the observed behaviour. They found that some samples showed good agreement in deformation moduli between the predicted and measured values while others showed poor correlation. Correlation was good between tests in which the mean net stress was monotonically increased and the suction was monotonically decreased, but correlation was poor if mean net stress was decreased or suction was increased. This suggested the possibility of irreversible behaviour, and the need therefore to use an elasto-plastic form of constitutive model (see Section 2.6).

Fredlund (1979) proposed that, for a limited range of stresses, the void ratio would vary linearly with the logarithmic of both mean net stress and suction :

$$e = e_0 - C_t \log \frac{(p-u_a)_f}{(p-u_a)_o} - C_m \log \frac{(u_a-u_w)_f}{(u_a-u_w)_o} \tag{2.14}$$

where C_t and C_m are compressibility coefficients and subscripts '*f*' and '*o*' indicate final and initial states. However the values of C_t and C_m were said to be controlled by the stress history of the soil. The relationship given in Equation (2.14) is in the form of a planar surface (with stresses on a logarithmic scale) as shown in Fig. 2.12. Thus it cannot model both swelling and collapse on wetting.

Lloret and Alonso (1985) also proposed constitutive relations linking volume change and stress for unsaturated soil. They proposed the following equation for the volume change, for suction greater than 1 kPa :

$$e = a + b\ln(p-u_a) + c\ln(u_a-u_w) + d\ln(p-u_a)\ln(u_a-u_w) \tag{2.15}$$

where *a, b, c* and *d* are constants. Equation (2.15) represents a warped surface linking *e*, to $u_a - u_w$ and $p - u_a$. A typical state surface for Pinolen clayey sand as represented by equation (2.15) is shown in Fig. 2.13. This representation is better than Equation (2.14), because it describes a warped surface where swelling and collapse can be modelled by a single equation. A similar equation for the degree of saturation was also proposed by *Lloret and Alonso* (1985)

$$S_r = a - \{1 - \exp[-b(u_a-u_w]\}[c + d(p-u_a)] \tag{2.16}$$

2.5 Shear strength

Fredlund, Morgenstern and Widger (1978) suggested an expression for the shear strength τ of an unsaturated soil in the following form :

$$\tau = c' + (\sigma - u_a)\tan\phi' + (u_a - u_w)\tan\phi^b \tag{2.17}$$

where τ was the shear stress on the failure plane at failure, $\sigma - u_a$ was the net stress normal to the failure plane at failure, and ϕ^b was a friction angle indicating the rate of change of shear strength with suction. Equation (2.16) describes a planar surface, which is called the extended Mohr-Coulomb failure envelope, as shown in Fig. 2.14. The surface is tangential to the Mohr's circles at failure. The equation was used by *Fredlund, Morgenstern and Widger* (1978) to plot data from *Bishop, Alpan, Blight and Donald* (1960), within a suction range from zero to 200 kPa, which showed that, for this soil over this range of suction, ϕ^b was constant.

Ho and Fredlund (1982) also carried out some multi-stage triaxial tests on unsaturated Hong Kong residual soils, which appeared to verify Equation (2.16). Multi-stage tests were used so as to obtain as much information as possible from a limited number of tests.

Later experimental data showed that the failure surface was not linear when higher values of suction were used. *Escario and Saez* (1986) carried out some direct shear tests on Madrid grey clay, Guadalix red clay and Madrid clayey sand to investigate the validity of Equation (2.16). The results are shown in Fig. 2.15 and it can be seen that for Madrid clayey sand, the shear strength envelopes plotted against $\sigma - u_a$ for various values of suction were roughly parallel within the pressure range used, suggesting that ϕ' was constant. However the test results for Guadalix red clay and Madrid grey clay showed that the failure envelopes diverged over the same pressure range. This indicated that ϕ' varied with suction for these two soils. Fig. 2.15 also shows graphs of the same test results, but replotted using $u_a - u_w$ as abscissa. The graphs all show curvature at low suction values, indicating that ϕ^b varied with suction (ϕ^b decreased as suction was increased).

Fredlund, Rahardjo and Gan (1987) and *Gan, Fredlund and Rahardjo* (1988) found that data from shear tests on unsaturated glacial till showed significant non-linearity of the strength envelope τ with respect to $u_a - u_w$ when considered over a large range of suction values (between 0 and 500 kPa) as shown in Fig. 2.16. The strength envelope was planar up to a value of suction of about 75 kPa. Up to this

point ϕ^b was equal to ϕ', but as suction was increased beyond 75 kPa the strength showed significant non-linearity and the value of ϕ^b decreased. At high values of suction (greater than 300 kPa) the value of ϕ^b tended to a constant value, much lower than ϕ' (see Fig. 2.17).

Escario and Juca (1989) carried out direct shear tests with controlled suction on Madrid clay, Guadalix red clay and Madrid clayey sand over a larger suction range than tested by *Escario and Saez* (1986). Typical results are shown for Madrid grey clay at σ - u_a = 0.3 MPa in Fig. 2.18 (a). At lower values of suction close to the origin, the tangent value of ϕ^b was roughly equal to ϕ'. As suction was increased the tangent value of ϕ^b decreased until the shear strength reached a maximum value (with a tangent value of ϕ^b of zero). Fig. 2.18 (c) shows that for Madrid clayey sand the value of ϕ' was found to be independent of suction, whereas Fig. 2.18(b) shows that ϕ' was dependent on suction for Guadalix red clay.

Gulhati and Satija (1989) carried out triaxial shear tests on Dhanuri clay at constant water content (Series -A) and fully drained (Series-B). Their findings were consistent with the earlier results of *Fredlund, Morgenstern and Widger* (1978), in that the failure surface was planar. ϕ^b was found to be less than ϕ' because $\sigma - u_a$ had more influence in generating shear strength in unsaturated soil than $u_a - u_w$

2.6 Critical state models for unsaturated soil

Sections 2.4 and 2.5 described how the volume change behaviour and the shear strength of unsaturated soils were both related to the stress state variables : net stress $\sigma - u_a$ and suction $u_a - u_w$. In all of the work presented in Sections 2.4 and 2.5 the volume change and shear strength were however treated completely independently. Only in the last few years have attempts been made to link the volume change behaviour and the shear strength of unsaturated soils, following the example of the development of critical state theory for saturated soil.

2.6.1 The elasto-plastic model of Alonso, Gens and Josa (1990)

Alonso, Gens and Hight (1987) presented a qualitative description of an elasto-plastic constitutive model for unsaturated soil. Subsequently the mathematical development of the model was given by *Alonso, Gens and Josa* (1990).

Alonso, Gens and Josa (1990) proposed an elasto-plastic critical state model for unsaturated soil which used concepts of the theory of hardening plasticity. The model reduced to the Modified Cam Clay critical state model for full saturation. The model was intended for unsaturated soils which are only slightly or moderately expansive, such as sands and clays of low plasticity.

2.6.1.1 Isotropic stress states (q = 0)

Under isotropic loading to virgin states at a given suction the specific volume was assumed to be given by :

$$v = \mathrm{N}(s) - \lambda(s) \ln\left(\frac{p'}{p^c}\right) \tag{2.18}$$

where $N(s)$ is the value of v at a reference stress p^c (defined below) and $\lambda(s)$ is the compressibility parameter for changes in mean net stress for virgin states of the soil. Both N(s) and λ(s) varied with suction s, with λ(s) decreasing monotonically from the saturated value λ(o) as the suction was increased from zero. The assumed isotropic normal compression lines for saturated and unsaturated states defined by Equation (2.18) are shown in Fig. 2.19 (a).

Alonso, Gens and Josa (1990) introduced the concept of a yield curve in the p'- s plane, which they named the Loading-Collapse (LC) yield curve (see Fig. 2.19 (b)). The shape of this yield curve was defined by,

$$\left(\frac{p_o'}{p^c}\right) = \left(\frac{p_o'(o)}{p^c}\right)^{\left(\frac{\lambda(0)-\kappa}{\lambda(s)-\kappa}\right)} \tag{2.19}$$

where p_o' was the yield value of mean net stress at a suction s, $p_o'(o)$ was the yield value of mean net stress for saturated condition (s = 0) and κ was the elastic swelling index for changes in mean net stress. Inspection of Equation (2.19) shows that when $p_o'(o) = p^c$, then $p_o' = p^c$. The reference stress p^c therefore defines the value of p' at which the yield stress p_o' is independent of suction and the LC yield curve forms a straight vertical line in the s-p' plane. On subsequent expansion the yield curve becomes curved in the s-p' plane, with p_o' greater than $p_o'(o)$.

The Loading-Collapse yield curve was coupled with a second section of yield curve, the Suction-Increase (SI) yield curve. The simplest assumption was to define the SI yield curve as a straight, horizontal line in the s-p' plane, as given by $s = s_o$ (where s_o was the maximum past suction ever experienced by the soil). The two sections of yield curve are shown in Fig. 2.20. The Suction-Increase (SI) yield curve was incorporated to take into account the irrecoverable compression which occurred when suction was increased beyond the previous maximum value (s_o).

For stress paths inside the LC and SI yield curves only elastic strains occur, with specific volume v varying with p' and s via two elastic constants κ and κ_s :

$$dv^e = -\frac{\kappa dp'}{p'} - \frac{\kappa_s ds}{s + p_{at}} \tag{2.20}$$

where atmospheric pressure p_{at} was included in the equation to avoid indeterminancy as suction reduces to zero.

The LC yield curve provides a means of modelling both swelling and collapse on wetting (reduction of s). At small values of $p - u_a$, say point A in Fig. 2.20, decreasing suction following path AB would result in a small elastic swelling within the yield curve. However at a larger value of $p - u_a$, say at point C, decreasing suction following path CDE would initially cause elastic swelling (from C to D) but this would be followed by irrecoverable (plastic) collapse (from D to E). The yield

curve would be displaced after stress path CDE to the new position shown in Fig. 2.20.

2.6.1.2 Anisotropic stress states (q>0)

For anisotropic stress states *Alonso, Gens and Josa* (1990) extended the LC yield curve up into $q:p':s$ space to form a yield surface as shown in Fig. 2.21. Cross-sections of this LC yield surface at constant suction were assumed to be elliptical in shape, with an equation

$$q^2 - \mathrm{M}^2(p' + ks)(p'_o - p') = 0 \tag{2.21}$$

where M is the critical state stress ratio for saturated soil.

The critical state line at any given suction passes through the apex of the relevant elliptical yield curve (see Fig. 2.22)). A single value of M was assumed for critical state lines for different values of suction. The model of *Alonso, Gens and Josa* (1990) resulted in the following expressions for deviator stress q and specific volume v at critical states :

$$q = \mathrm{M}p' + ks \tag{2.22}$$

$$v = \mathrm{N}(s) - \{\lambda(s) - \kappa\}\ln\left\{2 + \frac{ks}{p'}\right\} - \lambda(s)\ln\left(\frac{p'}{p^c}\right) \tag{2.23}$$

Equation (2.22) is equivalent to equation (2.17) proposed by *Fredlund, Morgenstern and Widger* (1978) i.e. no account is taken of the non-linearity of strength with suction reported by authors such as *Escario and Saez* (1986) (see Section 2.5).

Alonso, Gens and Josa (1990) assumed a non-associated flow rule, relating the plastic component of shear strain to the corresponding plastic component of volumetric strain (see Fig. 2.22).

2.6.2 Toll's critical state model

Toll (1990) carried out standard displacement controlled triaxial tests on samples of 100mm-diameter and 200mm-high lateritic Kiunyu gravel (9% clay). The soils were compacted in layers by using either static or drop hammer compaction. Six samples were tested under full saturation and twenty-three samples were tested under unsaturated conditions. Samples were sheared under constant water content, with flow of water being prevented.

Toll (1990) stated that at critical states the deviator stress q and specific volume v could be given by;

$$q = \mathrm{M}_a(p-u_a)+\mathrm{M}_w(u_a-u_w) \tag{2.24}$$

$$v = \Gamma_{aw} - \lambda_a \ln(p-u_a) - \lambda_w \ln(u_a-u_w) \tag{2.25}$$

$$\Gamma_{aw} = 1+\frac{\Gamma-1}{S_r} \tag{2.26}$$

where M_a was critical state stress ratio with respect to net stress, M_w was critical state ratio with respect to suction, Γ was the saturated critical state parameter and λ_a and λ_w were the slopes of the critical state plane with respect to net stress and suction respectively.

M_a M_w λ_a and λ_w were functions of the degree of saturation S_r as shown in Fig. 2.23. This means that five variables are involved in Toll's proposal (q, $p-u_a$, u_a-u_w, v and S_r), three of which are independent at critical states ($p-u_a$, u_a-u_w and S_r).

Wheeler (1991) argued that the use of S_r as an additional independent variable meant that Toll's equations could not be used for predictive purposes without an additional equation. *Wheeler* (1991) suggested that Toll's experimental critical state values of q could be modelled by an equation which did not involve S_r , of the form :

$$q = \mathrm{M}(p - u_a) + f(u_a - u_w) \tag{2.27}$$

where M was the critical state ratio for saturated soil and the last term was a non-linear function of suction. Equation (2.27) was therefore equivalent to the shear strength expression of Equation 2.17, but with a value of ϕ^b that varied with suction (as reported by authors such as *Escario and Saez* (1986)). *Wheeler* (1991) found that the experimental values of q from Toll's data were more accurately predicted by Equation (2.27) than by Equation (2.24). The only reason that *Toll* (1990) found that M_a and M_w had to vary with S_r was because in Equation (2.24) he was, incorrectly, attempting to force the values of q to fit a relationship that varied linearly with suction. *Wheeler* (1991) also expressed some doubt about the experimental values of v measured by *Toll* (1990), and hence on the validity of Equation (2.24). These experimental problems are discussed in Section 2.7.4.1

2.6.3 An elasto-plastic model showing a maximum of collapse

Josa, Balmaceda, Gens and Alonso (1992) extended the model of *Alonso, Gens and Josa* (1990) to include some aspects of soil behaviour not previously described in the earlier model. This included modelling the behaviour of unsaturated compacted soil with a maximum of collapse, whereas the original model predicted that the collapse on wetting would increase indefinitely on increasing p', because the normal compression lines for different values of suction diverged continously with increasing p'. *Josa, Balmaceda, Gens and Alonso* (1992) argued that this was physically unreasonable, because if an unsaturated soil is loaded to sufficiently high values of p' the suction is unable to continue to maintain an open structure; substantial plastic compression therefore occurs on loading, so that there is then reduced scope for further plastic collapse on wetting.

In the improved model for unsaturated soil of *Josa, Balmaceda, Gens and Alonso* (1992) the shape of the LC yield curve was modified in order to describe the maximum of collapse exhibited by the soil. The following equation was proposed

$$p_o' = (p_o'(o) - p_c) + p_c[(1-m)e^{-\alpha s} + m] \tag{2.28}$$

This means that, for a given position of the yield curve, the yield stress p_o' increases from $p_o'(o)$ at zero suction to a value of $p_o'(o)+(m-1)p_c$ as the suction tends to infinity (see Fig. 2.24 (a)). The parameter m (which is always greater than 1) therefore defines the increase of p_o' as suction is increased to very high values, with the increase of p_o' expressed in terms of a reference stress p_c. The initial rate of increase of p_o' with suction is determined by the exponential parameter α. The maximum of collapse was represented by having the parameter m vary with the expansion of the yield curve in the following manner :

$$m = 1 + \frac{\varsigma_y - 1}{\varsigma_x - p_c}\{p_o'(o) - p_c\}\exp\left(\frac{\varsigma_x - p_o'(o)}{\varsigma_x - p_c}\right) \tag{2.29}$$

m therefore has the value of 1 when $p_o'(o)$ is equal to the reference pressure p_c ; m increases to a peak value of ς_y when $p_o'(o)$ is equal to ς_x ; and m decreases again towards 1 as $p_o'(o)$ tends to infinity (see Fig. 2.24 (b)). The yield curve therefore expands from a straight line when $p_o'(o)=p_c$ to its maximum inclination when $p_o'(o)=\varsigma_x$, and it then tends back towards a straight vertical line as $p_o'(o)$ tends to infinity (see Fig. 2.24 (c)). The maximum collapse on wetting from a specified value of initial suction s_o occurs for a stress path starting on the position of the yield curve with maximum inclination, at $p_o'(o) = \varsigma_x$ (see path AB in Fig. 2.24 (c)). *Josa, Balmaceda, Gens and Alonso* (1992) stressed that their improved model did not involve an increased number of parameters. The model was able to reproduce most of the characteristics of unsaturated non-expansive soil.

2.6.4 An elasto-plastic model for highly expansive clays

Gens and Alonso (1992) presented a modified version of the earlier model of *Alonso, Gens and Josa* (1990) in order to represent the behaviour of unsaturated highly expansive clays. These materials show an irreversible component of swelling on first wetting, whereas the original model of *Alonso, Gens and Josa* (1990) assumed that swelling on wetting was a purely elastic (reversible) process. *Gens and Alonso* (1992) incorporated an additional yield curve, which they called the Neutral Line (NL) in order to model the irreversible component of swelling on first wetting (see Fig. 2.25)

2.6.5 Wheeler and Sivakumar's model

Wheeler and Sivakumar (1993a) pointed out that a second volumetric parameter (in addition to v), such as degree of saturation S_r or water content w should be included to fully define the volumetric state of unsaturated soil. This would mean that, for unsaturated soil, five state variables were involved : mean net stress p', deviator stress q, suction s, specific volume v and water content w (or degree of saturation, S_r). *Wheeler and Sivakumar* (1993a) argued that, although unsaturated soil involved two more state variables than saturated soil, there should be only one more degree of freedom, because there was only one additional phase i.e. the air. *Wheeler and Sivakumar* (1993a) therefore proposed an isotropic normal compression "hyper-line" defined by three equations of the form

$$q = 0 \tag{2.30}$$

$$v = f_1(p', s) \tag{2.31}$$

$$w = f_2(p', s) \tag{2.32}$$

The term "hyper" was introduced because of the need to work in a five- dimensional mathematical space (because of the existence of five state variables)

A critical state hyper-line was also postulated defined by

$$q = f_3(p', s) \tag{2.33}$$

$$v = f_4(p', s) \tag{2.34}$$

$$w = f_5(p', s) \tag{2.35}$$

A state boundary "hyper-surface" linking the normal compression hyper-line and critical state hyper-ine was also defined by the following form

$$v = f_6(p', q, s) \tag{2.36}$$

$$w = f_7(p', q, s) \tag{2.37}$$

Equations (2.30), (2.31), (2.33), (2.34) and (2.36) are present (either explicitly or implicitly) in the constitutive model of *Alonso, Gens and Josa* (1990), but Equations (2.32) , (2.35) and (2.37) are missing, because the model of *Alonso, Gens and Josa* (1990) provides no information on the variation of water content. This means, in particular, that the model of *Alonso, Gens and Josa* (1990) is unable to predict the stress-strain behaviour under undrained (constant water content) conditions.

Wheeler and Sivakumar (1993a, 1995) described triaxial tests on 50mm-diameter specimens of compacted kaolin performed by *Sivakumar* (1993). The samples were compacted in 9 layers in a mould at water content of 25% (4% less than optimum from the standard Proctor compaction test) using a displacement controlled compression machine to give an initial dry density of about 1200 kg/m^3 and degree of saturation of 54%.

The samples were first brought into equilibrium at a mean net stress p' of 50 kPa and suctions of zero, 100, 200 or 300 kPa. They were then isotropically consolidated to a virgin state by increasing p' (while holding s constant) to a stress level higher than that produced by the compaction process. Five different types of shearing stage were then performed :

(a) constant *v*/constant *s* shearing : u_a and u_w increased by equal amounts to keep *v* constant

(b) constant *p'*/constant suction shearing : u_a and u_w increased by equal amounts to keep *p'* constant

(c) fully drained/constant suction shearing : u_a and u_w both held constant

(d) constant *w*/ rising *s* shearing : u_a was maintained constant but no drainage of the water phase was allowed (leading to a decrease of u_w and hence an increase of *s*)

(e) constant p/ falling s shearing : u_a was increased to keep *p'* constant while u_w was increased at 1.5 times the rate of u_a.

The samples in type (a), (b) and (c) tests were sheared at suction values of 0, 100, 200 or 300 kPa whereas suction varied during shearing in type (d) and (e) tests. The cell pressure was held constant in all shear tests.

Wheeler and Sivakumar (1995) interpreted the data from the consolidation stages of the tests of *Sivakumar* (1993) (see Fig. 2.26), in terms of an isotropic normal compression hyper-line relationship for specific volume (Equation 2.31) which took the form

$$v = N(s) - \lambda(s) \ln\left(\frac{p'}{p_{at}}\right) \tag{2.38}$$

where N(s) was the intercept of the line with the *v*-axis at $p' = p_{at}$ and $\lambda(s)$ was the slope of the line. Atmospheric pressure (p_{at}) was introduced into the equation to ensure dimensional consistency. Both N(s) and $\lambda(s)$ were functions of suction, as shown in Table 2.1. N(s) increased monotonically with increasing suction, consistent with the model of *Alonso, Gens and Josa* (1990). $\lambda(s)$ did not however decrease monotonically with increasing suction (as suggested by *Alonso, Gens and Josa* (1990)).

Equation (2.38), which defined the isotropic normal compression hyper-line, as proposed by *Wheeler and Sivakumar* (1995) was slightly different from the normal compression line equation relating v and p' proposed by *Alonso, Gens and Josa* (1990) (see Equation 2.18). *Alonso, Gens and Josa* (1990) assumed the existence of a reference stress p^c at which the yield curve was a straight vertical line in the s-p' plane (see also Equation 2.19). However *Wheeler and Sivakumar* (1995) argued that the existence of this reference stress p^c had never been validated experimentally. Alternatively *Wheeler and Sivakumar* (1995) showed that the form of the LC yield curve could be defined in terms of the parameters defining the normal compression line relationship of Equation 2.38 :

$$(\lambda(s)-\kappa)\ln\left(\frac{p_o'}{p_{at}}\right)=(\lambda(0)-\kappa)\ln\left[\frac{p_o'(o)}{p_{at}}\right]+N(s)-N(o)+\kappa_s\ln\left[\frac{s+p_{at}}{p_{at}}\right] \tag{2.39}$$

Therefore N(s) and λ(s) together with κ and κ_s described the shape of the yield curve for all possible values of $p_o'(o)$. *Wheeler and Sivakumar* (1995) argued that it was more convenient and much simpler to measure N(s) and λ(s) for a few different values of suction in the laboratory than to attempt to measure the value of p^c as suggested by *Alonso, Gens and Josa* (1990). Equation (2.39) simplifies to the yield equation given by Equation (2.19) if it is assumed that there exists a reference pressure p^c at which the yield curve is a straight vertical line.

Wheeler and Sivakumar (1995) showed that the data from Sivakumar's shear stage (see Figs. 2.27 and 2.28) demonstrated the existence of critical state hyper-line relationships for q and v (Equations 2.33 and 2.34 respectively) which took the form

$$q=M(s)p'+\mu(s) \tag{2.40}$$

$$v=\Gamma(s)-\psi(s)\ln\left[\frac{p'}{p_{at}}\right] \tag{2.41}$$

The parameters M(s), μ(s), Γ(s), and ψ(s) were all functions of suction, as given in Table 2.1. M(s) varied slightly with suction, so that the critical state lines of q versus p' at various suctions were not quite parallel to each other (see Fig. 2.27) as assumed by *Alonso, Gens and Josa* (1990) (see Equation 2.22). This suggests slight variation of the value of ϕ' in Equation 2.17. The intercept μ(s) did not increase linearly with suction (as assumed by *Alonso, Gens and Josa* (1990) in Equation 2.22) and the variation was equivalent to reduction in the parameter ϕ^b in Equation 2.17 with increasing suction (as proposed by *Escario and Saez* (1986) and others). The shapes of the critical state line of v versus p' at various suctions (see Fig. 2.28) were very different to those predicted by the model of *Alonso, Gens and Josa* (1990), as given by Equation 2.23, where the curves should be convex upwards.

Wheeler and Sivakumar (1995) proposed elliptical constant suction yield curves passing through the yield point (p'_o) on the normal compression hyper-line and the intersection of the elastic wall with the critical state hyper-line (p'_x) (see Fig. 2.29). The elliptical yield curve was given by :

$$q^2 = M_*^2(p'_o - p')(p' + p'_o - 2p'_x) \tag{2.42}$$

where the aspect ratio M_* was given by,

$$M_* = \left[\frac{M(s)p'_x + \mu(s)}{p'_o - p'_x}\right] \tag{2.43}$$

p'_o and p'_x can both be expressed in terms of the values of p' and v at any general point C on the yield curve, so Equation 2.42 (in combination with Equation 2.43) gives the first state boundary relationship proposed in Equation 2.36.

Equations 2.42 and 2.43 were used to predict test paths in q-p'-v space for a number of constant suction shear tests (types (a), (b) and (c)). Results from the experimental programme were in good agreement with the predicted test paths. The

shear strains could also be predicted along any particular test path with reasonable success by assuming an associated flow rule (in contrast to the non-associated flow rule proposed by *Alonso, Gens and Josa* ,1990).

Wheeler and Sivakumar (1995) were unable to confirm conclusively the existence and form of the normal compression line, critical state and state boundary relationship for water content w (Equations 2.32, 2.35 and 2.37 respectively) from the experimental data of *Sivakumar* (1993). In particular, it was unclear whether a unique critical state relationship for w existed.

2.7 Experimental methods for testing unsaturated soil

The testing of unsaturated soils is more complicated than for saturated soils because of two additional requirements. Firstly the need to control or measure the suction $u_a - u_w$ in the sample, and secondly the need to measure the sample volume change. The sample volume change of a saturated sample is given by the volume of water draining out of the sample, whereas the sample volume change of an unsaturated sample is also affected by the changing volume of air inside the sample. In this section various methods of testing unsaturated soil are given but the experimental results will not be discussed as they have been covered elsewhere in this chapter.

2.7.1 Methods of applying suction

2.7.1.1 Axis translation technique

In the field the pore water pressure within unsaturated soil is negative and the pore air pressure is at atmospheric pressure. To simulate this condition in the laboratory is difficult, because the negative value of pore water pressure induces cavitation in the measuring system (along the water back pressure line).To overcome this problem, *Hilf* (1956) devised a system known as the "axis translation technique" whereby negative values of pore water pressure are avoided.

In the axis translation technique the total stress σ, the pore air pressure u_a and the pore water pressure u_w are all increased by equal amounts until the pore water pressure is increased above zero. In theory this should have no influence on the soil behaviour, because the net stress $(\sigma - u_a)$ and suction $(u_a - u_w)$ remain unchanged. This technique is widely used in testing unsaturated soils in the laboratory.

Because of the need to control or measure independently the pore air pressure and pore water presure, a fine porous ceramic disc known as a high air entry filter, is used to prevent air getting into the pore water pressure measuring system. The high air entry filter must have an air entry value higher than the suction present within the soil. Under these circumstances the filter remains saturated at all times, so that the water in the pores of the high air entry filter is in pressure equilibrium with the pore water pressure in the sample. The pore air pressure in the sample can be controlled or measured through a coarse porous stone, known as a low air entry filter, with a moisture retention so low that it is unable to draw water from the soil. The air contained in the pores of the low air entry filter remains in pressure equilibrium with the pore air pressure inside the sample.

The axis translation technique however has the disadvantage of not exactly replicating the in-situ stress condition. In particular the phenomenon of cavitation which may occur in unsaturated soil under in-situ stress conditions, and may influence its behaviour, cannot be simulated with the axis translation technique. This occurrence of cavitation within the soil is however thought to be important only during the process of de-saturation of an initially saturated soil. The axis translation technique is therefore considered valid for testing samples which are already in an unsaturated condition.

2.7.1.2 Osmotic method of applying suction

Delage, Suraj de Silva and Laure (1987) and *Cui and Delage* (1993) described an osmotic method used to control suction in a triaxial apparatus, and *Delage, Vicol and Suraj de Silva* (1992) described the application of the same

technique to a a suction-controlled oedometer. The soil sample was placed in contact at the top and bottom with two semi-permeable cellulotic dialysis membranes resting on a fine sieve mesh, as shown in Fig. 2.30. Behind the semi-permeable membranes, the top cap and base pedestal were provided with concentric grooves to provide circulation of a solution of polyethylene glycol 2000 through a closed circuit containing a reservoir and a pump. The reservoir was provided with three glass tubes, two of which provided circulation for the cell fluid and a third placed at the centre of the reservoir was used to monitor the volume of the water exchanges between the solution and the sample. The pore air pressure was applied at the bottom of the sample through a small air vent in the bottom pedestal. The semi-permeable membranes allowed the passage of small molecules of water but prevented the passage of the larger polyethylene glycol molecules. A supply of polyethylene glycol 2000 solution from the reservoir was applied to the top and bottom of the sample via the semi-permeable membranes and a difference in the osmotic pressure between the the solution and the water inside the sample was set up across the membrane. This osmotic pressure difference caused a flow of water from the sample to the solution. Under equilibrium conditions (with no flow) the osmotic suction of the polyethylene glycol 2000 must equal the total suction inside the soil sample. Thus by controlling the concentration of the solution under equilibrium condition the total suction of the soil could be controlled by means of a calibration chart of suction plotted aginst the concentration of the solution.

Cui and Delage (1993) claimed that their method of suction control was better than the axis translation technique because the pore water pressure within the sample was maintained at a realistic negative value.

2.7.2 Oedometer testing

Basically in an oedometer test the soil sample is laterally confined such that no horizontal movement is allowed. Thus loading and displacement only take place in

the vertical direction. A variety of oedometer test apparatus has been used in the laboratory for testing unsaturated soils.

Barden, Madedor and Sides (1969) used a modified form of Rowe consolidation cell, as shown in Fig. 2.31 to carry out tests on samples of unsaturated compacted soil having diameter of 150mm and a thickness of 25mm. The total stress σ was applied to the rigid plate by means of hydraulic pressure in the convoluted rubber jack. They used the axis translation technique to control the suction in the soil sample. The pore water pressure u_w was controlled via high air entry filters at the top and bottom of the sample. The pore air pressure u_a was controlled from a square grid of channels cut into the surface of the high air entry filters. Water was flushed through a spiral channel behind the high air entry filters to remove air bubbles, and the flow of water entering or leaving the sample was measured by monitoring the movement of mercury in horizontal tubes.

Fredlund and Morgenstern (1977) used a modified Anteus oedometer to carry out tests on unsaturated samples of silt and kaolin. The construction of the apparatus is shown in Fig. 2.32. The chamber of the oedometer was filled with air to regulate the pore air pressure in the sample. Air and water pressures were separated by means of a high air entry filter placed at the bottom of the sample, with pore air pressure being supplied to the top of the sample. All pressures were controlled by means of pressure regulators. The diffused air bubbles which went into solution in the water and passed through the high air entry filter were flushed into a diffused air volume indicator.

Lloret and Alonso (1985) used a specially built oedometer cell, shown in Fig.2.33 to perform one-dimensional compression tests under controlled suction. The pore water pressure was applied to the bottom of the sample through a high air entry filter while the pore air pressure was applied to the top of the sample through a low air entry filter. During the tests the pore air and pore water pressures were controlled.

In oedometer tests the behaviour of unsaturated soil has been investigated by means of:

a) Consolidation of the soil sample at constant suction (including loading and unloading) i.e variation of the net vertical stress $\sigma_v - u_a$ while holding the suction $u_a - u_w$ constant.

b) Wetting or drying at constant applied load i.e. variation of the suction $u_a - u_w$ while holding the net vertical stress $\sigma_v - u_a$ constant.

c) Wetting or drying of the sample with vertical strain prevented i.e. variation of suction $u_a - u_w$ with the corresponding change of net vertical stress $\sigma_v - u_a$ measured under conditions of zero volume change.

2.7.3 Direct shear testing

In principle, a direct shear test is carried out by shearing the sample at a constant rate of strain in a horizontal direction on a fixed shear plane under a constant vertical load. The size of the sample may vary but it is usually square in plan. Upon testing the sample fails on a pre-determined horizontal shear plane, due to the nature of the test set-up.

Escario and Saez (1986) used a shear box test to test unsaturated samples of Madrid soils as shown in Fig. 2.34. A direct shear box was placed inside a chamber into which nitrogen (serving as the pore air) was introduced at pressure. The nitrogen pressure was applied to the upper part of the soil through a coarse-grained porous stone (a low air entry filter). The lower face of the sample was in contact with water at atmospheric pressure through a high air entry filter. The vertical and horizontal forces and displacements were measured by using push rods. In their shear box tests, *Escario and Saez* (1986) used statically compacted samples of Madrid soils, 22mm thick.

Gan, Fredlund and Rahardjo (1988) also used direct shear box tests on unsaturated soils. The apparatus is shown in Fig. 2.35. A conventional direct shear apparatus was modified to control the pore air pressure and pore water pressures

using the axis translation technique. The sample dimensions were 50mm x 50mm x 20mm thick and the sample was sandwiched between a low air entry filter at the top and a high air entry filter at the bottom. The apparatus was placed inside a pressure chamber, and the air pressure inside the chamber was in direct contact with the top of the low air entry filter while the flow of water (at atmospheric pressure) into the bottom of the sample was controlled through the high air entry filter. Provision was made for flushing the diffused air bubbles in the solution of water into a diffused air volume indicator *(Fredlund*, 1975). The normal stress σ on the sample was applied vertically via a loading ram and the shear test was performed at a slow rate to ensure fully drained conditions.

As quoted by *Escario and Saez* (1986) and *Gan, Fredlund and Rahardjo* (1988), the advantage of the shear box test over a triaxial test was the use of a thin soil sample which shortened the time for equalization of suction during the test. In the direct shear test apparatus the behaviour of unsaturated soil was investigated under a constant vertical loading with both the air and water phases fully drained.

2.7.4 Triaxial testing

This is the commonest and most versatile technique of investigating the stress-strain behaviour of soil in the laboratory. In principle a cylindrical soil sample is subjected to unequal vertical and horizontal stresses, where the horizontal stress is provided by a cell fluid while the deviator stress (the difference between the vertical and horizontal stresses) is provided by a loading ram acting in the vertical direction. With the advent of modern testing techniques the soil sample can be loaded along any desired stress path. However in the testing of unsaturated soil in a triaxial test, the measurement of sample volume change cannot be achieved by simply measuring the the volume of water draining from the sample (as in saturated soil testing) because the sample volume change in unsaturated soil is the combined changes of the volume of air and water in the sample. Presently there are two methods available for

measuring sample volume change in unsaturated soil in the triaxial apparatus : the double-walled cell and local strain gauges mounted directly on the soil sample.

2.7.4.1 Double-walled cell

Bishop and Donald (1961) used a double-walled cell to carry out an experimental study on unsaturated soil. The experimental set-up is shown in Fig. 2.36. The soil sample was surrounded by mercury contained within an inner perspex cylinder. The upper part of the inner cell was filled with water, which was directly connected via a cut-away in the inner perspex cell wall to water in an outer cell. Equal pressures were therefore maintained on both inner and outer faces of the inner cell wall, so that any changes of cell pressure did not cause a change of inner cell volume. The sample volume change was measured by monitoring the level of mercury, which was detected by a cathetometer measuring the movement of a stainless ball floating on the mercury. The suction within the soil sample was controlled or measured by the axis translation technique. The pore water pressure was applied to the bottom of the sample through a high air entry filter while the pore air pressure was applied to the top of the sample via a glass fibre disc.

The disadvantages of the type of double-walled apparatus used by *Bishop and Donald* (1961) included the fact that the sample could not be seen and the hazard of handling a large quantity of mercury. In addition, significant variation of lateral stress over the height of the sample occurred because of the very high density of mercury.

Delage, Suraj de Silva and Laure (1987) developed a modified version of Bishop and Donald's double-walled triaxial cell, in which the mercury in the inner cell was replaced with water and the water in the outer cell and the upper section of the inner cell was replaced with air (see Fig. 2.30). This solved most of the problems inherent in Bishop and Donald's cell. The only remaining difficulty was that it was difficult to provide a method of automatically recording sample volume change, as this required a method for automatically measuring the movement of the water

surface in the inner cell. The triaxial cell of Delage, Suraj de Silva and Laure employed the osmotic method of controlling suction.

Wheeler (1988b) also used a double-walled triaxial cell to measure sample volume change of unsaturated soil samples as shown in Fig. 2.37. The principle of the double-walled cell as used by *Wheeler* (1988b) was that the volume change of the sample was given by the volume of water entering or leaving the inner cell. The pressures of the inner and outer cell were kept equal, to prevent any change of the inner cell volume that would be caused by expansion of the inner acrylic cylinder. A rolling diaphragm seal on the loading ram was used to prevent leakage of water from the inner cell. The double-walled cell was calibrated for any apparent volume change caused by cell pressure application, water absorption by the acrylic cell wall and ram displacement. The double-walled cell was successfully used by *Sivakumar* (1993) to measure the volume change of unsaturated compacted kaolin samples.

Wheeler (1991) questioned the accuracy of the critical state values of v reported by *Toll* (1990) (see Section 2.6.2) because Toll measured the sample volume change of the soil samples in his tests by simply measuring the volume of water entering or leaving his single-walled triaxial cell. This involved significant errors in the calculated values of v, due to expansion of the cell wall (which cannot be adequately calibrated, because of the marked creep and hyteresis of acrylic) and water absorption by the acrylic cell wall.

2.7.4.2 Local strain gauges

Another method of measuring sample volume change in unsaturated soil in a triaxial test is the use of local strain gauges (axial and radial) mounted directly on the soil sample. The use of local gauges in measuring the small strain behaviour of soil has been described in length by many authors. These local gauges include electrolevel gauges (*Burland and Symes*, 1982 ; *Jardine, Symes and Burland*, 1984), LVDTs (*Costa-Filho*, 1982), Hall-effect transducers (*Clayton and Khatrush*, 1987) and proximity transducers (*Hird and Yung*, 1989). The principle of the technique is that

the individual axial and radial displacements of the sample are measured directly by the local and radial gauges mounted directly on the soil sample as shown in Fig. 2.38. The axial and lateral strains are then combined to give the volumetric strain of the sample.

This technique may have an advantage over the double-walled cell technique at small strains where the high precision of the local gauges is significant. The disadvantage of the method is apparent at high values of strain, where non-uniform deformation of the sample (such as barrelling) becomes significant and the lateral strain measured at a single height on the sample become unrepresentative of the whole sample. Also the local gauge measurements become completely meaningless as a means of measuring sample volume change if a shear plane forms across the sample.

2.7.4.3 Overall performance of triaxial testing technique

In contrast to oedometer and direct shear tests on unsaturated soil, the triaxial test is the most versatile. The behaviour of unsaturated soil has been investigated in the triaxial apparatus by a variety of methods, some of which are :

a) Wetting and drying tests where the suction in the sample is varied under isotropic stress states with the mean net stress held constant.
b) Isotropic consolidation at constant suction (including loading and unloading), in which the mean net stress is varied at constant suction.
c) Shearing at constant water content (water phase undrained, air phase drained), giving rise to a variation of suction during shearing.
d) Fully drained shearing (both air and water phases drained), producing constant suction shearing.

Perhaps the most important feature of the triaxial test over any other type of shear test is the ability of the apparatus to simulate the stress conditions of the soil along any desired axisymmetric stress path. This is made possible by the advent of computerised logging and control systems. For example, *Sivakumar* (1993) used a

feedback control system in his triaxial apparatus to control independently cell pressure σ_3, pore air pressure u_a and pore water pressure u_w. With these facilities incorporated into the triaxial testing technique virtually any stress paths of the soil can be followed with ease.

2.8 Yielding of soil

One of the main aspects of the soil behaviour that was investigated in the research programme was the occurrence of yielding (see Chapter 3). An overview of the concept of yielding of soil and its identification is briefly given here.

The yield point of an engineering material (including soil) is defined as the point at which plastic (irrecoverable) strains commence. In practice, however, yield is normally identified by a sudden change of stiffness, rather than by investigating directly the onset of irrecoverable strains.

Yielding is an important feature of the stress-strain behaviour of over-consolidated clays (*Graham, Crooks and Lau*, 1988). Yielding of soil has been studied by many investigators, including *Tavenas and Leroueil (1979)*, *Tavenas, Des Rosiers, Leroueil, La Rochelle and Roy* (1979) *Graham, Noonan and Lew* (1983) and *Baracos, Graham and Domaschuk* (1983). Most of their studies have concentrated on natural saturated soils. *Roscoe and Burland* (1968) and *Parry and Nadarajah* (1973) studied soil yielding on reconstituted specimens of kaolin in the laboratory. *Cui and Delage* (1993) are perhaps the only authors to present results on the yielding of unsaturated soil under triaxial stress states.

Fig. 2.39 shows some typical curves used by *Graham, Noonan and Lew* (1983) to identify yielding in natural saturated soils. They pointed out that the initial straight sections of the curves are considered elastic and the break (or kink) in each stress-strain curve is considered to be a yield point. This is shown in Fig. 2.39 (a) and (b). They also said that in the absence of discontinuity of slope of the stress-strain curves, for natural saturated soil there generally exists two linear sections of the curve which

can be extended to meet at a point. This point was also identified as a yield point, as illustrated in Fig. 2.39 (c).

Roscoe and Burland (1968) used plots of specific volume v versus mean net stress p' (with p' plotted a logarithmic scale) and deviator stress q versus axial strain ε_1 to identify yield points from tests on kaolin subjected to isotropic loading and shear (see Fig. 2.40). Fig. 2.40 (a) shows the intersection of two linear sections of the v versus $ln\, p$ curve at a point, and this point was identified as the yield point. This yield point is also shown in Fig. 2.40 (b) which relates q to ε_1.

Parry and Nadarajah (1973) used a linear scale for the p' and q- axes in their plots to identify yield points from tests on lightly over-consolidated kaolin in a triaxial cell. Their method is shown in Fig. 2.41. They found from the graphs that there are two linear sections on the curves that meet a point which they termed the yield point (denoted by arrow in Fig. 2.41).

Cui and Delage (1993) used similar techniques *to Roscoe and Burland* (1968) and *Parry and Nadarajah* (1973) to identify yield points from triaxial shear tests on unsaturated Jossigny silt. Their methods are shown in Fig. 2.42. From the graph of v versus p' (with p' plotted on a logarithmic scale) two linear sections on the curve are joined together to determine the yield point. *Cui and Delage (1993) also found that* if the yield points shown in Fig. 2.42 (a) were plotted on q versus ε_1 diagram, yielding occurred at an axial strain of approximately 2% in all tests. However no distinct yield points were apparent from the plots of q versus ε_1, and it would have been difficult to use the q versus ε_1 plots to identify yield points (Fig. 2.42 (b)).

Graham, Crooks and Lau (1988) however cautioned that their methods of identification of yield points were applicable to natural soils which had experienced diagenetic aging, where the stress-strain curves were approximated by two straight lines intersecting at a point. They argued that the methods were inapplicable to re-constituted clay soils where linear pre-yield behaviour proceeded directly into exponential post-yield behaviour. However *Wood* (1990) pointed out that yielding was more or less associated with a transition from stiff to less stiff response of the

material and this criterion was more convenient in defining yield which was normally shown by more or less well-defined kinks in stress-strain curves.

To summarize, there is agreement amongst researchers that yield points can be identified from plots of v versus p' (with p' plotted on a logarithmic scale) and q versus ε_1 . Although a sharp kink or change in the curve is not always obvious, there is a suggestion that in most cases there exist two linear sections on the curves that can be extended to meet at a point defined as the yield point. However it seems likely that the volumetric behaviour of the soil (v versus $ln\ p'$) often gives a better indication of the yield point than the shear behaviour (q versus ε_1), even during shear tests.

Recent high quality experimental measurements of the behaviour of soil at small strains show that the stress-strain relationship is highly non-linear and the soil deformation is influenced by the current state and stress history of the soil (*Jardine and Potts*, 1988). This was substantiated by the fact that laboratory-measured stiffnesses under-estimated values back-calculated from field observations. There was also considerable evidence of plastic (irrecoverable) strains occurring for stress paths remaining well inside what was conventionally thought of as the yield surface, and the onset of yielding appeared to be a gradual process rather than a single distinct yield point. A new approach for modelling the yielding of soil by a series of nested kinematic yield surfaces was proposed by among others *Stallebrass* (1990) and *Smith, Jardine and Hight* (1992). The model of *Stallebrass* (1990), consisting of three yield surfaces, is schematically shown in Fig. 2.43. The stress-strain behaviour of the soil is controlled by the movement of the two inner kinematic surfaces and the expansion and contraction of all three surfaces. The outer third surface, called the 'bounding' surface, describes the overall stress history while the recent stress history of the soil is represented by the 'yield' and 'history' surfaces of the soil (see Fig. 2.43).

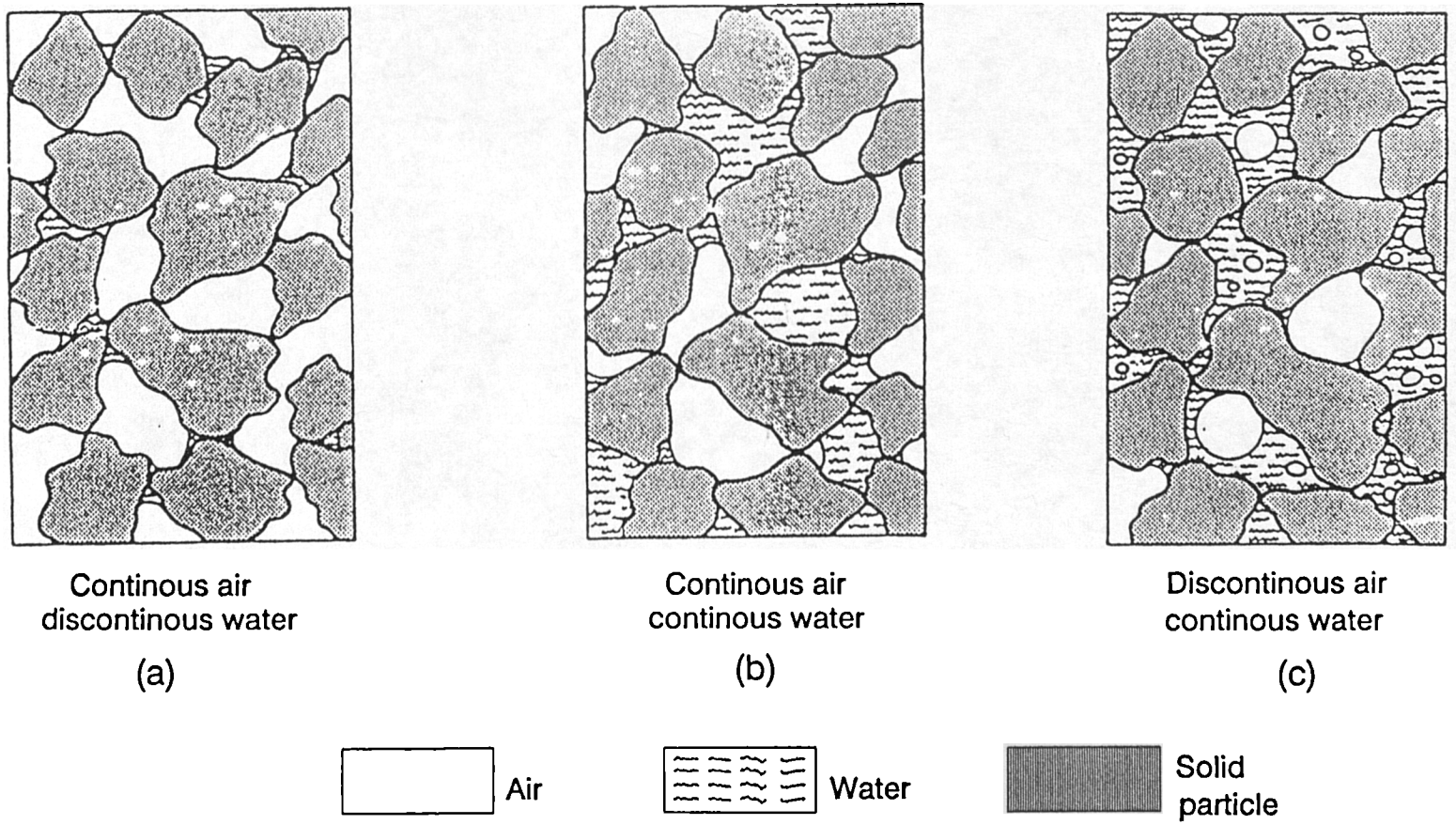

Fig. 2.1 : Continuity of air and water phases (Wroth and Houlsby, 1985)

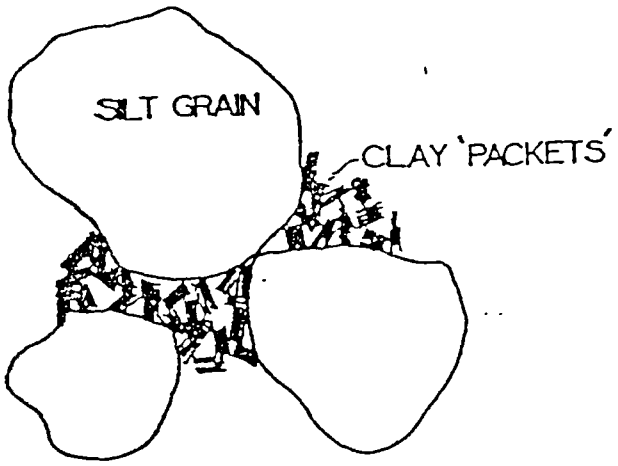

Fig. 2.2 : Fabric of unsaturated natural soil containing widely differing particle sizes (Burland, 1965)

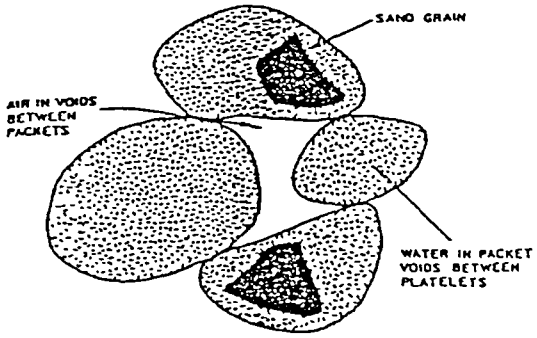

Fig. 2.3 : Model of unsaturated compacted clay soil (Brackley, 1975)

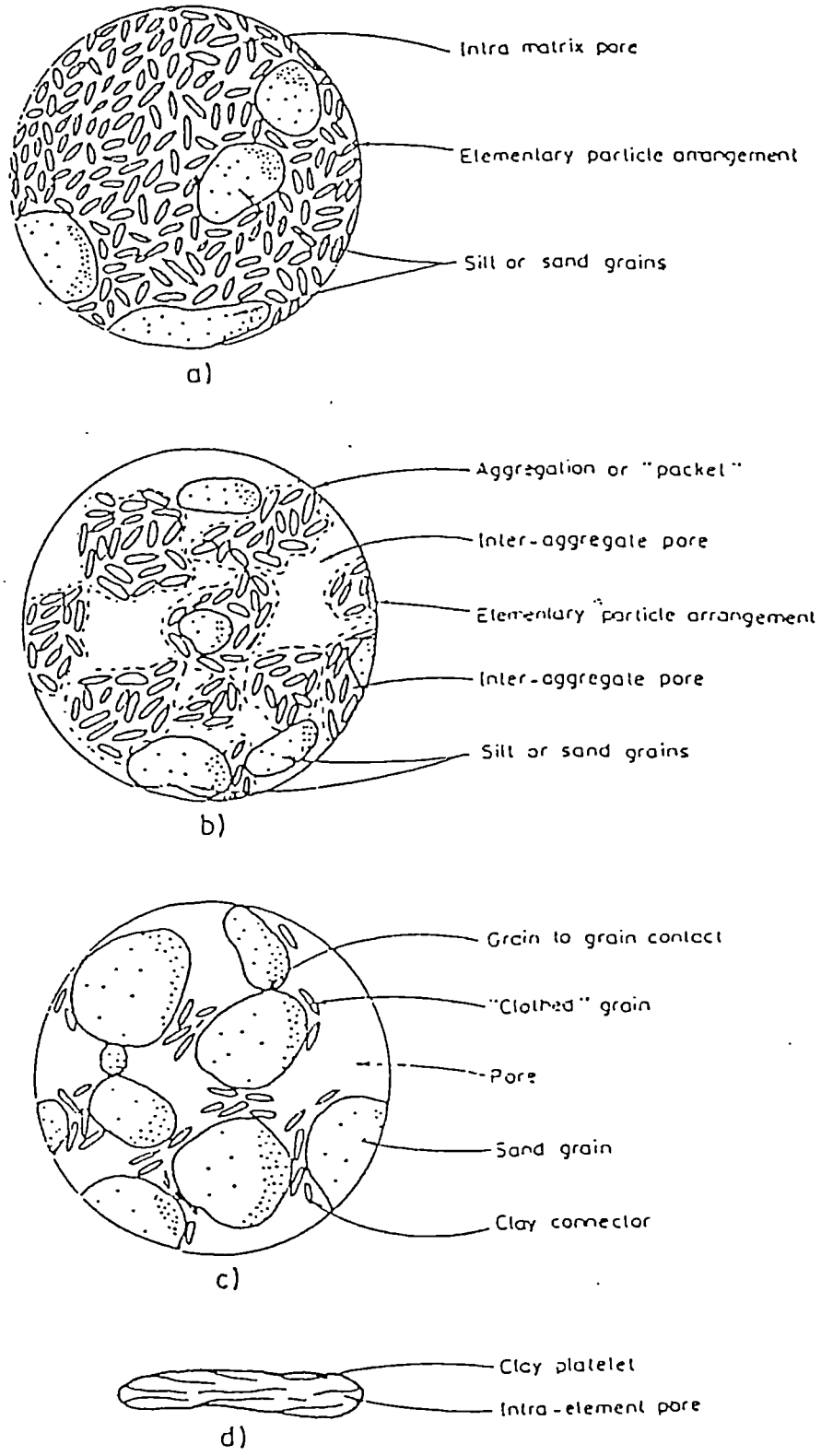

a) Clay matrix predominatly constituted by elementary particle arrangements of clay platelets and a few grains of silt and sand. b) Microfabric of a clay predominantly made up of aggregations of elementary particle arrangements. c) Sand or silt matrix with clay connectors. d) Elementary particle arrangement in a parallel configuration.

Fig. 2.4 : Types of microfabric for unsaturated compacted soil (Alonso, Gens and Hight, 1987)

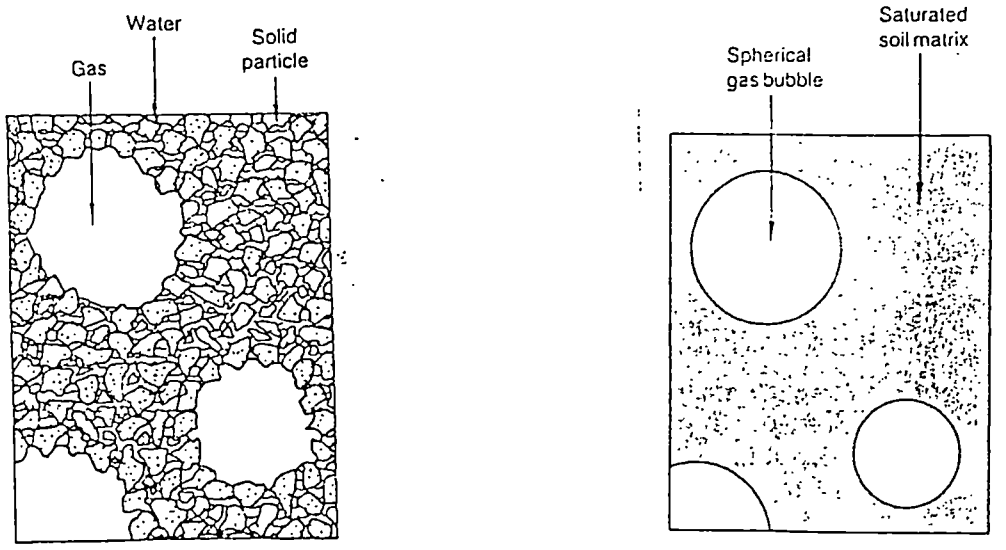

(a) soil structure (b) continuum model

Fig. 2.5 : Structure of soil containing gas bubbles (Wheeler, 1988a)

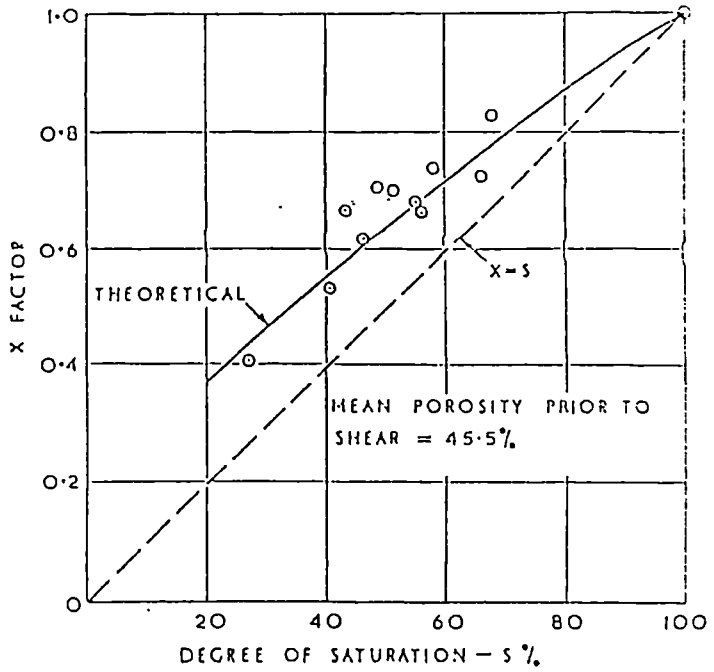

Fig. 2.6 : Values of χ back-calculated from drained triaxial tests on Braehead silt (Bishop, Alpan, Blight and Donald, 1960)

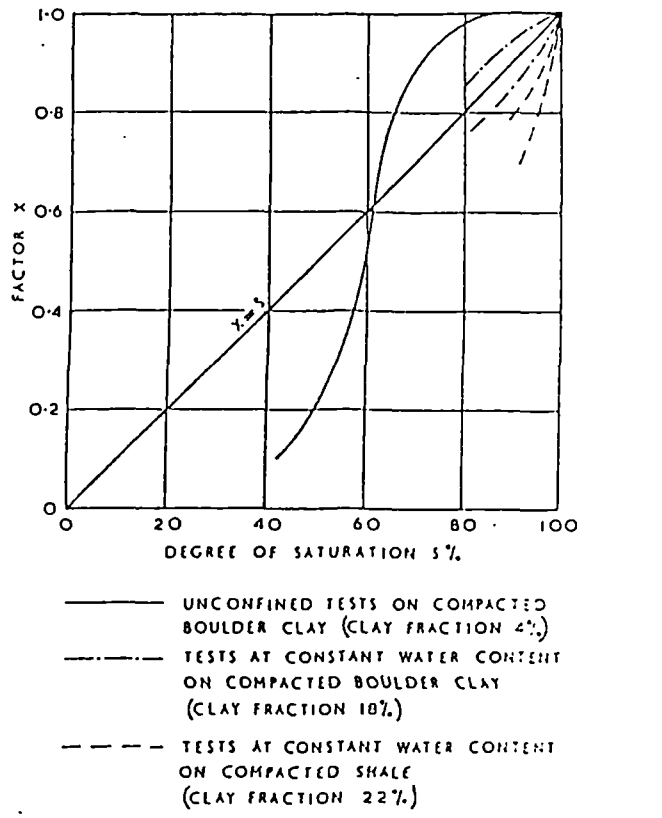

Fig. 2.7 : Relationship between degree of saturation and factor χ for three compacted soils (Bishop, Alpan, Blight and Donald, 1960)

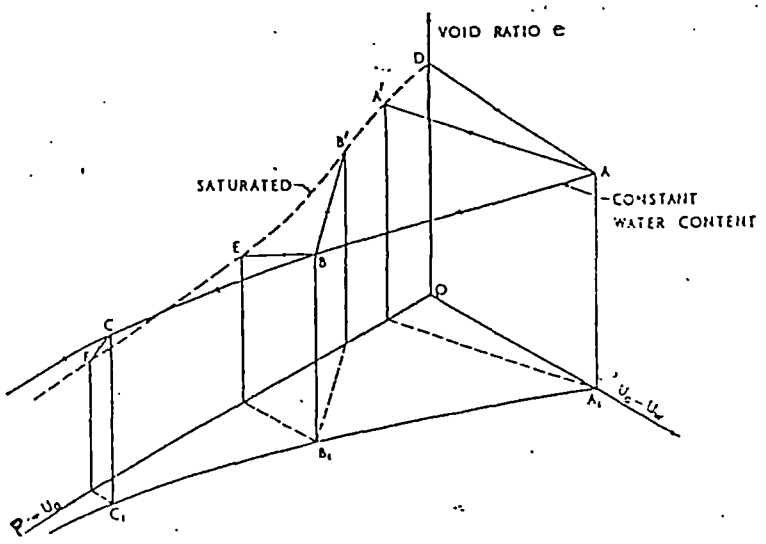

Fig. 2.8 : Volume change under isotropic loading plotted in void ratio : mean net stress : suction space (Bishop and Blight, 1963)

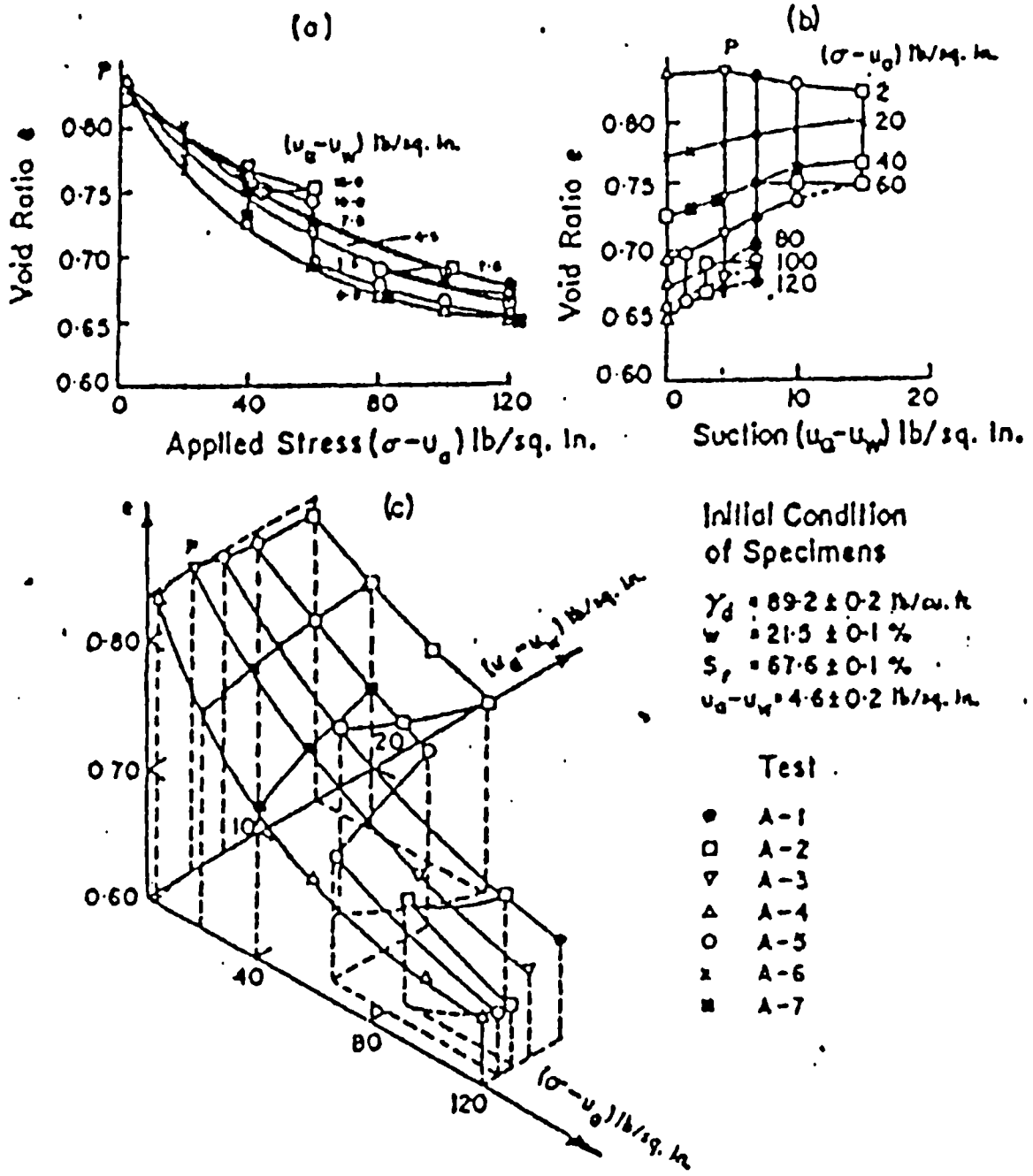

Test paths for series A (all-round compression)

Fig. 2.9 : Volume change behaviour of unsaturated flint/kaolin soil under isotropic conditions (Matyas and Radhakrishna, 1968)

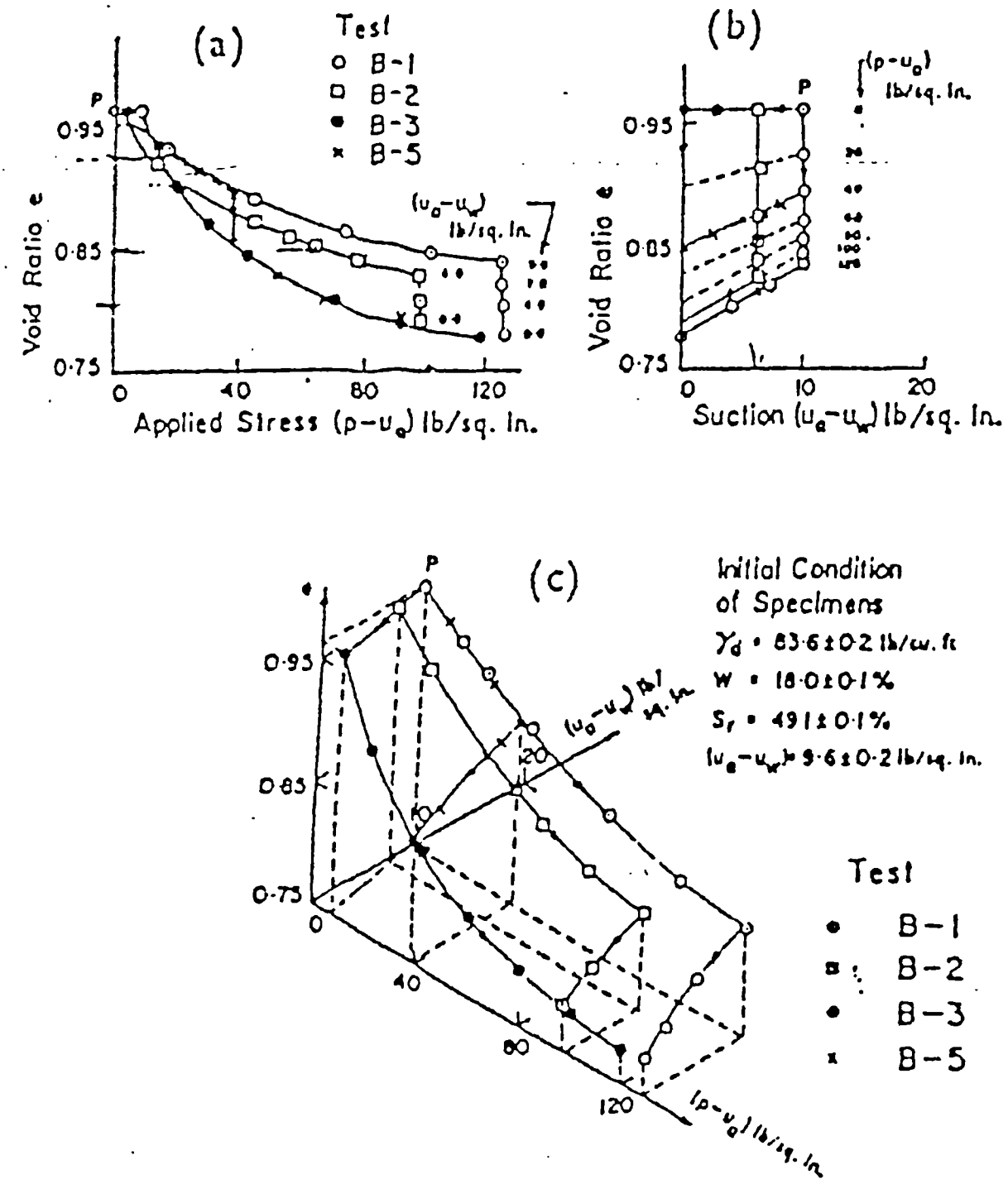

Test paths for series B (K_0 compression)

Fig. 2.10 : Volume change behaviour of unsaturated flint/kaolin soil under K_o- conditions
(Matyas and Radhakrishna, 1968)

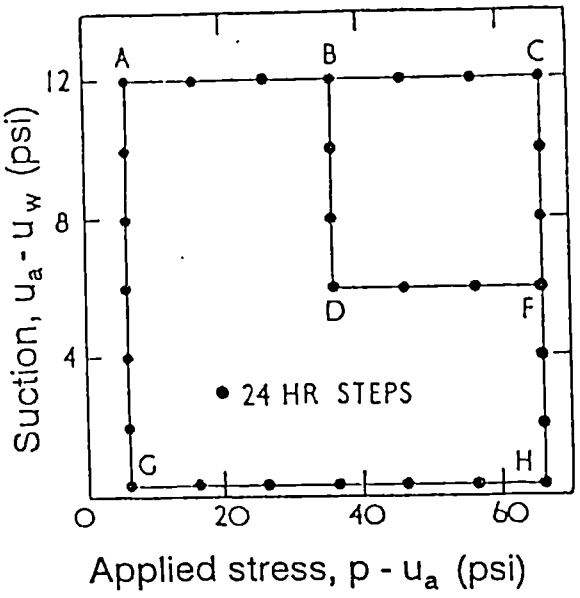

(a) stress paths for group 1

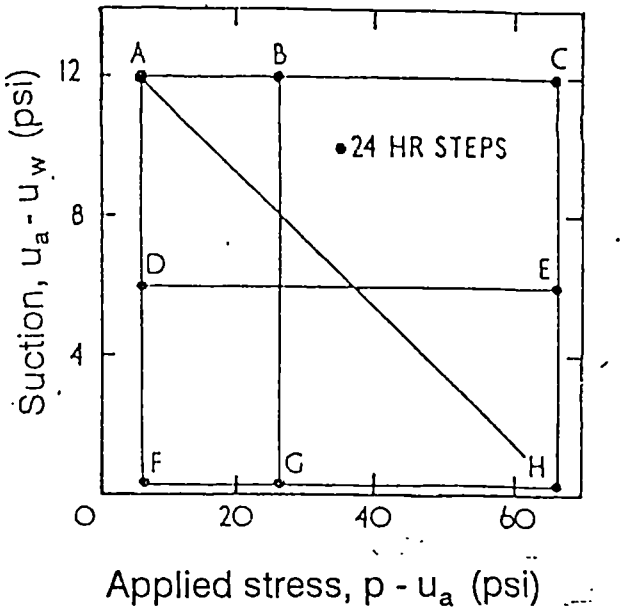

(b) stress paths for groups 2 through 11

Fig. 2.11 : Stress paths adopted in oedometer tests by Barden Madedor and Sides (1969)

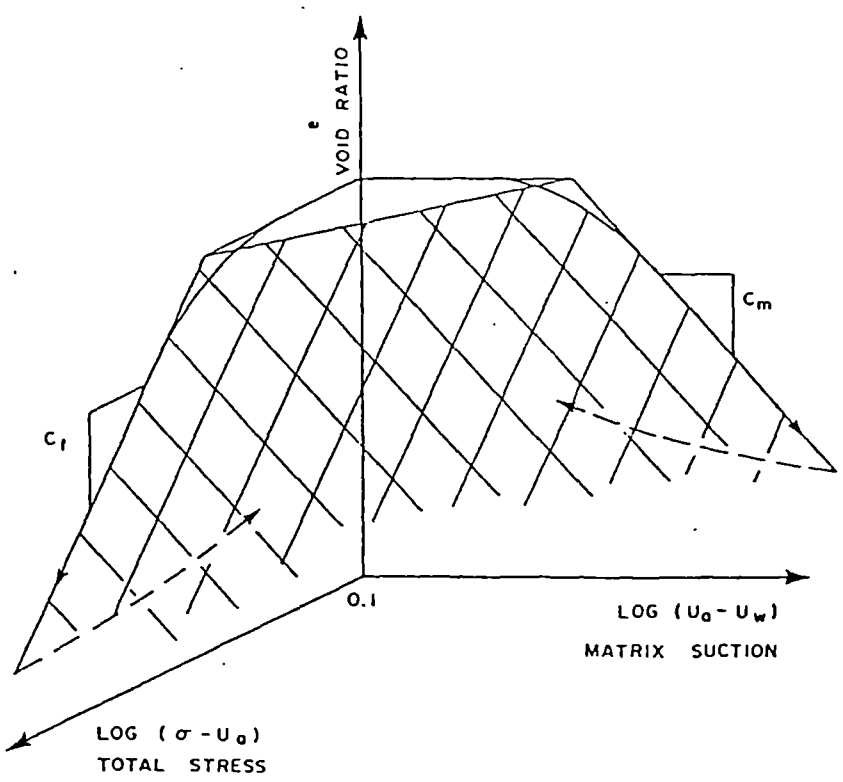

Fig. 2.12 : Planar state surface for void ratio proposed by Fredlund (1979)

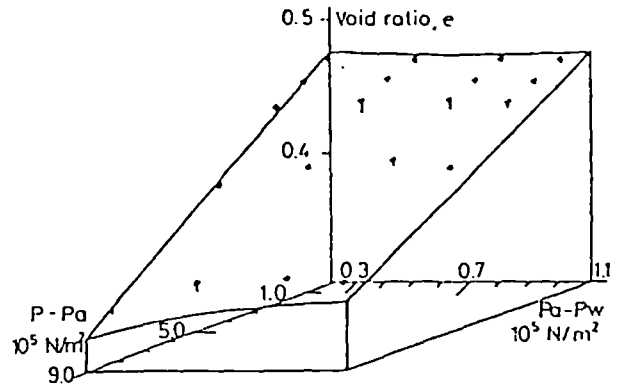

Fig. 2.13 : State surface for void ratio of Pinolen clayey sand under isotropic compression (Lloret and Alonso, 1985)

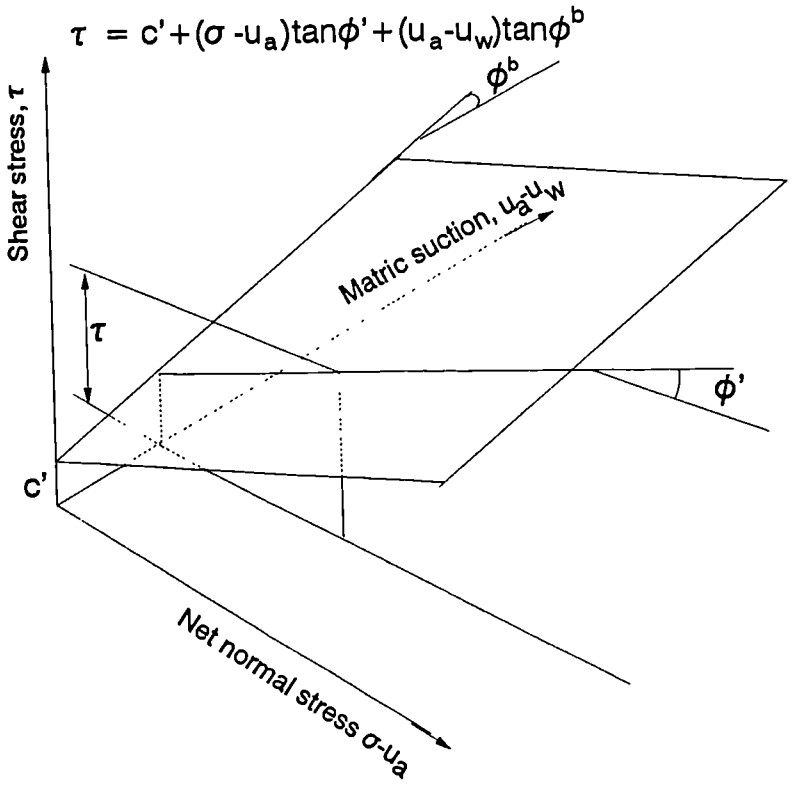

Fig. 2.14 : Extended Mohr-Coulomb failure envelope
(after Fredlund, Morgenstern and Widger, 1978)

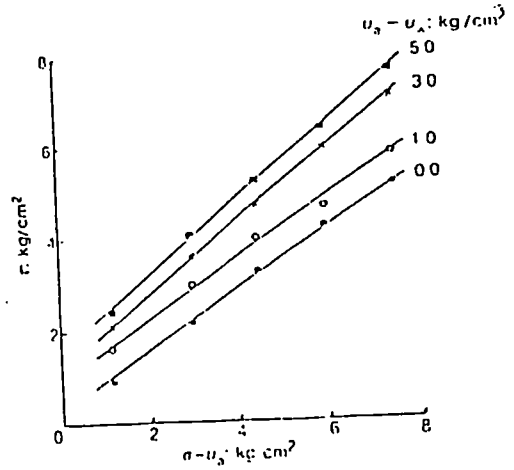

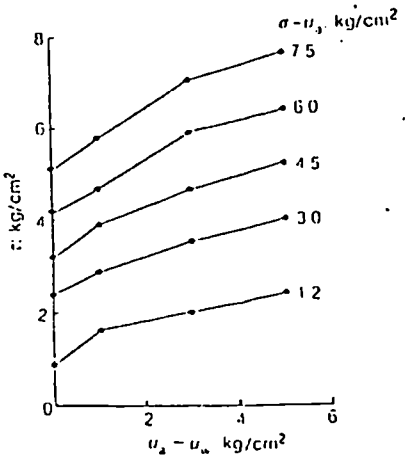

(i) τ versus net stress (ii) τ versus suction

(a) Test results for Guadalix red clay

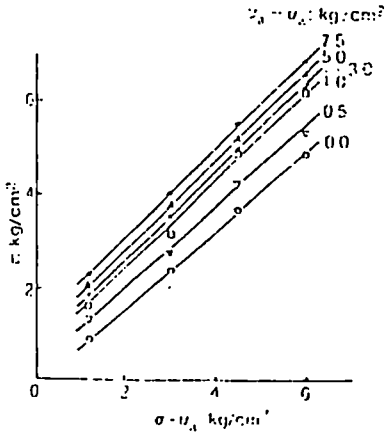

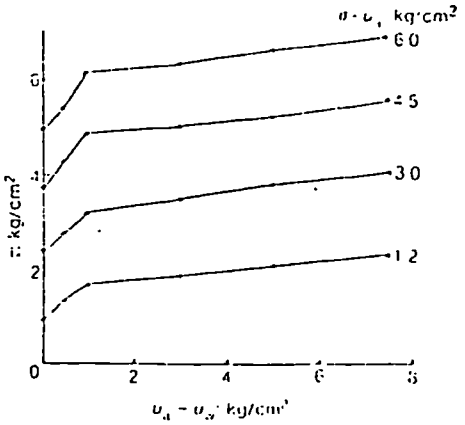

(i) τ versus net stress (ii)τ versus suction

(b) Test results for Madrid clayey sand

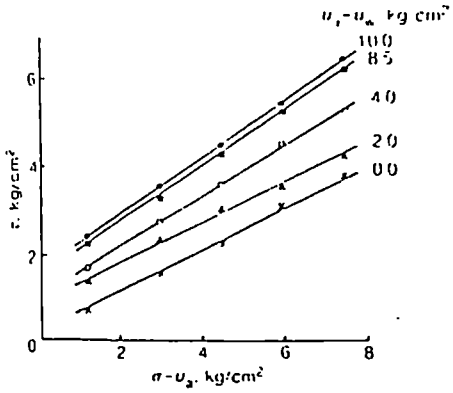

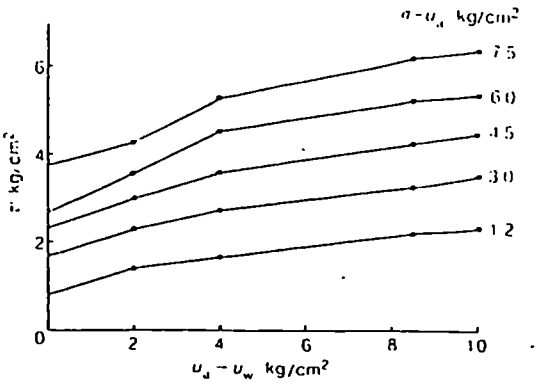

(i) τ versus net stress (ii)τ versus suction

(c) Test results for Madrid grey clay

Fig. 2.15 : Direct shear test results of Escario and Saez (1986)

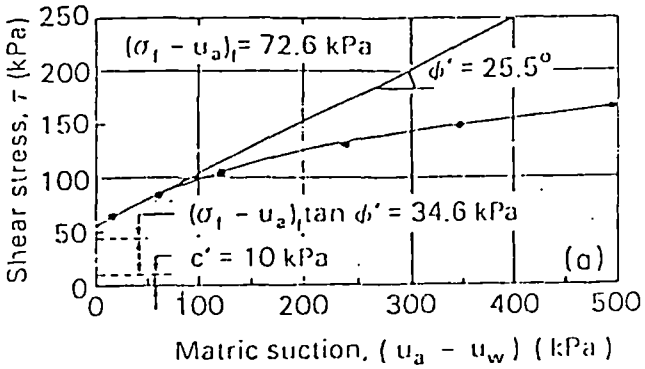

Fig. 2.16 : Non-linearity of failure envelope for unsaturated glacial till
(Fredlund, Rahardjo and Gan, 1987)

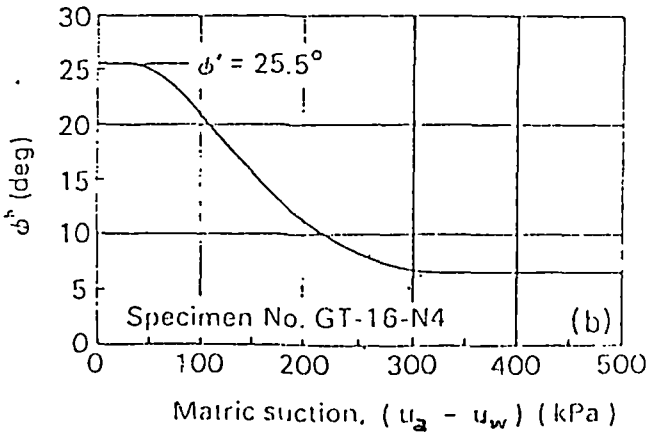

Fig. 2.17 : Variation of ϕ^b with suction for unsaturated glacial till
(Gan, Fredlund and Rahardjo, 1988)

(a)

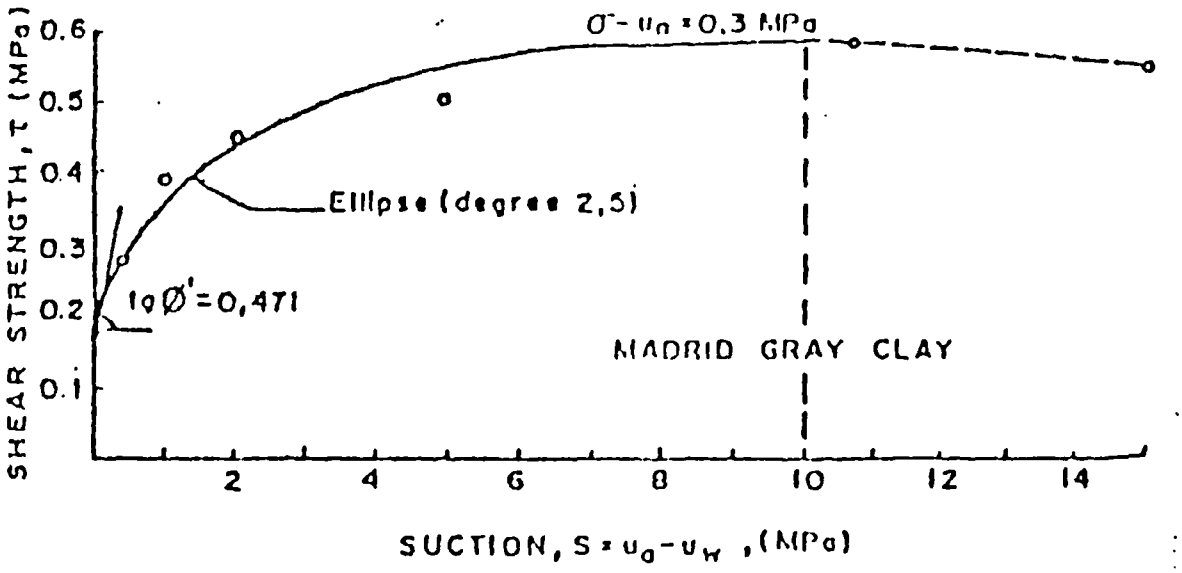

Variation of shear strength with suction for different values of vertical stress (direct shear tests)

(b)

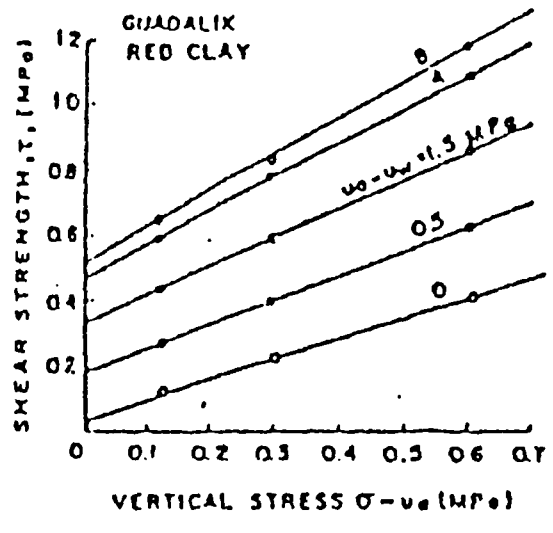

(c)

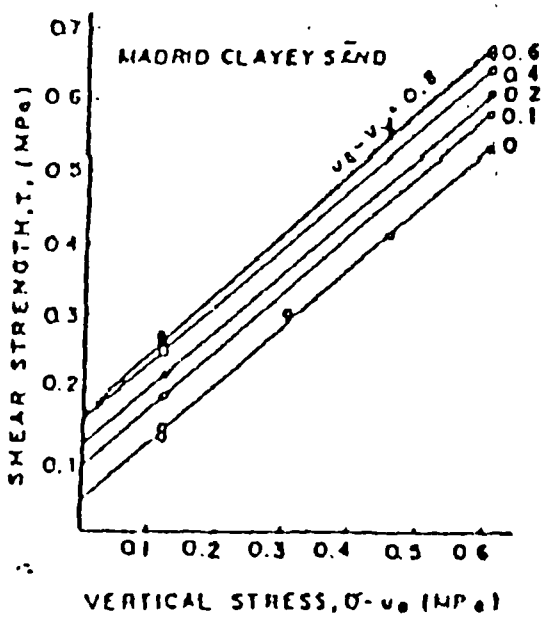

Variation of shear strength with vertical stress for different values of suction (direct shear tests)

Fig. 2.18 : Direct shear test results of Escario and Juca (1989)

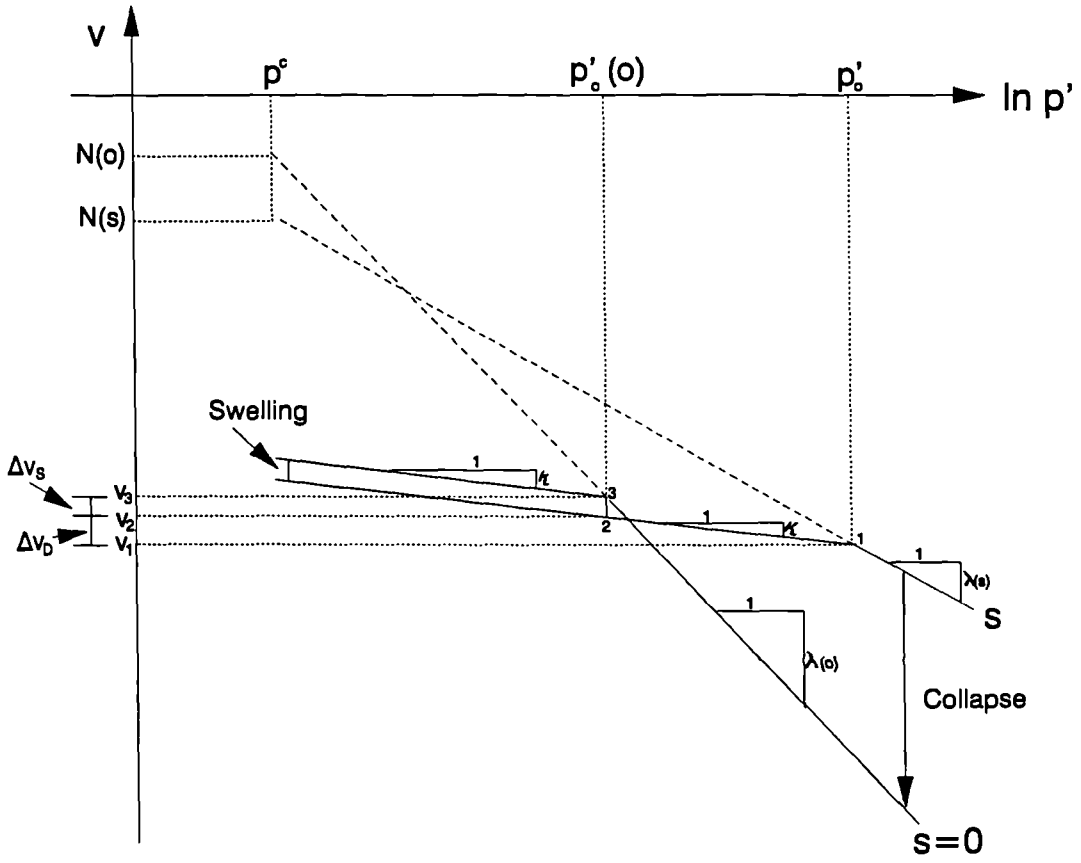

(a) compression curves for saturated and unsaturated soil

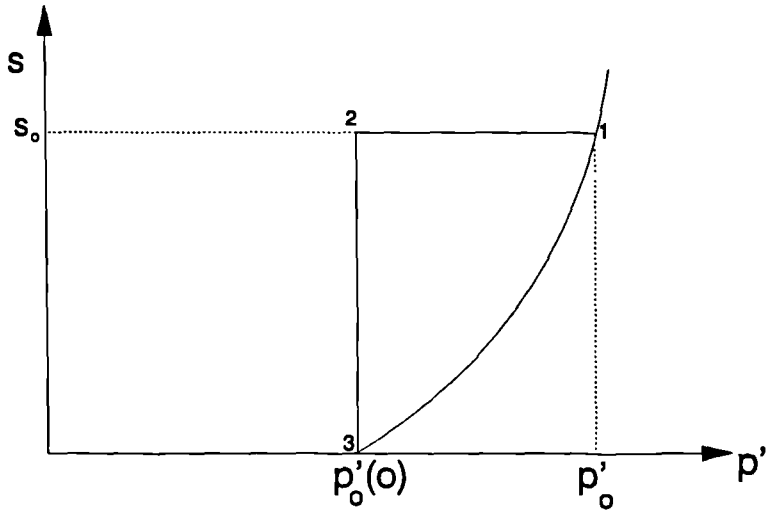

(b) stress paths and yield curve in s:p' plane

Fig. 2.19 : Isotropic normal compression lines and Loading-Collapse yield curve in constitutive model of Alonso, Gens and Josa (1990)

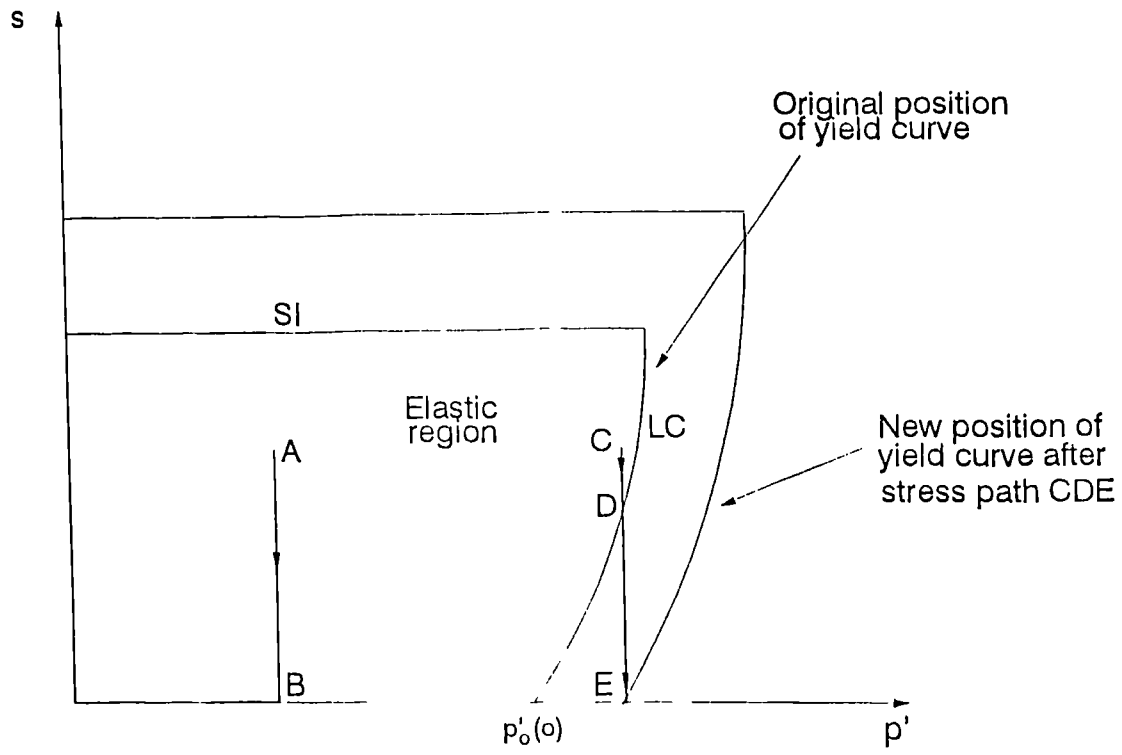

Fig. 2.20 : Yield curves for unsaturated soil under isotropic stress states (Alonso, Gens and Hight, 1987)

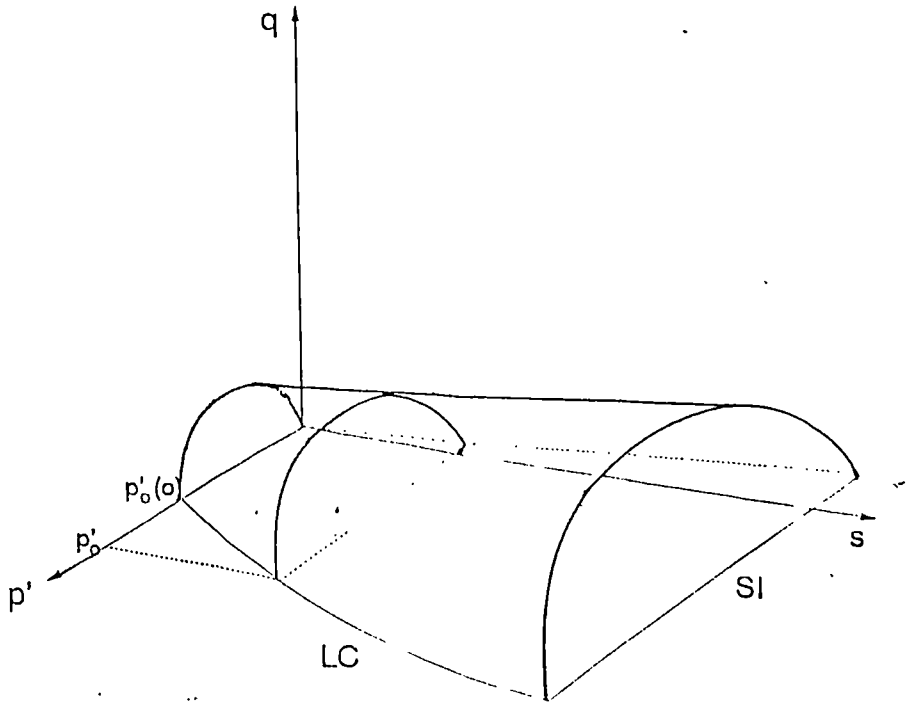

Fig. 2.21 : LC and SI yield surfaces for unsaturated soil in p' :q : s space (Alonso, Gens and Josa, 1990)

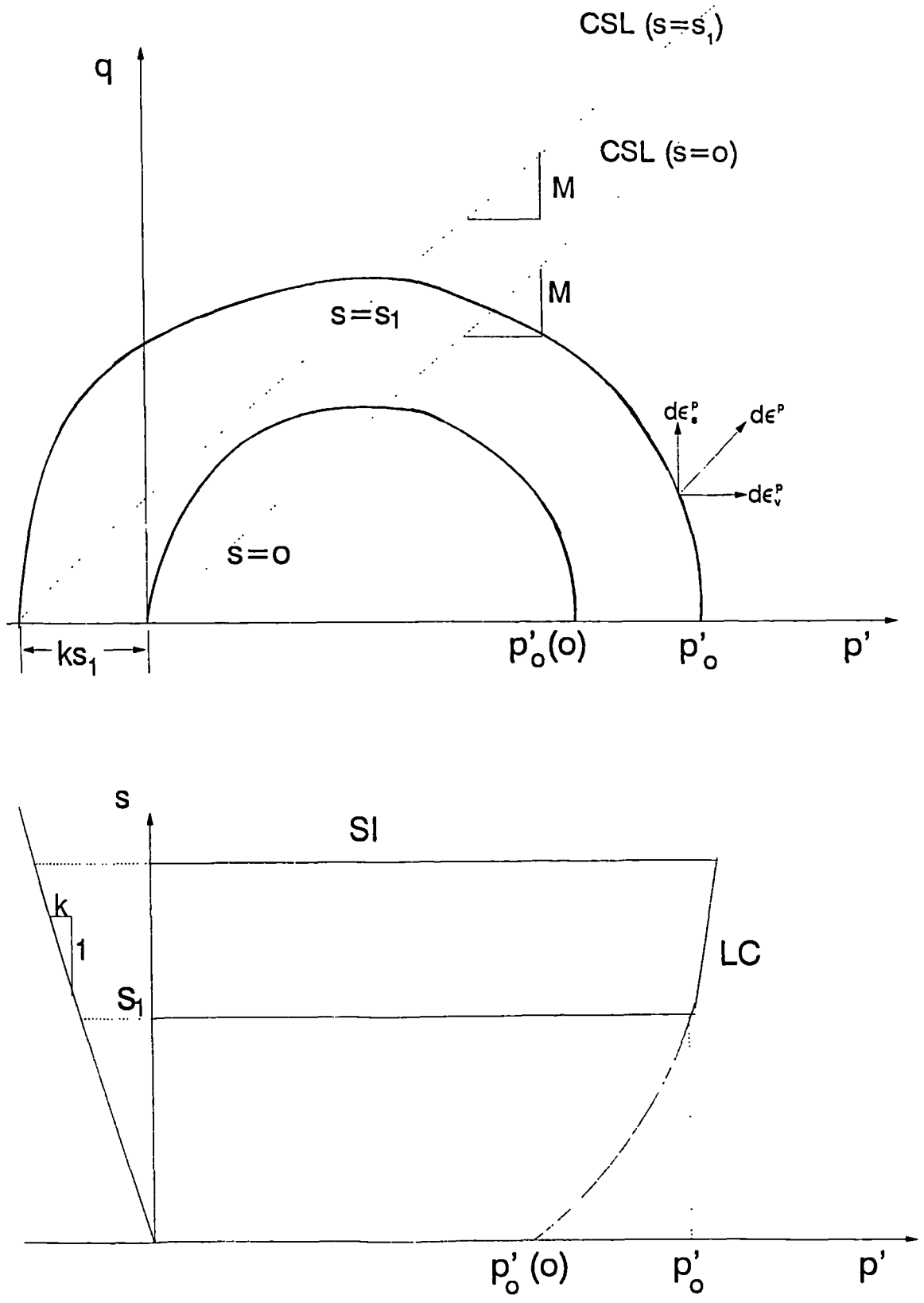

Fig. 2.22 : Cross-section of LC yield surface for unsaturated soil in p':q:s space (Alonso, Gens and Josa, 1990)

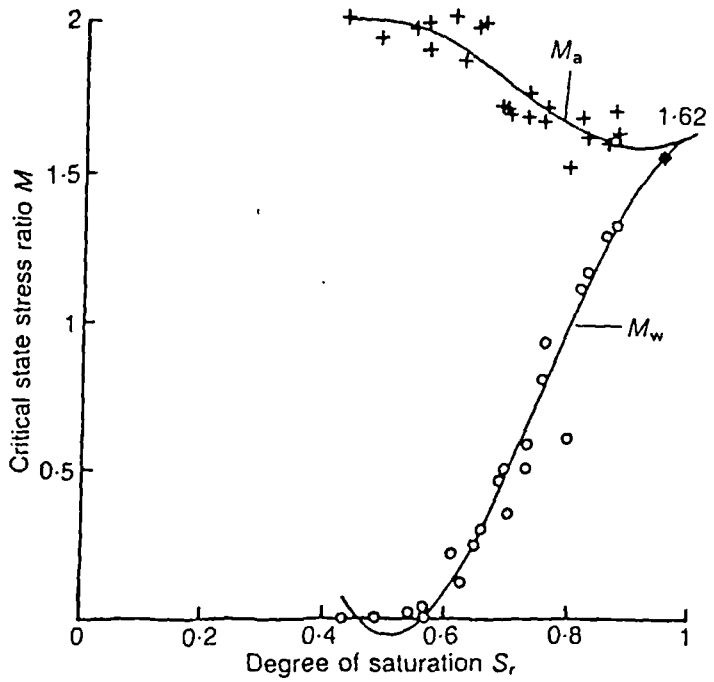

(a) stress ratios

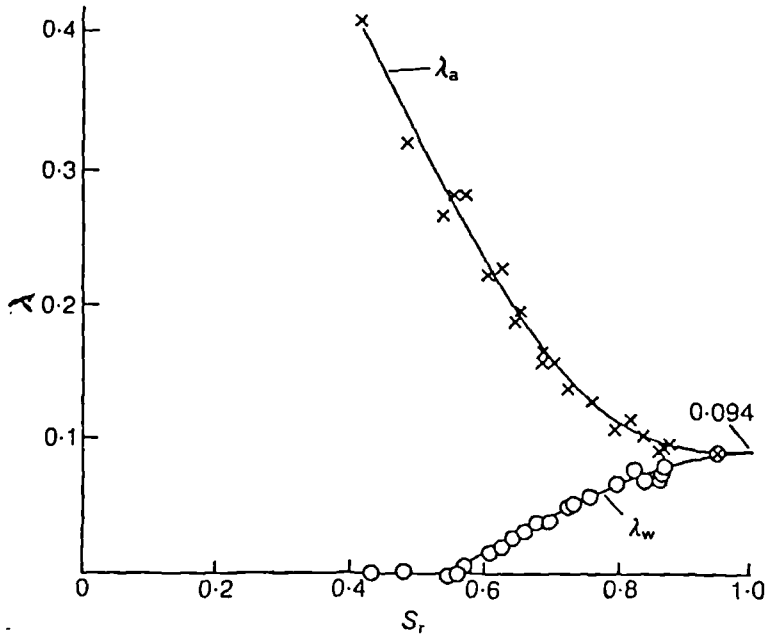

(b) compression indices

Fig. 2.23 : Variation of Toll's critical state parameters with degree of saturation for Kiunyu gravel (Toll, 1990)

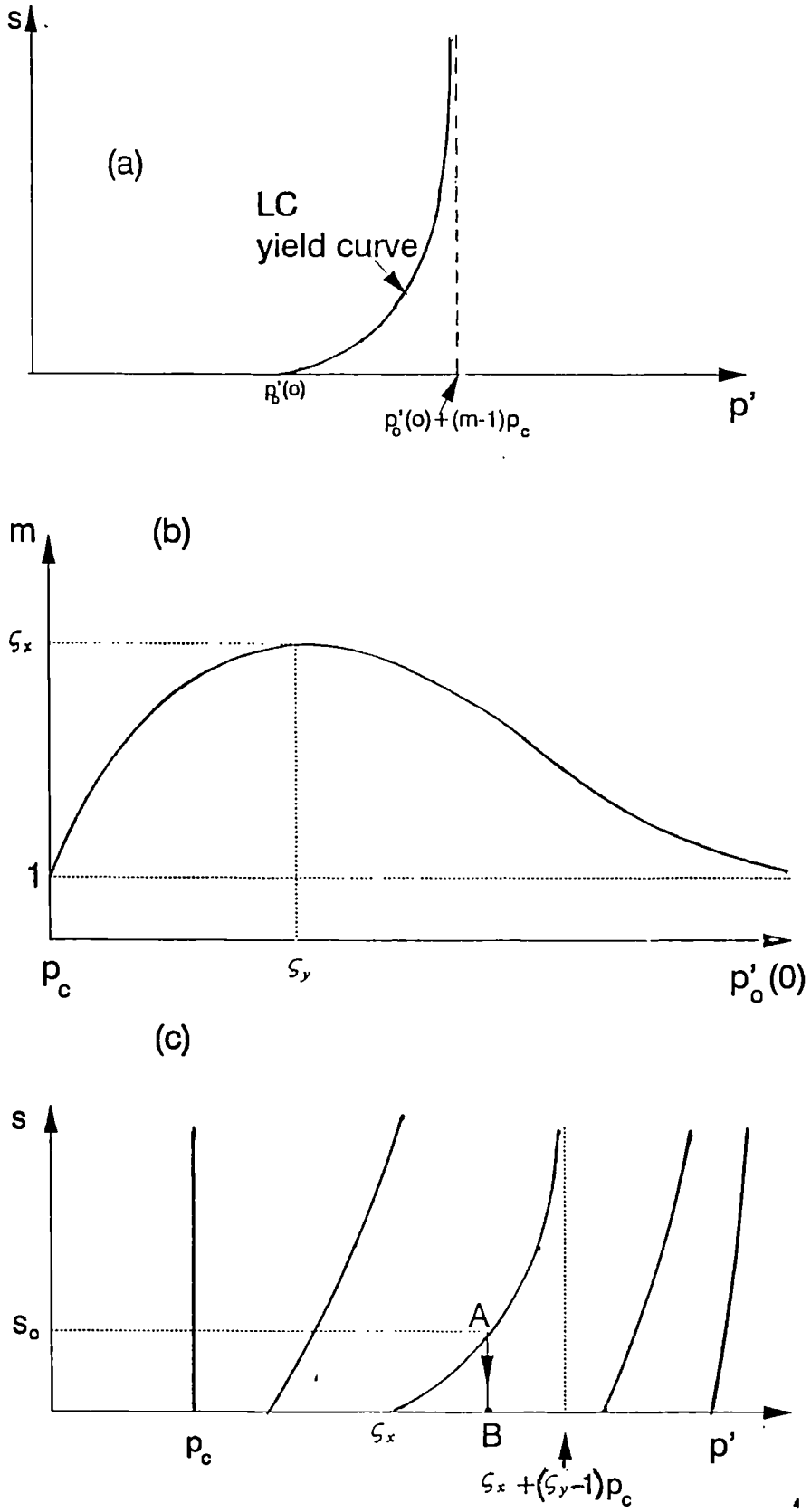

Fig. 2.24 : LC yield curve in the s : p' plane for unsaturated soil exhibiting a maximum of collapse (Josa, Balmaceda, Gens and Alonso, 1992)

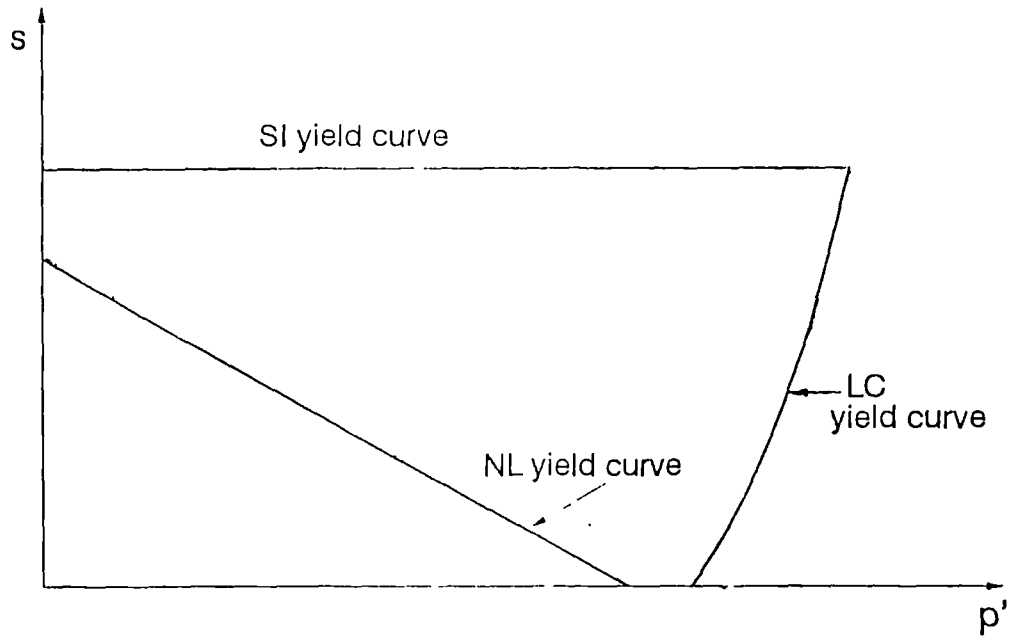

Fig. 2.25 : Additional Neutral Line (NL) yield curve in model of Gens and Alonso (1992) for highly expansive soils

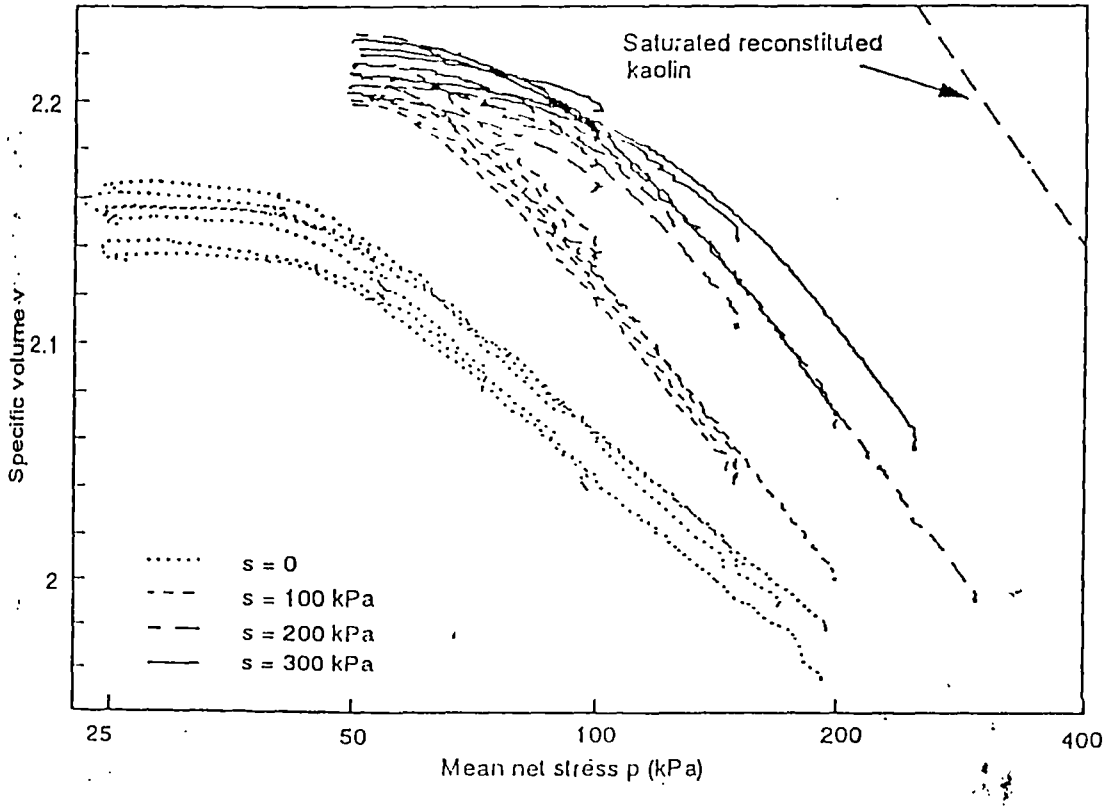

Fig. 2.26 : Variation of specific volume during ramped consolidation of compacted speswhite kaolin at various values of suction (Wheeler and Sivakumar, 1995)

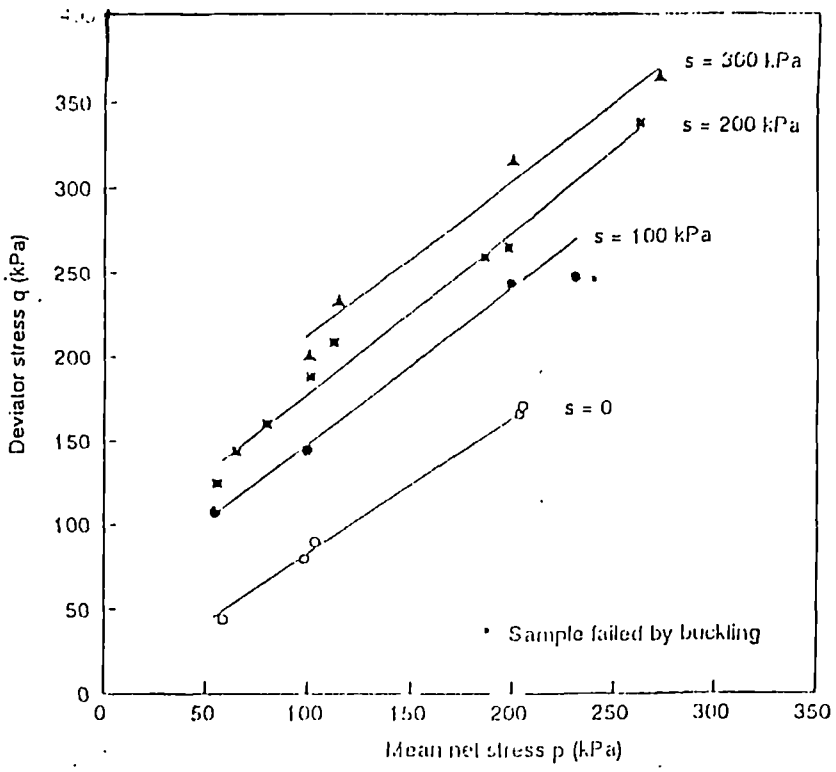

Fig. 2.27 : Deviator stress versus mean net stress at critical states for compacted speswhite kaolin (Wheeler and Sivakumar, 1995)

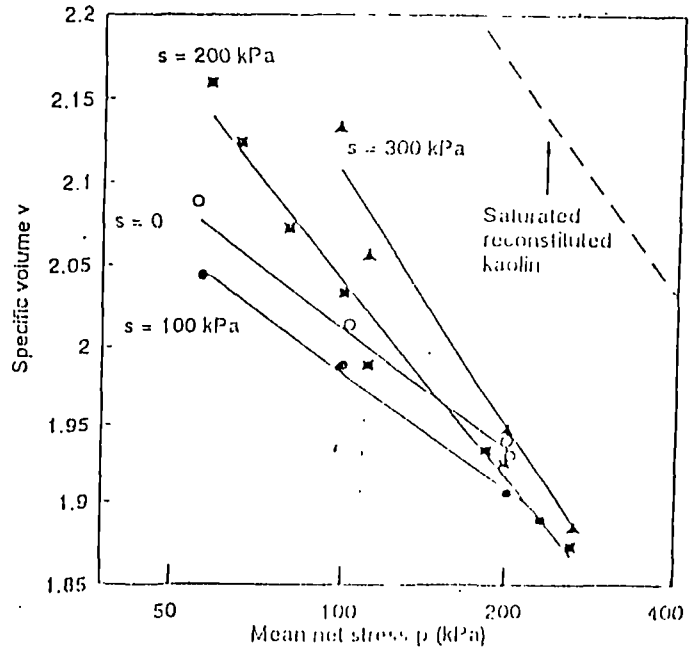

Fig. 2.28 : Specific volume versus mean net stress at critical states for compacted speswhite kaolin (Wheeler and Sivakùmar, 1995)

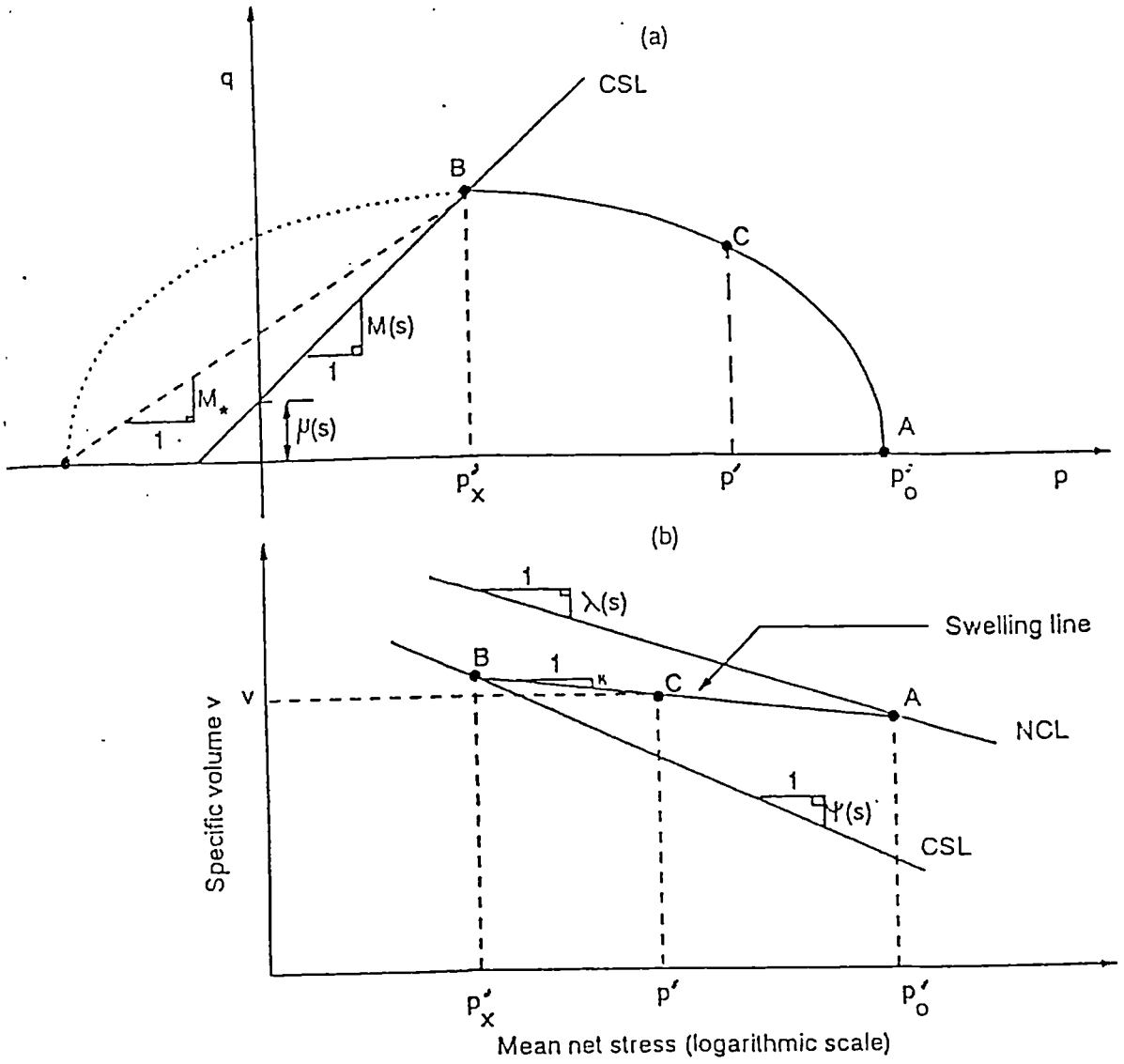

Fig. 2.29 : Constant suction yield curve
(Wheeler and Sivakumar, 1995)

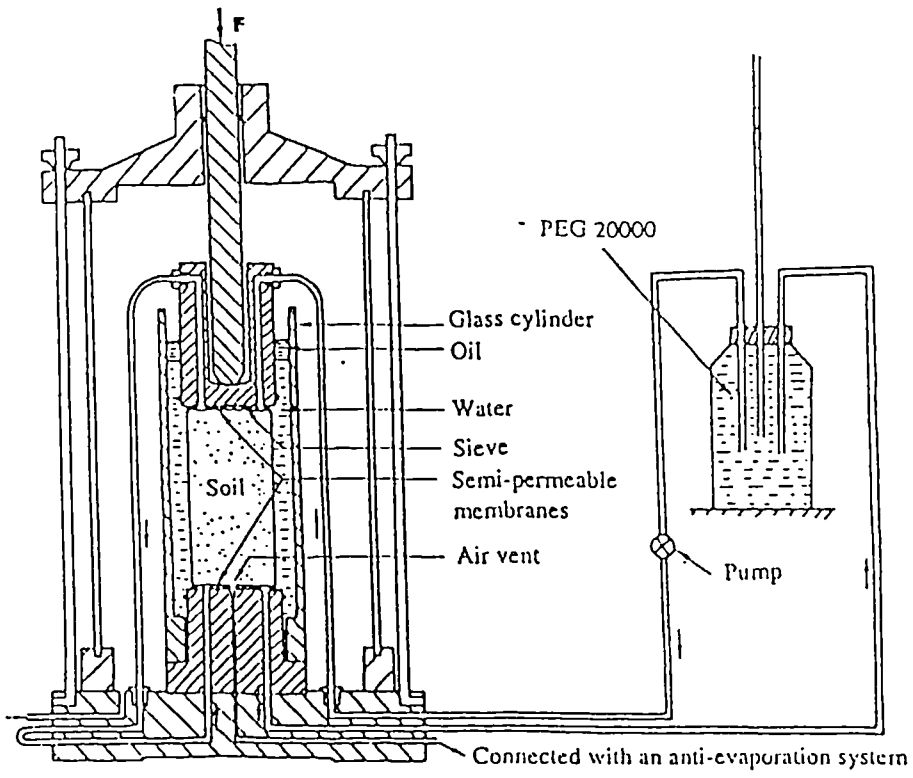

Fig. 2.30 : The osmotic triaxial apparatus for suction-controlled testing of unsaturated soil (Delage, Suraj de Silva and Laure, 1987)

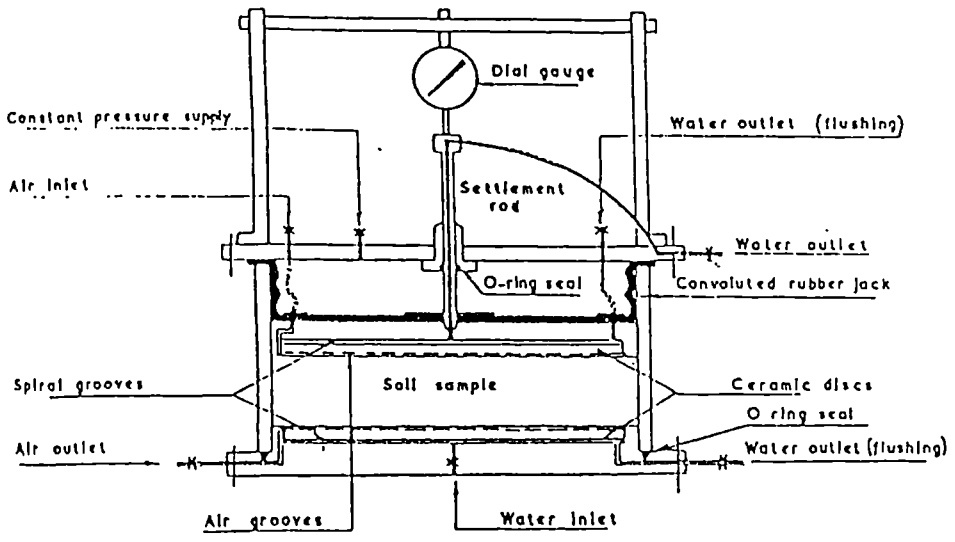

Fig. 2.31 : Modified Rowe cell for suction-controlled testing of unsaturated soil (Barden, Madedor and Sides, 1969)

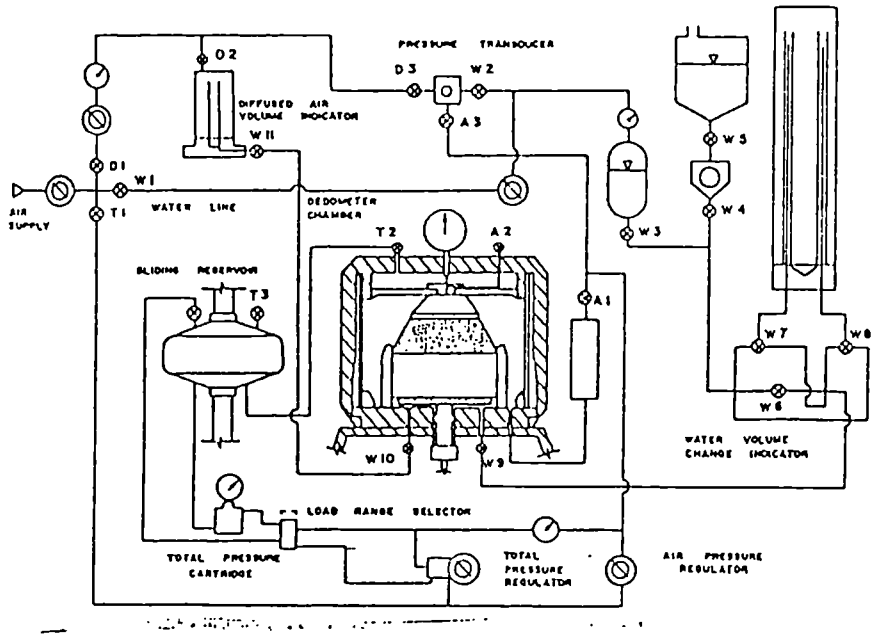

Fig. 2.32 : Modified Anteus oedometer for testing unsaturated soil under controlled suction (Fredlund and Morgenstern, 1977)

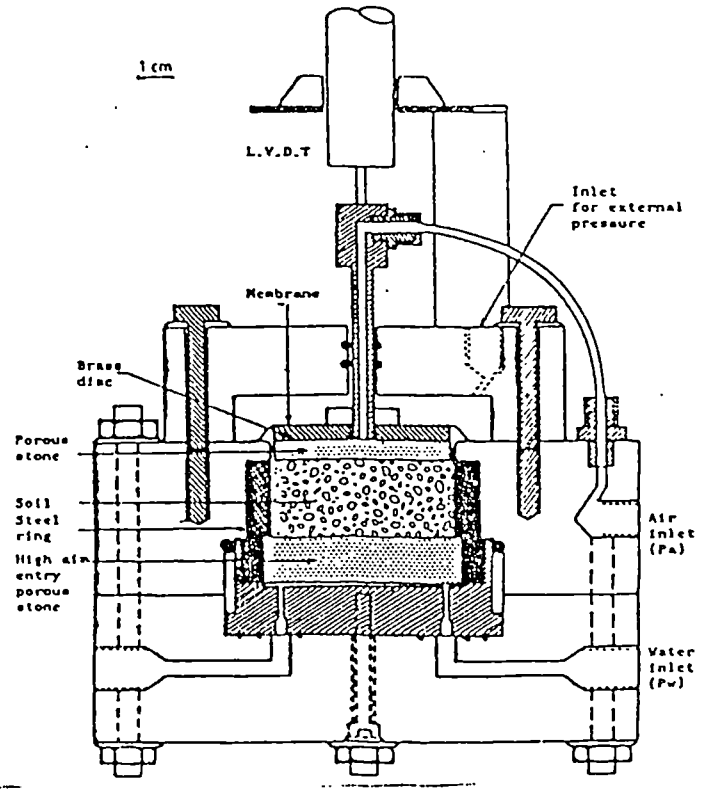

Fig. 2.33 : Oedometer apparatus for testing unsaturated soil under controlled suction (Lloret and Alonso, 1985)

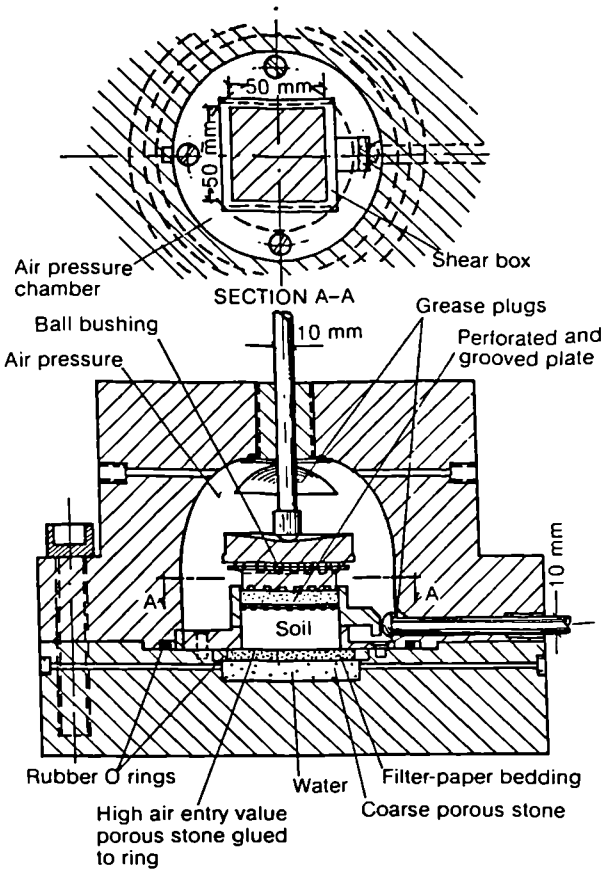

Fig. 2.34 : Direct shear test apparatus with controlled suction (Escario and Saez, 1986)

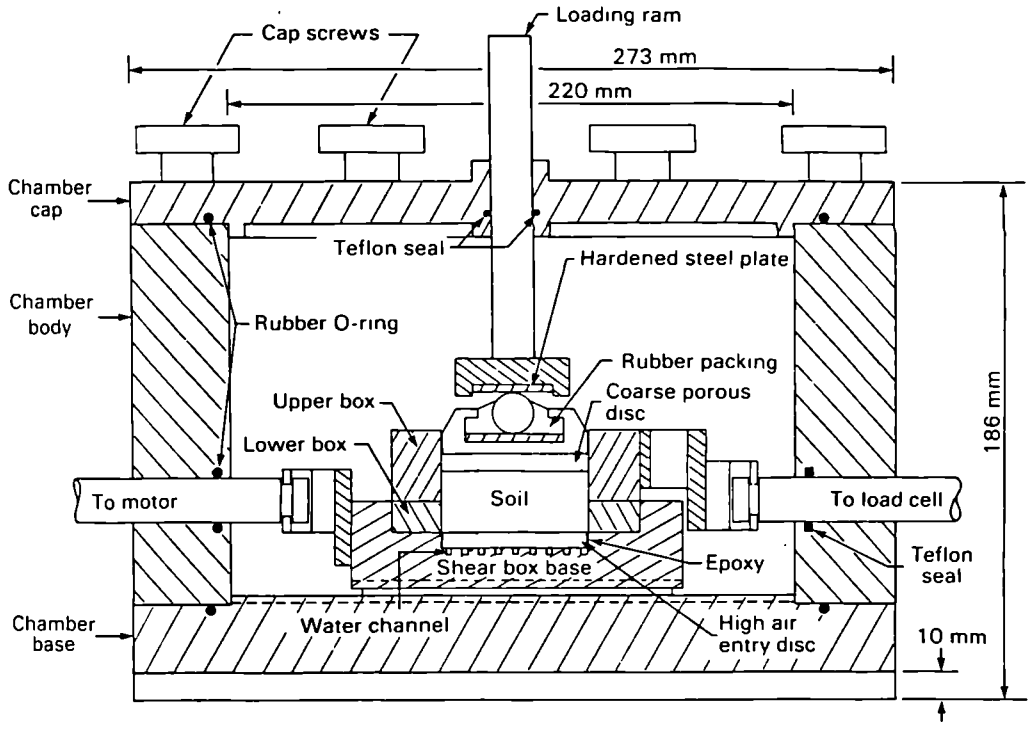

Fig. 2.35 : Modified direct shear apparatus for testing unsaturated soil (Gan, Fredlund and Rahardjo, 1988)

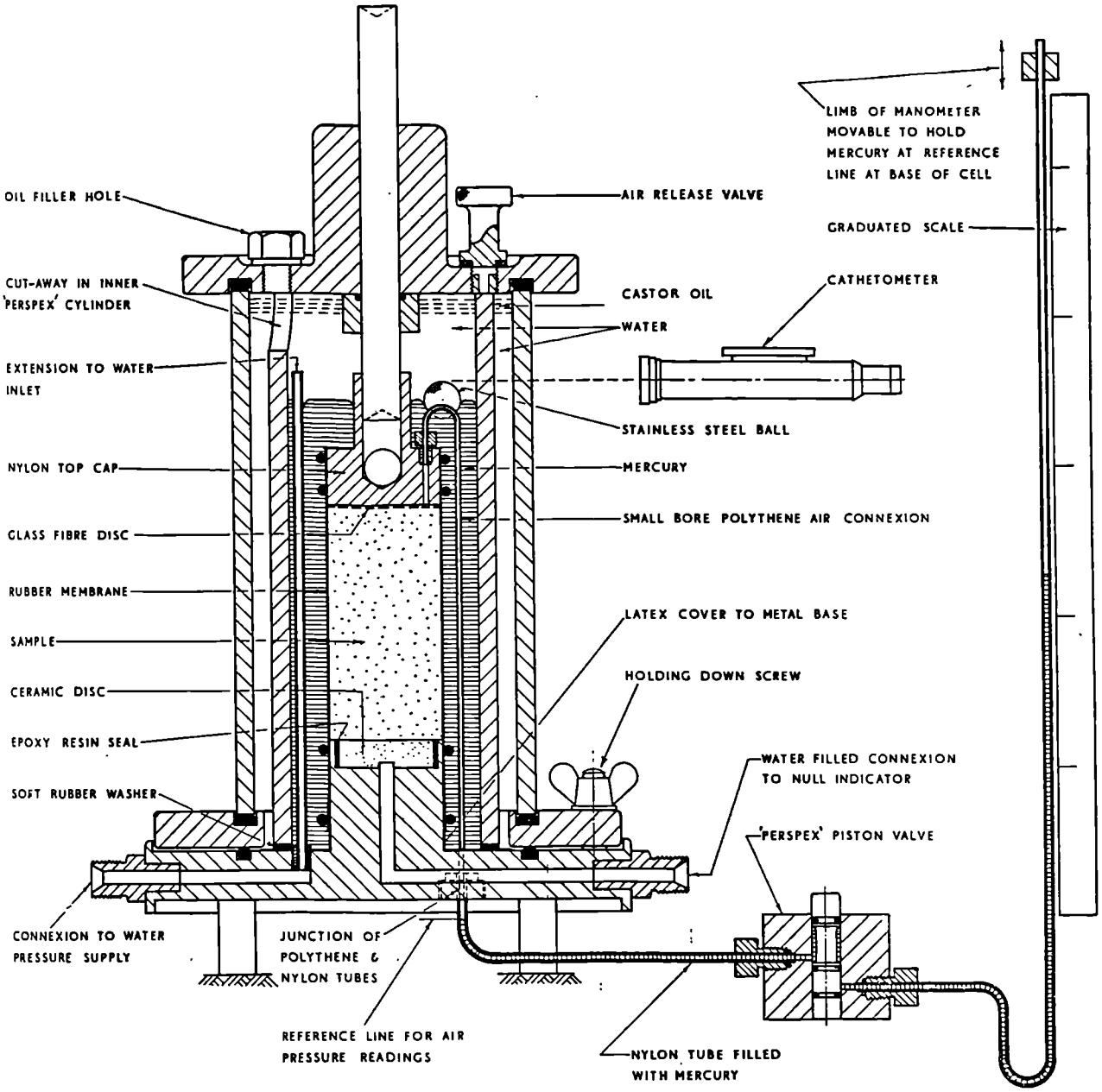

Fig. 2.36 : Double-walled triaxial cell for testing unsaturated soil (Bishop and Donald, 1961)

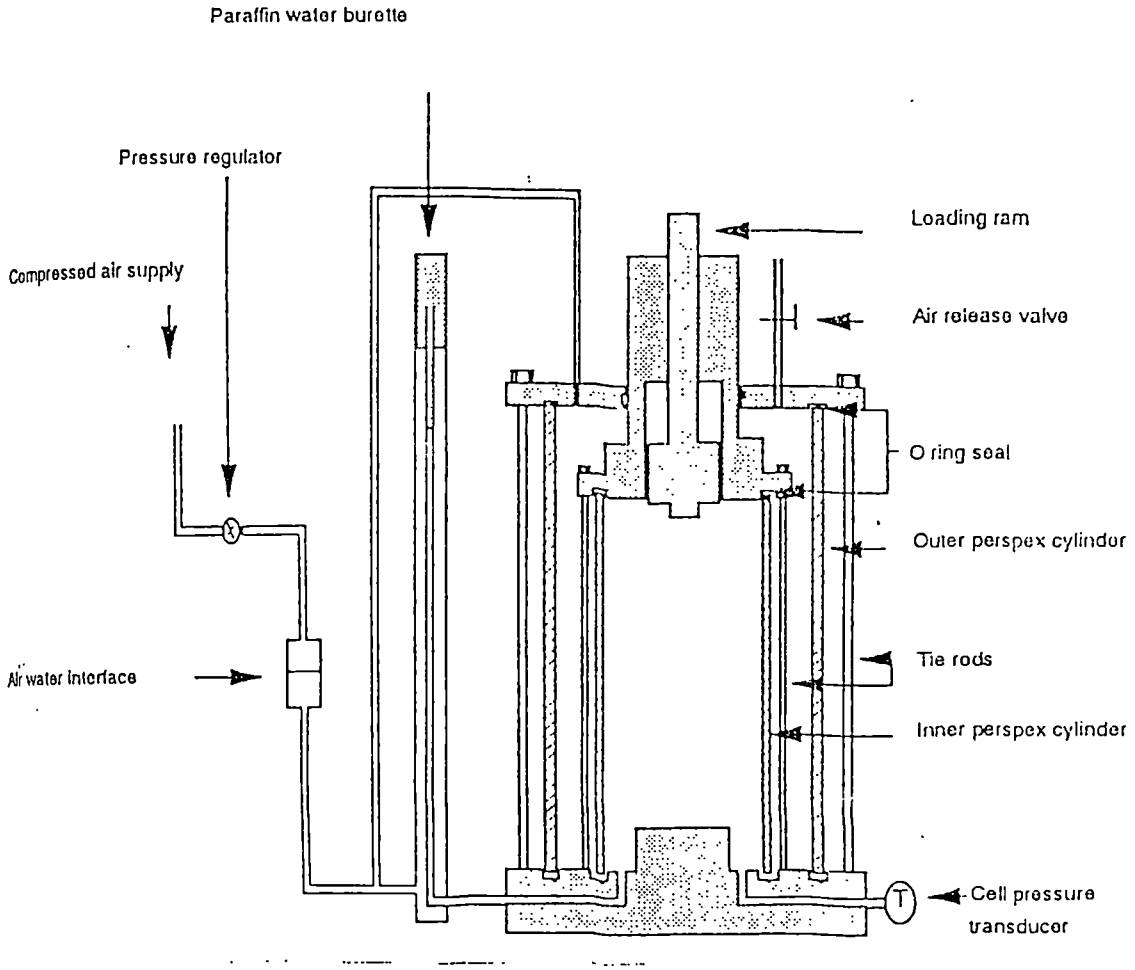

Fig. 2.37 : Double-walled triaxial cell for measuring sample volume change (Wheeler, 1988b)

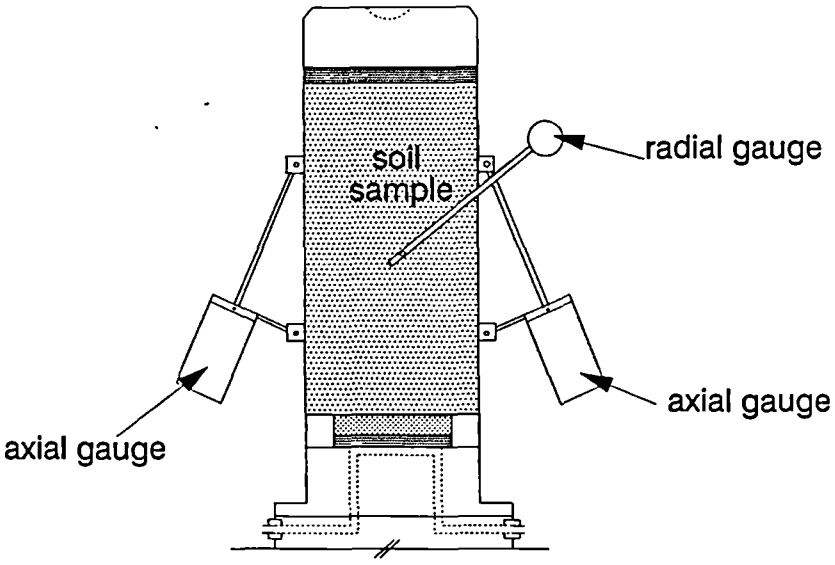

Elevation

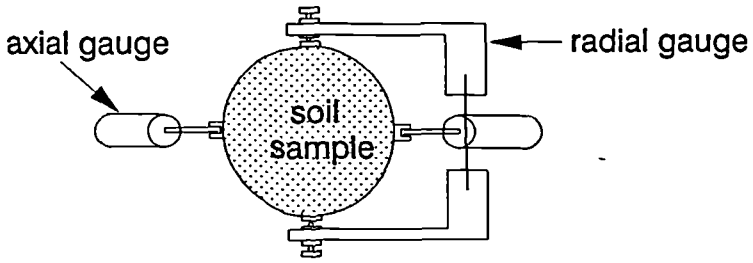

Plan

Fig. 2.38 : Local strain gauges for measuring sample volume change of unsaturated soil

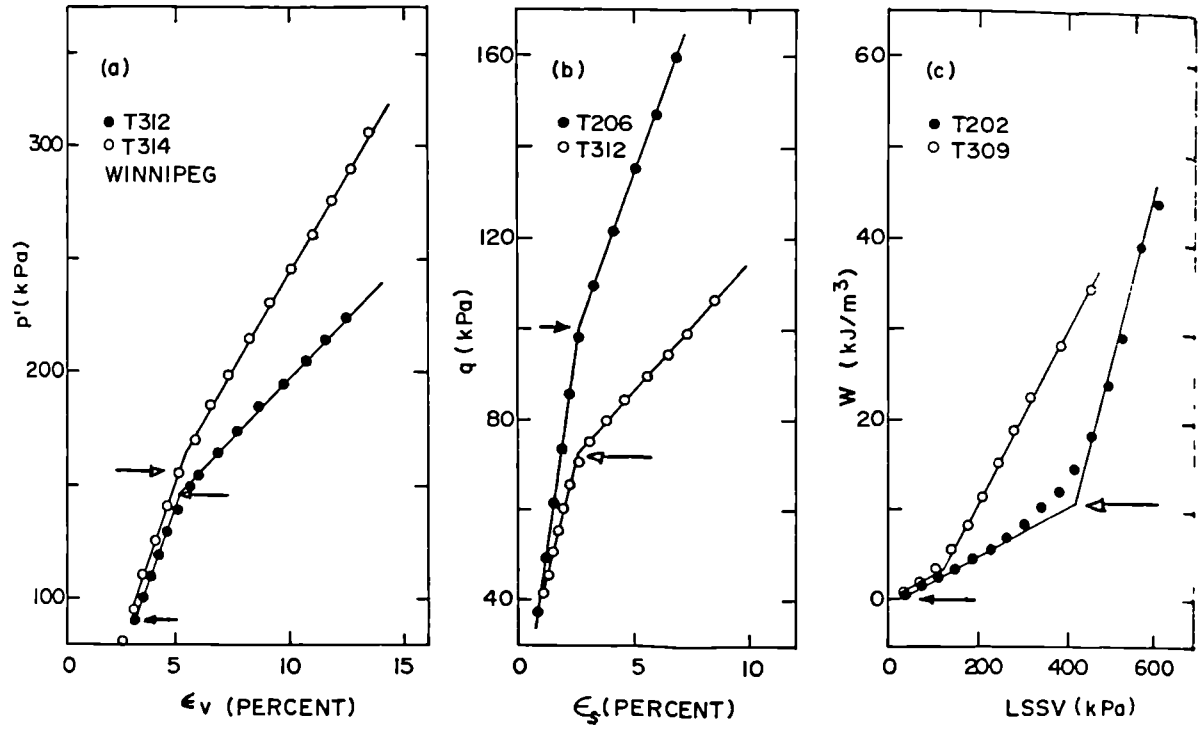

Yielding and bilinear behaviour in plots of (*a*) mean effective pressure p' vs. volume strain ε_v, (*b*) deviator stress q vs. shear strain ε_s, and (*c*) absorbed energy/unit volume vs. length of stress vector.

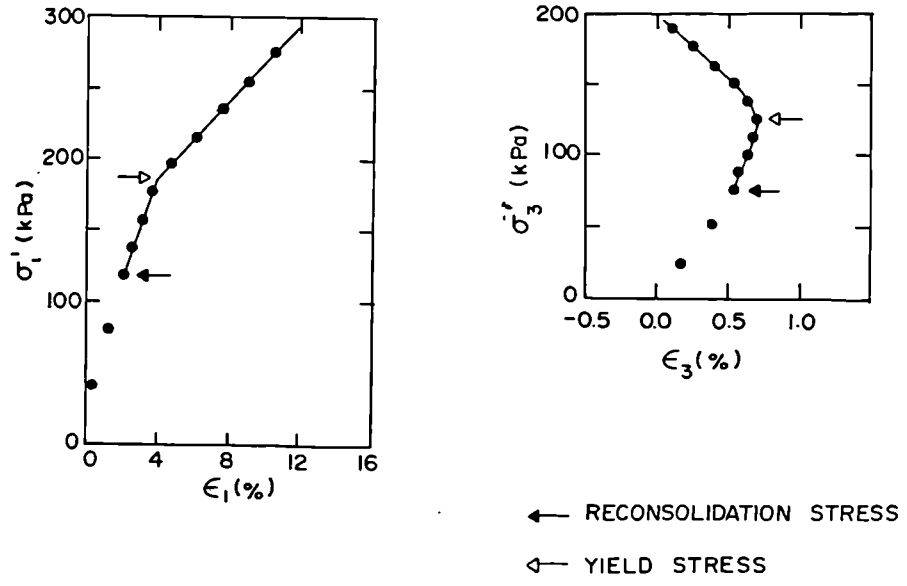

Fig. 2.39 : Techniques for evaluating yield points
(Graham, Noonan and Lew, 1983)

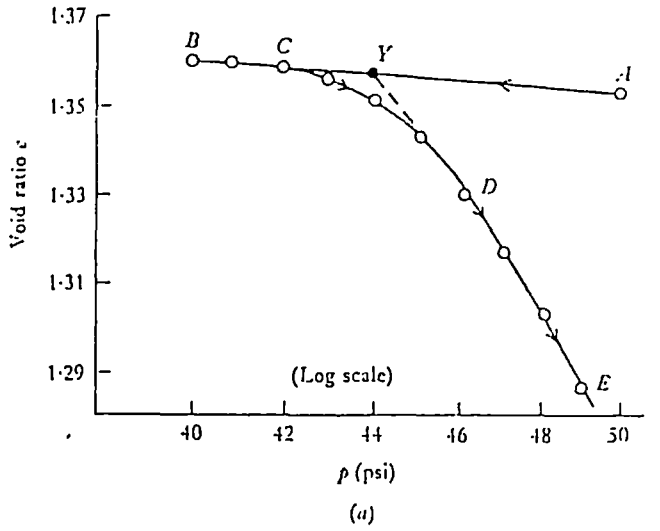

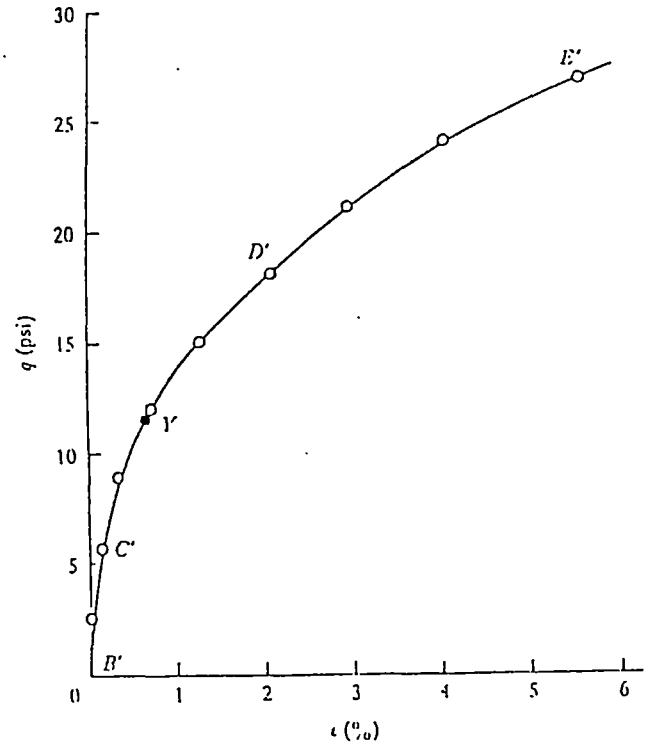

Y is the volumetric yield point.

Fig. 2.40 : Identification of yield points from tests on saturated kaolin (Roscoe and Burland, 1968)

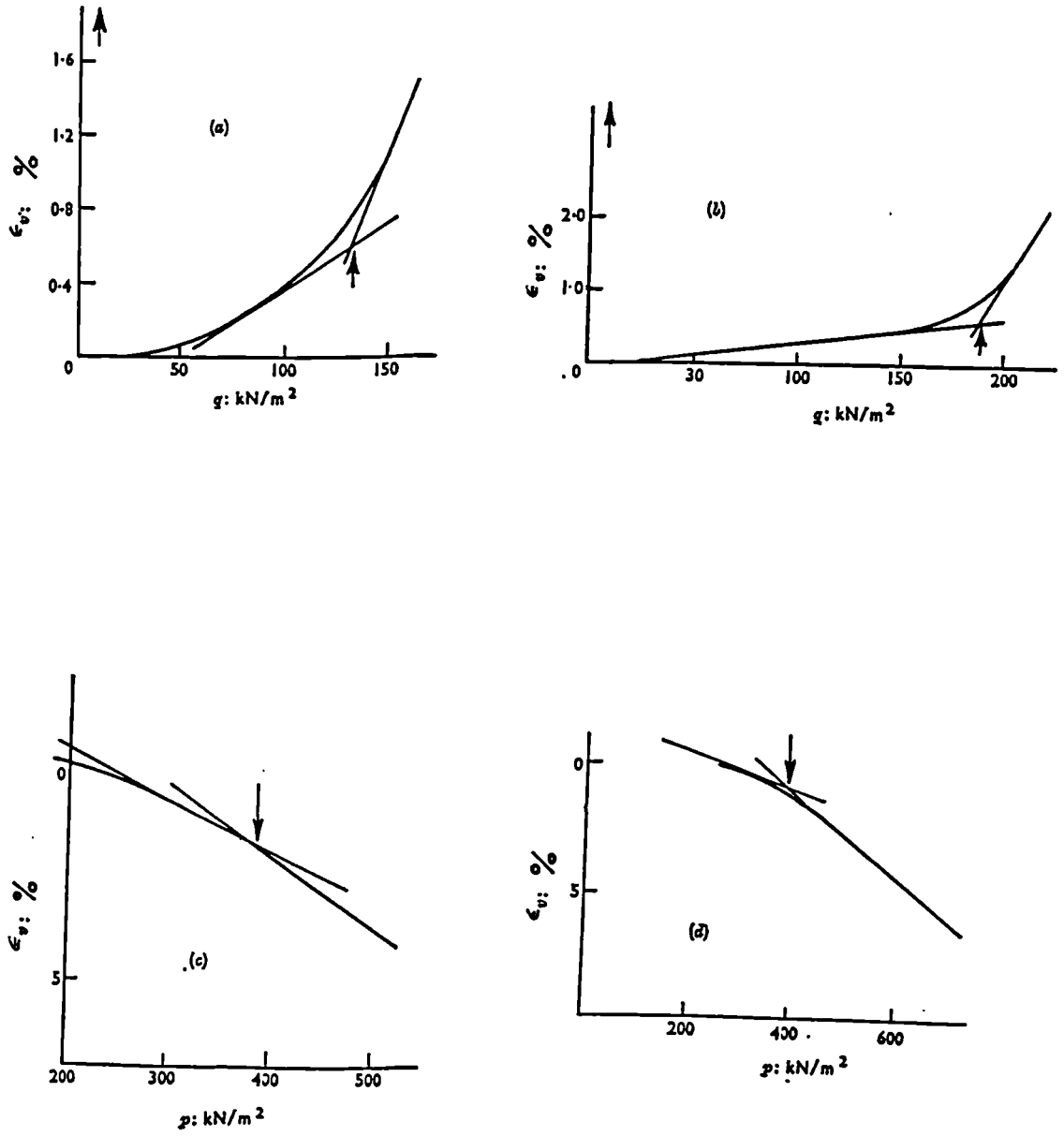

Fig. 2.41 : Determination of yield points from tests on lightly overconsolidated saturated kaolin (Parry and Nadarajah, 1973)

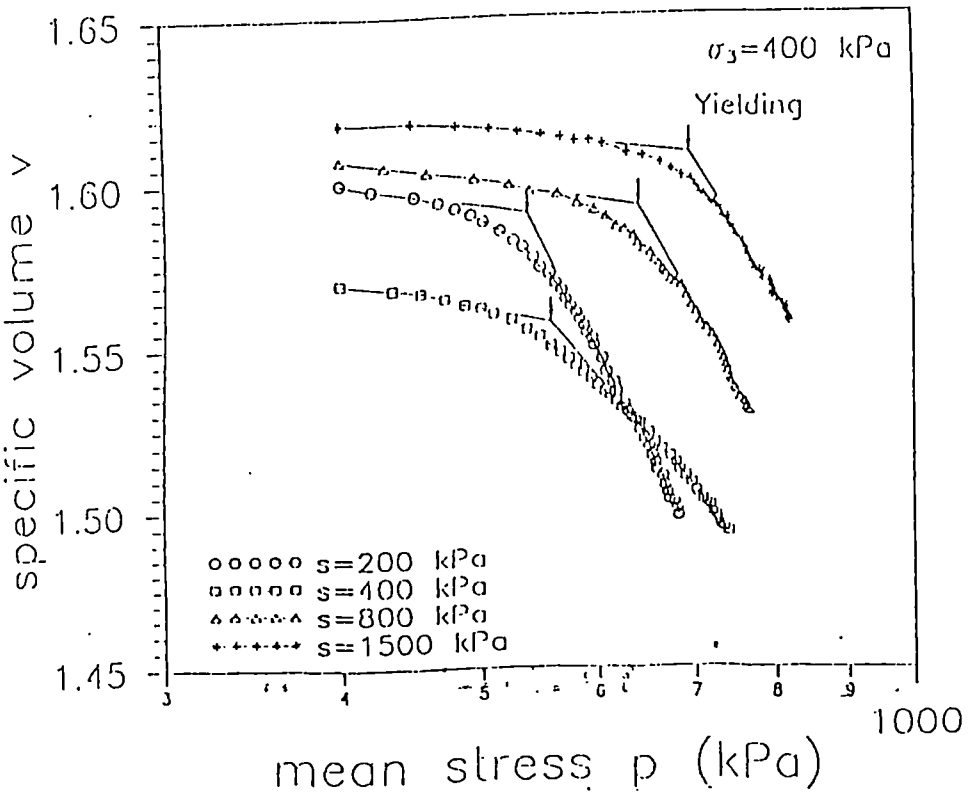

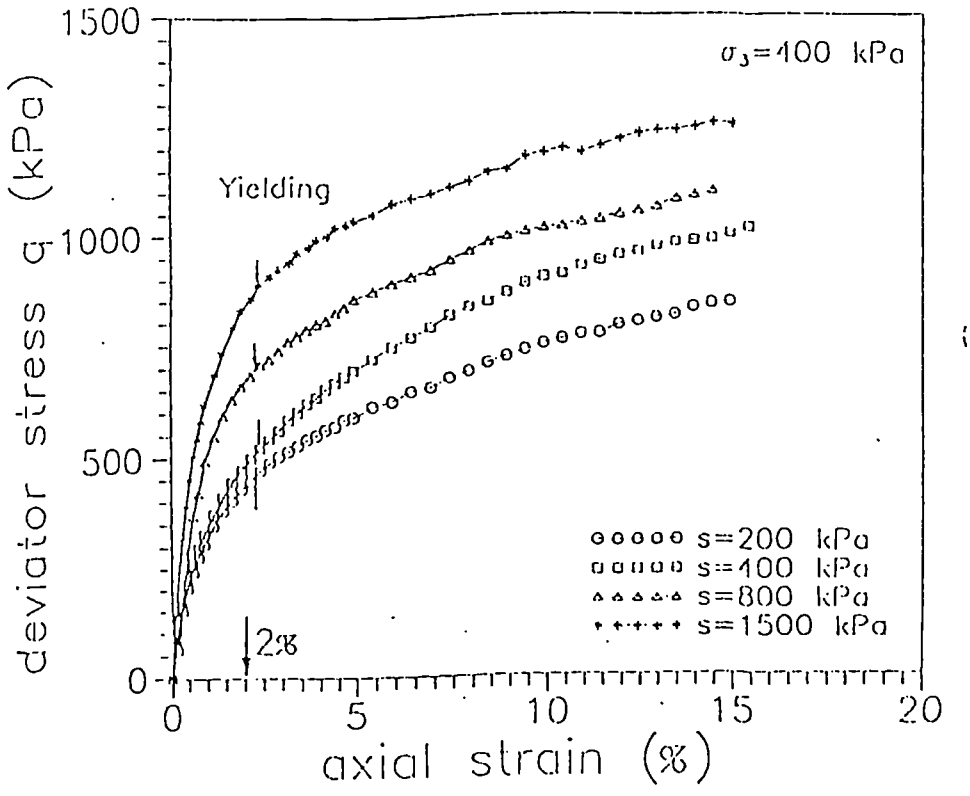

Fig. 2.42 : Identification of yield points from tests on compacted Jossigny silt (Cui and Delage, 1992)

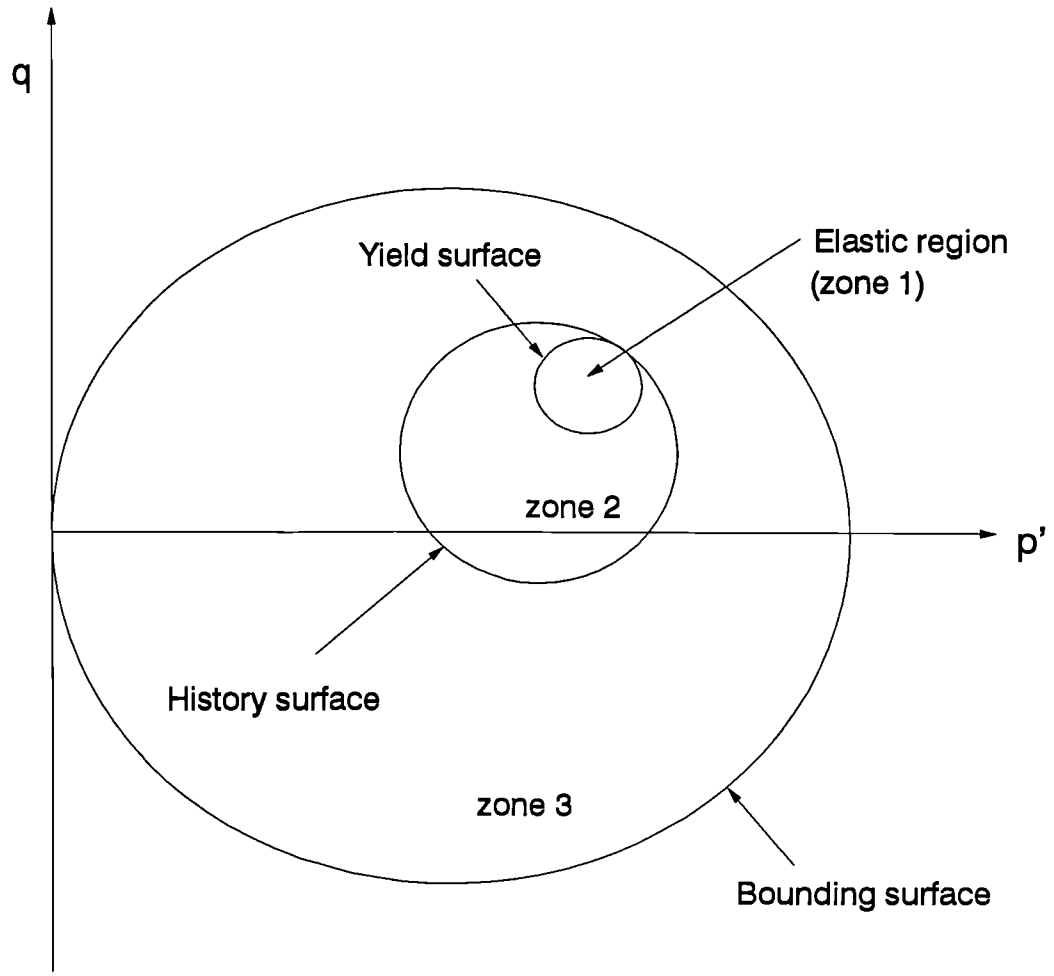

Fig. 2.43 : Three surface kinematic yield model
(Stallebrass, 1990)

s (kPa)	$\lambda(s)$	N(s)	M(s)	$\mu(s)$ (kPa)	$\psi(s)$	$\Gamma(s)$
0	0.128	2.052	0.813	0.0	0.110	2.011
100	0.182	2.122	0.933	54.2	0.108	1.984
200	0.196	2.196	0.959	83.5	0.181	2.042
300	0.176	2.212	0.910	122.0	0.223	2.105

Table 2.1 : Values of critical state soil parameters for compacted speswhite kaolin (*Wheeler and Sivakumar*, 1995)

CHAPTER 3

RESEARCH OBJECTIVES AND METHODOLOGY

3.1 Research objectives

Investigation of the literature review revealed that the shape of the yield surface in $q{:}p'{:}s$ space had not been well defined experimentally. Although *Wheeler and Sivakumar* (1995) showed that tests paths observed during the shear tests of *Sivakumar* (1993) were reasonably consistent with the suggestion that constant suction cross-sections of the yield surface were elliptical in shape, there had been no direct investigation of the shape of the yield surface.

In addition, the tests of *Sivakumar* (1993) provided little information on the elastic behaviour when the soil state was inside the yield surface, because no unloading stages were included in the tests and because all samples were sheared from virgin (normally compressed) states.

The form of the flow rule governing plastic behaviour was also rather uncertain. *Wheeler and Sivakumar* (1995) assumed an associated flow rule to predict the stress-strain behaviour in the tests of *Sivakumar* (1993), whereas *Alonso, Gens and Josa* (1990) selected a non-associated flow rule. In neither case however was there any direct evidence of the appropriate form for the flow rule.

Finally, the variation of water content w was not included within the elasto-plastic models of *Alonso, Gens and Josa* (1990) or *Wheeler and Sivakumar* (1995), partly because there was little high quality data available to develop this aspect of the models.

The overall aim of the project was therefore to conduct experimental research that would fill in some of these gaps in existing knowledge, thus enabling a fuller development of the elasto-plastic critical state framework for unsaturated soils.

Specific objectives of the research project were as follows:

1). To investigate the shape of the yield surface in q:p':s space by examining selected constant suction cross-sections of the surface. A particular interest was to examine whether an assumption of elliptical constant suction yield curves was reasonable.

2). To investigate the "elastic" behaviour of the soil inside the state boundary. Three particular areas of interest were :

a) the value of the swelling index κ and whether it varied with suction (this required unloading stages (reduction of p') within the test programme)

b) the value of the swelling index κ_s and whether it varied with p' (this required test stages in which the suction s was increased or decreased)

c) the value of the elastic shear modulus G and whether it varied with s and p' (this required test stages in which the soil was sheared starting from stress states inside yield surface).

κ, κ_s and G might also vary with the position of yield surface (as defined by $p_o'(o)$, see Section 2.6.1.1)), but this would not be examined in the project.

3). To define an appropriate form for the flow rule. By determining the plastic strain increments $d\varepsilon_v^p$ and $d\varepsilon_s^p$ occurring after yielding it would be possible to establish whether the flow rule was associated or non-associated.

4). To incorporate the variation of water content within the elasto-plastic framework for unsaturated soil. This required high quality data of the variation of water content under a variety of different loading and unloading conditions (including variation of p', s and q).

3.2 Research methodology

In order to achieve the objectives listed above, a programme of triaxial tests on unsaturated compacted speswhite kaolin was planned. All samples were compacted at the same water content and with the same compactive effort, to ensure that the intial soil fabric was identical in every case (*Sivakumar*, 1993). The position of the yield surface was, however, then set by controlled-suction consolidation, rather than by the original compaction process. It was thought that this would result in improved repeatability of the position of the yield surface and a better definition of the stress history. It was therefore decided that all samples would be initially consolidated to a virgin state at a mean net stress p' of 400 kPa and a suction s of 100 kPa, in order to set the position of the yield surface, prior to subsequent unloading.

The shape of the yield surface was examined by investigating three constant suction cross-sections, at s = 0, 100 and 200 kPa as shown in Fig. 3.1. Several tests, with different stress paths, were to be conducted at each value of suction.

Each sample was subjected to various test stages. Fig. 3.2 shows schematic representations of the test stages as dictated by the research objectives.

(a) The first stage was undrained application of net stress (see AB in Fig. 3.2 (a), (b) and (c)). This stage took place virtually instantaneously, with the undrained increase of p' generating an unknown increase of pore water pressure and hence a decrease of suction.

(b) The next stage in each test was an equalization (wetting) stage (see BC in Fig. 3.2 (a), (b) and (c)). In this stage the suction was reduced from its initial high value at B (set by the compaction process and subsequent undrained loading AB) to a value of 100 kPa, resulting in a flow of water into the sample. This took place at constant p', with a variety of different values of p' used in the different tests.

(c) The third stage was ramped consolidation (see CD in Fig. 3.2 (a), (b) and (c)). In this stage the mean net stress was increased to 400 kPa, while the suction s was held constant at 100 kPa. This stage was identical for all

tests, to ensure that the yield surface was expanded to the same position in all tests.

(d) Most tests included an unloading or swell-back stage (see DX in Fig. 3.2 (a), DE or FX in Fig. 3.2 (b) and DE in Fig. 3.2(c)). During this stage the mean net stress p' was reduced from 400 kPa to a final value p_c' (which varied in the different tests), while holding the suction constant.

(e) Some tests included a suction change stage (DF or EX in Fig. 3.2 (b) or (c)). In this stage the suction was changed from 100 kPa to a value of either zero or 200 kPa. This stage took place either before or after the unloading stage described before, with the mean net stress held constant at either 400 kPa or p_c'.

(f) The final stage of each test was a re-loading or shear stage (see Fig. 3.3). In this stage (starting at point X) the sample was re-loaded, either isotropically or with the application of a deviator stress q, with the suction held constant. For each of the three values of suction (zero, 100 and 200 kPa) the intention was that tests would be conducted starting at various different positions X and with various different values of $\Delta q/\Delta p$ (see Fig. 3.3).

A typical test showing all the stages in 3-dimensional $p':q:s$ space is shown in Fig: 3.4.

The first objective (to investigate the shape of the yield surface) was to be achieved by the final re-loading stages of the tests. In this stage, values of s, p' and q at yielding could be obtained and these values were to be used to plot cross-sections of the yield surface at specific values of suction, as depicted in Fig. 3.1. By having tests at various suction values the overall shape of the yield surface could then be examined.

The "elastic" behaviour of unsaturated soil inside the state boundary, as stated in the second objective, was examined in several different stages, with values of κ, κ_s

and G taken from the unloading stages, suction change stages and re-loading (shear) stages respectively.

The third objective was concerned with the post yielding behaviour of the soil. This behaviour would be investigated during the later part of the final re-loading or shear stage of the tests where the plastic strain increments $d\varepsilon_s^p$ and $d\varepsilon_v^p$ beyond yielding could be experimentally determined. From the relative magnitudes of the plastic strain increments $d\varepsilon_s^p$ and $d\varepsilon_v^p$ the direction of the total plastic strain increment $d\varepsilon^p$ with respect to the yield curve could be determined.

Lastly, the incorporation of water content within the elasto-plastic framework for unsaturated soil required the data showing the variation of water content in all stages of the test. It was suggested (*Wheeler*, 1991) that the change of water content was best expressed in terms of specific water volume v_w, defined as the volume of solids and water in a volume of soil containing unit volume of solids

$$v_w = 1 + eS_r = 1 + wG_s \tag{3.1}$$

Elastic changes of v_w caused by changes of p' and s could then perhaps be represented by an equation directly analogous to the one defining elastic variation of v (see Equation 2.20)

$$dv_w^e = -\kappa_w \frac{dp'}{p'} - \kappa_{sw} \frac{ds}{s + p_{at}} \tag{3.2}$$

where κ_w and κ_{sw} are two additional soil constants. The values of κ_w and κ_{sw} were investigated in the unloading stages and suction change stages respectively.

To investigate the behaviour of unsaturated soil inside the state boundary, it was necessary to provide accurate measurements of the specimen displacements at small strains. These requirements are discussed in detail in Chapter 4 (Experimental Equipment and Calibration).

Although the prime emphasis was the behaviour of unsaturated soil at relatively small strains, each soil sample was sheared to the highest strains possible in the available apparatus, so as to get as much information as possible from each test.

The research methodology was based on the assumption that unsaturated soil behaviour can be adequately represented by a constitutive model involving a single yield surface, rather than the type of multi-surface kinematic yield model developed recently for saturated soils (see Section 2.8). This is obviously a major simplication, but it was considered appropriate at this relatively early stage in the development of elasto-plastic constitutive models for unsaturated soil.

Finally it was envisaged that each multi-stage test would take a long time to accomplish and therefore the number of tests that could be completed would be limited. This constraint had to be borne in mind when planning the detailed test programme (see Chapter 5).

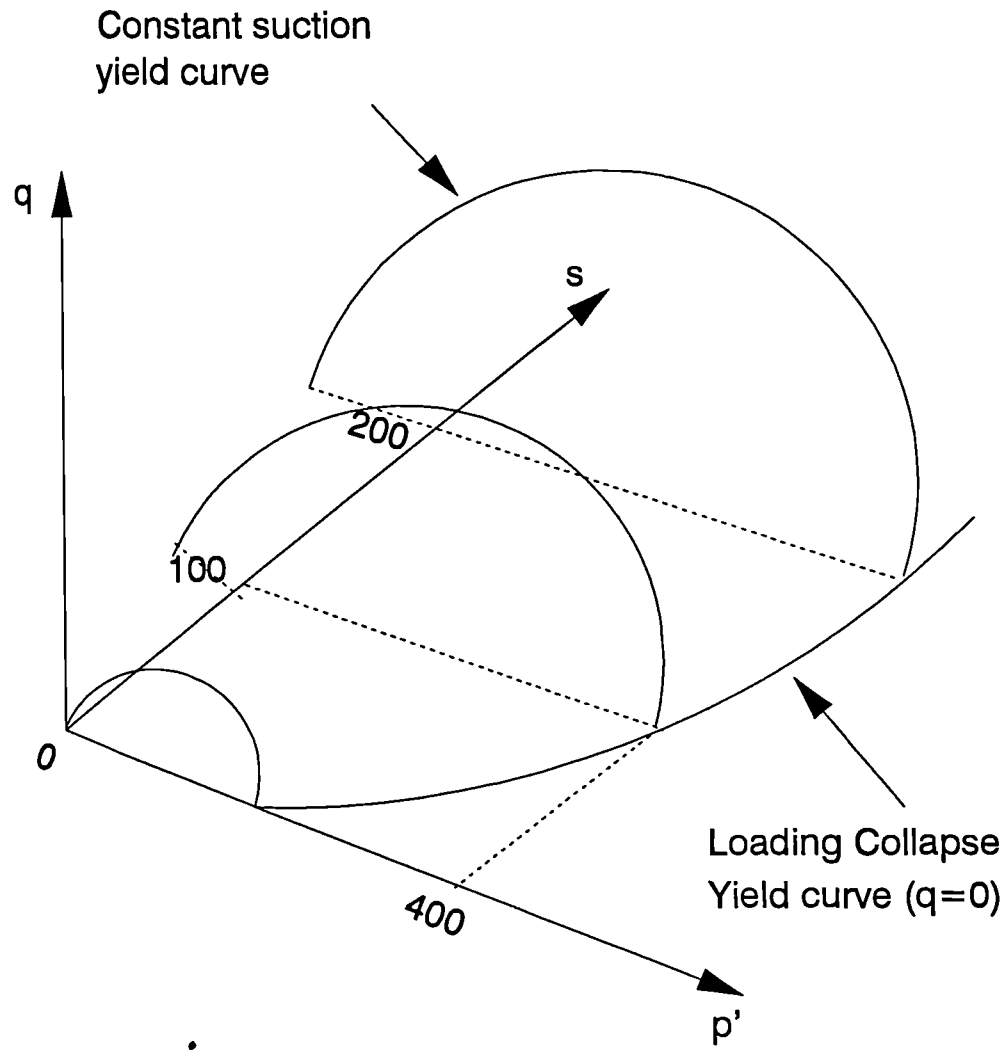

Fig. 3.1 : Yield surface for unsaturated soil

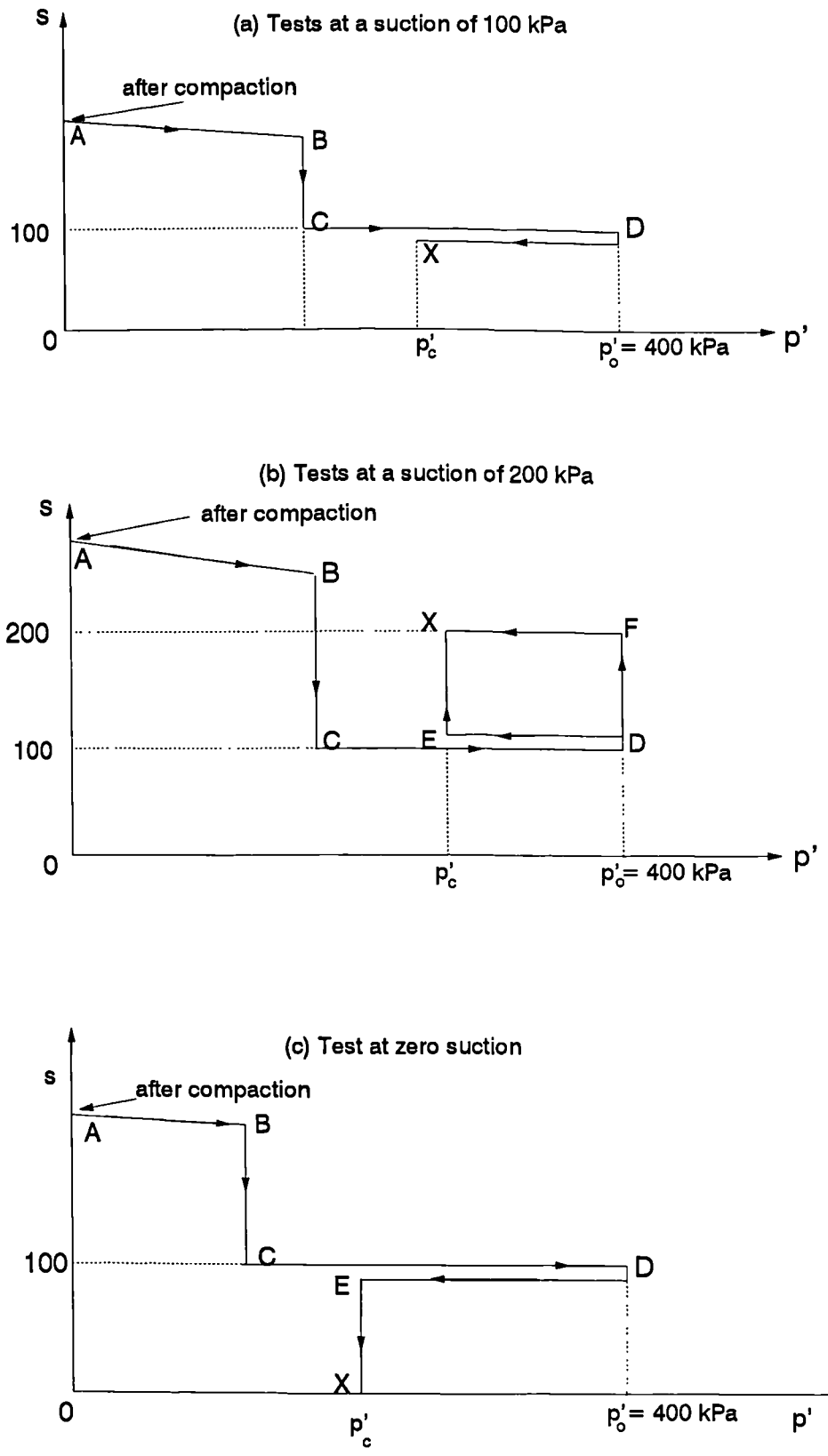

Fig. 3.2 : Stress paths during equalisation, consolidation, unloading and suction change stages

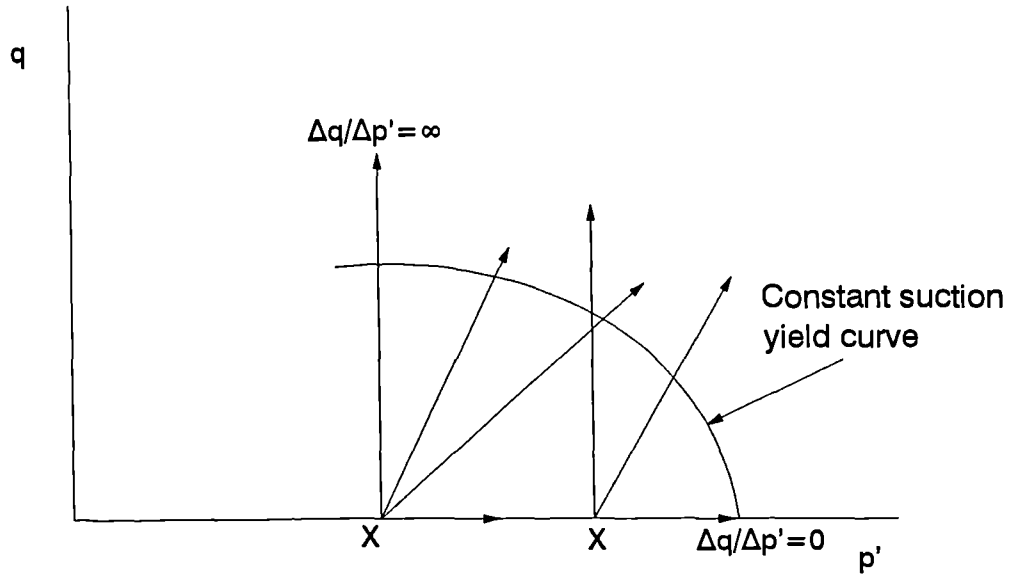

Fig. 3.3 : Stress paths during re-loading or shear stage

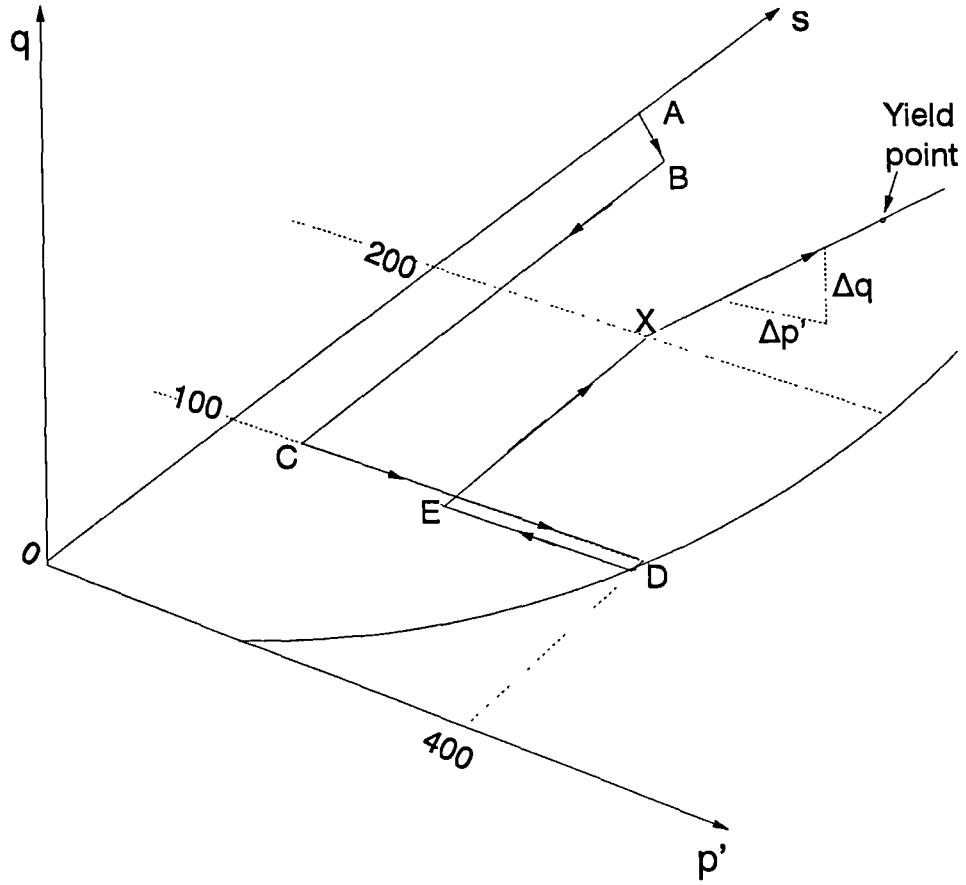

Fig. 3.4 : 3-D view of a typical stress path in p':q:s space

CHAPTER 4

EXPERIMENTAL EQUIPMENT AND CALIBRATION

To apply the research methodology outlined in Section 3.2 the experimental apparatus had to be suitable for conducting isotropic consolidation (under controlled suction), isotropic swell-back (again under controlled suction), change of suction and finally shearing or isotropic re-loading (still under controlled suction). The overall layout of the experimental equipment designed to fulfil these needs is shown in Fig. 4.1

4.1 Triaxial cell and pressure connections

4.1.1 Bishop-Wesley hydraulic triaxial cell

A wide-bodied Bishop-Wesley hydraulic triaxial cell, manufactured at Imperial College, was used in the experimental work. The cell was designed for soil specimens up to 50mm in diameter and 100mm in length, and the maximum working pressure was 1300 kPa.

The specimen size was chosen after due consideration of the following factors:

1) The soil sample must be considerably larger than the dimensions of the largest structural elements forming the soil fabric (the arrangement of saturated packets and large, unsaturated inter-packet voids forming the soil) (see *Sivakumar*, 1993).

2) The larger the size of the soil specimen the longer would be the time required for each test (because of the need for pore water pressure

equalisation throughout the specimen). This would limit the number of tests that could be performed.

3) The existing triaxial cell was suitable for soil samples up to 50 mm in diameter and 100 mm in height (including the attachment of local displacement gauges).

After consideration of these points a sample size of 50 mm in diameter and 100 mm in height was selected.

The travel limit of the loading ram of the triaxial cell was about 26 mm, giving a maximum axial strain of about 26 % for a soil sample with a height of 100 mm. As a result it was not possible to achieve critical states in the shear stages of all tests (see Section 5.3.6). Fortunately, however, the attainment of critical states was not a prime objective of the research.

4.1.2 Cell pressure connection

The pressure to the cell was provided from a digital pressure/volume control unit supplied by Geotechnical Digital System Instruments Ltd. of Surrey (hereafter called GDS Unit 1 for simplicity) which was available in the department and had a pressure limit of 2000 kPa and a maximum volume displacement of 200 cm^3. The GDS unit could be used in a stand alone mode or computer-driven via an IEEE-488 interface card which could be plugged into the computer motherboard. Without computer control the GDS unit could be used to hold either pressure or volume constant or it could be used to ramp either pressure or volume at a constant rate (specified by the operator) to a target value (specified by the operator). This facility to ramp the cell pressure was particularly useful for the ramped consolidation and swell-back stages (see Chapter 5).

The GDS unit was connected via an oil/water interface to an outlet in the cell base and hence to the main chamber of the triaxial cell (see Fig. 4.1). Transparent

nylon tubing was used for the connections so that any trapped air (if present) was visible.

The cell pressure transducer was rigidly fixed to a de-airing block attached to a separate outlet on the cell base. The same outlet was also connected to an oil supply tank, located on the floor, which was used when filling and emptying the cell (see Chapter 5).

4.1.3 Lower chamber pressure connection

The lower chamber of the triaxial cell was connected to a second GDS unit through a nylon tube (see Fig. 4.1). The function of this GDS unit 2 was to drive the loading ram of the hydraulic triaxial cell during shearing. By ramping the volume or pressure with GDS Unit 2 it was possible to provide either strain-controlled or stress-controlled shearing.

The cross-sectional area of the Bellofram seal inside the lower chamber was 29.4 cm^2. Therefore, if a shear test were to be conducted under strain-control then 29.4 cm^3 of water had to be pumped into the lower chamber of the triaxial cell to produce 1 cm of piston movement. By knowing this relationship any rate of strain on the soil specimen could be calculated to suit the test requirements. The lower chamber was provided with only one outlet so a careful de-airing procedure had to be performed to ensure that the lower chamber was free of air.

4.1.4 Control of pore air pressure

The pore air pressure u_a was controlled at the top face of the soil specimen. Compressed air from a supply line with a maximum pressure of 600 kPa was supplied via a pressure regulator to a connection in the triaxial cell base and then via a flexible tube to the top cap on the soil specimen (see Fig. 4.1). The detail of the top

cap is shown in Fig. 4.2. A standard (low air entry) porous stone was used to make the pressure connection to the soil specimen (see Fig. 4.3).

4.1.5 Control of pore water pressure

The pore water pressure $u_w$was controlled at the base of the soil specimen. Compressed air from the supply line, having passed through a pressure regulator with the outlet pressure read by a pressure gauge, was delivered to the top of a bladder-type air/water interface 1. The air then pressurised the water (forming the water back pressure line) leading to the bottom of an automatic volume gauge (supplied by Imperial College). This water back pressure line then passed through a connection in the triaxial cell base to the bottom of the soil specimen through a system of filters as shown in Figs. 4.1 and 4.3.

For unsaturated soil under in-situ conditions the pore air pressure is normally zero (atomspheric pressure) and the pore water pressure is therefore negative. It is very difficult to reproduce this condition in the laboratory, because cavitation may occur in the water back presure line. To alleviate the problem, *Hilf* (1956) devised a system known as the 'axis translation technique' whereby the total stress, pore air pressure and pore water pressure were all increased by identical amounts until the pore water pressure was positive. In this way any positive value of suction $u_a - u_w$ could be generated without the need to apply or measure negative values of pore water pressure.

With the pore air pressure u_a within the soil specimen maintained at a higher value than the pore water pressure u_w applied at the base of the specimen, it was necessary to use a high air entry filter in order to prevent air from the specimen blowing through into the line providing the water back pressure.

A ceramic filter with an air entry value of 500 kPa was used in the test programme. The filter was manufactured by Soilmoisture Equipment Corp. of

California and came in large circular sheets about 300 mm in diameter and 8 mm thick. A small disc, 30 mm in diameter and 6 mm thick, of the high air entry filter material was cut from the sheet and used in the filter system as shown in Fig. 4.3 and Fig. 4.4. The filter system also included a 4mm thick standard (low air entry) porous stone placed underneath the high air entry filter. The function of the low air entry porous stone was to increase the rate of flow through the filter and into the fine bore drainage lines , by reducing the constriction of the flow lines through the low permeability , high air entry ceramic (see *Sivakumar*, 1993). Both filters were securely glued within an annular filter housing made of perspex (see Fig. 4.4). It was extremely important to have a complete seal between the filters and the filter housing to prevent the air inside the specimen from entering the water back pressure system. The filter system was screwed onto a bottom pedestal, the details of which are shown in Fig. 4.5

4.2 Transducers for stress and strain measurement

4.2.1 Measurement of water volume change

The water volume change in the soil specimen was monitored by means of an automatic volume gauge supplied by Imperial College. The water draining from the sample flowed along the water back pressure line, through a 3-way valve and then to the volume gauge (see Fig. 4.6). Water flowing into the volume gauge displaced a piston inside the gauge and this movement of the piston was detected by an LVDT attached to the side of the gauge with its armature resting on an arm fixed to the piston.

With high values of pore air pressure inside the specimen there was a possibility that the air could go into solution in the pore water and then diffuse through the high air entry ceramic filter. This phenomenon was undesirable because the dissolved air could then come out of solution to form air bubbles within the back

pressure line. A flushing system, to remove any bubbles of diffused air from beneath the ceramic filter, was therefore included as shown in Fig. 4.6.

The flushing system consisted of a diffused air volume indicator (*Fredlund,* 1975), and a second bladder-type air/water interface and a system of 3-way valves. The flushing line originating from the base of the specimen passed through the 3-way valve and into a 10 cm^3 glass burette via a nylon tube. The glass burette was surrounded by water contained inside a larger diameter perspex tube (to avoid pressure differences across the glass walls of the burette) and the pressure to the inner (glass) and outer (perspex) tubes was supplied from the compressed air supply via bladder-type air/water interface 2. The flushing was accomplished by having a small differential head between the two air/water interfaces, causing air bubbles to be flushed into the diffused air volume indicator, where the air collected at the top of the graduated glass burette. The flow through the drainage grooves beneath the high air entry filter was reversed several times during flushing, using the 3-way valves, to ensure that all diffused air was removed.

4.2.2 Measurement of sample volume change

The sample volume change occurred as a result of the combined volume changes of the air and water phases (assuming that the solid particles were incompressible). There were two options available for measuring the sample volume change : either monitoring the flow of water in and out of the surrounding cell or measuring the individual lateral and axial strains of the sample. The first option required the use of a double-walled cell, as described by *Bishop* and *Donald* (1961) and *Wheeler* (1988b). The method was found by *Sivakumar* (1993) to give accurate values of overall sample volume change at small and large strains (including shearing to failure, when the sample was highly deformed). The second option required the use of local strain gauges mounted directly on the sample. This method gives accurate values of sample volume change at small strains, when it is reasonable to

the sample deforms as a cylinder, but becomes increasingly inaccurate as the sample is sheared towards failure.

In the research project one of the main objectives was to investigate the behaviour of unsaturated soil at small strains including the measurement of both volumetric and shear strains. The measurement of small shear strains could only be achieved by the use of local axial and radial strain gauges. Unfortunately , financial constraints meant that it was not feasible to provide both local strain gauges and a double-walled cell. It was therefore necessary to select the second option for measurement of sample volume change i.e. the local axial and radial strain gauges were used to calculate values of both shear and volumetric strains. Clearly this had significant implications for the accuracy of the volumetric strain measurements when the sample became very distorted.

4.2.3 Measurement of axial strain

Axial strain was measured directly on the soil specimen using inclinometer type axial gauges developed at Imperial College (*Ackerly, Hellings and Jardine*, 1987) as shown in Fig. 4.7. The inclinometer type axial gauge used in the experimental work was a revised version of the original electrolevel type gauge (*Jardine, Symes and Burland,* 1984). The gauge consisted of a heavy metal pendulum bob suspended by a thin strip of spring steel which had been strain gauged to provide a full 350 Ω Wheatstone bridge. It could be used for various-sized specimens in conventional or stress path triaxial cells.

The axial devices had a gauge length of 45 mm between the footings mounted on the soil sample and a working range of about 15 mm. This gave an axial strain range of over 30%, which was greater than the limit of 26% set by the maximum travel of the triaxial cell piston (see Section 4.1.1).

The axial gauges were mounted on the specimen by attaching their footing pads onto the vertical face of the rubber membrane enclosing the soil specimen. Two gauges were mounted on opposite sides of the specimen to reduce the influence of any sample tilting. The gauges were fixed to the rubber membrane by applying superglue on the faces of the pads, as shown in Fig. 4.7. The detailed procedure for mounting the axial gauges onto the soil specimen is given in Section 5.2.3 including the use of a suspension system to support the bouyant weight of the gauges.

Local axial gauges have been used for many years to minimise the errors in the measurement of small axial or shear strains (*Burland and Symes,* 1982 ; *Jardine, Symes and Burland,* 1984 ; *Costa Filho,* 1982). This was because in the conventional method of measuring axial strains, by external LVDTs or dial gauges, errors arise due to the compliance of the loading system and "bedding-in" at the top and bottom of the specimen.

The triaxial cell was also provided with facilities for measuring the axial strain of the specimen external to the cell. This was done by the use of two LVDTs mounted vertically on the cell top plate, with the spindles of the LVDTs resting on vertical bars supported on the cross-arms of the loading ram. The LVDTs had a travel limit of about 26 mm (corresponding to the maximum travel of the loading ram itself).

4.2.4 Measurement of radial strain

A radial gauge capable of measuring the lateral displacement of soil samples was custom-built in the department. The radial gauge consisted of two L-shaped brass arms joined together by a stainless steel strip as shown in Fig. 4.8. Mounted on both sides of the stainless steel strip were two electrical resistance strain gauges. The strain gauges were exposed, because coating them with a flexible sealant was found to affect their performance (resulting in hysteresis, creep and lack of repeatability).

With the electrical resistance strain gauges exposed it was not possible to use water as the cell fluid. Instead a strain gauge oil called Diala-B was used as the cell fluid. Experiments had shown (see Chapter 5) that the oil had no effect on the strain gauges.

Each brass arm of the gauge was provided with an adjusting screw so that the arms could be set at any aperture. A small hole was drilled in each arm so that the gauge could be suspended by strings from two cantilevers attached to the acrylic cell wall to avoid the weight of the radial gauge being carried solely by the soil specimen. The detailed procedure for mounting the radial gauge on the specimen is given in Section 5.2.3.

The arrangement of axial and radial strain gauges on a soil sample is shown in Fig. 4.9.

4.2.5 Measurement of pressures

Pressure transducers were used to measure cell pressure, pore air pressure and pore water pressure (Fig. 4.1). The pore air pressure and pore water pressure transducers were manufactured by Bell & Howell Ltd. and had a range of 500 kPa. The cell pressure transducer had a maximum capacity of 1000 kPa and was made by Druck Ltd.

The pore air pressure transducer was fixed to a de-airing block mounted on the air back pressure line. The pore water pressure transducer on the water back pressure line was set at the specimen mid-height by clamping it to the exterior of the cell.

4.2.6 Measurement of deviator load

The deviator load on the soil was measured by means of an Imperial College load cell with a maximum capacity of 4.5 kN. The load cell was rigidly attached to

the cell cover and it could be raised or lowered by turning a nut placed on top of the cell top plate.

The load cell was also provided with an alignment collar (designed and fabricated in the department), shown in Fig. 4.3 and Fig. 4.10. A small clearance of about 0.4 mm was provided between the inner cylindrical surface of the alignment collar and the vertical cylindrical surface of the top cap, to avoid friction between the two. The alignment collar prevented the soil specimen from tilting to one side during consolidation or swell-back prior to shearing.

4.3 Logging system

The logging system consisted of an IBM-PC compatible computer, Quicklog PC™ software and an interface card. The computer was provided with 640 kB of RAM, a 40 MB hard disk, a 1.22 MB 5.25in. floppy disk drive and a 1.44 MB 3.5in. floppy disk drive. The disk space was sufficient to store the large amount of data from any single test. Data from each test were then stored on floppy disk at the end of the test. A VGA colour monitor was used to display data from the gauges and transducers.

A computer program called Quicklog PC™, produced by Strawberry Tree Inc. of California, was used to log and save data on disk. Data from each channel could be displayed on the screen in engineering units. However only a limited amount of data processing was possible with the Quicklog PC™, and the data was therefore subsequently transferred to a spreadsheet program, LOTUS 1-2-3, for further manipulation (as described in Section 5.4.1). Unfortunately this transfer to LOTUS 1-2-3 could only be performed when the test was complete, so it was not possible to complete data-processing while a test was in progress.

The logging system is schematically represented in Fig. 4.11. Two interface boxes were used in the logging system and each interface box was provided with 8

channels so that a maximum of 16 channels could be used for logging data from transducers. Channels 1- 8 on the first interface box were connected to a 10V DC power supply and these were used for the LVDTs, the pressure transducers, the volume gauge and the load cell. Channels 9 - 16 on the second interface box were connected to a 5V DC power supply and channels 9 - 12 were used for the local strain gauges. Channels 13 - 16 were not used. The interface boxes were individually connected to an interface card mounted inside the computer motherboard via interface cables.

An interface card ACPC 16-16 manufactured by Strawberry Tree Inc. of California was used to convert I/O signals from all channels. The ACPC 16-16 interface card had 16-bits resolution and had 16 analogue channels, where each channel was individually programmable as input or output. The interface card received an analogue signal from each channel and converted it to digital signal for subsequent manipulation by the computer software.

If multiple channels were used to log data in a test, the manufacturer claimed that the maximum scan rate was 60 Hz divided by the number of channels in use (in the low noise mode as selected in the Quicklog PC software).

4.4 Calibration of transducers

In this section the calibration of the various devices is discussed. However only a few calibration methods will be given in detail, because standard procedures were used for many transducers. Channels 8 and 12 were used to monitor the 10V and 5V supply voltages, by simply inserting blank plugs into the channels, as a check on the supply voltage stability (see Section 5.4.2) All transducers were calibrated in exactly the same configuration (power supply and logging) as was subsequently used in the actual soil testing. Table 4.1 shows the various transducers and gauges connected to specific channels for reading and logging the data.

4.4.1 Calibration of pressure transducers

The pressure transducers for measuring cell pressure, pore air pressure and pore water pressure were calibrated against a Budenburg dead load tester over their full working range. Three calibrations were performed for each transducer, as a check of repeatability. This resulted in a linear calibration equation for each transducer, with, in each case, a standard error in the measured pressure of less than ±0.2 kPa.

4.4.2 Calibration of load cell

The load cell was calibrated against the dead load tester over a range of 0.2 kN to 3.8 kN, because the minimum load of the dead load tester was 0.2 kN and the maximum load envisaged during soil testing was about 3.5 kN.

It was found that regression analysis on the data using a first order polynomial yielded a standard error of ±6.5 N on the deviator load over the full range of 3.8 kN. This was considered unacceptable. Regression analysis using a third order polynomial gave standard error of ±2.5 N on the deviator load over the same range. This was equivalent to an error of about ±1.3 kPa in the deviator stress, assuming a specimen cross-sectional area of about 1960 mm^2. This was considered satisfactory.

4.4.3 Calibration of LVDTs

The two LVDTs used for external measurement of axial strain were calibrated against a micrometer gauge with a precision of 1 μm. The standard errors of the two LVDTs using linear regression were found to be ±7.6 μm and ±7.4 μm respectively over a range of 25 mm. This was equivalent to a standard error in the axial strain measurement of about 0.0075%, for a specimen height of 100 mm. This was considered acceptable, given that the local axial displacement devices were to be used for accurate measurements of axial strain.

4.4.4 Calibration of volume gauge

The volume gauge used for measuring the volume of water draining from the specimen was calibrated against a 10 cm^3 burette with a precision of ± 0.02 cm^3. The layout for the calibration is shown in Fig.4.12. The volume gauge unit was calibrated over the full working range of 40 cm^3 by re-filling the burette as necessary.

Before the volume gauge was calibrated it was flushed under a pressure of about 50 kPa with de-aired water so that no air was trapped inside the gauge cylinder and the drainage line. This was done by opening the bleed valve at the top of the volume gauge and slowly allowing water to drain out under the action of the applied back pressure. While water was still flowing out, the bleed valve was tightened. The system was left under a pressure of 200 kPa for 24 hours before calibration could be done so that no trapped air was present. This could be detected by observing the connecting tubes to the volume gauge . Any trapped air was visible through the transparent tubes.

To calibrate the volume gauge the burette was initially filled with water by opening valves 1 and 4 while closing valves 2, 3, 5 and 6 (see Fig. 4.12). A known volume of water (typically 5 cm^3) was drained from the burette into the volume gauge under a back pressure of 50 kPa by opening valves 2, 4, 5 and 6 and closing valves 1 and 3. Back pressure increments were then applied without changing the volume of water in the gauge, by opening valves 1, 3 and 5, closing valves 2, 4 and 6 and then adjusting the regulator on the compressed sir supply. The change in voltage output of the LVDT attached to the volume gauge was noted for each back pressure increment. The water back pressure was increased at intervals of 50 kPa until it reached 300 kPa, the probable maximum water back pressure to be used in the test programme. An additional 5 cm^3 was then drained into the volume gauge from the burette, and at every increment of water volume the same increments of water back pressure were applied. The process was repeated until the volume gauge reached its working limit of 40 cm^3.

The calibration of the volume gauge included the influence of back pressure on the calibration equation. It was found that at a given value of back pressure u_w, the volume of water V within the gauge could be related to the output voltage x by a linear equation :

$$V_w = A + Bx \tag{4.1}$$

where the intercept A and slope B varied with the back pressure u_w as shown in Fig. 4.13. Inspection of Figs. 4.13(a) and 4.13 (b) showed that both A and B varied approximately linearly with back pressure u_w i.e.

$$A = A_o + A_1 u_w \tag{4.2}$$

$$B = B_o + B_1 u_w \tag{4.3}$$

where A_o= 48.060 cm^3, A_1= -0.000109 cm^3/kPa, B_o= 0.66656 cm^3/mV, B_1 = −0.00000568 $cm^3/mV.kPa$. The calibration equation was therefore given by :

$$V_w = A_o + A_1 u_w + (B_o + B_1 u_w)x \tag{4.4}$$

The standard error in using Equation 4.4 was about ±0.015 cm^3. This corresponded to a standard error of about ±0.006% in the change of water content w or better than ±0.00016 in the change of specific water volume v_w, assuming that the typical mass of solid particles was about 245 g. This was considered acceptable in the experimental work.

4.4.5 Calibration of local axial displacement gauges

The method of calibration for the local axial displacement gauges is shown in Fig 4.14. The two gauges were mounted on a winding frame in an upright position. The body of a micrometer gauge, with a precision of 1 μm, was rigidly attached to the base of the winding frame. The bottom footing pads of the gauges were fastened to a stationary lower plate mounted on the frame, while the top footing pads were fastened to a movable upper steel plate. The movable plate was securely attached to the spindle of the micrometer gauge. The movement of the spindle could be adjusted by turning the knob of the micrometer gauge.

The centre-to-centre distance between the top and bottom footing pads was initially set at 45 mm, corresponding to the gauge length to be used during soil testing, and initial readings of the voltage outputs from the two gauges recorded. The axial gauges were calibrated at intervals of 0.2 mm over the full range of 15 mm. The calibration was carried out in such a way that the footing pads moved towards each other, as would be expected in the soil test when the soil specimen shortened during consolidation and shearing. However outward movement of the footing pads was also carried out to check if hysteresis was present.

From the calibration data, regression analysis using a third order polynomial gave standard errors of ±1.3 μm and ±1.0 μm for the two gauges. This meant that the standard error in the measured axial strain was about ±0.0025% over the soil gauge length of 45 mm. This was considered adequate for the experimental work (given that the objectives of the research project did not require the measurement of very small strains). The standard error may well have reflected the micrometer precision, rather than the accuracy of the axial displacement gauges, and lower errors might have been obtained if a more precise method of calibration had been employed. However this was not considered necessary.

4.4.6 Calibration of radial displacement gauge

The calibration of the radial gauge is shown schematically in Fig. 4.15. The radial gauge was supported on a solid block at roughly the same level as the winding frame, which was laid down on the bench. A small circular stud with a conical recess on the outer face was glued to the outer side of the fixed steel plate mounted on the winding frame. Another circular stud was also attached to the outer side of the movable steel plate which was securely fixed to the spindle of the micrometer gauge. The tips of the adjusting screws fixed to the radial gauge arm were then positioned over the studs. The screws were adjusted so that the radial arm exerted a slight force on the stud recess to ensure proper contact.

The calibration was performed using intervals of 0.2 mm. The maximum range used was 5 mm outwards (gauge arm moving away from each other), starting from an initial separation of 48 mm. This was because during the ramped consolidation stage the sample would decrease in diameter and in the subsequent unloading and shearing its diameter would increase. The overall change in specimen diameter was unlikely to exceed -2 mm or +3 mm from the initial diameter of 50 mm.

Linear regression analysis of the first order on the data gave a standard error of ±1.7 μm. This represented a standard error of just over ±0.003% on a 50 mm diameter specimen. The gauge was dismantled from the winding frame and another independent run was carried out to check the reproducibility of the results. The device was found to be sound and acceptable.

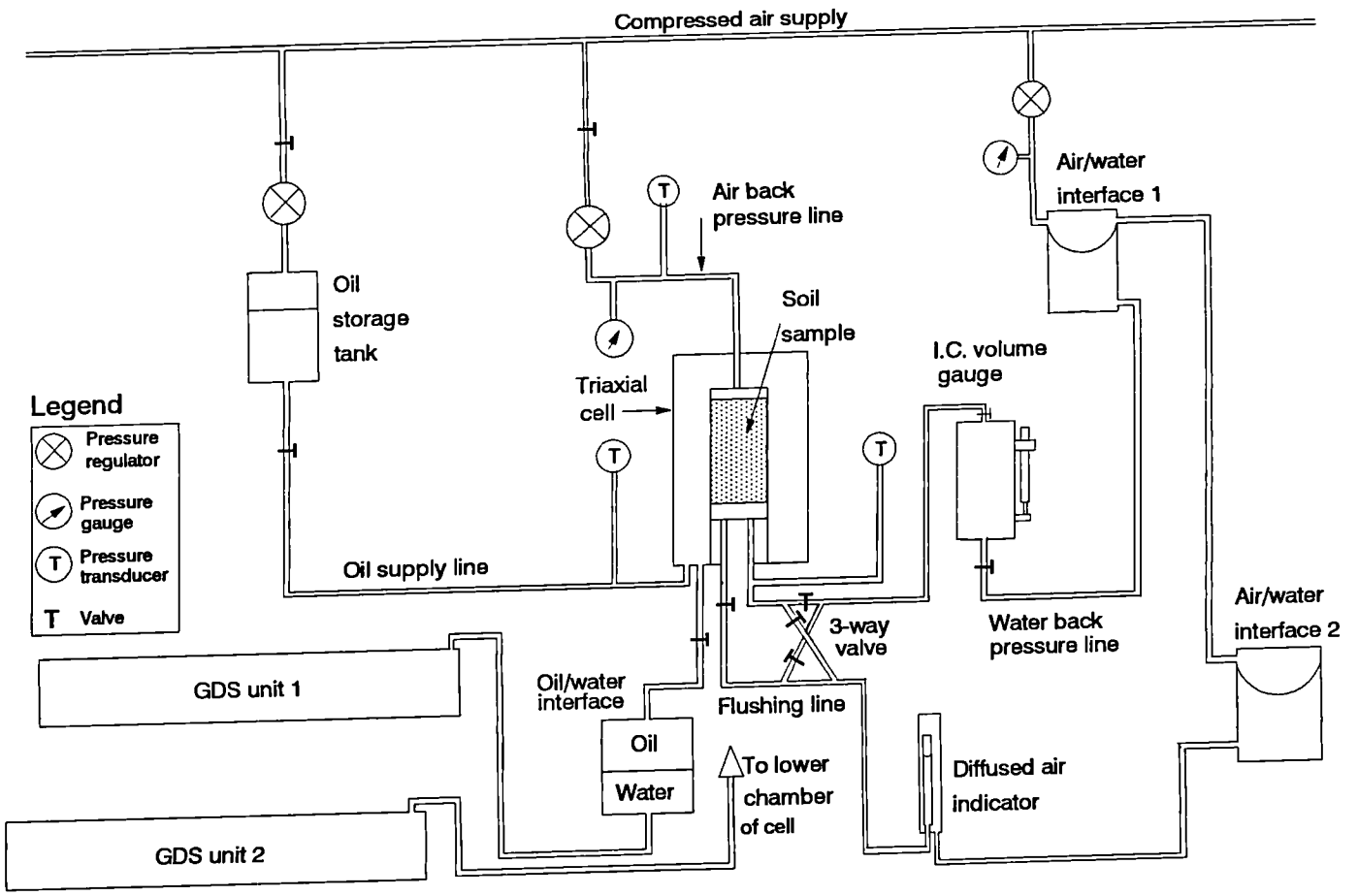

Fig.4.1 : Experimental set-up

Note : not to scale

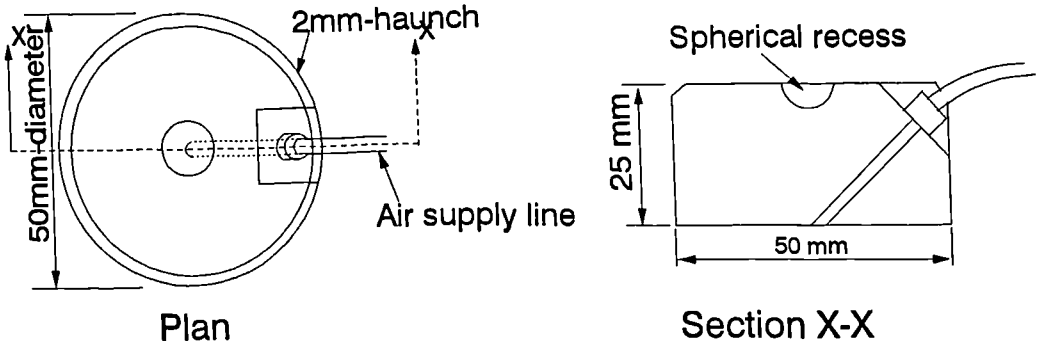

Fig. 4.2 : Details of top cap

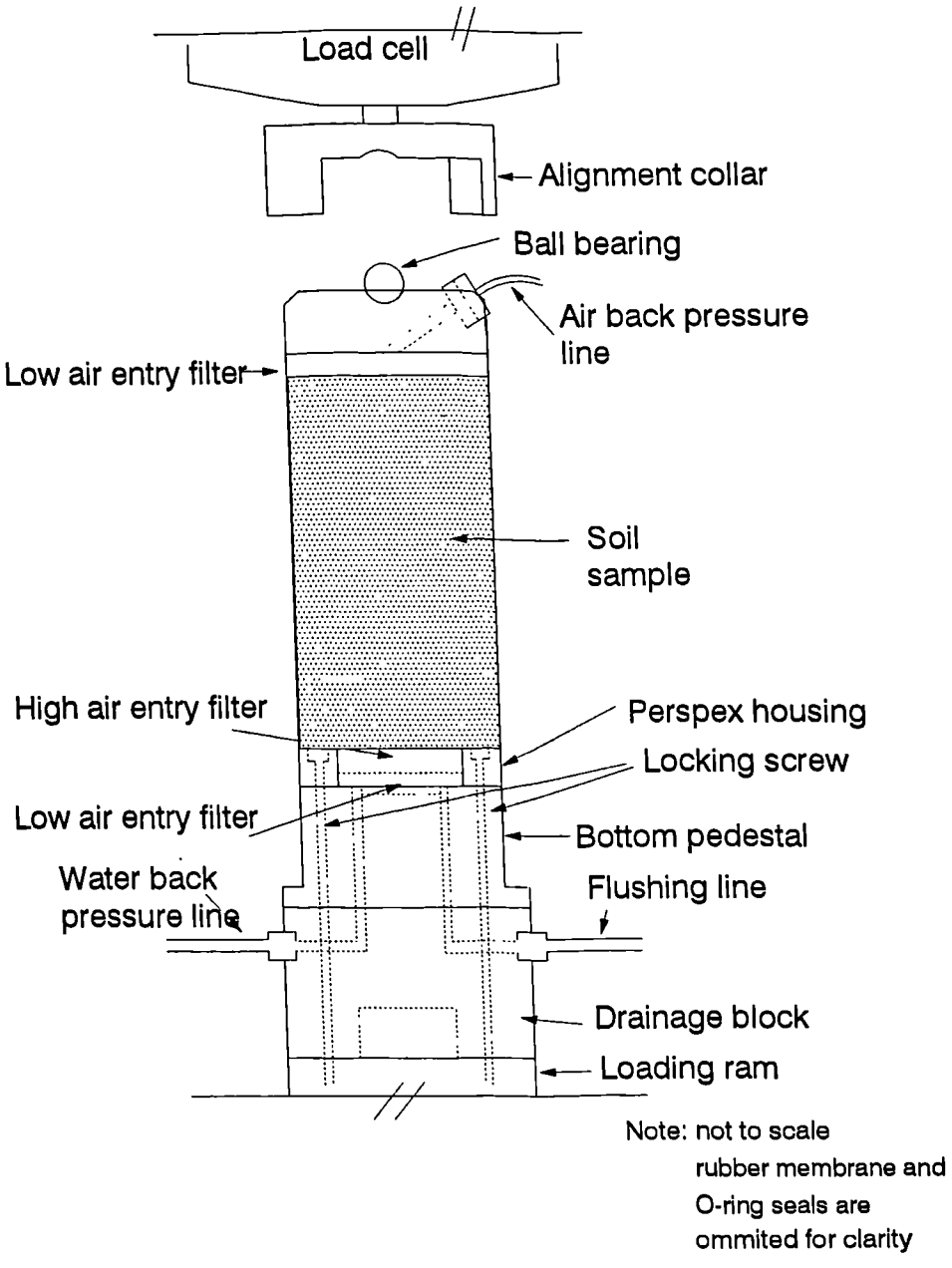

Fig. 4.3 : Drainage connections to soil sample

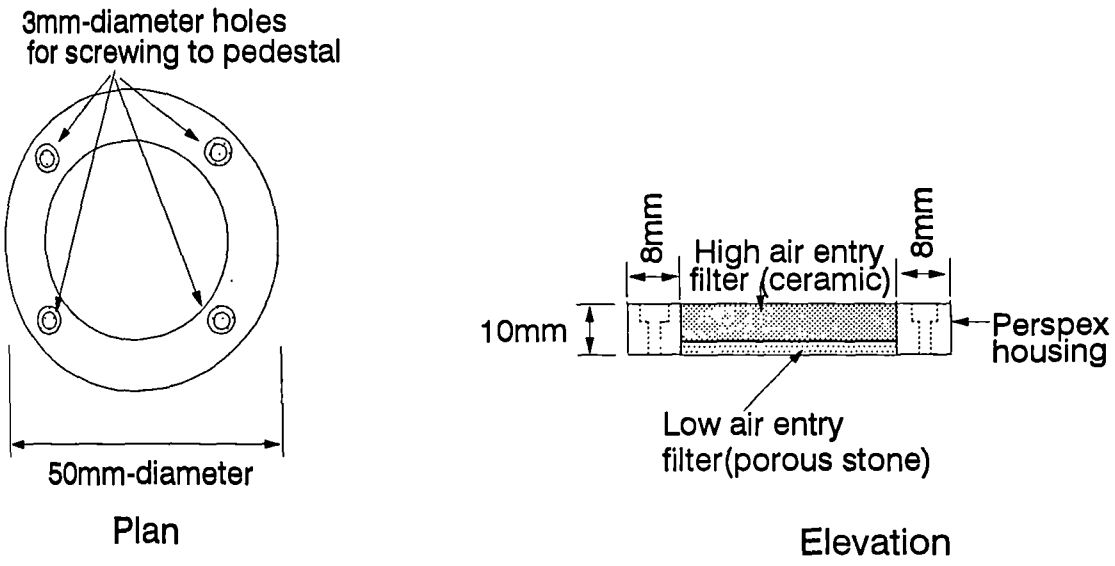

Fig. 4.4 : Details of bottom filter system

Note : not to scale

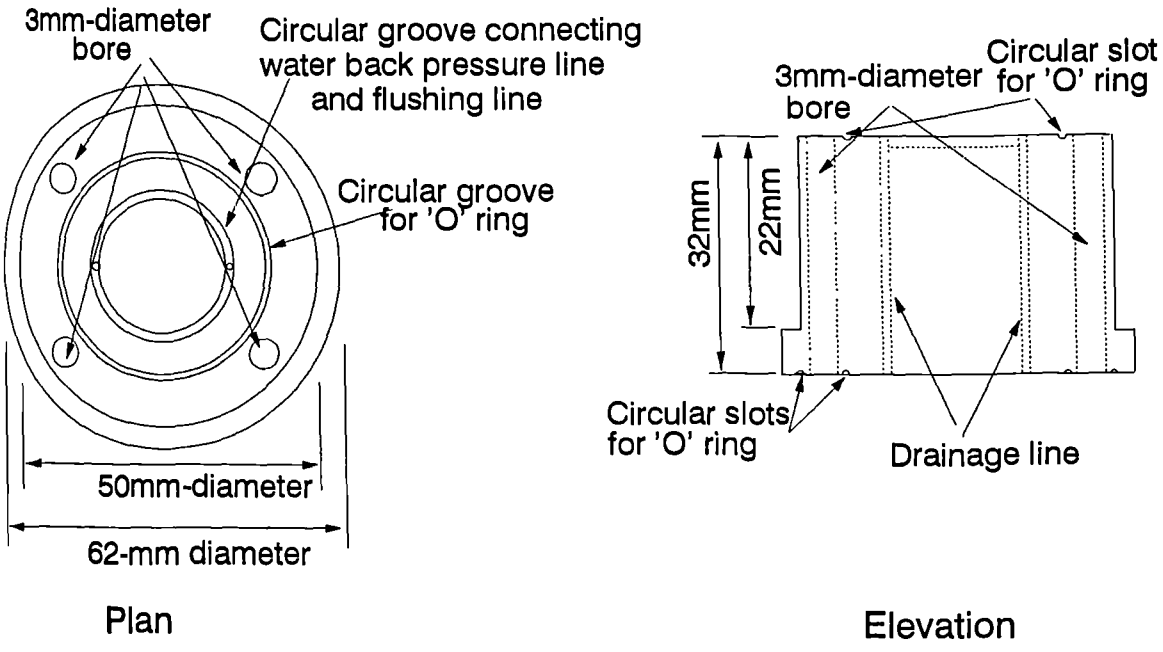

Fig. 4.5 : Details of bottom pedestal

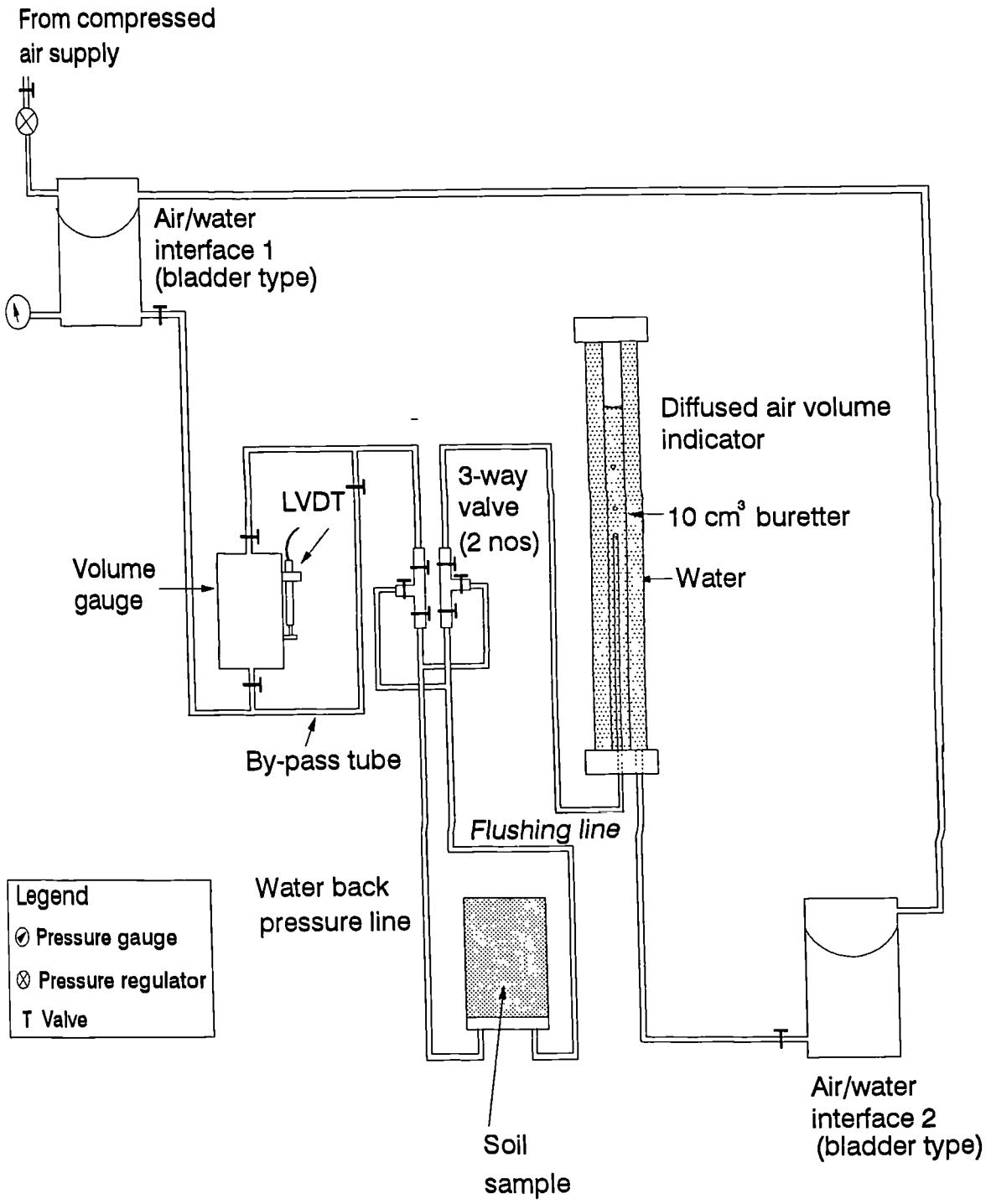

Fig. 4.6 : Flushing system

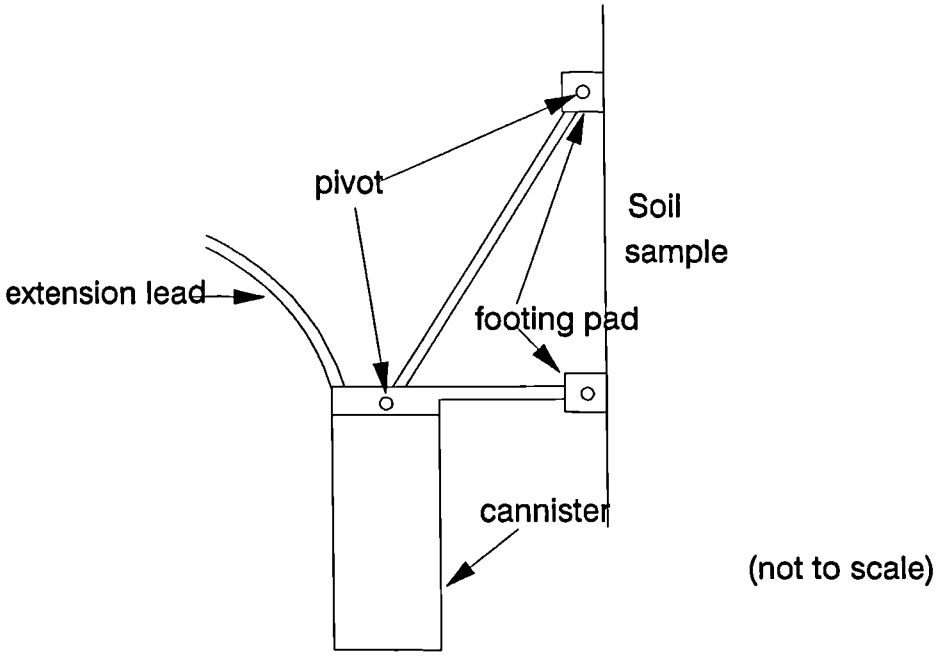

Fig. 4.7 : Inclinometer type axial gauge

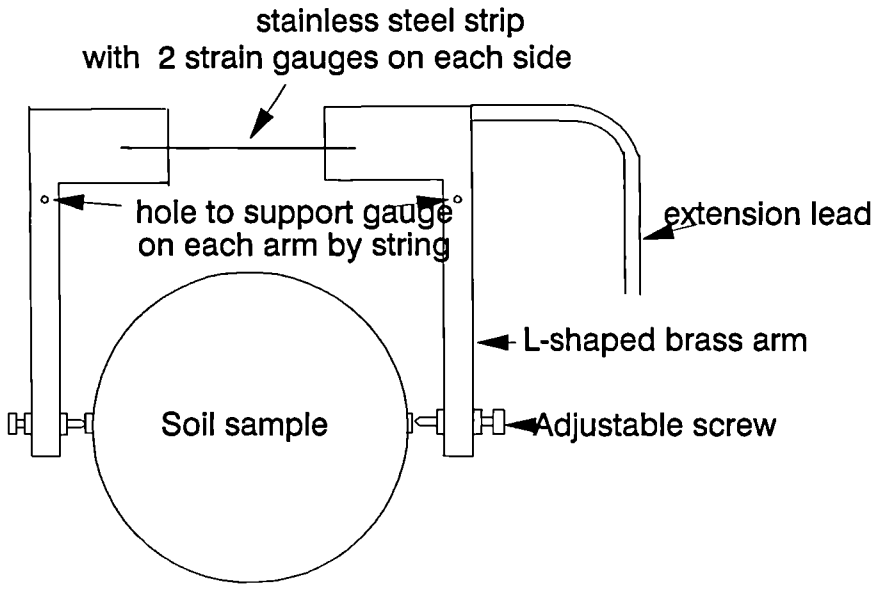

Fig. 4.8 : Radial displacement gauge

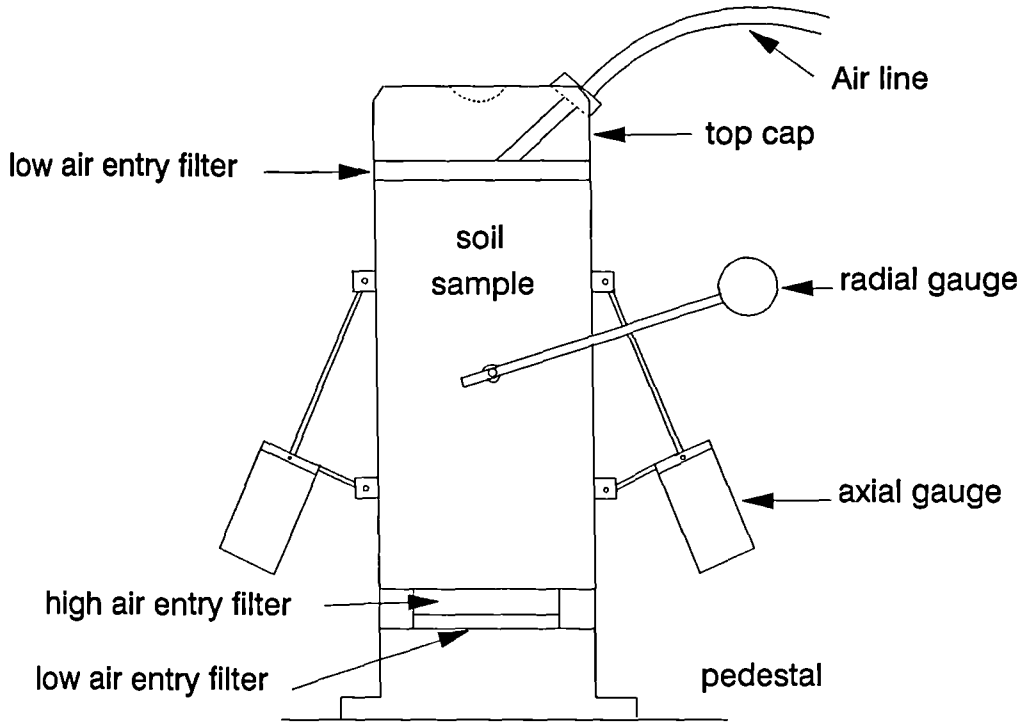

Note : suspension systems to balance buoyant weight of axial gauges in oil are ommited for clarity

Elevation

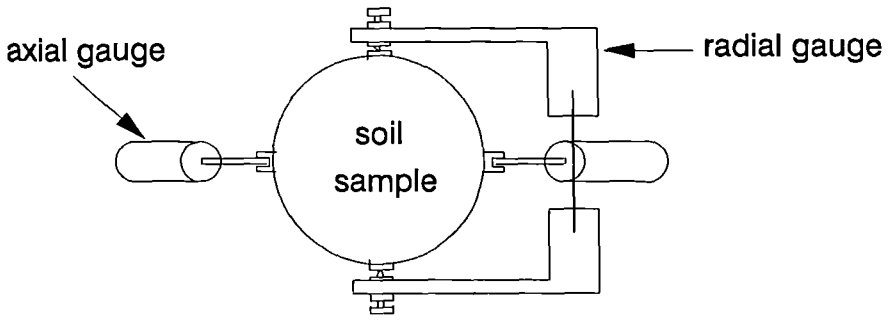

Plan

Fig. 4.9 : Local strain measuring devices mounted on soil sample

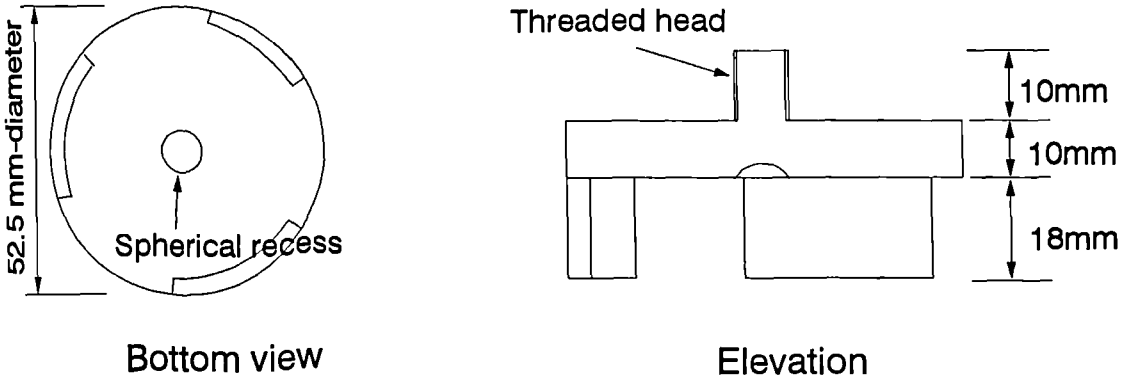

Fig. 4.10 : Alignment collar

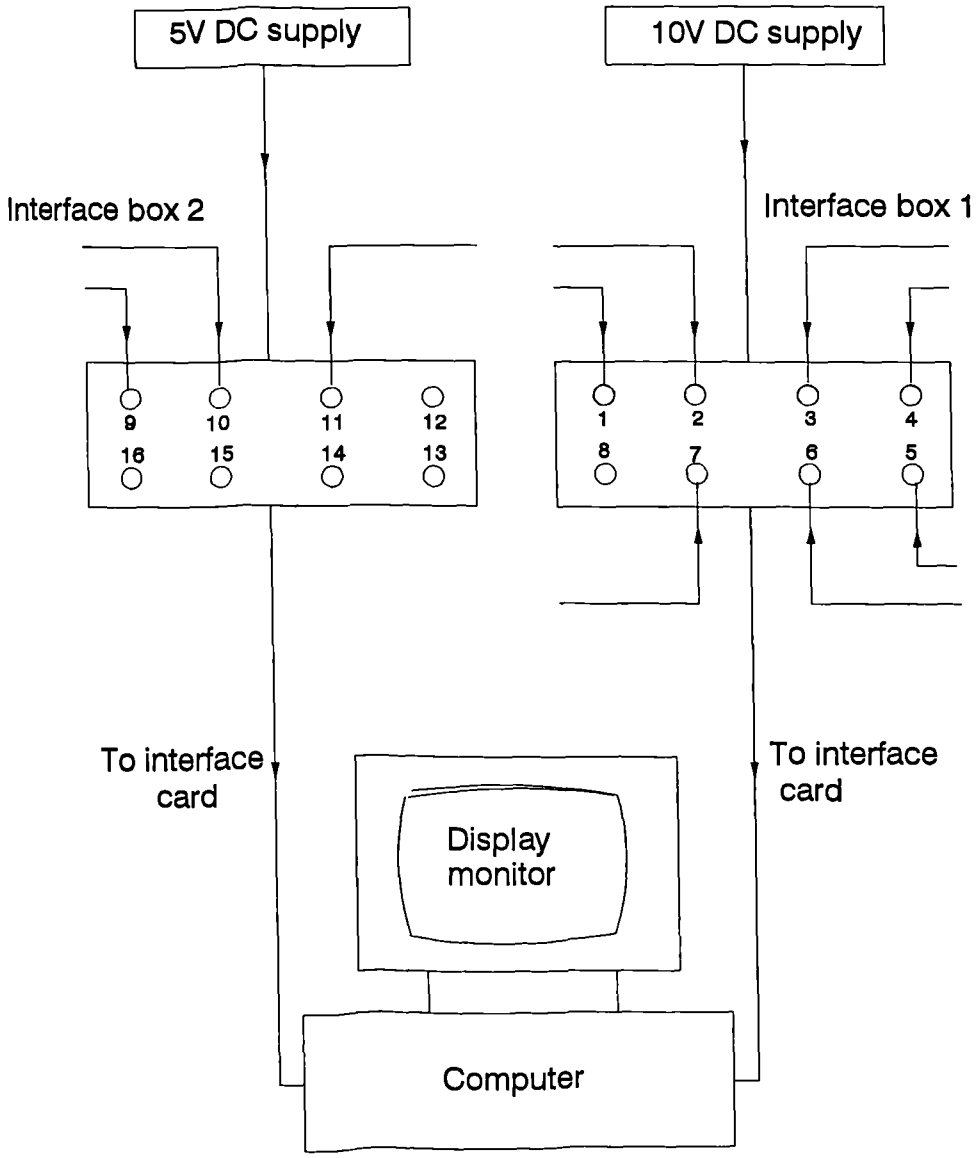

Fig. 4.11 : Logging system

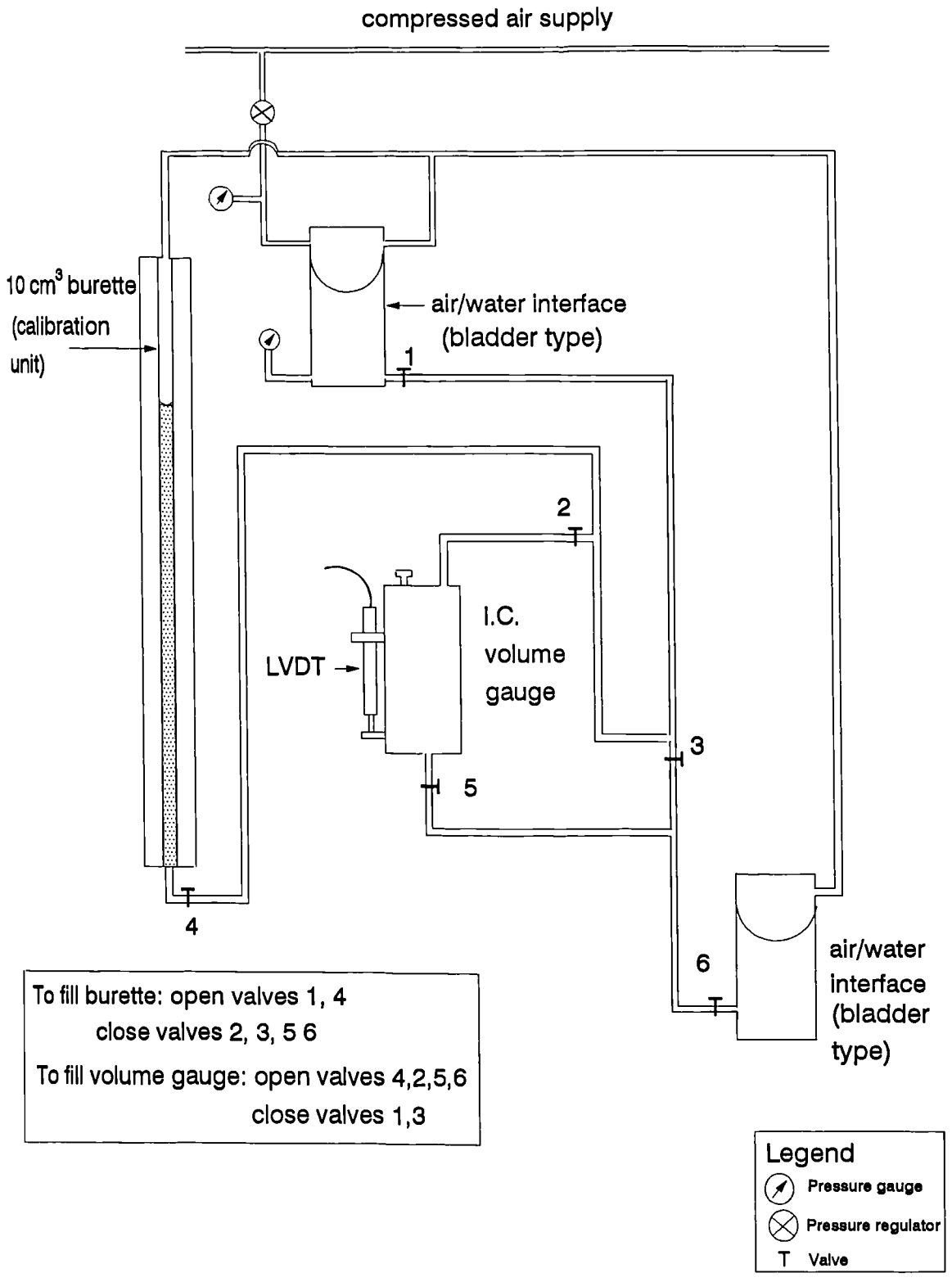

Fig. 4.12 : Calibration of volume gauge

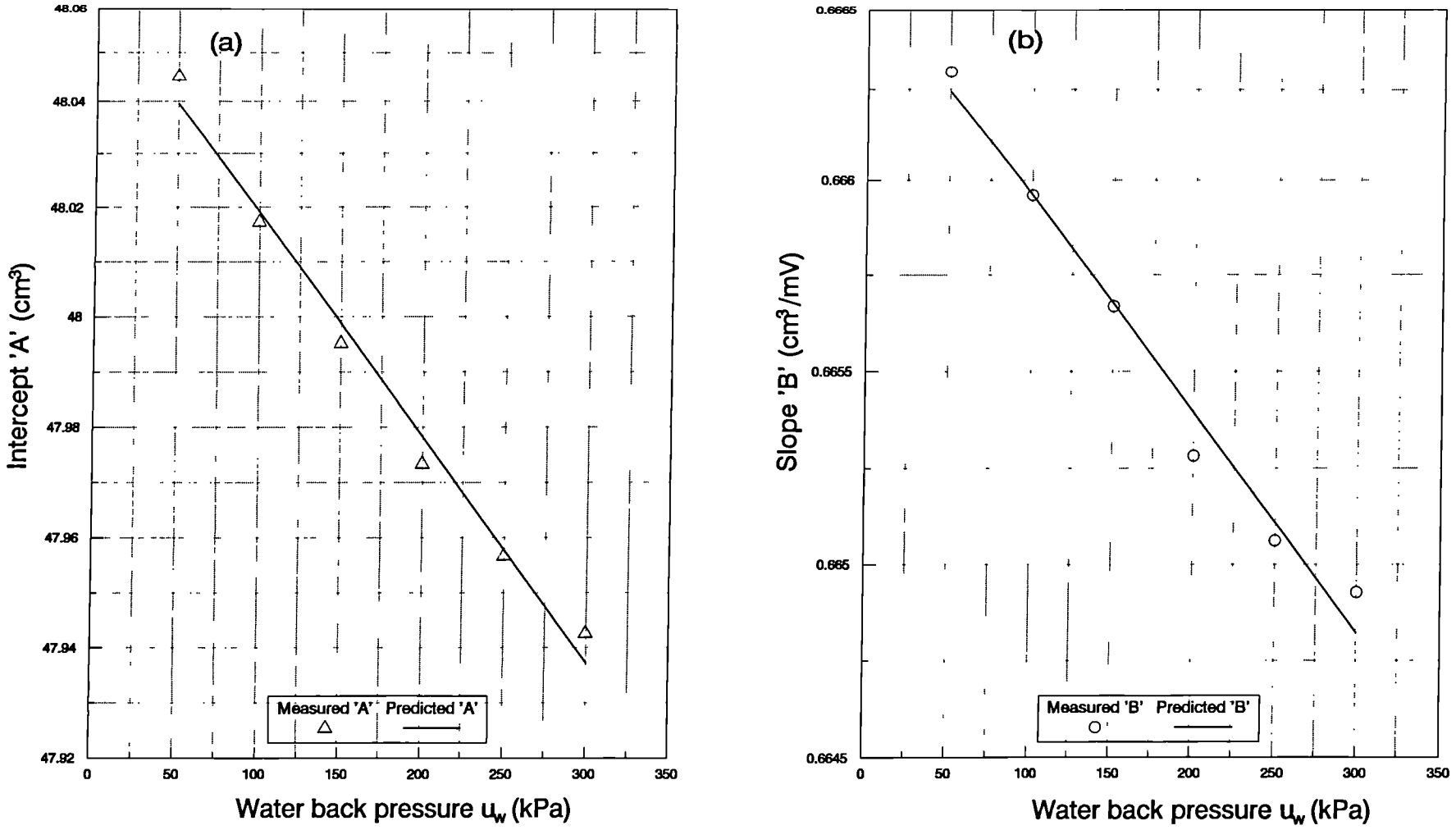

Fig. 4.13 : Calculation for intercept 'A' and slope 'B' for calibration of volume gauge

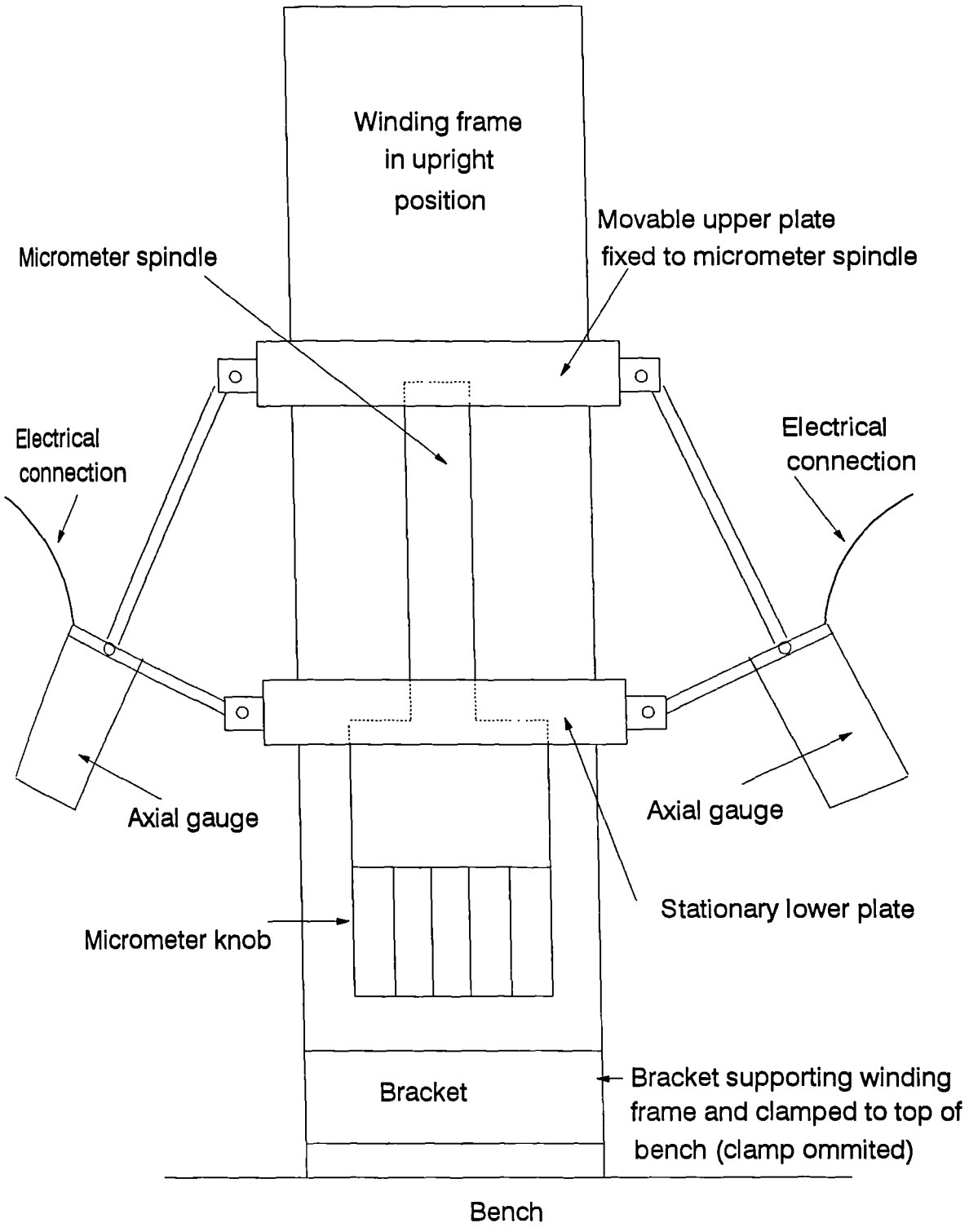

Fig. 4.14 : Calibration of axial gauges

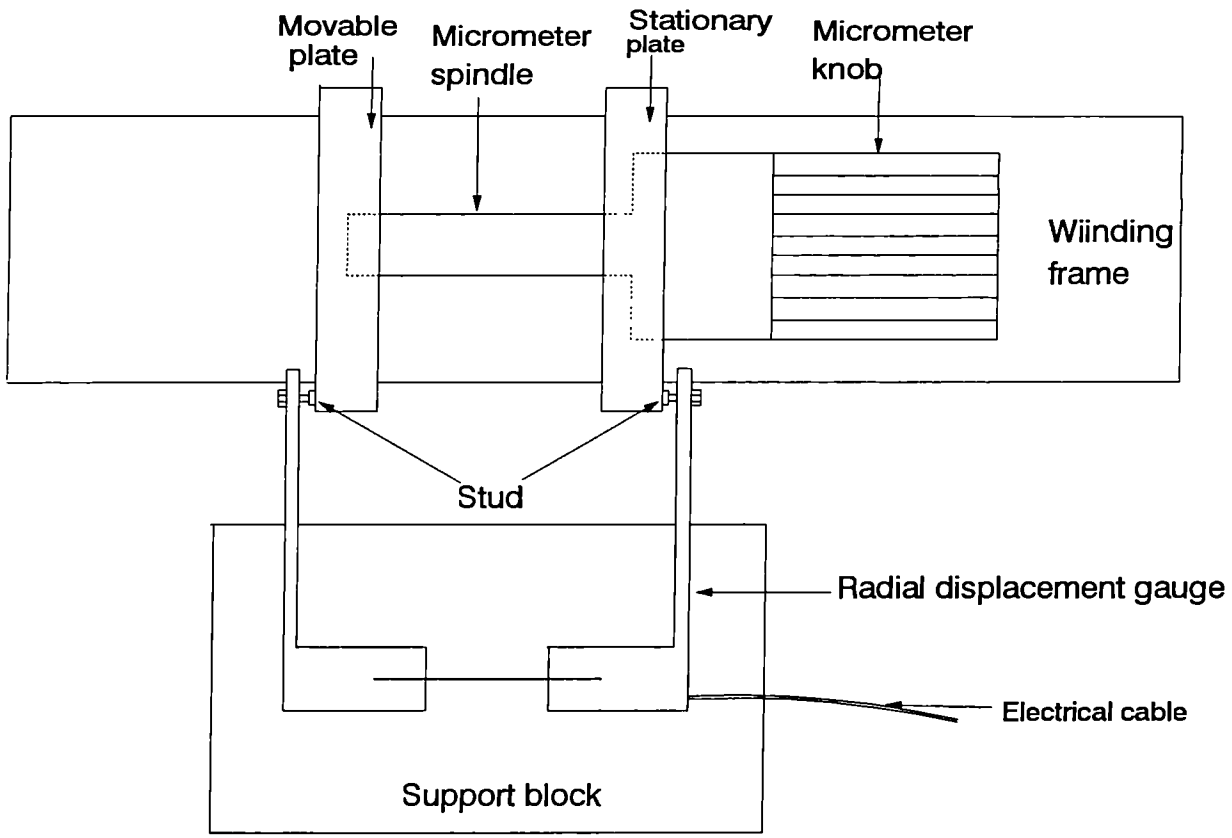

Plan view

Note : not to scale

Fig. 4.15 : Calibration of radial displacement gauge

Channel	Measurand	Device
1	External axial strain	LVDT
2	External axial strain	LVDT
3	Water volume change	I.C. volume gauge
4	Deviator load	I.C. load cell
5	Pore water pressure	Pressure transducer
6	Pore air pressure	Pressure transducer
7	Cell pressure	Pressure transducer
8	10V input supply	
9	Local axial strain	Inclinometer type axial gauge
10	Local axial strain	Inclinometer type axial gauge
11	Radial strain	Radial gauge
12	5V input supply	

Table 4.1 : Channel number and device

CHAPTER 5

EXPERIMENTAL PROCEDURES

5.1. Sample Preparation

5.1.1 Choice of soil type

Speswhite kaolin (LL = 75%, PL = 38%) was chosen as the soil type for the experimental work. There were many advantages of using kaolin as the test material in this type of fundamental research :

1) It was readily and cheaply available in a uniform and homogeneous form.
2) Kaolin contains about 75% clay fraction and it is therefore representative of the fine-grained soils which were of interest in this work.
3) Kaolin has a higher rate of consolidation than most other fine-grained soils, thus reducing the time required for testing. This is especially important for tests involving many stages, as described in Chapter 3.
4) The concept of an elasto-plastic critical state constitutive model was already well established for saturated kaolin (see for example *Schofield and Wroth* (1968), *Roscoe and Burland* (1968) and *Balasubramaniam* (1974)).
5) The proposed research project was an extension of previous research work on the development of an elasto-plastic critical state model for unsaturated soil by *Sivakumar* (1993), and Sivakumar used speswhite kaolin in his experimental work.

Inevitably compacted kaolin may not be fully representative of the full range of unsaturated clays found in practice. However in this type of fundamental research work it was useful to start with a relatively simple, homogeneous material, the condition of which could be readily controlled in the laboratory. The model could then be extended to other types of unsaturated soil at a later date.

The work of *Sivakumar* (1993) and that described in this thesis is restricted to unsaturated soils containing relatively inactive clay minerals (such as kaolinite), and it is not necessarily fully applicable to unsaturated soils containing active (highly expansive) clay minerals (such as montmorillonite). Additional features are required in the elasto-plastic model if these highly expansive unsaturated soils are to be represented (see *Gens and Alonso*, 1992).

5.1.2 Compaction procedure

Fig.5.1 shows the compaction characteristics for speswhite kaolin obtained by *Sivakumar* (1993). The figure shows compaction curves produced by the standard Proctor dynamic compaction (upper curve) and by the static compaction technique actually employed to produce the soil samples used in the programme of triaxial tests (lower curve). The static compaction curve was obtained by statically compacting the soil in 9 layers, each layer being given a vertical pressure of 400 kPa. Static compaction was selected in preference to dynamic compaction because it was envisaged that static compaction would give more repeatable results.

The optimum water content obtained from the standard Proctor compaction was 29% at a maximum dry density of about 1440 kg/m^3. The static compaction technique used by Sivakumar produced samples of lower density than the standard Proctor dynamic compaction (with a maximum dry density of about 1360 kg/m^3 at a water content of about 34%). This lower compactive effort was desirable, in order to produce samples at sufficiently low density that they could subsequently be consolidated to virgin states in the triaxial apparatus. It was considered desirable to prepare samples in a substantially unsaturated state, with a significant air content. *Sivakumar* (1993) therefore decided to prepare samples by static compaction at a water content of 25% (4% below the standard Proctor optimum and 9% below the static compaction optimum). This method produced compacted samples at a dry density of about 1210 kg/m^3 (see point P in Fig.5.1). The static compaction

procedure selected for the experimental research described in this thesis was identical to that employed by Sivakumar.

To prepare compacted soil samples, a known mass of dry kaolin powder (normally 1 kg) was thoroughly mixed with the required quantity of de-aired water (to give a water content of 25%) in a domestic food mixer for between 5 and 10 minutes. Large lumps of soil formed by the mixing process were broken down to smaller lumps by using a mortar and pestle.

The soil was then sieved through a 1.18mm aperture BS sieve and material passing through the sieve was transferred to a plastic bag. Material retained on the sieve was again ground and sieved as before. The process was repeated until only a very small amount of material was retained on the sieve. The preparation of mixed soil using this technique had to be done as quickly as possible to avoid moisture loss during grinding and sieving. The plastic bag containing the sieved soil was sealed with tape and kept in an air-tight container for at least 7 days. This allowed the moisture in the soil to distribute evenly throughout the mass. Water content tests on the soil showed that the moisture content remained constant even after several weeks. This preparation technique yielded sufficient material for two soil samples 50mm in diameter and 100mm long.

The split compaction mould, shown in Fig. 5.2, was made of brass and fabricated in the department. The mould consisted of three sections : a top collar, a middle section and a bottom collar. Each section was split vertically into two halves. The mould section was designed in such a way that dismantling was easy (see later) and caused little disturbance to the compacted sample. The middle section of the mould was 100 mm high and the top and bottom collars were used to prepare an over-length sample, which was subsequently trimmed to a length of 100 mm. The compaction mould was set on a rectangular brass base 120mm x 85mm in plan and 10mm thick. The mould was also provided with four 49.75-mm diameter steel plugs, having lengths of 112.5 mm, 87.5mm, 57.5mm and 17.5mm respectively. The plugs

were used in turn to compress the sample inside the mould when it was placed in the compression frame.

Three circular aluminium clamps were use to hold together the various sections of the split mould during compaction (see Fig.5.2). The top clamp was positioned at the interface between the top collar and the middle section of the mould, the middle clamp was positioned at the mid-height of the mould and the bottom clamp was placed at the interface between the middle section and the bottom collar. All clamps were provided with a tightening screw at one end. Hook-shaped guides on the middle and upper clamps were located on two vertical threaded bars mounted on the base plate (see Fig.5.2). These guides were held in place during compaction by wing nuts on the threaded bars, so that the entire split compaction mould was clamped firmly down onto the base plate.

The inner surfaces of the various sections of the compaction mould were sparingly cleaned with silicone grease to reduce friction during compaction. To prepare a compacted soil sample, 9 identical portions of the soil mixture, each weighing about 52.5 g, were taken from the sealed plastic bag and kept in a small sealed plastic container to prevent moisture loss to the atmosphere while each portion was being compacted in the mould in turn. The soil was then compacted in the compaction mould in 9 layers in a mechanical loading frame (see Fig. 5.3). A displacement rate of 1.5 mm/min was used and each layer was compressed to a vertical pressure of 400 kPa. This procedure was identical to that employed by *Sivakumar (1993)*. The top surface of each layer was scarified a little to provide better continuity with the oncoming layer.

After compaction, the mould was placed on a flat, rigid surface. The top clamp was loosened, by unscrewing the tightening screw, and pushed downward a little until it was clear of the interface between the top collar and the middle section. The top collar was removed first by inserting a sharp-ended knife into one of the vertical lines separating the two halves, after which they opened slightly. The two halves of the top collar were then removed completely from the mould. It was extremely

important to carry out this operation carefully to avoid damage to the sample. The top surface of the sample was then trimmed with a knife, flush with the top of the middle section of the mould.

To remove the bottom collar the mould was then turned upside down and the process of removing the bottom collar was exactly the same as the top collar. Again, the bottom surface of the sample was trimmed while it was still inside the middle section of the mould. Finally, to remove the middle section, all three clamps were removed and a sharp-ended knife was inserted into the top part of one of the vertical lines separating the two mould halves and the knife was then twisted a little. The two halves opened and the mould was turned upside down. The two halves were detached from each other as before and then completely removed from the compacted soil sample.

Immediately after its removal from the mould the soil sample was left exposed to the atmosphere for 30 minutes, so that the pore air pressure inside the sample equalized to atmospheric pressure. A period of 30 minutes was considered adequate for pore air pressure equalization, while keeping water content changes (due to evaporation) to an acceptably low level.

Sivakumar (1993) found that soil samples produced by the static compaction technique showed a maximum variation of bulk density throughout a given sample of only 1.4% (compared to 3.4% for dynamic compaction). Visual examination of soil samples compacted by the static method also confirmed that there was little evidence of significant interfaces between layers.

5.1.3 Measurement of sample dimensions

A portion of the compacted soil trimmed from the two ends of the sample was weighed, dried in the oven for 24 hours and then weighed again for water content determination. This served as a check on the consistency of the sample preparation technique with regards to water content. These water content tests showed values between 24% and 25% (the latter being the value of water content at which the soil

was originally mixed). After the 30 minute equalization period the sample was weighed to the nearest 0.01 g.

A technique to measure the specimen dimensions was devised by *Sivakumar* (1993) to enable measurements to be taken to a precision of 0.01mm. The apparatus for carrying out this operation is shown in Fig. 5.4. It consisted of a jig assembled on an aluminium base, fitted with a micrometer for measuring the sample height. The sample was placed on the aluminium base via a spacer, and an aluminium cap provided with an upstand which ran through a slot in the top jig assembly was placed on the top of the sample. A lateral retention spacer attached to the bracket supporting the micrometer provided horizontal alignment of the sample.

A dial gauge (facing upward) was horizontally mounted on a holder with its spindle pressing against one end of the micrometer holder (see Fig. 5.4). The intention was that, as the micrometer spindle moved downward, when it came in contact with the top cap upstand on the soil sample this triggered a movement of the dial gauge as the jig flexed slightly. A reading on the micrometer scale was then taken. The micrometer spindle was moved upward and the top cap spacer lifted so that the sample could be freely rotated a little and more readings were taken. An average reading from nine trials was taken. The soil sample was later replaced by a dummy or 'standard' sample made of solid brass having a length of 104.07 mm and measurements were taken in exactly the same fashion as for the soil sample. The length of the sample was given by the length of the dummy minus the difference in readings of the dummy and the sample taken by the vertical micrometer scale.

The diameter of the sample was taken as the average internal diameter of the split mould (49.997mm). This was subject to slight error, because of changes in sample diameter on removal from the mould and during the subsequent 30 minute equalization period. However *Sivakumar* (1993) found that this method was more reliable than attempting to measure the sample diameter with a micrometer, because of the difficulty of measuring accurately to the curved vertical surface of the compressible soil sample.

It was sometimes observed that a small amount of soil remained stuck to the inner sides of the compaction mould, but measurements of the weight of this soil indicated that it never exceeded 0.25% of the sample weight and normally it was considerably less than this. This problem would lead to a small error in the calculations of the overall volume of the specimen.

5.2 Setting-up in the triaxial cell

5.2.1 De-airing of apparatus

Before the sample was set-up in the triaxial apparatus the two GDS units , the lower chamber of the triaxial cell, the high air entry filter and the drainage line providing water back pressure had to be de-aired.

The de-airing procedure for the GDS units is shown in Fig. 5.5. The unit was laid on a slope, supported on a rigid wooden block. The piston of the GDS unit was driven forward towards the outlet forcing the water from inside the pressure cylinder into a container of de-aired water. This operation also forced out any trapped air bubbles from inside the pressure cylinder. The piston was then driven backward, so that de-aired water was taken back into the cylinder. The process was repeated several times until the GDS unit was properly de-aired. It was not necessary to de-air the GDS units every time a test was to be conducted if this procedure was properly performed.

To de-air the lower chamber of the triaxial cell, the de-airing procedure shown in Fig. 5.6 was adopted. The triaxial cell was placed on a wooden saddle in a slightly inclined position with the lower chamber pressure inlet at the highest point. Having positioned the cell as shown, the loading ram was positioned at the forward end of its travel (upper end in its normal orientation) and de-aired water was injected into the lower chamber through the pressure inlet of the cell (only one inlet was provided) by using a syringe. The loading ram was then pushed manually backward (downward in its normal orientation) to expel the water and any trapped air. As the loading ram

neared the end of its travel, a nylon tube from the pressure outlet of a de-aired GDS unit was quickly connected to the pressure inlet of the lower chamber of the triaxial cell. The GDS unit had previously been set to a small positive pressure, so that a steady outflow of water was emanating from the unit at the time of connecting to the triaxial cell (thus minimising the chances of trapping any air during connection). Once the connection had been made, the pressure of the GDS unit was reduced to zero, so that the weight of the loading ram took it down to its bottom position when the cell was returned to an upright position (leaving the maximum travel of the ram available for subsequent testing). The de-airing procedure for the lower chamber of the triaxial cell was done only once at the beginning of the test programme and it was not necessary to carry out this procedure again.

The apparatus used to de-air the high air entry filter is shown in Fig. 5.7. The filter system, consisting of high air entry filter, low air entry stone and perspex holder (see Fig. 4. 4) and the pedestal of the triaxial cell were securely screwed onto the base of the de-airing cell. The de-airing cell was filled with de-aired water through an inlet in the cell base and then connected to an air/water interface. The procedure of de-airing the filter involved four steps. Firstly with valve 1 open and valve 2 closed, the water pressure inside the cell was increased to 600 kPa and held at this value for 24 hours. This forced most of the air into solution. Secondly the drainage valve 2 was opened (still with valve 1 open and a pressure of 600 kPa applied) resulting in a slow flow of water through the high air entry filter. *Sivakumar* (1993) showed that for a properly prepared high air entry filter the flow of water through the filter was between 2 and 3 drops per minute. This flow through the filter, which was maintained for 24 hours, flushed any remaining air from the pore spaces of the filter. Thirdly drainage valve 2 was closed and the pressure of 600 kPa in the cell was left for a further 24 hours. Finally, the pressure supply valve 1 was closed, the drainage valve 2 was opened and the cell was left for another 24 hours while the pressure gradually decreased to zero. For a new (dry) filter the entire procedure was repeated once

more, after changing the water inside the cell, but for a filter that had been used previously and was still virtually de-aired this was unnecessary.

Immediately prior to setting up a soil sample, a triaxial cell pedestal with a de-aired high air entry filter system was taken from the de-airing cell and screwed onto the loading ram of the triaxial cell. De-aired water under a pressure of about 50 kPa from a bladder-type air-water interface was passed through the water back pressure line into the connecting groove at the top of the pedestal (beneath the high air entry filter system) and out via the flushing line, until the connecting tubes were completely de-aired. The valve on the flushing line was then closed, the pressure on the water back pressure line was reduced to zero and finally the valve on the water back pressure line was closed.

5.2.2 Setting-up a soil sample in the triaxial cell

Two lengths of fuse wire, 0.3mm in diameter and about 30mm in length, were placed on the top of the high air entry filter mounted on the pedestal of the triaxial cell. The intention was to prevent direct contact between the soil sample and the high air entry filter until the cell pressure was applied. Direct contact between the soil sample and the filter before the cell pressure was applied would transmit a large negative value of pore water pressure to the water in the filter and in the water back pressure line, which might induce cavitation in the water back pressure line. This technique, of using lengths of fuse wire to temporarily avoid contact between the sample and the high air entry filter, was first developed at Imperial College and was used successfully by *Sivakumar* (1993). The use of the fuse wire technique introduced a small error in the measurement of sample volume change, because the wires intruded into the bottom of the sample when the cell pressure was subsequently applied. This error was estimated at 0.59 cm^3 (based on the diameter of the fuse wire, which was 0.3mm, and the cross-sectional area of the soil sample), and the measurements of sample volume change during application of the cell pressure were adjusted accordingly.

The soil sample was carefully placed on the high air entry ceramic filter. A special Neoprene rubber membrane was slowly sleeved onto the specimen by using a membrane stretcher. An ordinary latex rubber membrane could not be used in the experimental work because the Dialla-B oil used as the cell fluid would attack it, causing the membrane to perish. The Neoprene membrane, which had a thickness of 0.35 mm, was stiffer than the standard latex membrane. Two 'O'-rings were used to seal the bottom of the membrane on the bottom pedestal. An ordinary porous stone, which had been dried in an oven for 24 hours, was placed on the top of the sample, followed by the perspex top cap with the air back pressure line already connected (see Fig. 4.8). Two more rubber 'O'-rings were used to seal the membrane on the top cap. Finally any excess rubber membrane was trimmed off with scissors.

5.2.3 Mounting of local strain gauges on soil sample

Three hollow tubes (16 mm internal diameter and 235 mm long) were sleeved onto the tie bars of the triaxial cell to provide a temporary support for the top plate of the cell while the local strain gauges were being mounted on the soil sample. The cell top plate was carefully placed in position so that the alignment collar attached to the load cell (see Fig. 4.3) located on the sample top cap. The purpose of this operation was to ensure verticality of the sample and to minimise sample disturbance while the local strain gauges were being mounted.

The arrangement of the radial and axial gauges on the sample is shown in Fig. 5.8. The positions of the feet of the axial gauges and the radial gauge were marked on the membrane with a permanent ink. Two circular studs, each with a conical recess to support the tip of one of the adjusting screws on the radial gauge arms, were glued to the membrane using a gel type superglue. The studs were positioned at the mid-height of the sample and diametrically opposite each other. The positions for the footing pads of the axial gauges were marked at a distance of 27.5mm from the top and bottom of the soil sample, giving a gauge length of 45 mm for each gauge. The two axial gauges were positioned diametrically opposite each other and at 90° to the

attachment points of the radial gauge (see Fig. 5.8). The axial gauges were assembled on the membrane one at a time by smearing the feet with superglue and then pressing them against the rubber membrane. It was extremely important to carry out this operation quickly and efficiently so that the axial gauges were properly mounted at the right positions on the rubber membrane. This was because the superglue bonded in seconds and improper mounting of the local strain gauges would affect the whole specimen set-up in the triaxial cell. The buoyant weights of the radial and axial gauges were supported by counterweight systems mounted on the triaxial cell wall (see next section).

Results from one of the early triaxial tests (Test 2) suggested that the local strain gauges attached to the membrane moved relative to the soil sample. The nature of the problem is shown in Fig.5.9, where the local strain readings (axial and radial) were plotted against time during the equalisation stage. There were abrupt changes in the axial and radial strains in very short intervals of time which it was thought were unlikely to represent sample deformation and were more likely to be caused by slippage of the membrane relative to the sample.

This problem of membrane slippage had not been observed in earlier tests using the same axial and radial gauges on reconstituted kaolin samples. There were two possible explanations for this. Firstly the adhesion between the rubber membrane and the surface of a compacted, unsaturated sample may not have been as great as for a reconstituted saturated sample. Secondly the Neoprene membrane was stiffer than a standard latex membrane and it did not grip the sample as well as a latex membrane. It was observed that after the shear test it was very easy to strip the Neoprene membrane from the sample, as if there was no frictional resistance between the sample and the membrane.

To rectify the problem of membrane slippage, from Test 3 onwards the inner face of each of feet of the axial gauges and the studs used to mount the radial gauge was provided with a pin which had a length of about 8mm and diameter of 0.3mm. A small hole was made in the footing or the stud and the pin was inserted so that it

tightly fitted the hole. During mounting of the gauges, the footing pads or the studs were slightly pressed into the soil sample. The perimeter of the footings pad and the studs in contact with the membrane was smeared with superglue to prevent leakage (see Detail 'x' in Fig. 5.8). This method prevented leakage effectively as the superglue bonded in seconds and sealed any gap between the membrane and the footings or studs. No evidence of leakage was observed in the later tests. This pinning method caused some localized disturbance to the soil fabric, but this was unavoidable. Further test results showed that the pinning method was successful in attaching the axial and radial gauges firmly to the soil sample and that there was no further evidence of membrane slippage (see Fig. 5.10 for typical test).

5.2.4 Cell asssembly

After attaching the radial and axial guages, the cell top plate and the hollow tubes sleeves supporting it were withdrawn. The acrylic cell wall was then placed in position.

Each axial strain gauge was suspended by a fine string attached to the canister of the gauge. The string passed over two pulley wheels which were supported on a cantilever attached to the cell wall (see Fig. 5.8). The other end of the string was tied to a brass weight with a buoyant mass in oil of about 49.5g, equal to the buoyant mass of the axial displacement gauge. The radial displacement gauge was suspended by two strings, one attached to each arm of the gauge. These two strings were tied directly to two hooks mounted on the cell wall. The whole operation of attaching the counterbalancing systems had to be done carefully to avoid disturbance to the specimen.

A ball bearing was placed in the conical recess within the top cap, and the exterior surface of the rubber membrane was then coated with a thin layer of silicone grease to reduce any attack by the cell fluid. The top plate of the cell was again placed in position and securely tightened against the cell wall. The alignment collar attached to the load cell was raised a little, by turning an adjusting nut provided on the cell top

plate, so that when the nuts on the tie-rods were tightened the alignment collar was well clear of the sample top cap. The alignment collar was then carefully lowered, by using the adjusting nut, until the sample top cap located within the alignment collar but the ball bearing was not yet seated in the recess with the collar. The required level was indicated by a line marked on the top cap.

Finally Dialla-B oil from a storage tank was pumped at a slow rate into the cell, via an inlet at the bottom of the cell base, until the cell was full. Any trapped air inside the oil supply line or within the cell escaped through a bleed valve in the cell top plate. The valve on the oil supply line and the bleed valve on the cell top plate were closed, and the test was now ready to proceed.

5.3 Test stages

5.3.1 Application of net stress

The valves on the water back pressure line and the air back pressure line were opened prior to ramping the cell pressure. The initial readings of the water back pressure, air back pressure and cell pressure were all set at zero. The GDS unit 1 supplying the cell pressure was then used to ramp the cell pressure at relatively fast rate of 2 kPa/min from zero to the required target values of 200 kPa in Tests 1, 2, 3, 4, 5 and 10, 400 kPa in Tests 6 and 7, 350 kPa in Test 8 and 450 kPa in Test 9.

When the cell pressure reached 40 to 50 kPa the air back pressure was manually increased to about 20 kPa by adjusting the pressure regulator on the air back pressure line.The air back pressure was manually increased in further steps of 10 to 20 kPa every few minutes as the cell pressure steadily increased. The difference between the cell presure and the the air back pressure at any time was kept to a minimum of 20 kPa to avoid the membrane being blown up inside the cell.

In Tests 1, 2, 3, 4, 5 and 10 the final value of air back pressure was set at 150 kPa while in Tests 6, 7, 8 and 9 the final value air back pressure was set at 250 kPa. This meant that the value of mean net stress $(p-u_a)$ for the subsequent equalisation

stage p_e' was 50 kPa in Tests 1, 2, 3, 4, 5 and 10, 100 kPa in Test 8, 150 kPa in Tests 6 and 7, and 200 kPa in Test 9 (see Table 5.1).

In Tests 1, 2, 3, 4, 5 and 10 the water back pressure was manually increased by using a pressure regulator on the water back pressure line, in a single step to 50 kPa when the air back pressure was beyond 70 kPa. In Tests 6, 7, 8 and 9 the water back pressure was increased to a final value of 150 kPa in three increments of 50 kPa each when the air back pressure readings were 100 kPa, 200 kPa and 250 kPa respectively. This meant that the final difference between air back pressure and water back pressure (i.e. the suction) was 100 kPa in all tests.

GDS Unit 1 stopped ramping when the target cell pressure was achieved. The cell pressure was maintained constant thereafter until the GDS was re-programmed. The stage normally took between 2 and 3 hours, depending upon the target value of cell pressure.

5.3.2 Equalization stage

The equalization stage followed immediately after the application of net stress. The purpose of the equalization stage was to enable the pore water pressure within the sample to equalize to the water back pressure value. During this stage, the suction (the difference between pore air pressure and pore water pressure) within the sample was brought down from its high initial (unknown) value after compaction to the required value s_o of 100 kPa in all tests (see Table 5.1). This reduction in suction took place at a mean net stress p_e' of 50 kPa in Tests 1, 2, 3, 4, 5 and 10, 100 kPa in Test 8, 150 kPa in Tests 6 and 7, and 200 kPa in Test 9.

The water inflow into the sample and the axial and radial strains of the sample were logged every 100 minutes throughout the equalization stage. The stage took 8 to 10 days to complete. Full equalization corresponded to no further flow of water into the sample, and the criterion used for terminating the stage was that the rate of water flowing into the sample had decreased to less than 0.1 cm^3 / day. This was

equivalent to a change in specific water volume v_w of less than 0.001 per day, given that the solids content of a typical sample was about 100 cm^3.

5.3.3 Ramped consolidation stage

In the ramped consolidation stage the suction was kept constant at 100 kPa, by maintaining air back pressure and water back pressure constant, while the value of mean net stress was increased to a final value p_o' of 400 kPa in all tests (see Table 5.1). This increase of p' was achieved by ramping the cell pressure with GDS unit 1 to a new target value of 550 kPa in Tests 1, 2, 3, 4, 5 and 10 and 650 kPa in Tests 6, 7, 8 and 9.

Ramped consolidation was preferable to conventional step-loading consolidation, so as to limit the excess pore water pressure generated at the top face (water undrained) of the sample to an acceptably low value. A particular problem associated with the generation of high excess pore water pressure in unsaturated samples is illustrated in Fig. 5.11. Fig 5.11 shows Loading-Collapse yield curves for unsaturated soil as proposed by *Alonso, Gens and Josa* (1990). *Sivakumar and Wheeler* (1993b) pointed out that for a point within the interior of an unsaturated sample subjected to a step increment of total stress the stress path would be of the form ABC shown in Fig.5.11. As the increment of total stress is applied to the sample, excess pore air and pore water pressures are generated. The excess pore air pressure dissipates quickly, because of the high air permeability, but the excess pore water pressure takes much longer to dissipate because of the relatively low water permeability. As a result, the stress state moves initially from A to B (at the desired final value of p' but a reduced suction s) and it then moves slowly at constant p' from B to the desired final point C, as the excess pore water pressure dissipates. The consequence of this stress path ABC is that the yield curve expands from an initial position Y_A to a position Y_B during stress path AB and it then remains at this position (Y_B) during stress path BC (which corresponds to elastic unloading inside the yield curve). Thus the soil is not at a virgin state at the end of consolidation, and additional

plastic compression has occurred (compared with the desired stress path direct from A to C). It is therefore very important that consolidation of unsaturated soil samples should be done in a ramped fashion, to ensure that the excess pore water pressure remains acceptably small and the suction is held sensibly constant. This ramped technique was employed in the experimental work.

Another advantage of using ramped consolidation was that it was possible to produce continous plots of specific volume v or specific water volume v_w against the mean net stress p'. These represented constant suction compression curves if the external load (cell pressure) was applied slowly enough that the excess pore water pressure was minimal throughout the loading process. The continuous plot of v versus p' was useful in accurately identifying the yield stress produced by the compaction process.

Thomas (1987) presented a relationship for the equilibrium value of excess pore water pressure u_{ex} produced at the undrained face of a saturated soil sample loaded by ramped consolidation with the total stress increasing with time at a constant rate A

$$u_{ex} = \frac{Ah^2}{2c_v} \tag{5.1}$$

where c_v was the coefficient of consolidation and h was the drainage path length. u_{ex} is the value to which the excess pore water pressure would tend if ramped loading continued indefinitely. The value of c_v for compacted unsaturated speswhite kaolin was measured as $c_v = 7.1*10^{-8} m^2/s$ by *Sivakumar* (1993) from trial step-loading isotropic consolidation tests. Inserting $c_v = 7.1*10^{-8} m^2/s$ and h = 100 mm into equation (5.1) the following relationship was obtained;

$$u_{ex} = 19.5A \tag{5.2}$$

where A was the rate of increase of cell pressure expressed as a rate per hour. A rate of increase of cell pressure of 1.2 *kPa/hr* was selected, suggesting an equilibrium value of excess pore water pressure at the undrained face of about 24 kPa. This was considered acceptably small, as it corresponded to only 6% of the final value of p' of 400 kPa. With this rate of pressure increase, the ramped consolidation stage took approximately 14 days. Although a slower rate of presure ramping would have decreased the calculated value of excess pore water pressure below 24 kPa, it would have resulted in fewer tests being achieved within the research programme.

It should be pointed out that Equation 5.1 was strictly true only for saturated soil. In the case of unsaturated soil, the equilibrium value of excess pore water pressure generated at the undrained face would be probably be less than predicted by Equation 5.1 (because of the undrained compressibility of an unsaturated sample).

At the end of ramped consolidation, when p' reached 400 kPa, a period of 24 hours was allowed for complete dissipation of any excess pore water pressure.

5.3.4 Swell-back stage

In the swell-back stage the mean net stress p' was reduced from 400 kPa to a lower value p_c' which varied for the different tests between 100 kPa and 300 kPa, as shown in Table 5.1.The suction s was held constant during this reduction of p'. The reduction of p' was achieved by decreasing the cell pressure at the same rate of 1.2 kPa/hr used in the previous ramped consolidation stage.

In Tests 2, 4, 7 and 10, p' was decreased from 400 kPa to 300 kPa; in Tests 1,3, 5 and 8, p' was decreased from 400 kPa to 200 kPa ; and in Test 6, p' was decreased from 400 kPa to 100 kPa (see Table 5.1). No swell-back stage was included in Test 9, so that p' remained at 400 kPa.

A period of 24 hours was allowed to elapse after the sample reached its target p_c' value of 100, 200 or 300 kPa, to ensure complete equalization of pore water pressure throughout the sample.

5.3.5 Suction-change stage

In this stage the suction was increased from 100 kPa to 200 kPa or decreased from 100 kPa to zero. Four tests involved a suction increase to 200 kPa (Tests 5, 7, 8 and 9, see Table 5.1), while one test involved a suction decrease to zero (Test 6, see Table 5.1). In the remaining tests (Tests 1, 2, 3, 4, 5 and 10) no suction change stage was included, and the suction therefore remained at 100 kPa. In Test 6, the reduction of suction to zero took place after the swell-back to a mean net stress of 100 kPa. In the tests where suction was increased to 200 kPa, this took place before any swell-back (at $p_o^{'}$ = 400 kPa) in Tests 8 and 9, but after swell-back (at $p_c^{'}$=200 kPa or 300 kPa) in Tests 5 and 7.

The suction change was carried out by adjusting the water back pressure regulator manually while keeping the cell pressure and the air back pressure constant. The water back pressure was adjusted manually in small steps at a rate of about 24 kPa/day. Unfortunately adjustment of the water back pressure was not possible during the night (a period of about 12 hours). Increments of water back pressure were applied manually at intervals of about four hours during the day and then left overnight for about 12 hours with a single large increment applied the following morning.

On reaching the target value of applied suction (200 kPa or zero), the sample was left to achieve equilibrium , until the rate of flow of water entering or leaving the sample was less than 0.1 cm^3 / day (a rate of change of specific water volume of less than 0.001 per day).

5.3.6 Reloading / shear stage

In the final reloading stage the sample was either isotropically re-loaded at constant suction or sheared at constant suction. For isotropic reloading (Tests 3, 5 and 6, see Table 5.1) the cell pressure was ramped at a rate of 1.2 kPa/hour while the water back pressure and the air back pressure were held constant. All but one of the

remaining tests involved drained shearing with the cell pressure, water back pressure and air back pressure all held constant (giving $\Delta q / \Delta p' = 3$).

In one test (Test 4) an attempt was made to carry out a shear test with p' constant ($\Delta q / \Delta p' = \infty$), by reducing the cell pressure during shearing. For constant p', $\Delta\sigma_3 = -0.5\Delta\sigma_1$, so the cell pressure was reduced at half the rate at which the axial stress was increased (this test was performed under stress-control, with GDS Unit 1 (providing the cell pressure) and GDS Unit 2 (providing the lower chamber pressure) both set to ramp pressure at a constant rate). Unfortunately, it was found that fluctuations of loading ram friction resulted in major deviations from the desired stress path (see Section 6.7), and it was therefore concluded that this form of stress path testing was impractical without the provision of feedback control. The purchase or development of software for such feedback control was not possible within the budget or timescale respectively of the project, and therefore no further attempt was made to conduct constant p' shear tests.

The drained shear tests at constant cell pressure ($\Delta q / \Delta p' = 3$) were all performed under strain control, because the fluctuations of loading ram friction made stress control an undesirable option without the provision of feedback control to the lower chamber pressure. The method for determining the required rate of strain in the shear stage was based on the equation proposed by *Bishop and Henkel* (1962) for the time t for a sample to reach 95% dissipation of excess pore water pressure. The equation is given as

$$t = \frac{20h^2}{\eta c_v} \tag{5.3}$$

where h was half the sample height, η was a factor depending on the drainage conditions at the sample boundaries ($\eta = 0.75$ for drainage from one end only) and c_v was the coefficient of consolidation. Using $h = 50$ mm and $c_v = 7.1 * 10^{-8} m^2 / s$, t was found to be about 10 days. The prime objectives of the test were to investigate soil

yielding and the elastic behaviour of the soil before yielding. A trial test showed that yielding occurred at axial strains of less than 2%. Therefore the early part of the shear test, up to an axial strain of 2.5% to 3%, was conducted at a displacement rate of about 0.00018 mm/min, giving an axial strain rate of about 0.26% per day. The remainder of the shear stage was done at a faster rate of 0.0018 mm/min, giving a strain rate of about 2.6% per day.

Shearing was discontinued when the limit of travel of the loading ram of the triaxial cell was reached (at an axial strain of about 24%). This often preceded attainment of a true critical state. The entire shear stage normally took about 18 days to complete.

5.3.7 Dismantling of cell

When the test was completed, logging was halted and the valves on the water back pressure line and the air back pressure line were closed. All applied pressures were reduced to zero, the bleed valve in the cell top plate was opened and oil was then drained from the triaxial cell into the storage tank under the bench. The cell top plate was carefully removed and the acrylic cell wall was detached from the cell base. The axial gauges were removed from the membrane by cutting the membrane around footing pads. The radial gauge was dismantled by slightly pulling the arms of the gauge away from the sample. Finally the rubber membrane was stripped from the sample.

The wet weight of the sample was measured to the nearest 0.01 g and the sample was then dried in an oven for 24 hours before measuring the dry weight. The wet weight of the sample at the end of the test was considered less reliable than the value measured at the beginning of the test, because of the difficulty of preventing additional water or oil contaminating the sample during dismantling of the cell. The wet weight of the sample at the beginning of the test was therefore used in the subsequent calculations of the variation of specific water volume v_w throughout the

test, and the final value of the wet weight was simply used as an additional check on the consistency of the results.

5.4 Logging procedure

The Quicklog PC™ software was used to log all transducer channels every 100 minutes throughout the complete test.

5.4.1 Transfer of logged data to LOTUS 1-2-3 spreadsheet

The raw data from the test were stored in the floppy disk in the form of a spreadsheet, but no manipulations were possible because the Quicklog PC software lacked these facilities. Instead the raw data was transferred to a LOTUS 1-2-3 spreadsheet and saved as a LOTUS 1-2-3 worksheet file for further manipulations. The Quicklog PC™ software logged data from every channel for every stage of the tests. However for some stages, data from some of the channels were irrelevant. For example, the external axial displacements and deviator load were not relevant in the ramped consolidation stage because the loading ram was not in contact with the sample. In these circumstances the irrelevant data were simply not used in the calculations.

5.4.2 Voltage corrections

It was observed that while a test was in progress, the input voltages from the 5V DC and 10V DC supplies fluctuated slightly with time (probably due to variation in the mains supply). In the worst case the fluctuation was about ±0.2 V in the 5V DC supply as recorded during the equalization stage in Test 4. The variation of the 5V supply in this worst case is shown in Fig 5.12. This variation resulted in fluctuations of the local axial and radial gauge readings. The typical variation in the 5V input voltage was much less than shown in Fig.5.12, at about ± 0.004V.

To overcome the problem of fluctuating supply voltages a number of steps were taken. Firstly, from Test 4 onwards a filtering device RS 236-924 (maximum

current 13 Amp) was plugged into the mains power socket and then connected to the 5V and 10V power supplies via a multiple socket. The 5V and 10V power supplies then showed more stabilised voltages, with the voltage fluctuation now being ± 0.003V on the 5V supply (see Fig.5.13). Secondly, from Test 4 onwards the 5V and 10V power supplies were continously logged (using channels 8 and 12 of the logging system), and the calibration equations for the local axial and radial strain gauges were continously corrected for the current value of the input voltage to the gauges.

A simple test was carried out to see the effect of variations in the input supply voltage on the output of the axial and radial gauges, within the range of ±0.2V . This showed that the output voltage was directly proportional to the input supply voltage, so the appropriate calibration equations for the local gauges were adjusted accordingly. No adjustments for supply voltage were considered necessary for any of the remaining transducers.

5.5 Calculation of stress and strain parameters

5.5.1 Calculations of strains

Axial strain ε_1 was measured over a gauge length of about 45 mm centred on the mid-height of the soil sample. Theoretical analysis by *Moore* (1966) suggested that the stresses and strains over the central part of the sample were relatively uniform. Two measurements of axial strain were made on opposite sides of the sample, with ε_1 based on the average of the two measurements (to avoid any effects of sample tilting).The axial strain ε_1 during any stage of a test was calculated from the relative movement of the axial displacement gauge footings during the stage divided by the separation of the footings at start of the stage

Radial strain ε_3 was measured at the sample mid-height. The radial strain ε_3 was calculated from the change in separation of the radial displacement gauge divided by the gauge length (sample diameter) at the start of the stage.

The shear strain ε_s was then given by :

$$\varepsilon_s = \frac{2}{3}(\varepsilon_1 - \varepsilon_3) \tag{5.4}$$

and the volumetric strain ε_v was given by :

$$\varepsilon_v = 1-(1-\varepsilon_1)(1-\varepsilon_3)^2 \tag{5.5}$$

Compressive strains were considered positive and tensile strains were considered negative.

5.5.2 Calculation of deviator stress

The deviator stress q during the final reloading/shear stage was given by

$$q = F/A \tag{5.6}$$

where F was the deviator force and A was the current cross-sectional area of the central part of the sample which was based on the measurements from the radial displacement gauge. However the deviator stress q had to be corrected to take account of the membrane stiffness. The correction for membrane stiffness as given by *Bishop and Henkel* (1962) was

$$\sigma_r = \frac{\pi DM\varepsilon_1(1-\varepsilon_1)}{A_o} \tag{5.7}$$

where D was the diameter of the sample at the start of shearing, M was the membrane modulus, ε_1 was the axial strain during the shear stage and A_o was the cross-sectional area of the central part of the sample at the start of shear test. The value of σ_r

obtained from Equation (5.7) was substracted from Equation (5.6) to get the corrected deviator stress.

The method of determining the membrane modulus M was in accordance with that of *Bishop and Henkel* (1962), but the test method was modified to investigate the variation of M with the time of exposure to the cell fluid and the cell pressure at which the exposure took place (because of deterioration of the rubber in the Diala-B oil). Three newly cut loops of Neoprene membrane, each 25 mm wide, were soaked and pressurised in Diala-B oil (the cell fluid) in a pressure cell as shown in Fig. 5.14. These rubber loops were tested at a confining pressure of 450 kPa and another three were later tested at 550 kPa (the latter was the maximum cell pressure applied in any triaxial test). For each set of three membrane loops, the membrane modulus M was measured after various intervals of time up to 48 days (the duration of a typical triaxial test), using the method given by *Bishop and Henkel* (1962), as shown in Fig.5.15. After testing, the Neoprene membrane loops were put back into the pressurising cell, where they were left for a further interval of time before re-testing.

The variation of membrane modulus with time is shown in Fig. 5.16. For both confining pressures the modulus M dropped sharply during the first 10 to 15 days of exposure to the oil, after which the reduction of M with time was more gradual. From an initial value for fresh unsoaked membrane, of about 2.4 kN/m width, the value of M dropped after 40 days to about 1.4 kN/m width at σ_3 = 450 kPa and to about 1.2 kN/m width at σ_3 = 550 kPa. The behaviour shown in Fig.5.16 suggested that coating the membrane with silicone grease did not fully eliminate attack of the membrane by the Diala-B oil.

The variation of membrane modulus with time was relatively slight for the period corresponding to the final re-loading/shear stage of the triaxial tests (after about 28 days of exposure to the oil). The procedure used was therefore to measure a value of M at the end of each triaxial test (on the actual membrane used in the test) and then to assume that this value of M was applicable throughout the re-

loading/shear stage of that test. The values of M measured on completion of the triaxial tests were generally consistent with the curves shown in Fig. 5.16.

5.5.3 Calculation of mean net stress

The mean net stress p' was calculated as follows

$$p' = \sigma_3 + \frac{q}{3} - u_a \tag{5.8}$$

where σ_3 was the cell pressure, q was the deviator stress and u_a was the pore air pressure.

5.5.4 Calculation of specific volume

The specific volume v, during any stage of the test, was calculated from

$$v = \frac{V_o(1-\varepsilon_v)}{V_s} \tag{5.9}$$

where V_o was the sample volume at the start of the stage, ε_v was the volumetric strain during the stage and V_s was the volume of solid particles (calculated from the dry weight of the sample measured at the end of the test and the specific gravity of the soil particles). The value of V_o for each stage was calculated from the initial sample volume measured at the beginning of the test, which was then corrected for any volumetric strains in preceding test stages.

5.5.5 Calculation of specific water volume

The specific water volume v_w, defined in Equation 2.36 was calculated from

$$v_w = \frac{V_{wo} + \Delta V_w}{V_s} \tag{5.10}$$

where V_{wo} was the volume of water within the sample at the start of the stage and ΔV_w was the inflow of water into the sample during that stage. The value of V_{wo} for the first test stage was calculated as the difference between the wet weight of the sample measured at the beginning of the test and the dry weight of the sample measured at the end of the test. Values of V_{wo} for subsequent test stages were corrected for any water inflow or outflow from the sample during preceding stages.

The degree of saturation S_r was calculated from

$$S_r = \frac{v_w - 1}{v - 1} \tag{5.11}$$

5.6 Programme of tests

The test programme is shown in Table 5.1. A total of 10 tests were conducted, with an average duration for each test of 45 days.

After equalization to a suction s_o of 100 kPa at a mean net stress p_e', which varied between 50 kPa and 200 kPa in the different tests (see Table 5.1), all samples were consolidated to mean net stress p_o' of 400 kPa at a constant suction s_o of 100 kPa. Subsequent test stages involved swell-back to a lower value of mean net stress p_c', change of suction to a value s_c and then a reloading / shear stage at constant suction and various values of $\Delta q/\Delta p'$ (see Table 5.1). The tests were divided into three different series, based on the value of suction s_c during the final reloading stage.

5.6.1 Test series at $s = 0$

Only one test (Test 6) was included in this series, where the suction was decreased to zero after first establishing the position of the yield surface by consolidating at a suction of 100 kPa to a mean net stress of 400 kPa. The stress path is shown in the s-p' and q-p' planes in Fig. 5.17 (a). The value of mean net stress during equalisation p_e' was 150 kPa and after consolidation to a mean net stress p_o' of 400 kPa at a suction of 100 kPa, the sample was allowed to swell-back at a suction of

100 kPa to a mean net stress of 100 kPa. The suction decrease from 100 kPa to zero, was done after the swell-back stage at mean net stress p_c' of 100 kPa. During the reloading stage, the sample was loaded isotropically ($\Delta q / \Delta p' = 0$) at a constant suction of zero. The test was terminated at a mean net stress of 590 kPa, considerably after passing the yield point.

5.6.2 Test series at s = 100 kPa

The stress paths in the s-p' plane and q-p' plane for tests in this series are shown in Fig. 5.17 (b). Five tests were performed (Tests 1, 2, 3, 4 and 10). The value of mean net stress during equalization p_e' was 50 kPa for all five tests. After consolidation at a suction of 100 kPa to mean net stress p_o' of 400 kPa , each sample was allowed to swell-back at a constant suction of 100 kPa to a mean net stress p_c' of 200 kPa (Tests 1 and 3) or 300 kPa (Tests 2, 4 and 10).

In Test 3 the sample was isotropically reloaded ($\Delta q/\Delta p'=0$), and in Tests 1, 2 and 10 the samples were sheared at constant cell pressure ($\Delta q / \Delta p' = 3$). Test 10 was a repeat of Test 2. In Test 4, an attempt was made to conduct constant p' shearing ($\Delta q / \Delta p' = \infty$), by reducing the cell pressure during shearing, but this was not entirely successful (see Sections 5.3.6 and 6.7). For all five tests in this series the reloading/shear stage was conducted at a constant suction of 100 kPa.

5.6.3 Test series at s = 200 kPa

Fig. 5.17 (c) shows the stress paths in the s-p' plane and q-p' plane for tests done in this series. Four tests were included (Tests 5, 7, 8 and 9). The values of mean net stress during equalisation p_e' for Tests 5, 7, 8 and 9 were 50 kPa, 150 kPa, 100 kPa and 200 kPa respectively. In Tests 5 and 7, the suction increase from 100 kPa to 200 kPa was performed after the swell-back stage, whereas in Test 8 the suction increase was applied before the swell-back stage. No swell-back was done in Test 9. The sample in Test 8 was reloaded isotropically at a constant suction of 200 kPa. All

remaining samples in the series were sheared with $\Delta q / \Delta p' = 3$ at a constant suction of 200 kPa.

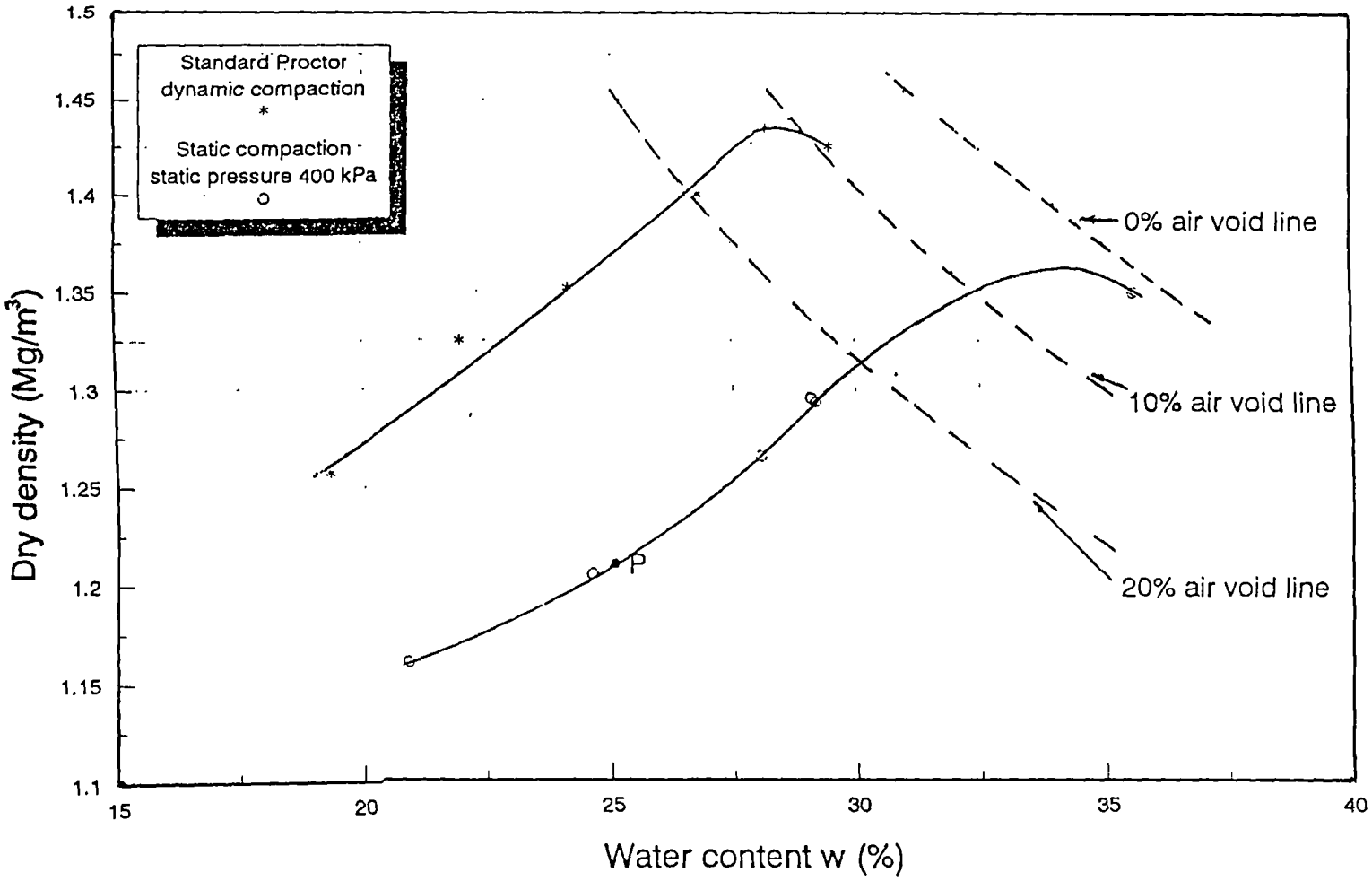

Fig. 5.1 : Compaction characteristics for speswhite kaolin
(reproduced from Sivakumar, 1993)

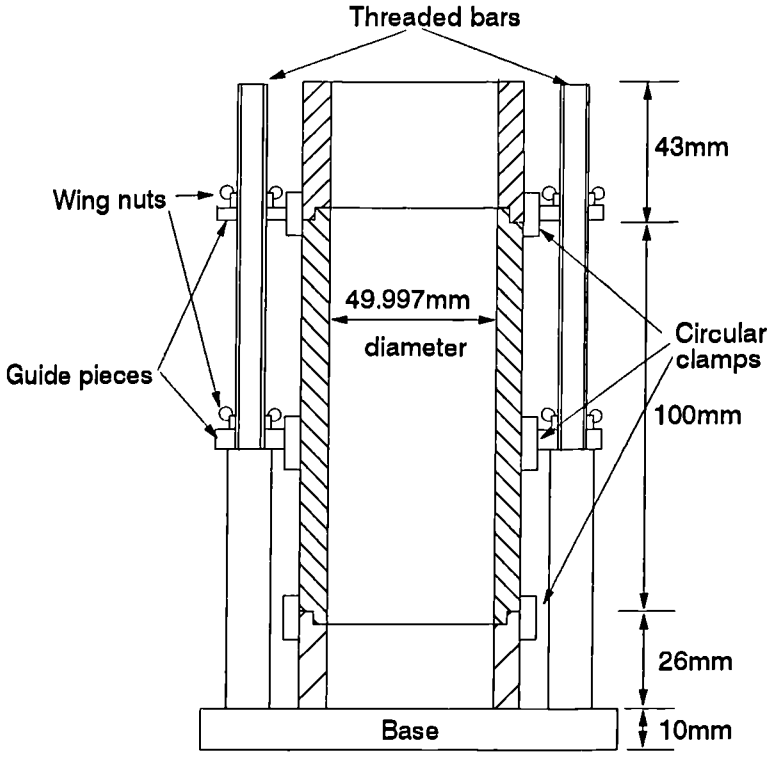

Sectional elevation across X-X

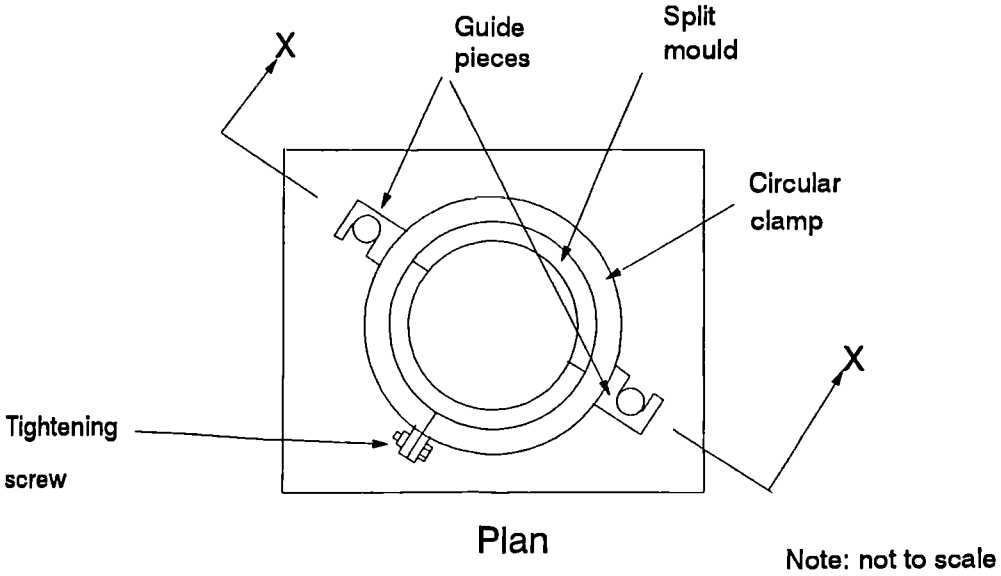

Plan

Note: not to scale

Fig. 5. 2 : Compaction mould

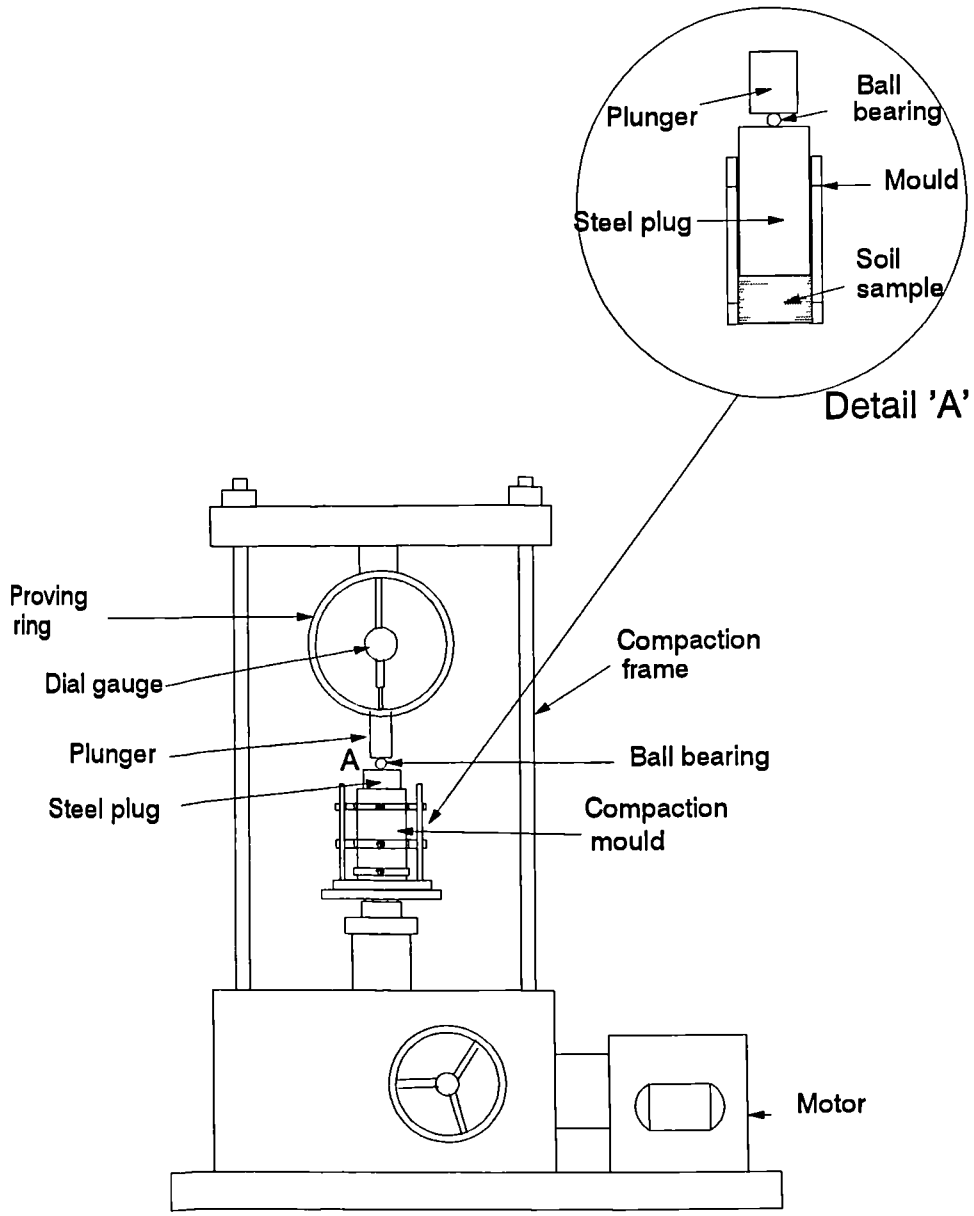

Fig. 5.3 : Compaction of soil sample in compression frame

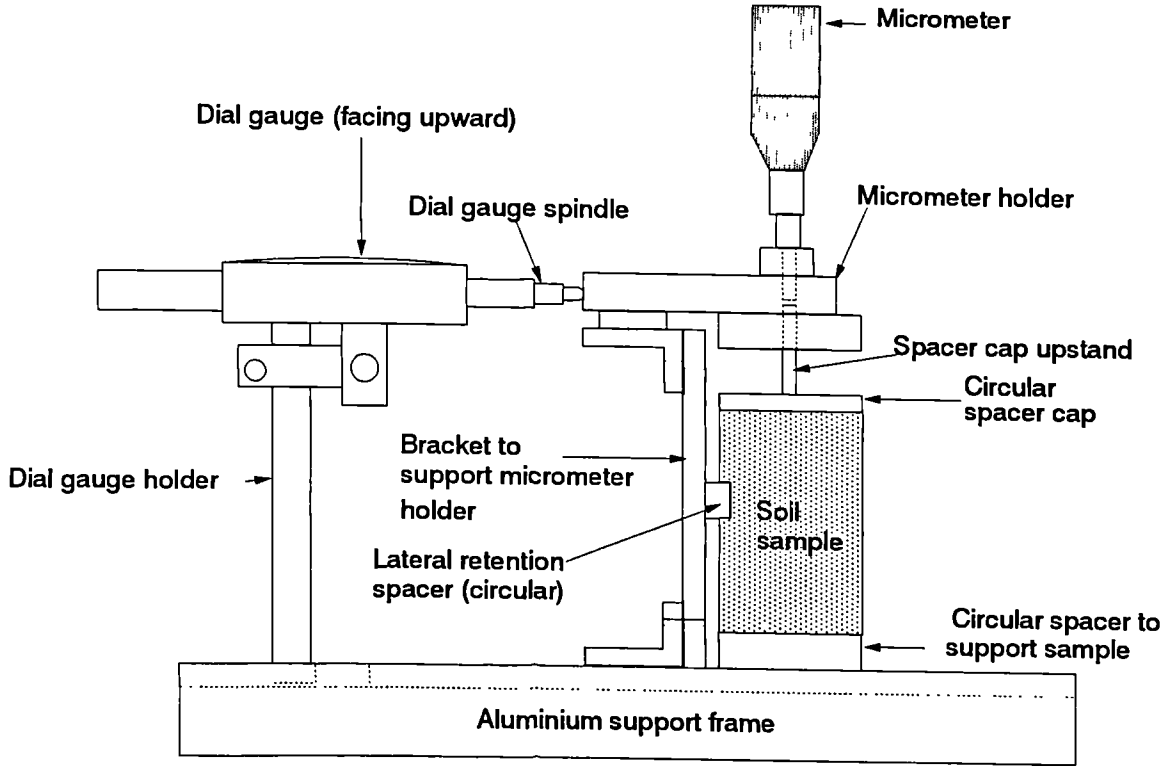

Note : not to scale

Fig. 5.4 : Method of measuring sample height

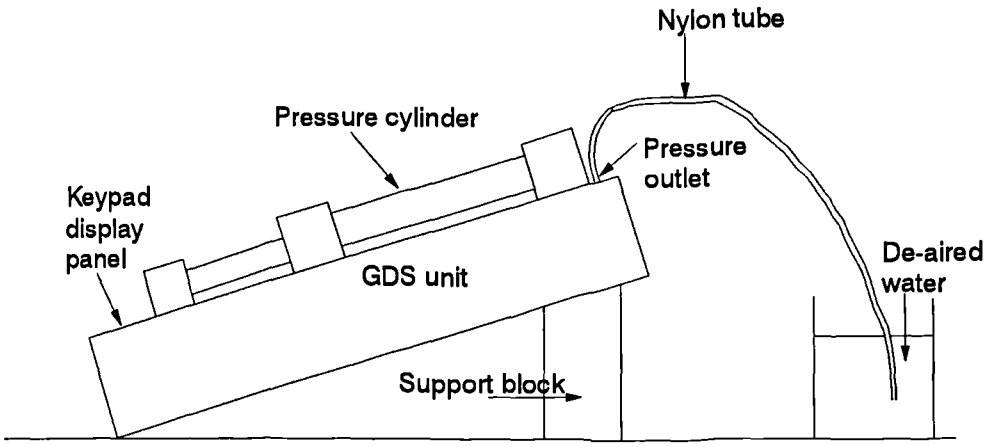

Fig. 5.5 : De-airing of GDS unit

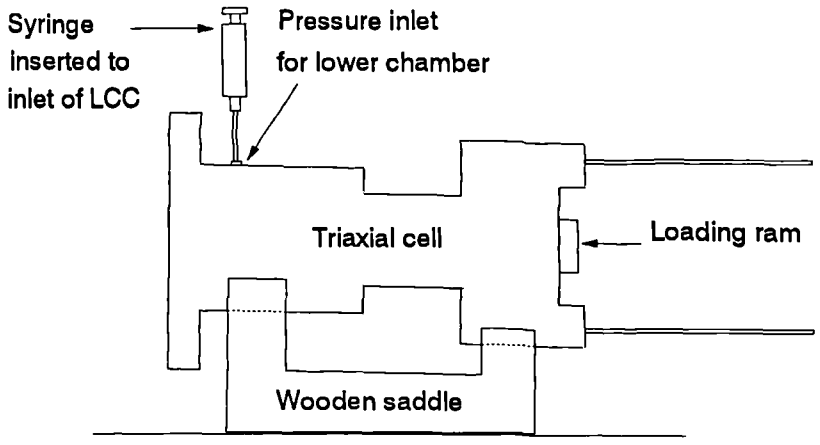

Fig. 5.6 : De-airing of lower chamber of triaxial cell

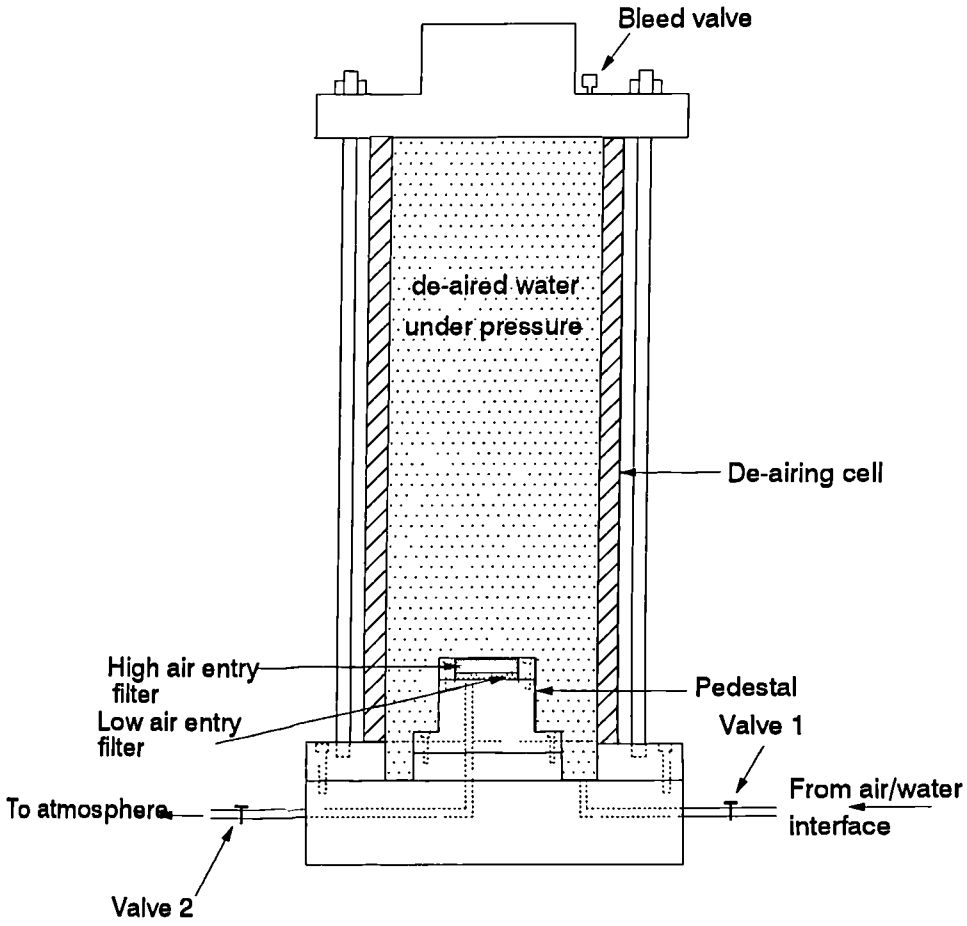

Fig. 5.7 : De-airing of high air entry filter

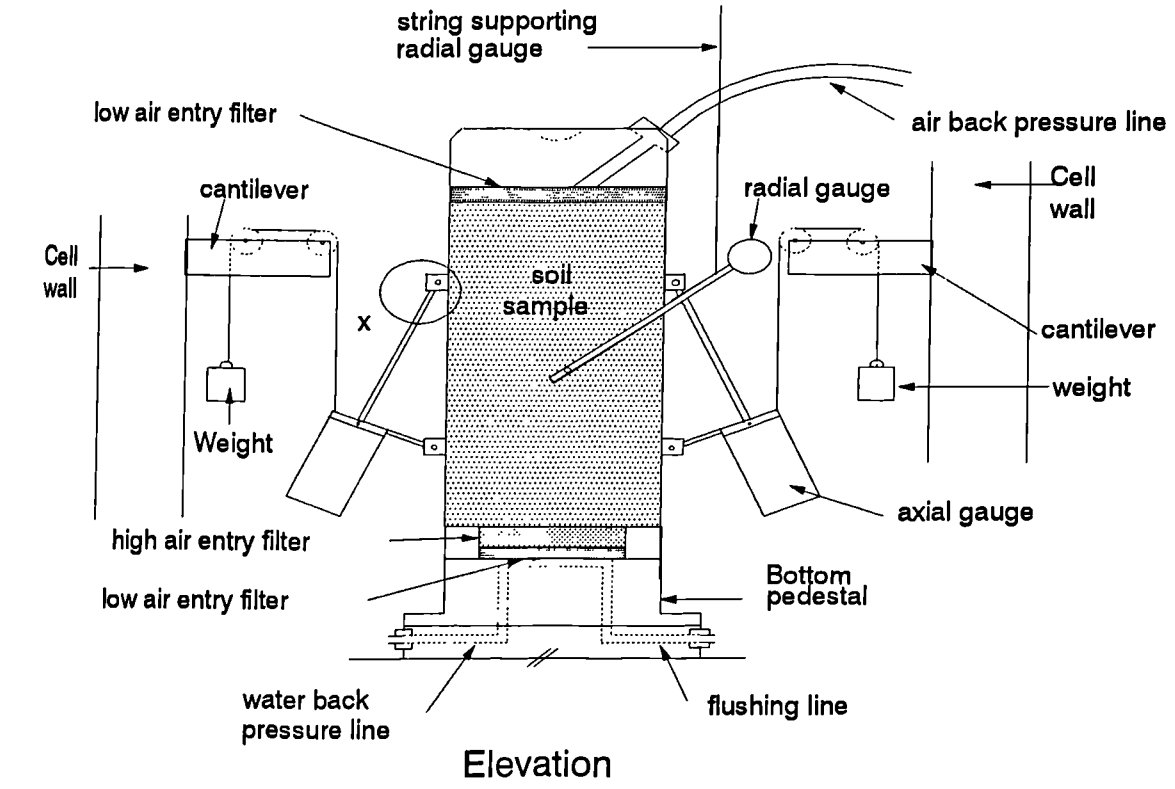

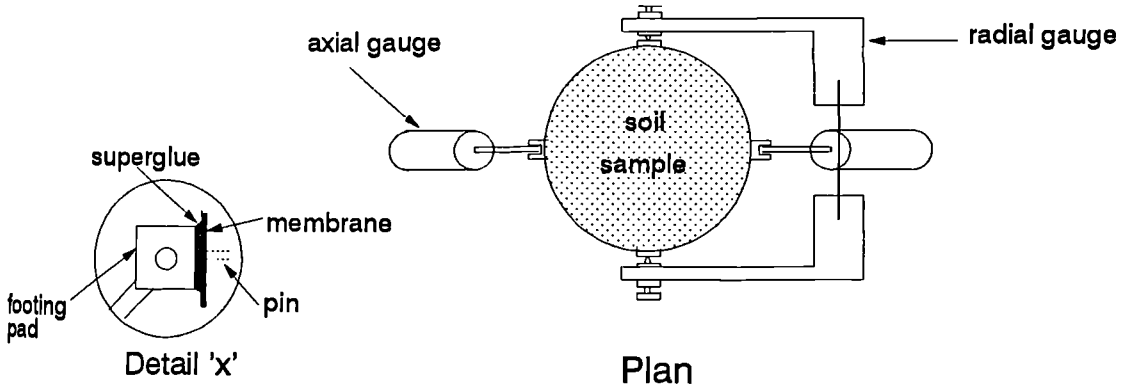

Fig. 5.8 : Local strain gauges mounted on soil sample

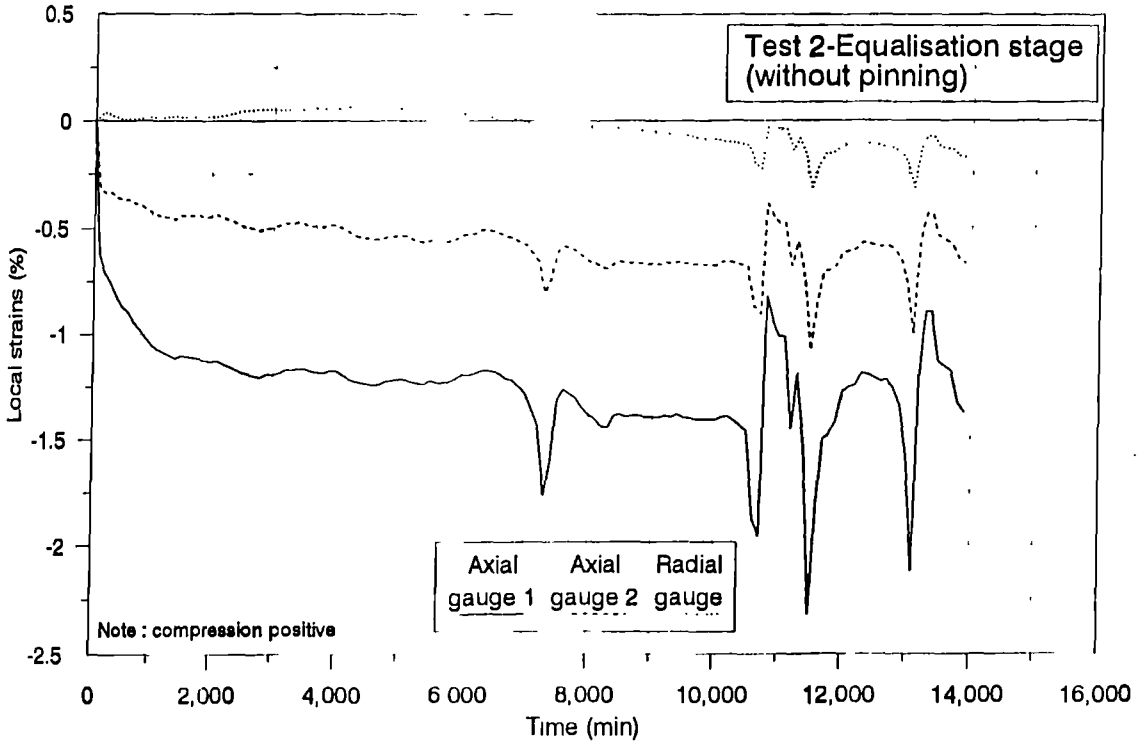

Fig. 5.9 : Membrane slippage observed in Test 2

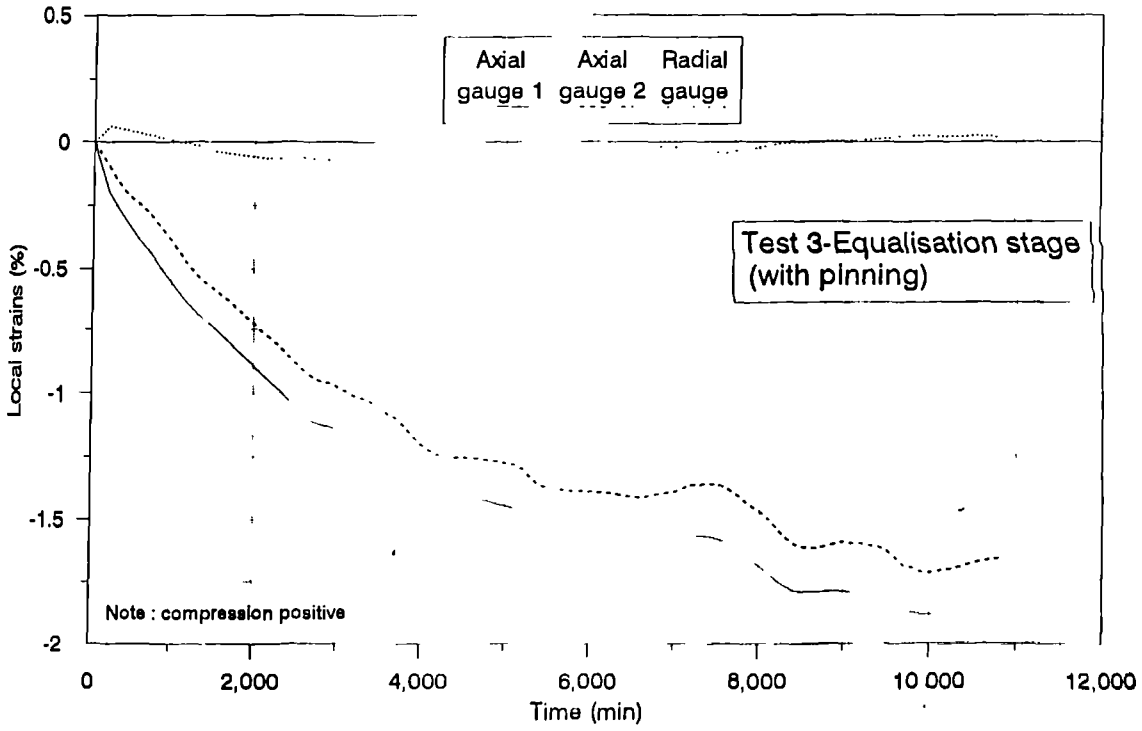

Fig. 5.10 : Typical strain readings after using pinning method

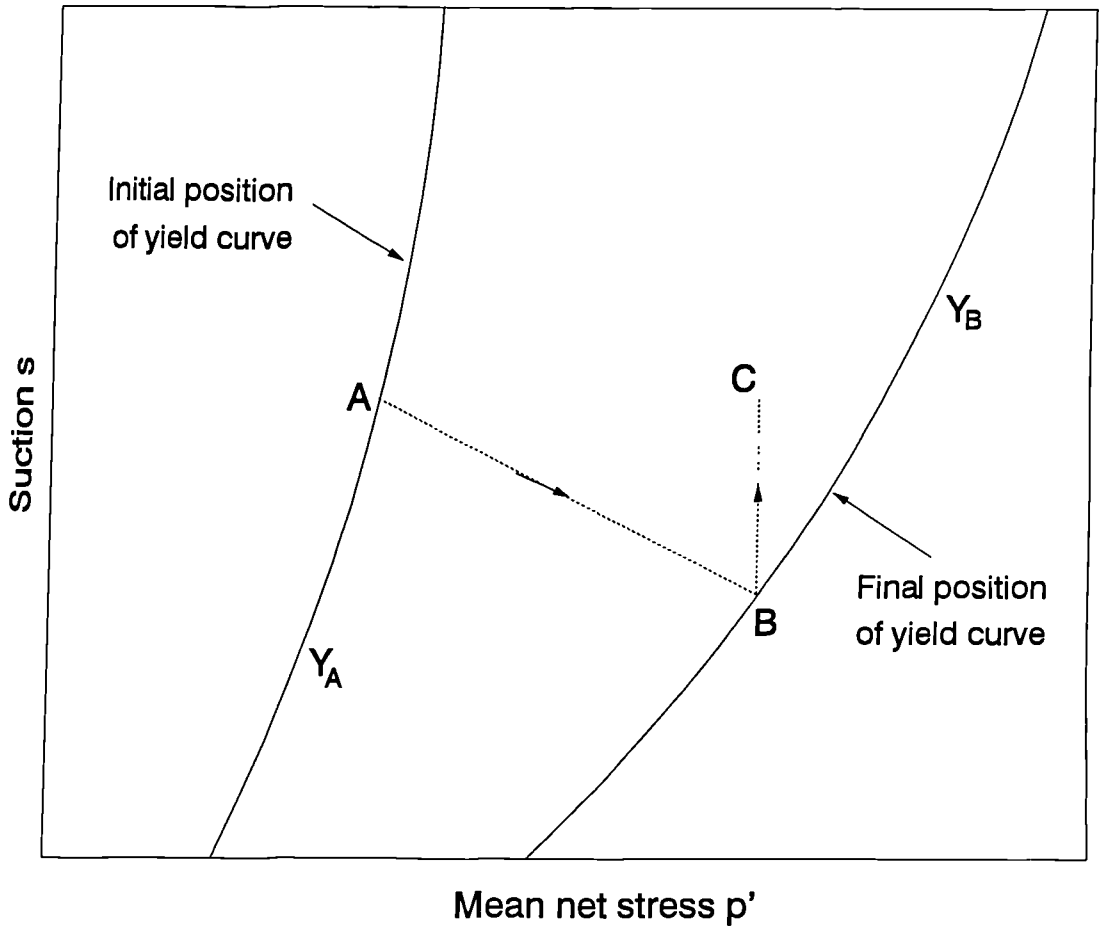

Fig. 5.11 : Stress path for isotropic consolidation by step-increment of cell pressure
(after Sivakumar and Wheeler, 1993)

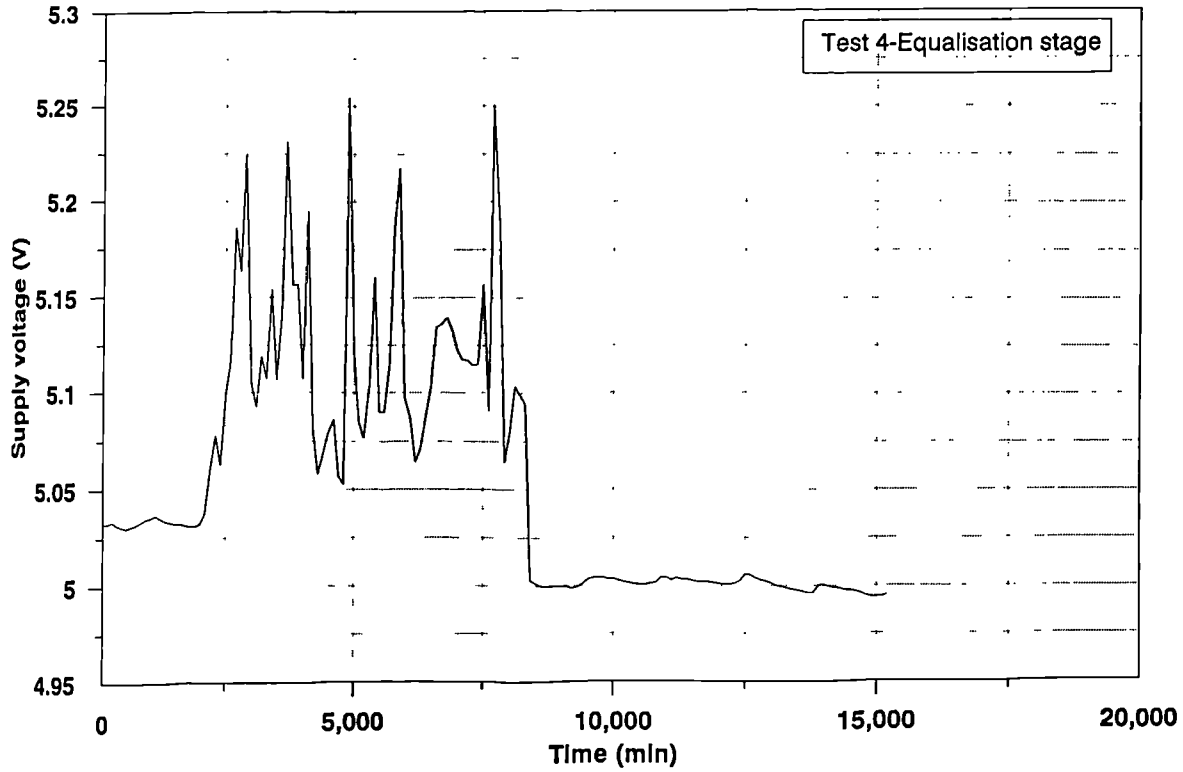

Fig. 5.12 : Variation of 5V supply with time during worst test (without filtering)

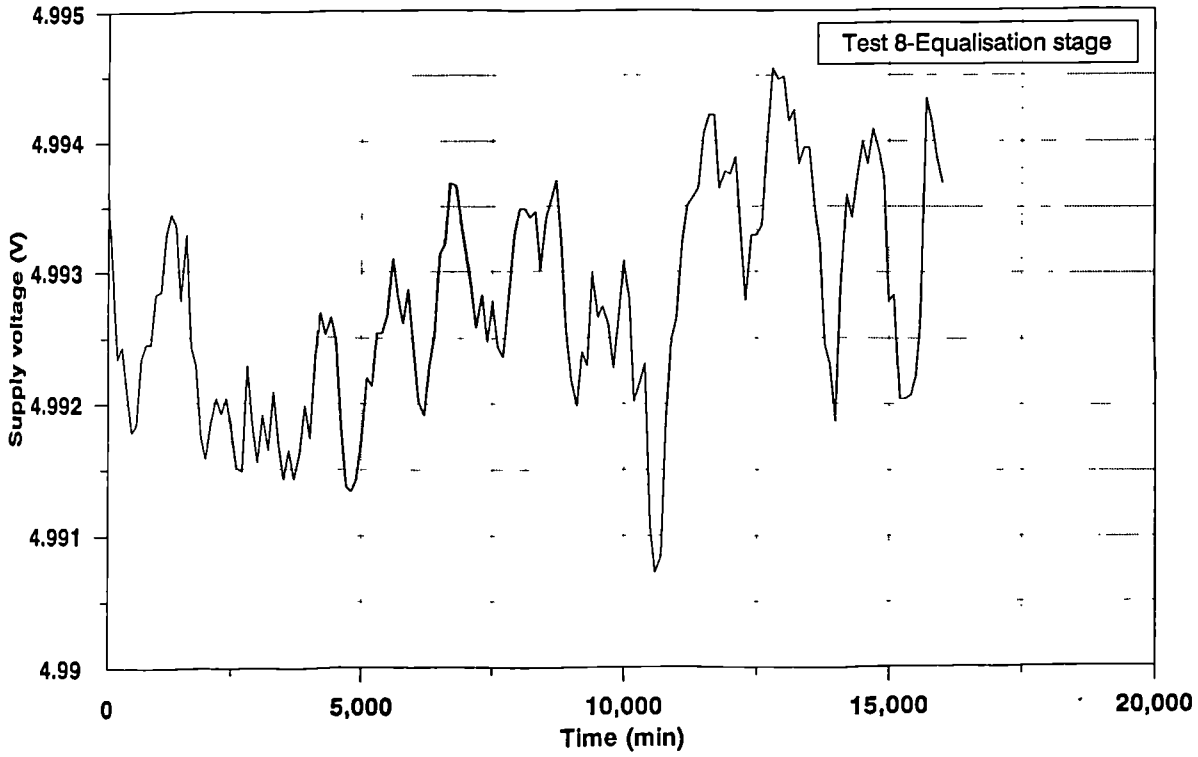

Fig. 5.13 : Variation of 5V supply with time during typical test (after filtering)

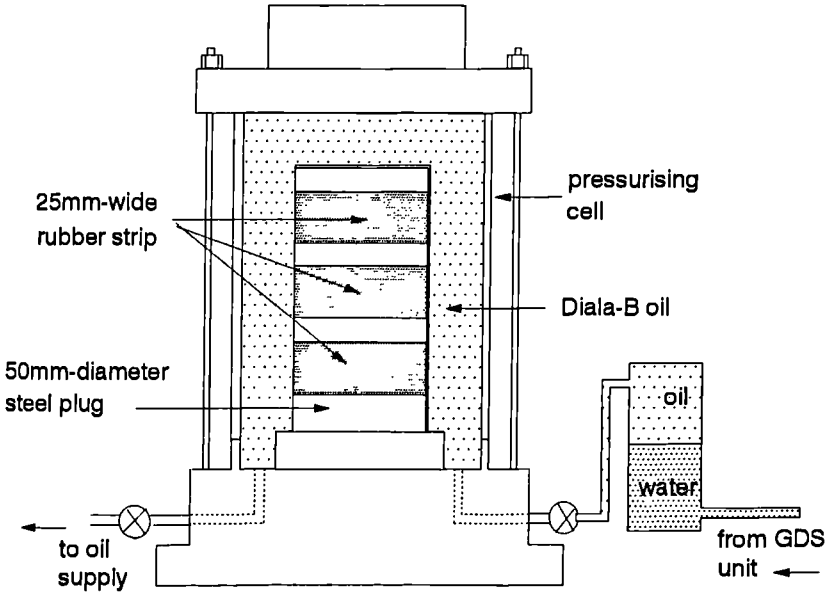

Fig. 5.14 : Soaking of rubber membrane in oil

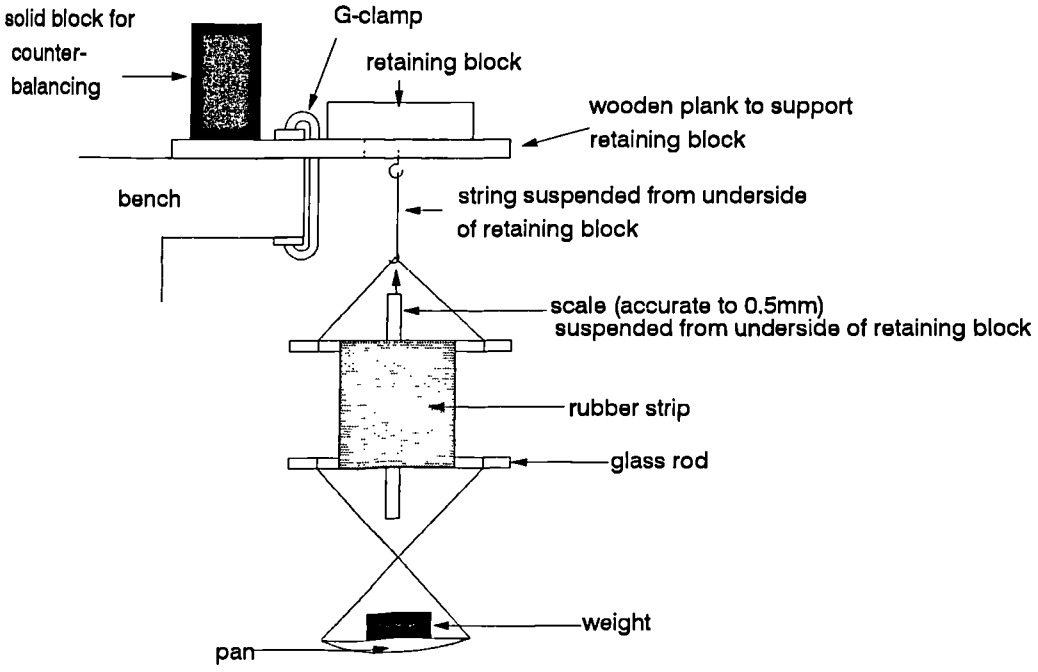

Fig. 5.15 : Method of measuring membrane extension
(after Bishop and Henkel, 1962)

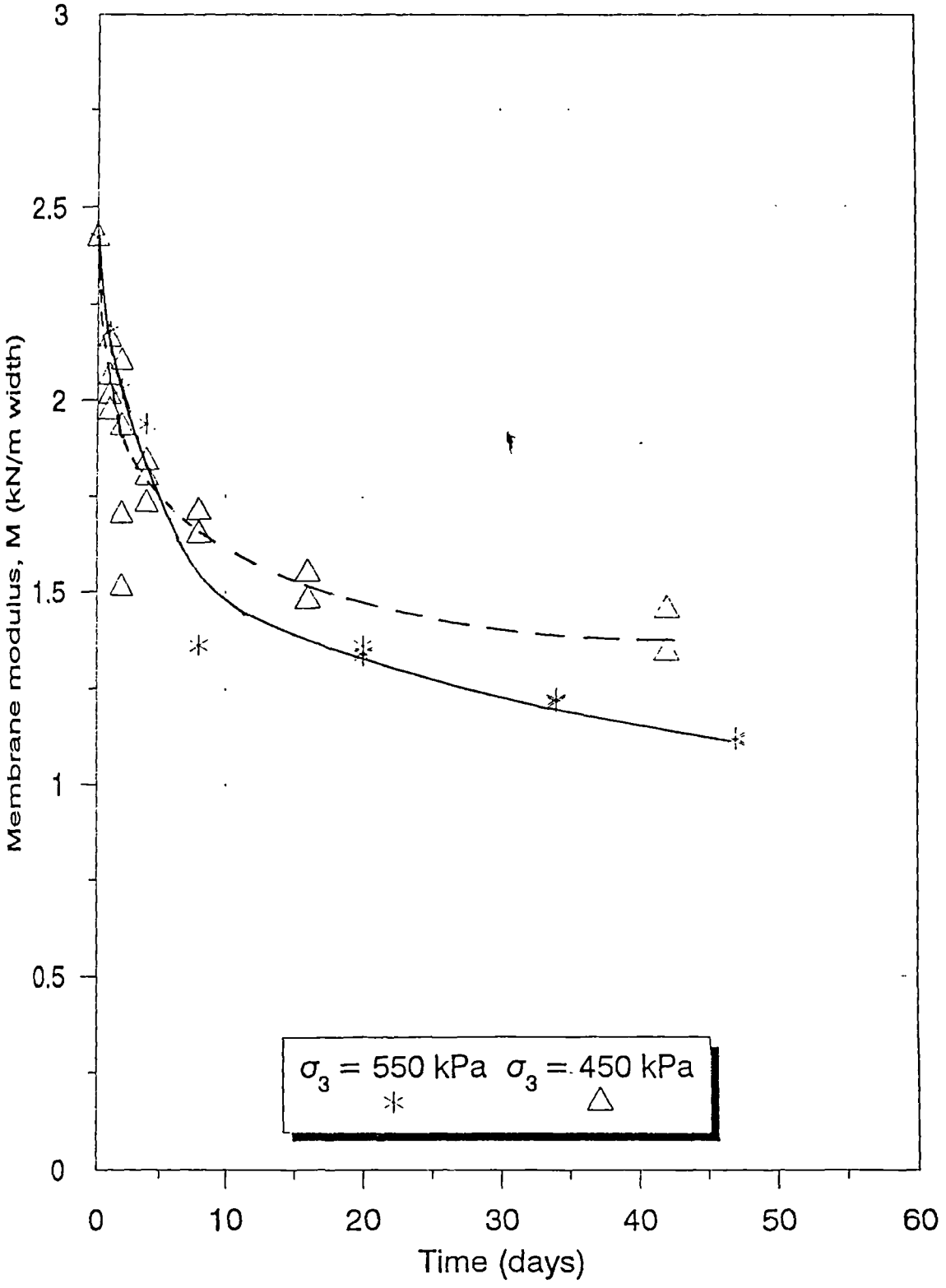

Fig. 5.16 : Variation of membrane modulus for Neoprene membrane soaked in oil at different confining pressures (σ_3)

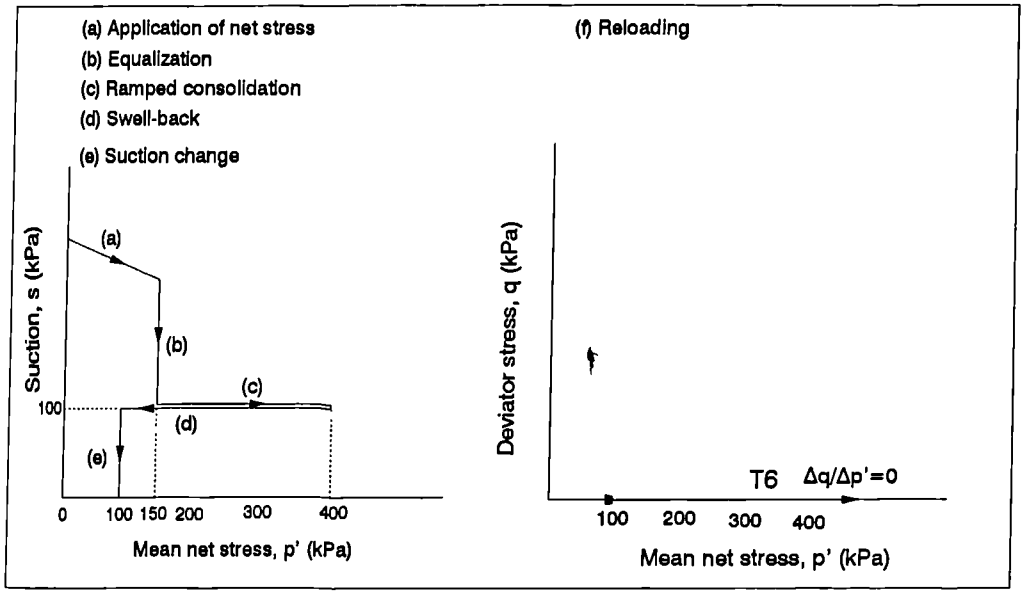

Fig. 5.17 (a) : Stress paths for test series at s = 0 kPa

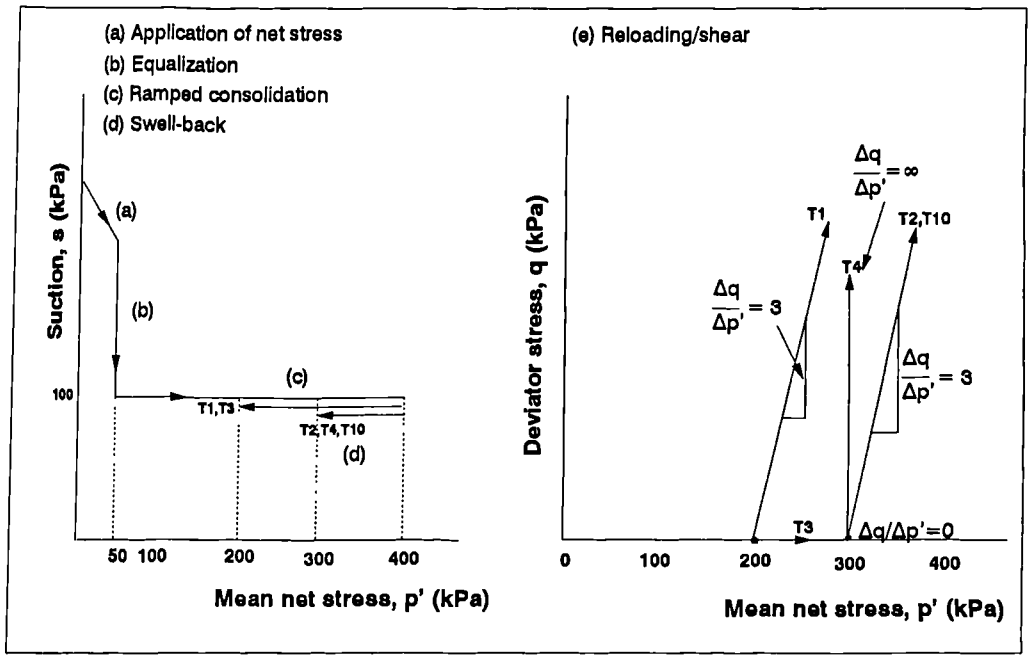

Fig. 5.17 (b) : Stress paths for test series at s = 100 kPa

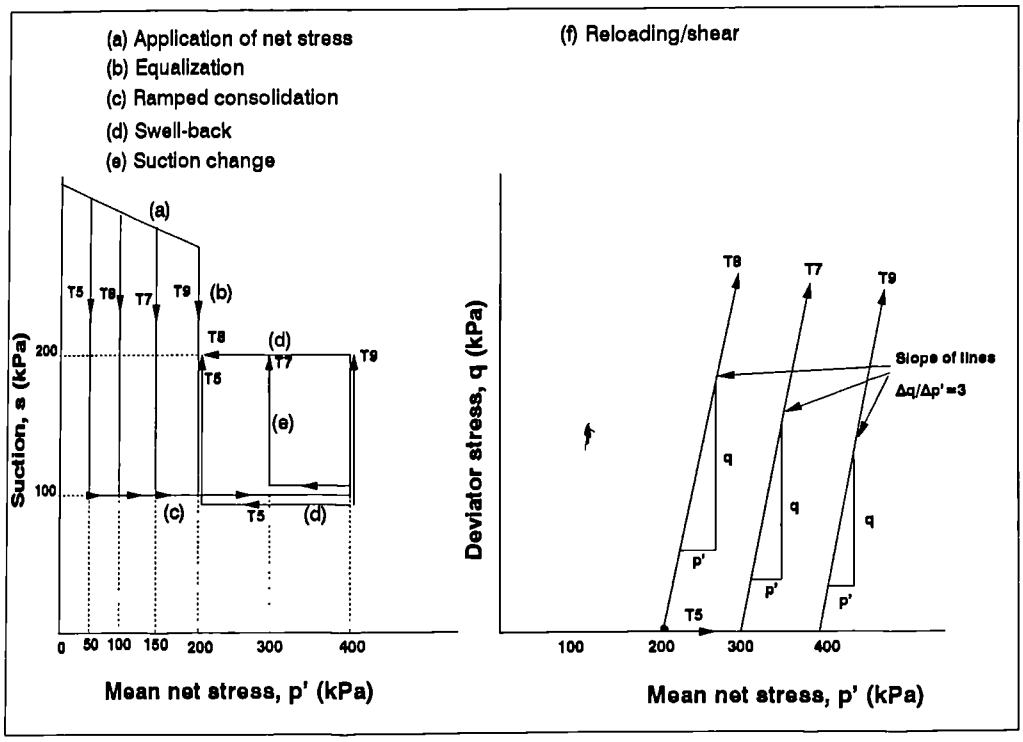

Fig. 5.17 (c) : Stress paths for test series at s = 200 kPa

Test	Mean net stress during equalization p'_e (kPa)	Suction at end of equalisation s_e (kPa)	Mean net stress at end of consolidation p'_o (kPa)	Mean net stress after swell-back p'_c (kPa)	Mean net stress at which suction change occurred (kPa)	Suction after suction change s_c (kPa)	Slope of reloading stress path $\Delta q / \Delta p'$	Duration of test (days)
1	50	100	400	200	-	100	3	44
2	50	100	400	300	-	100	3	45
3	50	100	400	200	-	100	0	37
4	50	100	400	300	-	100	∞	51
5	50	100	400	200	200	200	0	52
6	150	100	400	100	100	0	0	53
7	150	100	400	300	300	200	3	41
8	100	100	400	200	400	200	3	58
9	200	100	400	400	400	200	3	46
10	50	100	400	300	-	100	3	46

Table 5.1 Test programme

CHAPTER 6

EXPERIMENTAL RESULTS

This chapter summarizes the results obtained from the experimental programme. The order of presentation follows the various test stages, beginning with the equalization stage (including initial application of mean net stress), followed by the ramped consolidation stage, the swell-back stage, the suction-change stage and finally the reloading/shear stage. Interpretation of the results is given where appropriate, with more general discussion provided in Chapter 7.

Table 6.1 shows the values of the soil state parameters after compaction for all tests, calculated in accordance with Section 5.5.4. From Table 6.1 the water content after compaction varied from 23.99% to 25.35% i.e. a difference of 1.36% between tests. This caused variation in the degree of saturation from about 55% to about 61%, and variation in the specific volume v from 2.098 to 2.176, with an increase of w tending to cause a decrease of v (because the samples were on the dry side of optimum) and an increase of S_r.

6.1 Equalization stage

The mean net stress during the equalization stage p'_e was 50 kPa in Tests 1, 2, 3, 4, 5 and 10, 100 kPa in Test 8, 150 kPa in Tests 6 and 7 and 200 kPa in Test 9. During equalization, the suction was brought down from its high initial value (unknown) to 100 kPa in all tests.

Table 6.2 gives the values of soil state parameters, calculated in accordance with Sections 5.5.4 and 5.5.5, for all tests at the end of the equalization stage. The mean net stress p' at the end of equalization stage was maintained within ± 2 kPa of the target value, and the suction s was maintained within ± 1 kPa of the target value.

At the end of the stage the degree of saturation varied between 68.8% and 73.1% for the seven samples prepared at p_e' = 50 kPa or 100 kPa, but S_r was considerably higher (80.5% to 81.2%) for the three samples prepared at p_e' = 150 or 200 kPa. The wide variation in the values of S_r was therefore attributed to the range of p_e' values.

6.1.1 Variation of specific water volume

Fig. 6.1 shows the increase of specific water volume Δv_w with time during the equalization stage for all tests. It can be seen that, in all cases, water entered the samples during equalization, showing that the suction inside the sample after compaction and application of the mean net stress p_e' was higher than 100 kPa.

In most cases the equalization stage was terminated when the rate of change of v_w was less than 0.001 per day. Unfortunately however, due to a mistake, the equalization stages of Tests 3 and 5 were terminated prematurely, when the rate of change of v_w was still considerably in excess of 0.001 per day (see Fig. 6.1). This had implications for the behaviour observed during the early phase of the subsequent ramped consolidation stage (because equalization would still have been continuing).

From Fig. 6. 1, and discounting Tests 3 and 5 (in which incomplete equalization occurred), the final increase in v_w varied between 0.135 (Test 9) and 0.21 (Test 1). The scatter in the final values of Δv_w for the six tests conducted at p_e' = 50 kPa was greater than any difference between tests at different values of p_e', and Fig. 6.1 shows no apparent trend with changing p_e' during the equalization stage.

The final values of v_w at the end of equalization were (presumably) dependent on the value of suction after the equalization stage s_o (100 kPa in all tests), as found by *Sivakumar* (1993) (who used a variety of different values of s_o). The results shown in Fig. 6.1 suggest however that the final values of v_w after equalization were relatively insensitive to the mean net stress p_e'.

6.1.2 Variation of specific volume

Fig. 6.2 shows the variation of specific volume v with time during the equalization stage for all tests.. The erratic variation of v observed in Test 2 was attributed to membrane slippage, as discussed in Section 5.2.3.

Most of the six samples wetted at p_e' = 50 kPa (Tests 1, 2, 3, 4, 5 and 10) underwent a small reduction in v during the initial 'undrained' application of p_e' as shown in Fig. 6.2 . The values of Δv during this 'undrained' loading varied between zero and -0.004 for the six samples. Swelling was then observed as drainage occurred and equalization started to take place. The amount of swelling varied between the six tests, ranging from Δv = 0.006 to Δv = 0.037. In some of the tests at p_e' = 50 kPa (Test 1 in particular and Test 10 to a lesser extent), the swelling phase was followed by a small volume reduction (collapse). For example, in Test 1 a reduction in v of about 0.011 occurred after the swelling phase, while the corresponding value for Test 10 was about 0.002. No collapse was observed in Tests 2, 3, 4 and 5.

For the single test at p_e' = 100 kPa (Test 8), a small immediate 'undrained' compression during the application of p_e' (Δv = -0.005) was followed by a very small amount of swelling (Δv = +0.001) and then a significant amount of collapse (Δv = -0.028).

For the two samples tested at p_e' = 150 kPa (Tests 6 and 7) and the single sample tested at p_e' = 200 kPa (Test 9), a much larger 'immediate' undrained compression was observed (Δv = -0.03 in Tests 6 and 7 and Δv = -0.05 in Test 9). This was then followed by a large amount of collapse as equalization took place (Δv = -0.07 to -0.09), with no evidence of any prior swelling.

The behaviour of the soil during the 'undrained' application of mean net stress and the subsequent equalization stage can be explained by means of the concept of a Loading-Collapse yield curve in the *s-p'*, plane as proposed by *Alonso, Gens and Josa* (1990) (see Section 2.6.1.1) and as shown in Fig. 6.3. Y_0 is the approximate

initial position of the yield curve after compaction, deduced from the experimental results. The behaviour of the soil inside the yield curve is elastic, with an increase in p' (a loading path) causing elastic compression and a reduction in s (a wetting path) causing elastic swelling. The small amounts of immediate 'undrained' compression that occurred during Tests 1, 2, 3, 4, 5 and 10 (p_e' = 50 kPa) and Test 8 (p_e' = 100 kPa) are consistent with the fact that points B and D in Fig. 6.3 are inside the initial position of the yield curve produced by the compaction process. Conversely, the substantially greater values of immediate 'undrained' compression during Tests 6 and 7 (p_e' = 150 kPa) and Test 9 (p_e' = 200 kPa) are consistent with the fact that the points F and H in Fig. 6.3 are outside the initial position of the yield curve i.e. expansion of the yield curve from position Y_O to position Y_F (Tests 6 and 7) or position Y_H (Test 9) occurred during 'undrained' application of p_e'.

During subsequent equalization (wetting) the swelling observed in Tests 1, 2, 3, 4, 5 and 10 (p_e' = 50 kPa) was consistent with the wetting stress path BC in Fig. 6.3 remaining inside the yield curve (the small amount of collapse observed in the later stages of Tests 1 and 10 suggests that point C may be just outside the initial position of the yield curve Y_O). The very small amount of swelling in Test 8 (p_e' = 100 kPa) followed by a significant amount of collapse was consistent with wetting path DE starting inside the yield curve but then involving significant expansion of the yield curve to a final position Y_E. Finally, the major collapse observed in Tests 6 and 7 (p_e' = 150 kPa) and Test 9 (p_e' = 200 kPa) was consistent with wetting paths FG and HI involving major expansion of the yield curve (to final positions Y_G and Y_I respectively).

6.1.3 Axial and radial strains

Fig. 6.4 shows the variation of axial strain (ε_1) and radial strain (ε_3) with time during the equalization stage for tests conducted at p_e'.=50 kPa. The values of ε_1 shown in the figure are the average from the two local axial gauges. The erratic

variation of axial and radial strains in Test 2 was attributed to membrane slippage (see Section 5.2.3). The variation of specific volume v illustrated in Fig. 6.2 is, of course, the result of the individual axial and radial strains shown in Fig. 6.4. In Tests 1, 2, 3, 4, 5 and 10 (p_e'=50 kPa) the swelling seen in Fig. 6.2 was mainly due to expansion in the axial direction (see Fig. 6.4) with very little strain (even slight compression) occurring in the lateral direction (see Fig. 6.4).

In Tests 6 and 7 (p_e' = 150 kPa), Test 8 (p_e' = 100 kPa) and Test 9 (p_e'= 200 kPa) the collapse observed in Fig. 6.2 was mainly due to compression in the lateral direction, with small expansions actually occuring in the axial direction (see Fig. 6.5). Thus it follows that, irrespective of whether the overall effect was swelling or collapse, compression was more likely radially and expansion was more likely axially. This shows that behaviour of the soil during the equalization stage was highly anisotropic. This anisotropy was presumably induced by the one-dimensional compaction procedure used to prepare the soil samples.

6.2 Ramped consolidation stage

In the ramped consolidation stage the mean net stress p' was increased from 50, 100, 150 or 200 kPa to p_0'= 400 kPa (the target value of p') while holding suction constant at 100 kPa.

Table 6.3 shows the soil state parameters at the end of the ramped consolidation stage calculated according to Sections 5.5.4 and 5.5.5. The final values of p' and s varied slightly from their target values of 400 kPa and 100 kPa respectively, reflecting the accuracy of the control system. The variation in p_o' and s_o for all tests was generally less than ±2 kPa, which was considered acceptable. The degree of saturation S_r varied between 83.5% and 95.2%. It was not clear whether this relatively large variation of S_r represented a true variation between samples or was due to measurement inaccuracies in either v or v_w (see Equation 5.9 or 5.10).

6.2.1 Variation of specific volume

Fig. 6.6 shows for all tests the variation of specific volume v with mean net stress p' (with p' on a logarithmic scale). The erratic nature of the curve for Test 2 was presumably due to membrane slippage.

From Fig. 6.6 Tests 1, 2, 3, 4 ,5 and 10 showed evidence of an initially stiff (elastic) response, followed by yielding. This was consistent with point C in Fig. 6.3 lying just inside the yield curve. Fig. 6.6 shows almost immediate yielding take place in Tests 6, 7, 8 and 9 at the beginning of ramped consolidation stage, consistent with points E, G and I in Fig. 6.3 lying on the relevant yield curve.

The straight line portions of the curves shown in Fig. 6.6 define the normal compression line for a suction of 100 kPa. As described in Section 2.6.5, *Wheeler and Sivakumar* (1995) showed that this normal compression line, for any value of suction, can be represented by the equation

$$v = \mathrm{N}(s) - \lambda(s) \ln\left(\frac{p'}{p_{at}}\right) \qquad (6.1)$$

where p_{at} is atmospheric pressure and the intercept N(s) and slope λ(s) are both functions of suction. Inspection of Fig. 6.6 shows that, for a suction of 100 kPa, the average value of λ(s) obtained from the tests was 0.136 and the average value of N(s) was 2.108 (see Table 6.4). The scatter in the value of N(s) was probably due to the difficulty of accurately measuring absolute values of v (whereas changes of v can be measured much more accurately). For a suction of 100 kPa, *Sivakumar* (1993) obtained values of λ(s) and N(s) of 0.182 and 2.122 respectively. The differences between the values of λ(s) and N(s) obtained from Fig. 6.6 and those obtained by *Sivakumar* (1993) were probably due to the stress range over which the measurement took place. In his tests Sivakumar used values of p_0' ranging from 100 to 200 kPa for a suction of 100 kPa while in the present tests all samples had a value of p_0' of 400 kPa (all under a suction of 100 kPa). As p_0' became larger, the 'linear' portion of the

compression lines tended to flatten slightly, giving lower values of λ(s) and N(s). The scatter in N(s) measured by *Sivakumar* (1993) was also considerably less than shown in Fig. 6.6. Possible reasons for this are discussed in Section 7.2.

6.2.2 Variation of specific water volume

Fig. 6.7 shows, for all tests, the variation of specific water volume v_w during the ramped consolidation stage. The variation of v_w during each test was small: typically 0.01 to 0.03 (see Fig. 6.7 which has a large scale for v_w). The large separation of the different graphs probably reflects the difficulty in accurately measuring absolute values of v_w, whereas the changes in v_w were measured relatively accurately.

Tests 2, 4, 6, 7, 8, 9 and 10 showed a slight increase in v_w, (typically less than 0.01) during the early phase of the ramped consolidation stage. After reaching a peak, v_w then decreased again until the stage was terminated at $p_0^{'}$ = 400 kPa. Tests 3 and 5 showed larger increases in v_w during the early phase of ramped consolidation (see Fig. 6.7), which was probably due to the incomplete equalization during the preceding equalization stage (see Section 6.1.1). In contrast, Test 1 showed a completely different variation in v_w during the consolidation stage. Initially there was very little variation in v_w, and this was then followed by a significant increase in v_w in the later phase of the stage. It was thought that this might have been due to imperfect testing technique employed in the first test.

The final straight line portion of the curves shown in Fig. 6.7 defines the normal compression line for specific water volume for a suction of 100 kPa. By analogy with Equation 6.1, the equation relating the specific water volume v_w to changes in mean net stress p' for virgin states can be given by

$$v_w = A(s) - \alpha(s)\ln\left(\frac{p'}{p_{at}}\right) \tag{6.2}$$

where A(s) and α(s) are the intercept and slope of the normal compresion line for specific water volume. Both A(s) and α(s)are presumably dependent on suction. The average values of A(s) and α(s) were 0.026 and 1.849 respectively (see Table 6.4). The values of A(s) and α(s) from Tests 1, 3 and 5 were not included because of the problems of experimental procedure described above.

6.2.3 Axial and radial strains

Figs. 6.8 and 6.9 show the axial and radial strains, given by the local strain gauges, during the ramped consolidation stage. Fig. 6.8 shows the average local axial strain (ε_1) for all tests. The erratic nature of the axial strain variation in Test 2 was attributed to membrane slippage (see Section 5.2.3). In Tests 1, 3, 4, 5 and 10 where the samples started from p_e'=50 kPa in the ramped consolidation stage, the final values of ε_1 varied from 1.10 to 1.7% whereas in Tests 6, 7, 8 and 9, where p_e' varied from 100 to 200 kPa, the final values of ε_1 varied from 0.45 to 1.00%. Samples that had been previously subjected to higher values of p_e' in the equalization stage had smaller axial compressive strains in the subsequent ramped consolidation stage, because they had smaller axial tensile strains in the equalization stage (the total axial strain during equalization and consolidation stages was approximately the same for all samples).

Fig. 6.9 shows the variation of radial strain (ε_3) with p' (with p' plotted on a logarithmic scale) for all tests. The values of ε_3 show excellent consistency between tests, reflecting the high accuracy of measuring radial strains by the local radial gauge. Final values of ε_3 for Tests 1, 2, 3, 4, 5 and 10 (p_e' = 50 kPa) were about 5.5%, whereas the final values of ε_3 in Test 8 (p_e' = 100 kPa) was 3.8%, in Tests 6 and 7 (p_e' = 150 kPa) was 3.0% and in Test 9 (p_e' = 200 kPa) was 1.5%. The total

radial strain in the equalization stage and consolidation stage combined was very similar in all tests.

Examination of Figs. 6.8 and 6.9 shows that in the early phase of the stage ε_3 was increasing at a much faster rate than ε_1. This was to be expected from the anisotropic nature of the soil as observed in the earlier equalization stage (compression in the lateral direction was much higher than in the vertical direction). As the stage progressed the radial strain rate decreased (see Fig. 6.9) whereas the axial strain rate increased (see Fig. 6.8). The increase in rate of axial strain and the decrease in rate of radial strain brought the samples much closer to isotropic straining by the end of the stage. The anisotropic history produced by the one-dimensional compaction procedure was therefore gradually erased by continued isotropic consolidation.

6.3 Swell-back stage

Eight of the ten tests involved swell-back at a suction of 100 kPa from a mean net stress p_o' of 400 kPa to a lower mean net stress p_c' of 100, 200 or 300 kPa. The exceptions were Test 9, which did not include a swell-back stage, and Test 8, which involved swell-back to p_c' = 200 kPa but at a suction of 200 kPa (after a suction-change stage).

The soil state parameters at the end of swell-back stage are shown for all tests in Table 6.5.

6.3.1 Variation of specific volume

Fig. 6.10 shows the variation of v during the swell-back stage for all tests. The vertical lines at end of all curves correspond to the rest period of 24 hours at the end of the stage (to ensure complete equalization of pore water pressure throughout the sample). The variation of v during the 24-hour rest period was much greater in Test 1

than in any other tests, which might have been due to imperfect testing technique in the first test.

From Fig. 6.10 the separation between curves is quite apparent. This reflects the difficulty of accurately measuring absolute values of v, rather than changes in v. However the slopes of the curves are reasonably consistent which implies that the changes in v were accurately measured in all tests.

In the elasto-plastic model of *Alonso, Gens and Josa* (1990), as described in Section 2.6.1.1, the elastic changes of v are given by

$$dv^e = -\kappa \frac{dp'}{p'} - \kappa_s \frac{ds}{s + p_{at}} \qquad (6.3)$$

where κ and κ_s are elastic swelling indices with respect to changes of p' and s respectively. In the swell-back stage, s was held constant and therefore the slope of each curve in Fig. 6.10 gives a value for the elastic swelling index κ.

Test 8 was the only swell-back stage conducted at $s = 200$ kPa and this gave a κ value of 0.022 All the remaining swell-back stages were conducted at a suction of 100 kPa, and these gave κ values ranging from 0.010 to 0.041 (see Table 6.4), with an average of 0.025. There is therefore no strong influence of suction on the value of κ apparent in the data shown in Fig. 6.10 (any influence of suction is swamped by the scatter between supposedly identical tests).

6.3.2 Variation of specific water volume

Fig. 6.11 shows the variation of specific water volume v_w with p' (with p' on a logarithmic scale) for all tests. The vertical lines at end of all curves correspond to the 24 hour rest-period at the end of the stage. All tests except Test 8 should have been identical at this stage, so the separation between the remaining curves in Fig. 6.11

shows the difficulty of accurately measuring absolute values of v_w. However the slopes of all curves conducted at s = 100 kPa are consistent, suggesting that changes of v_w were accurately measured in all tests.

By anology with Equation (6.2), the elastic variation of specific water volume can be proposed as follows:

$$dv_w^e = -\kappa_w \frac{dp'}{p'} - \kappa_{sw} \frac{ds}{s + p_{at}} \qquad (6.4)$$

where κ_w and κ_{sw} are elastic indices relating reversible changes of v_w to changes of p' and s respectively. For the eight tests at s = 100 kPa in Fig. 6.11 the values of κ_w varied between 0.010 and 0.041 (see Table 6.4), with an average value of 0.024. For Test 8 (s = 200 kPa) κ_w was -0.022. It follows that κ_w can be negative or positive, and κ_w appears to decrease significantly with increasing suction. However at this juncture this conclusion is based on evidence from a single test, and it must therefore be somewhat tentative.

6.3.3 Axial and radial strains

Figs. 6.12 and 6.13 show, for all tests, the axial strain (ε_1) and radial strain (ε_3) during the swell-back stage. From Figs. 6.12 and 6.13 the axial and radial strains are negative, showing that the samples expanded during the swell-back stage, which was to be expected. The slopes of all curves in Fig. 6.12 are very similar, suggesting consistency of results. The curves in Fig. 6.13 also show excellent agreement between tests. Test 1 showed a surprisingly high value of negative strain during the final 24-hour rest period, which was probably due to membrane slippage (the pinning method described in Section 5.2.3 was not employed in this test).

It can be seen from Figs. 6.12 and 6.13 that the rates of change of ε_1 and ε_3 were very similar i.e. both reached a value of about -0.25% when the swell-back was carried out from 400 kPa to 200 kPa. This shows that the initial anisotropic behaviour of the soil (caused by the one-dimensional compaction procedure) had been virtually eliminated by subsequent isotropic loading during the ramped consolidation stage.

6.4 Suction-change stage

Five tests involved a suction-change stage. Test 6 involved a reduction of suction from 100 kPa to zero, whereas Tests 5, 7, 8 and 9 involved an increase in suction from 100 kPa to 200 kPa. The suction-change was performed by adjusting the pore water pressure manually at intervals, as described in Section 5.3.5.

Table 6.6 shows the soil state parameters at the end of the suction-change stage. In tests involving a suction increase, S_r decreased very slightly. In Test 6 which involved a suction decrease to zero, full saturation was not achieved (S_r=98% instead of 100%).

6.4.1 Variation of specific volume

Fig. 6.14 shows, for Tests 5, 6, 7, 8 and 9 the variation of specific volume v with suction, with suction on a scale corresponding to the logarithm of suction plus atmospheric pressure (see Equation 6.3). The direction of suction-change is shown by arrows in the figure. The stepped shape of the curves was due to the fact that the suction was adjusted manually in increments of 4 to 12 kPa (see Section 5.3.5).

From Fig. 6.14, for suction-increase tests (Tests 5, 7, 8 and 9) the elastic parameter κ_s in Equation 6.3 varied between zero (Test 5) and 0.030 (Test 8), with an average value of 0.014 (see Table 6.4). In these four tests in which the suction was increased, the value of κ_s seemed to increase with increasing p'. For the single

suction-decrease test (Test 6), κ_s was 0.053, which was significantly greater than the values of κ_s found in the four suction-increase stages.

6.4.2 Variation of specific water volume

The variation of specific water volume v_w with suction for tests involving a suction-change stage (Tests 5, 6, 7, 8 and 9) is given in Fig. 6.15, with suction on a scale corresponding to the logarithm of suction plus atmospheric pressure (see Equation 6.4). From the results, it appears from the four suction-increase stages that κ_{sw} increased with increasing p' (see Table 6.4). For example : at p' = 200 kPa, κ_{sw} = 0 (Test 5); at p' = 300 kPa, κ_{sw} = 0.032 (Test 7) ; and at p' = 400 kPa, κ_{sw} = 0.075 (average of Tests 8 and 9). For the single test with a suction-decrease stage (Test 6) the value of κ_{sw} was 0.116 (at p' = 100 kPa). This value was much higher than the value of κ_{sw} that would have been expected at this value of p' on the basis of the suction-increase test results.

6.5 Isotropic re-loading stage

Three tests, at three different values of suction, were conducted with a final isotropic re-loading stage ($\Delta q/\Delta p' = 0$). The tests were conducted by increasing the cell pressure, while holding suction constant at zero, 100 or 200 kPa. Tests 6, 3 and 5 were conducted at suctions of zero, 100 kPa and 200 respectively. The main objective of these isotropic re-loading stages was to evaluate the yield points under isotropic stress state conditions p_o' at three different values of suction.

6.5.1 Variation of specific volume

Fig. 6.16 shows the variation of specific volume v with mean net stress p' (with p' plotted on a logarithmic scale) during the isotropic re-loading stage for Tests 3, 5

and 6 . In Test 3 the suction was held at 100 kPa throughout all stages of the test, whereas Test 5 involved a suction increase to 200 kPa and Test 6 involved a suction decrease to zero. Test 3 was mistakenly terminated at p' = 400 kPa. The yield points in Tests 5 and 6 were identified by following the procedure suggested by Casagrande. The yield values of p' for Tests 6 and 5 were evaluated as 170 and 450 kPa respectively, with an estimated precision of about ±10 kPa and ±20 kPa respectively. If Test 3 had been continued, yield would have been expected at p' = 400 kPa, because the suction applied to the sample had been maintained at 100 kPa throughout the consolidation, swell-back and isotropic re-loading stages, and the consolidation stage involved loading to p_o' = 400 kPa.

From the yield points shown in Fig. 6.16 it was possible to sketch in the *s-p'* plane the position of the Loading-Collapse (LC) yield curve produced by the ramped consolidation stage (see Fig. 6.17). The shape of the curve is such that the isotropic yield stress p_o' increases dramatically from the value at zero suction (p_o'(o)=170 kPa) as suction is increased to about 100 kPa. However, for further increase of suction above 100 kPa the additional increase of p_o' is quite small, and there is suggestion that the curve tends to an asymtotic value of p' with increasing suction. This is consistent with the model of *Josa, Balmaceda, Gens and Alonso* (1992) (see Section 2.6.3), which postulates that the yield curve reaches a maximum value of p_o' with increasing suction. *Josa, Balmaceda, Gens and Alonso* (1992) argued that p_o' could not increase indefinitely with increasing suction because there was a maximum possible value of collapse on wetting.

6.5.2 Variation of specific water volume

The variation of specific water volume v_w with p' during the isotropic re-loading stage of Tests 3 , 5 and 6 is shown in Fig.6.18. Test 5 shows a marked yield point (following Casagrande's method) at about p' = 390 kPa. This value was lower than the value of 450 kPa obtained from the plot of *v versus lnp'* shown in Fig. 6.16.

No yield point was apparent in Test 3 (s = 100 kPa), because the test was prematurely terminated at p'=400 kPa. Presumably yield would have taken place at p' = 400 kPa had the test been continued further. Test 6 (s = 0) shows a peak in the curve i.e. a change in slope of v_w against lnp' . This occurs at $p' \approx 130$ kPa which is somewhat lower than the yield value of p' (170 kPa) obtained from the *v versus lnp'* plot shown in Fig. 6.16.

The value of κ_w (from the pre-yield section of the curve) for Test 5 (s=200 kPa), was found to be 0.007. This value clearly does not agree with the negative value (κ_w = -0.023 measured during the swell-back stage of Test 8 conducted at a suction of 200 kPa (see Section 6.3.2). The value of κ_w from the isotropic re-loading stage for Test 3 was 0.010 (see Fig. 6.18). This value was less than one half of the average value of κ_w = 0.025 measured in the swell-back stage for Tests at s = 100 kPa.

For Test 6 the initial slope of the curve during the re-loading stage suggests a negative value of κ_w at s = 0. Note that full saturation of the sample was not achieved despite the fact that the suction was zero (see Table 6.6). This lack of full saturation was further supported by the fact that the change in v_w was not equal to the change in v during the isotropic re-loading stage. The saturation increased during re-loading as a result of a larger reduction in v than the reduction in v_w. In fact the measured absolute values of v and v_w suggest that v was less than v_w at the end of re-loading stage. This was clearly impossible, because, for a fully saturated soil $v=v_w$ and the fact that $v < v_w$ implies $S_r>1$. This contradiction therefore emphasizes the difficulty in accurately measuring absolute values of v and v_w.

6.6 Shear stage conducted at constant cell pressure ($\Delta q / \Delta p' = 3$)

Six fully drained shear tests were conducted with the cell pressure held constant. Three tests were conducted at a suction of 100 kPa (Tests 1, 2 and 10) and

the remaining three tests were conducted at a suction of 200 kPa (Tests 7, 8 and 9). Unfortunately Test 2 was unsuccessful, due to failure of the load cell, and Test 10 was therefore performed as a repeat of Test 2.

The objectives of conducting shear tests at constant suction and cell pressure were as follow:

1) To investigate yielding under anisotropic stress states ($q \neq 0$)

2) To investigate "elastic" shearing prior to yielding (i.e. evaluation of the elastic shear modulus, G)

3) To investigate the form of the flow rule after yielding.

6.6.1 Performance of local strain gauges

Each soil sample was fully instrumented with local strain gauges (two axial gauges and one radial gauge), to monitor the sample displacements in all stages of the test. Of particular interest was the performance of these gauges in the early part of the shear stage where the pre-yield behaviour of the soil was one of the main concerns of the test programme.

Fig. 6.19 shows the variation of local axial strain from the individual axial gauges and the radial strain from the local radial gauge for the shear stage of three typical tests (Tests 4, 8 and 10) plotted against the corresponding external measurement of axial strain. Note that Test 4 was a fully drained shear stage conducted at contant p' (see Section 6.7) at a suction of 100 kPa, whereas Tests 8 and 10 were constant cell pressure shear tests conducted at suctions of 200 kPa and 100 kPa respectively. Generally the axial strains given by the two axial gauges in each test were very similar, suggesting that relatively little tilting of the sample occurred. However the use of two axial gauges (positioned diametrically opposite each other on the sample) can detect tilting of the sample only within one plane, and tilting cannot be observed in the vertical plane orthogonal to the plane containing the

axial gauges. This technique could be improved by having four axial gauges mounted on the sample, but this would have complicated the test procedure given the size of the sample and size of the triaxial cell.

At axial strains greater than about 2% the percentage difference between the average local strain and the external axial strain was quite small (see Fig. 6.19), suggesting that external measurement of axial strain is adequate at large strains. The significant advantage of the local axial gauges was the improved accuracy during the early part of the shear stage and the elimination of bedding errors, as shown in Fig. 6.20 for two typical tests (Tests 9 and 10). In Test 9 there was relatively little bedding error, but the initial stiffness of the sample would have been considerably under-estimated by the use of external strain measurement. In Test 10 the external strain measurement also involved a significant bedding error (about 0.4% axial strain) together with an under-estimate of the yield value of q (by about 11 kPa).

6.6.2 Stress-strain curves

The stress-strain curves for the five successful shear tests conducted at constant cell pressure are shown in Figs. 6.21 and 6.22. Fig. 6.21 shows the deviator stress q plotted against the axial strain ε_1 for the complete set of tests, with ε_1 based on the average of the two local strain gauge measurements. Fig. 6.22 shows q plotted against the shear strain ε_s, with ε_s calculated from Equation 5.4. The apparent increase in stiffness at an axial strain of about 2.5% observed for all tests in Figs. 6.21 and 6.22 was due to the tenfold increase in axial strain rate applied at this point.

The erratic nature of the early part of stress-strain curves for Test 1 (see Figs. 6.21 and 6.22) was attributed to membrane slippage, because this test was conducted before the introduction of the procedure of pinning the feet of the local strain gauges (see Section 5.2.3). Inspection of Figs. 6.21 and 6.22 shows an initially stiff response in shear, with more than 50% of the maximum deviator stress achieved in less than

2.5% axial strain. The shear stiffness then decreased significantly. This general behaviour is consistent with expectations, with the initial stiff response corresponding to 'elastic' behaviour inside the yield surface and the reduction of stiffness corresponding to the onset of plastic strains on reaching the yield surface.

Inspection of Figs. 6.21 and 6.22 shows that all samples except Test 7 reached a maximum value of deviator stress prior to termination of the test (when the limit of travel was reached). This maximum value of deviator stress occurred at an axial strain of 15 to 20% . The maximum value of q generally increased with both the mean net stress at the start of shearing p_c' and the suction s . This was consistent with expected behaviour for unsaturated soil (see Equation 2.21).

In Tests 8 and 10 there was a significant post-peak reduction of deviator stress, and it is unclear whether this would also have occurred in the other tests if it had been possible to continue them to higher strains. In general, true critical states were not achieved. The critical state behaviour had, however, already been investigated by *Sivakumar* (1993), and it was not the main area of study within the current project.

6.6.3 Specific volume and specific water volume

Fig. 6.23 shows the specific volume v plotted against the mean net stress p' (with p' on a logarithmic scale) for the five successful shear stages conducted at constant cell pressure. The effects of membrane slippage are again apparent in the erratic nature of the curve for Test 1. All five curves show an initially stiff volumetric response (with only small reductions of v for a given increase of $ln\ p'$) and then the suggestion of yielding, as the compression of the samples increased significantly. Tests 8 and 10, which were continued through post-peak reductions of deviator stress (see Figs. 6.21 and 6.22), finally show a sudden increase of v. This was probably caused by the formation of shear planes, such that the local strain gauges

gauges no longer gave true readings of the sample displacements. This invalidates the use of local strain gauges at higher strains.

Fig. 6.24 shows the variation of specific water volume for five successful shear stages conducted at constant cell pressure. Tests 1 and 10 involved shearing at a suction of 100 kPa, whereas Tests 7, 8 and 9 involved shearing at a suction of 200 kPa. In Tests 1 and 10, there was very little change of v_w during most of the shear stage, except towards the end where there was an increase in v_w of about 0.01.

In Tests 7, 8 and 9 there was a reduction in v_w ranging from 0.025 (Test 7) to 0.050 (Test 9), indicating that water was expelled from the samples during the shear stage (see Fig. 6.24).

6.6.4 Identification of yield points

To assist in the identification of the yield points, the stress-strain curves for the initial part of each test (up to an axial strain of 2.5%, when the strain rate was increased tenfold) were plotted to enlarged scales. Fig. 6.25 shows a plot of deviator stress q versus axial strain ε_1 and Fig. 6.26 shows q versus shear strain ε_s. Fig. 6.27 shows specific volume v versus mean net stress p' (with p' on a logarithmic scale). Various other plots were also investigated, including p' versus volumetric strain ε_v (with p' on a linear scale) and stress increment $\delta\sigma'$ versus energy per volume W (as recommended by *Graham, Noonan and Lew* (1983) (see Section 2.8). It was however found that yield was even more ambigious in these additional plots than it was in the curves shown in Figs. 6.25 to 6.27.

The erratic nature of the curves for Test 1 in Figs. 6.25 to 6.27 clearly shows the effects of membrane slippage, and identification of a yield point was therefore impossible for this test. For the remaining four tests, yield points were identified by approximating the stress-strain curves in Figs. 6.25 and 6.26 to two linear sections, and by using a Casagrande construction in Fig. 6.27. The change from a stiff

response to a less stiff response was not always indicated by a sharp change in the slope of the graphs, and identification of the yield points was therefore subject to a considerable degree of uncertainty. This was particularly true for the q versus ε_1 or ε_s plots for Tests 7 and 9 (see Figs. 6.25 and 6.26).

Yield values of deviator stress q_y and mean net stress p'_y were calculated from Fig. 6.25 (q versus ε_1) and Fig. 6.27 (v versus $ln\ p'$) and these are listed in Table 6.7. Final values of q_y and p'_y were then calculated by averaging the two independent sets of values (see Table 6.7). Yield values from Fig. 6.26 (q versus ε_s) were not included in this averaging process, because these essentially duplicated the values from Fig. 6.25 The final values of q_y and p'_y were considered to have precisions of about ± 15 kPa and ± 5 kPa respectively.

6.7 Shear stage at constant mean net stress

In the experimental programme an attempt was made to conduct a fully drained shear test at constant p' and Test 4 was designated for this purpose. The test was performed under stress control, and the cell pressure was reduced at half the rate at which the axial stress was increasing (calculated from the applied rate of pressure increase to the lower chamber of the triaxial cell, see Section 5.3.6). Fig. 6.28 shows the stress path actually achieved in Test 4. Due to friction on the loading ram, there were considerable fluctuations from the desired path (no feedback control was available to maintain p' exactly constant, see Section 5.3.6). As a result, p' varied by as much as 10 kPa from the target value of 300 kPa. Even worse, there were large step increases of q (of up to 25 kPa) and several periods when q reduced temporarily. It was therefore decided that no further tests of this type should be conducted.

The variation of deviator stress q with axial strain ε_1 during Test 4 is shown in Fig. 6.29. The large step increases of q and the minor reductions of q are apparent in

the graph. The variation of q with ε_1 and ε_s during the early part of the test (up to ε_1 = 2.5%) is shown in Fig. 6.30 on an enlarged scale. The yield point was identified from Fig. 6.30 in the usual way, and corresponding yield values q_y and p'_y are tabulated in Table 6.7.

Fig. 6.31 shows the variation of v and v_w during the shear stage of Test 4, plotted against the deviator stress q (with q on a logarithmic scale). The initially stiff volumetric response followed by more significant compression suggests a yield point at a deviator stress of about 100 kPa (consistent with the value calculated from Fig. 6.30). The rapid increase of v at the end of the shear stage presumably corresponded to the formation of a shear plane, such that the local strain measurements became unreliable.

6.8 Yield surface

The estimated values of q_y and p'_y for each test from Table 6.7 were used to plot constant suction yield curves in the $q : p'$ plane at suction values of 100 and 200 kPa, together with a single isotropic yield point $p'_o(o)$ at zero suction (see Fig. 6.32). From Fig. 6.32 it can be seen that the yield curves at suction values of 100 and 200 kPa are both approximately elliptical in shape, with the p' axis forming one axis of the ellipse. This agrees well with the models of *Alonso, Gens and Josa* (1990) and *Wheeler and Sivakumar* (1995) which were based on elliptical yield curves at constant suction (see Sections 2.6.1.2 and 2.6.5). The shape is also consistent with the behaviour of an isotropic material. This confirms the earlier observations that the anisotropic nature of the soil produced by the compaction process had been eradicated by subsequent isotropic ramped consolidation and swell-back.

Expansion of the curve with increasing suction was greater when the suction was increased from zero to 100 kPa than it was when the suction was increased from 100 to 200 kPa. This is consistent with the model of *Josa, Balmaceda, Gens and*

Alonso (1992) which suggested that expansion of the yield curves could not continue indefinitely with increasing suction (see Section 2. 6.4).

Figs. 6.17, showing the LC yield curve in the s:p' plane from the isotropic re-loading stage, and 6.32, showing the yield curves in the q:p' plane at different suction values, can be combined to form the complete yield surface for the compacted kaolin sample. This surface in p': q : s space, which defines the limits of 'elastic' behaviour for soil samples isotropically consolidated to p'_o = 400 kPa and s_o= 100 kPa, is shown in Fig. 6.33. This form of yield surface is in qualitative agreement with the models of *Alonso, Gens and Josa* (1990) and *Wheeler and Sivakumar* (1995).

6.9 Shear modulus

The shear modulus G was evaluated by assuming an isotropic behaviour of the soil within the linear 'elastic' region at the beginning of the shear test on the q versus ε_s plot. This required an even more enlarged plot of q versus ε_s, up to a shear strain of about 0.2% (see Fig. 6.34). The slope of the initial linear portion was equal to $3G$, and the values of G obtained from Tests 4, 7, 8, 9 and 10 are shown in Table 6.4.

The measured values of G are plotted against the initial value of mean net stress at the beginning of the shear stage p'_c in Fig. 6.35. The results show considerable scatter but, from the tests at s = 200 kPa, there was evidence of an increase in G with increasing mean net stress. Comparing the results at s = 100 kPa with those at s = 200 kPa it was unclear (because of the scatter) whether the change of suction had any influence on the value of G.

6.10 Flow rule

The flow rule represents the relationship between the yield curve and the direction of the plastic strain increment vector. To obtain the direction of the plastic strain increment vector after yielding, plots of q versus ε_s and p' versus ε_v were

used. The elastic shear strain increment $\delta\varepsilon_s^e$ and the plastic shear strain increment $\delta\varepsilon_s^p$ were evaluated from the q versus ε_s plot, whereas the elastic volumetric strain increment $\delta\varepsilon_v^e$ and the plastic volumetric strain increment $\delta\varepsilon_v^p$ were evaluated from the p' versus ε_v plot. The method is illustrated in Fig. 6 .36 for Test 8.

Fig. 6. 36 (a) shows the variation of q with ε_s plotted on a large scale (up to 2.5% shear strain). X is the yield point determined earlier and OX is the initial linear ('elastic') part of the curve extended upward. An increment of deviator stress dq was then selected (which in this example was 30 kPa), denoted by the line AX. A horizontal line ABC was drawn through A to meet the projected initial linear part of the curve at B and the straight line approximation of the plastic part of the curve at C. AB then represented $\delta\varepsilon_s^e$ and BC represented $\delta\varepsilon_s^p$. Similar techniques were used to evaluate $\delta\varepsilon_v^e$ and $\delta\varepsilon_v^p$ (see Fig. 6. 36 (b)), with the interval of dp' taken as $dq/3$ (10 kPa in Fig. 6. 36 (b)).

By using the values of plastic strain increments calculated as described above, the plastic strain increment vectors for the successful shear tests (Tests 4, 7, 8, 9 and 10) were superimposed on the relevant yield curve, with the components $\delta\varepsilon_s^p$ and $\delta\varepsilon_v^p$ aligned with q and p' respectively (see Fig. 6.37).

The plastic strain increment vectors for isotropic re-loading tests (Tests 5 and 6) were inclined slightly upward, because small plastic shear strains occurred after yielding for these tests. This was true even though the samples were only subjected to isotropic loading during the final re-loading stage. For Test 3 however the direction of $\delta\varepsilon_s^p$, was not available because the test was mistakenly terminated at $p' = 400$ kPa and no investigation of the plastic strain increment vectors was possible. The yield point of 400 kPa for Test 3 was assumed rather than measured in the test (see Fig. 6.17).

It can be seen in Fig. 6.37 that the total plastic strain increment vectors $\delta\varepsilon^p$ at each yield point, were approximately perpendicular to the yield curve, indicating that the flow rule was associated.

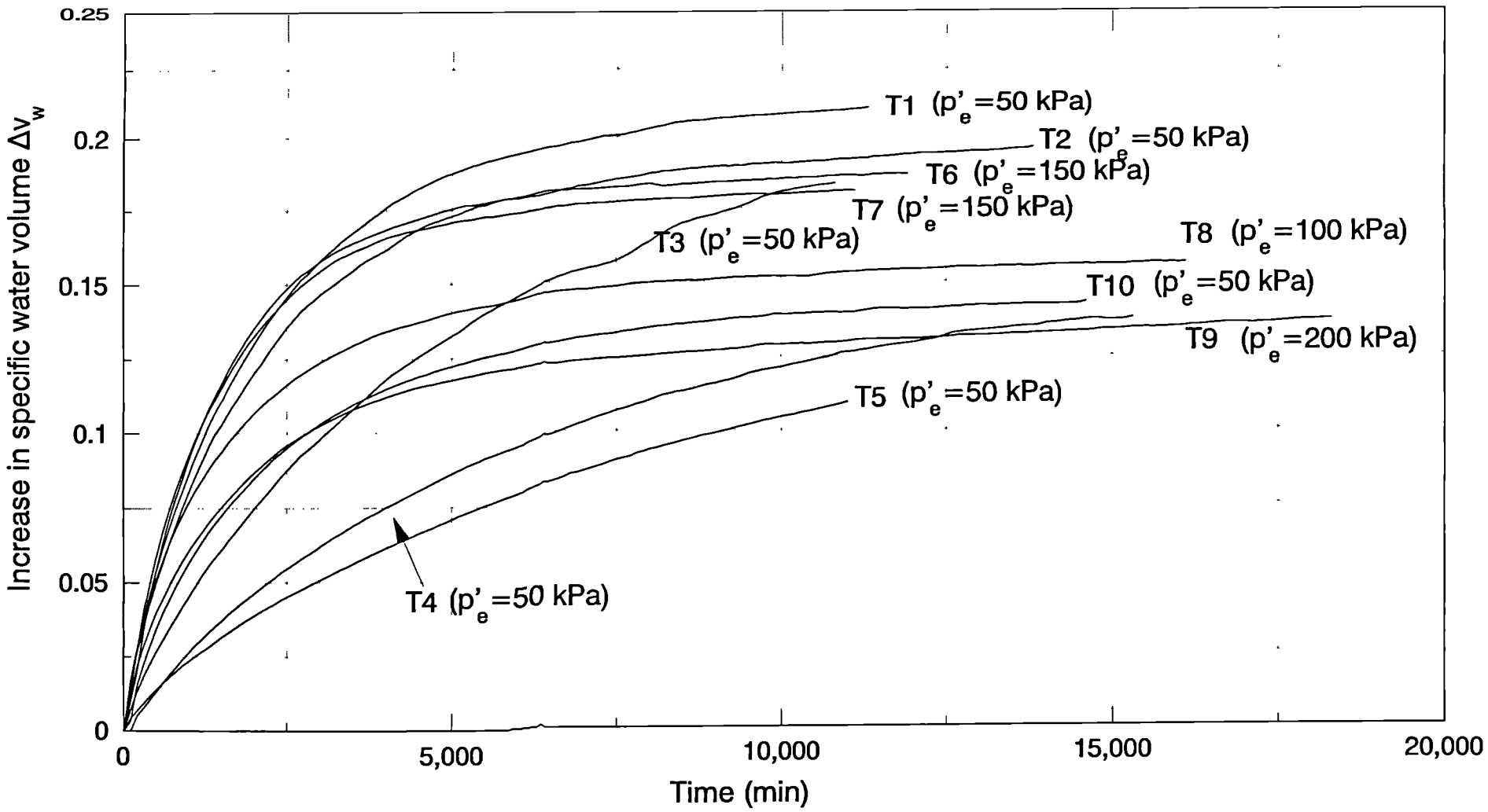

Fig. 6.1 : Increase in specific water volume for all tests during the equalization stage

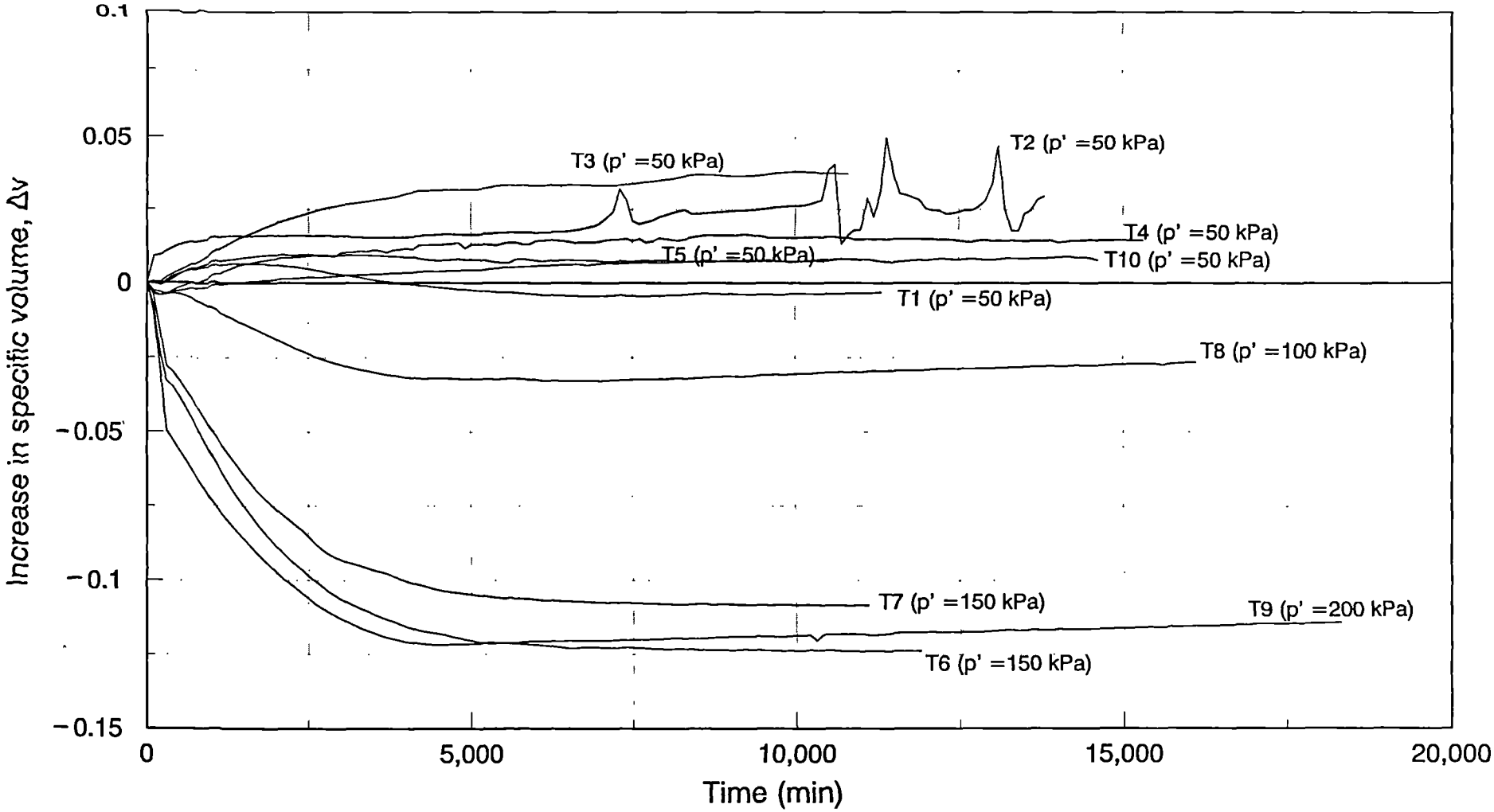

Fig. 6.2 : Variation of specific volume for all tests during equalization stage

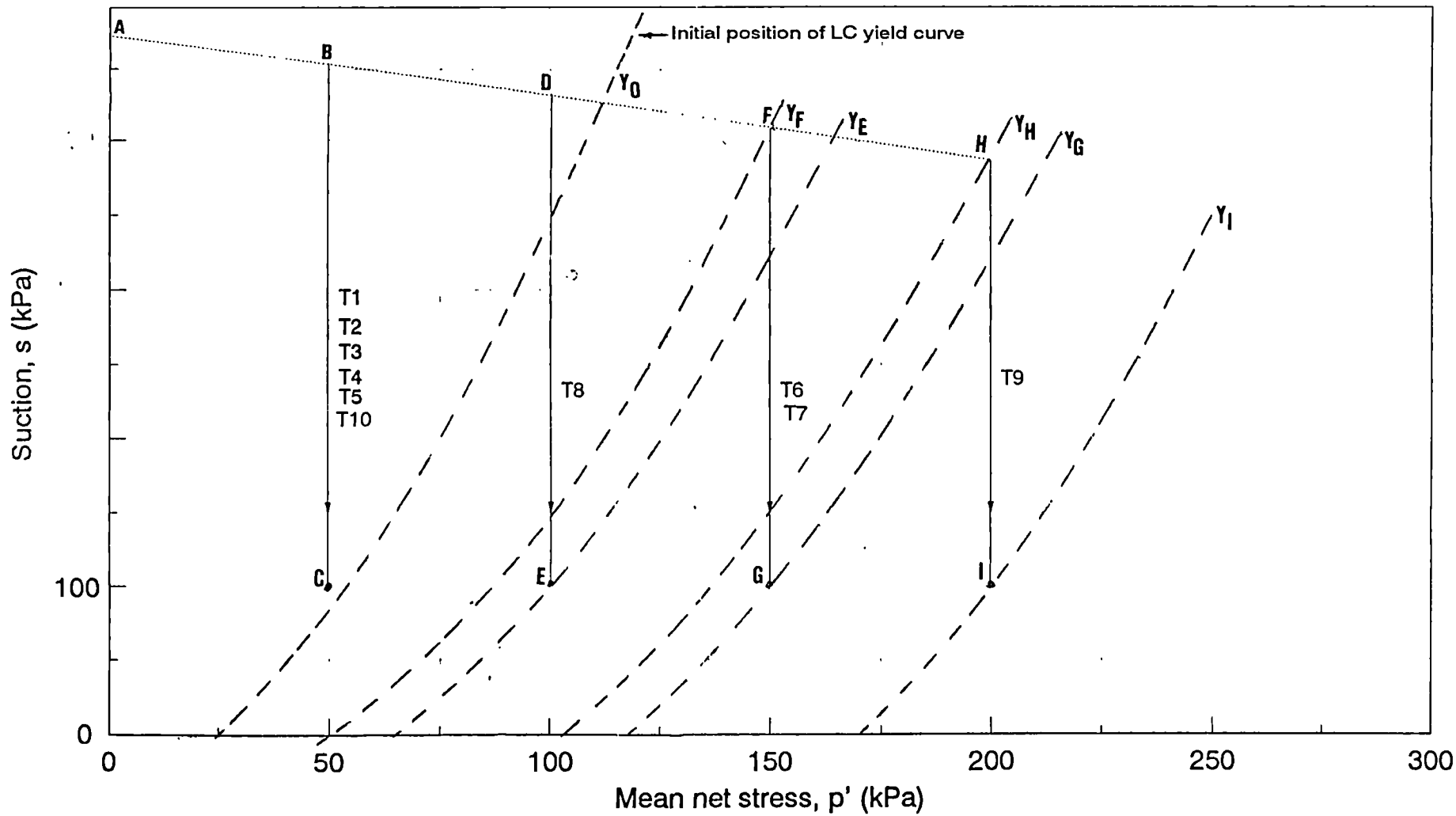

Fig. 6.3 : Stress paths during equalization stage and resulting expansion of the yield curve

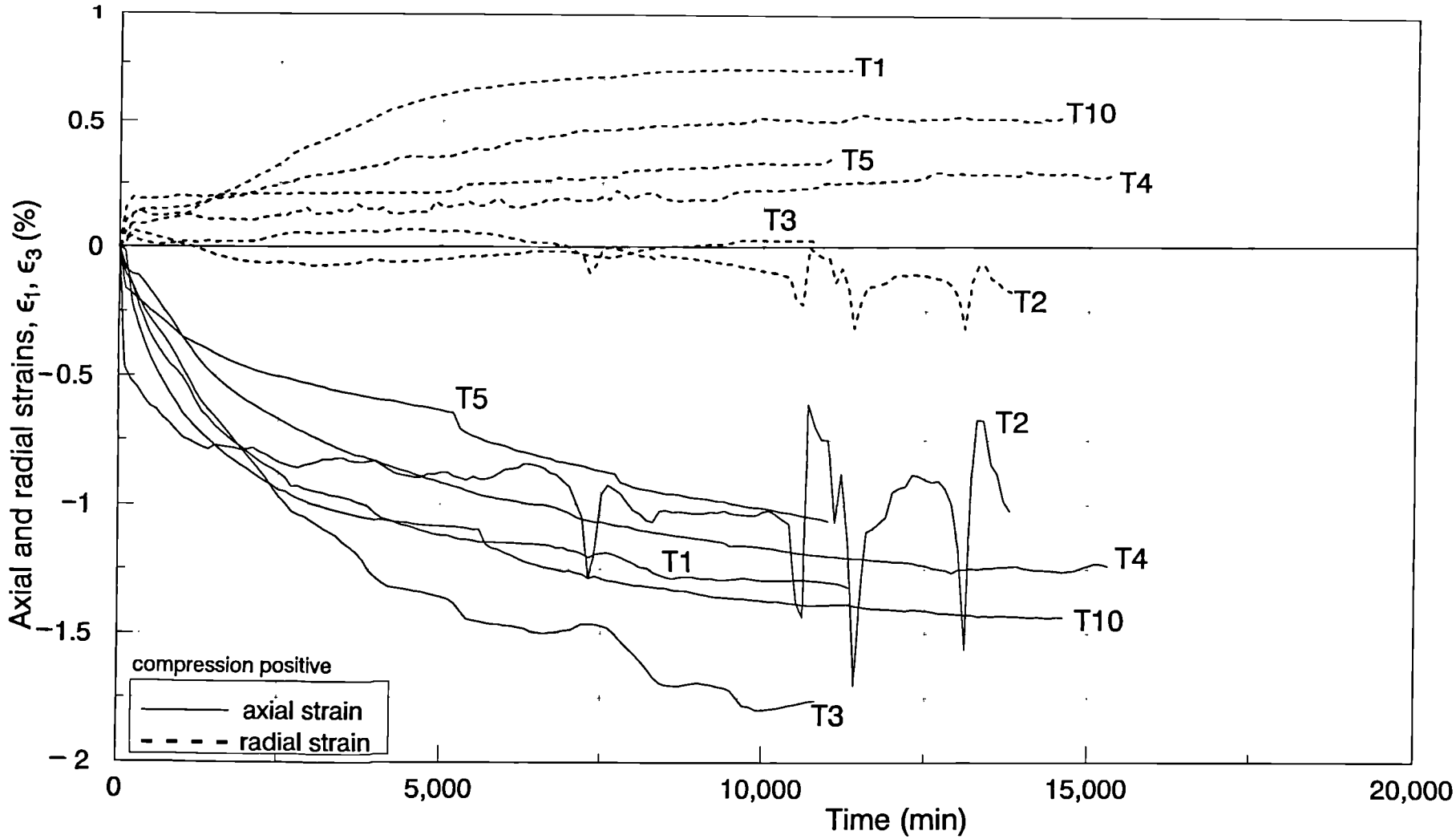

Fig.6.4 : Variation of axial and radial strains for tests at p'_e = 50 kPa during equalization stage

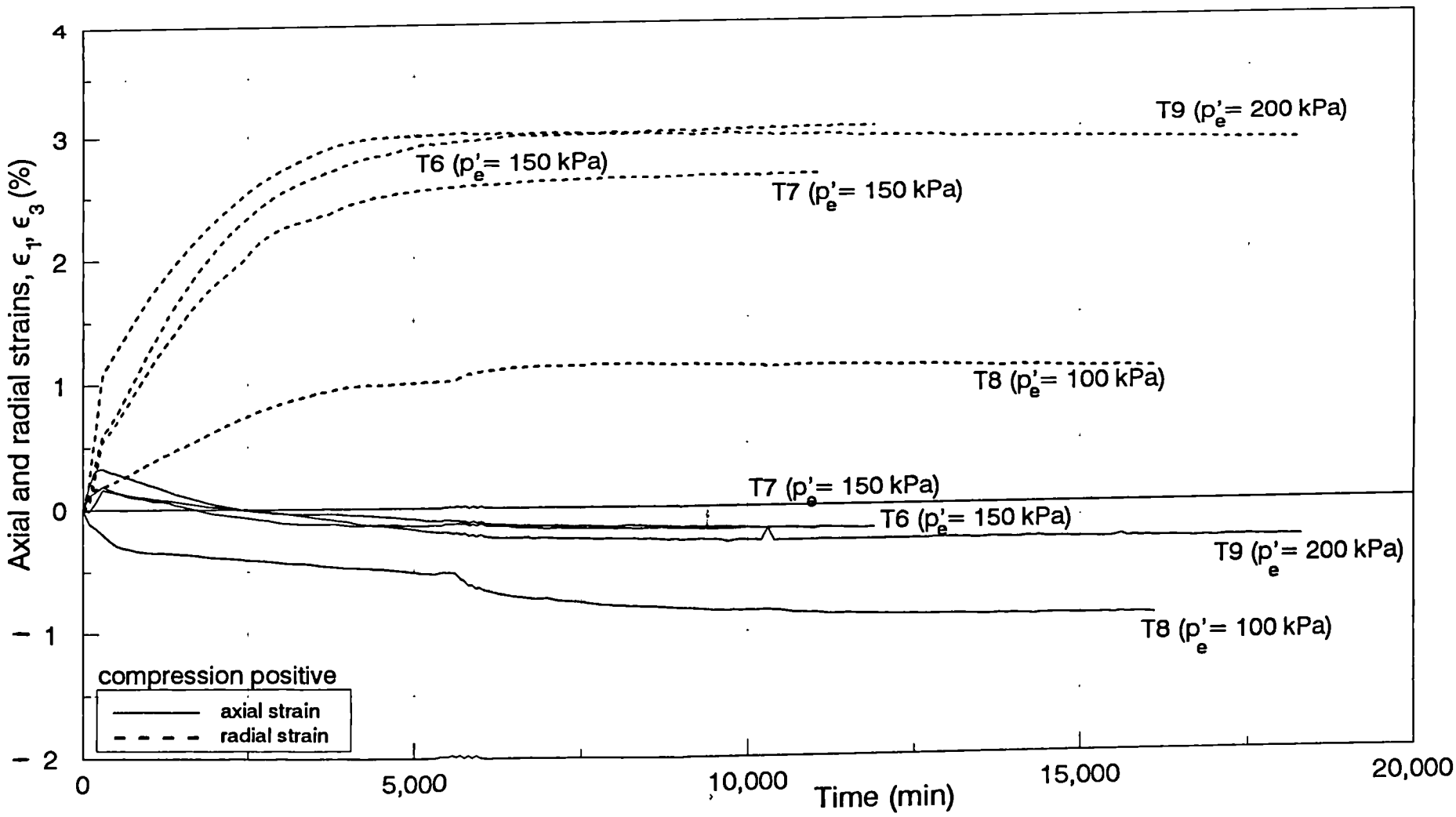

Fig. 6.5 : Variation of axial and radial strains for tests at p'_e > 50 kPa during equalization stage

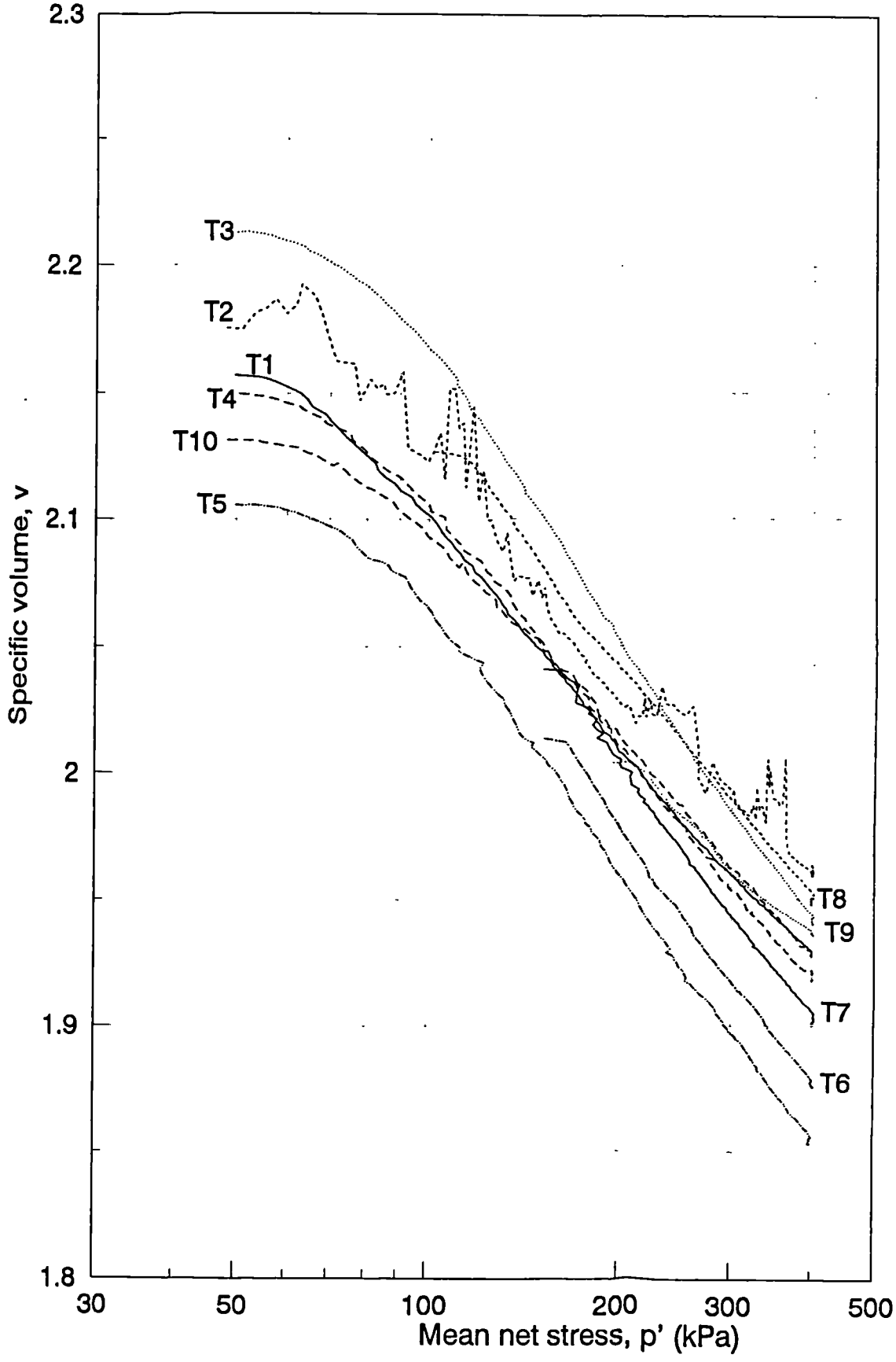

Fig. 6.6 : Specific volume versus mean net stress for all tests during ramped consolidation stage

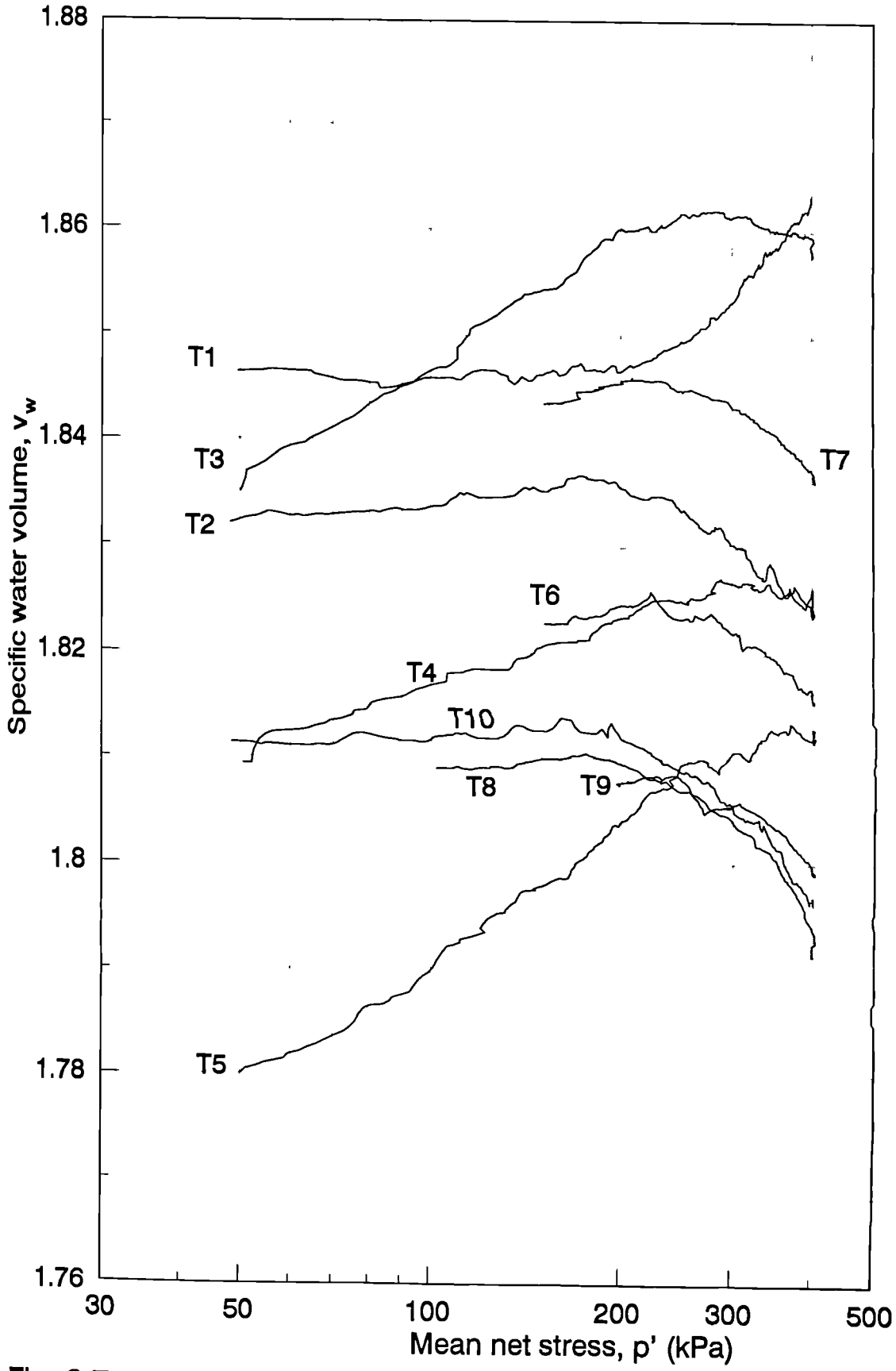

Fig. 6.7 : Specific water volume versus mean net stress for all tests during ramped consolidation stage

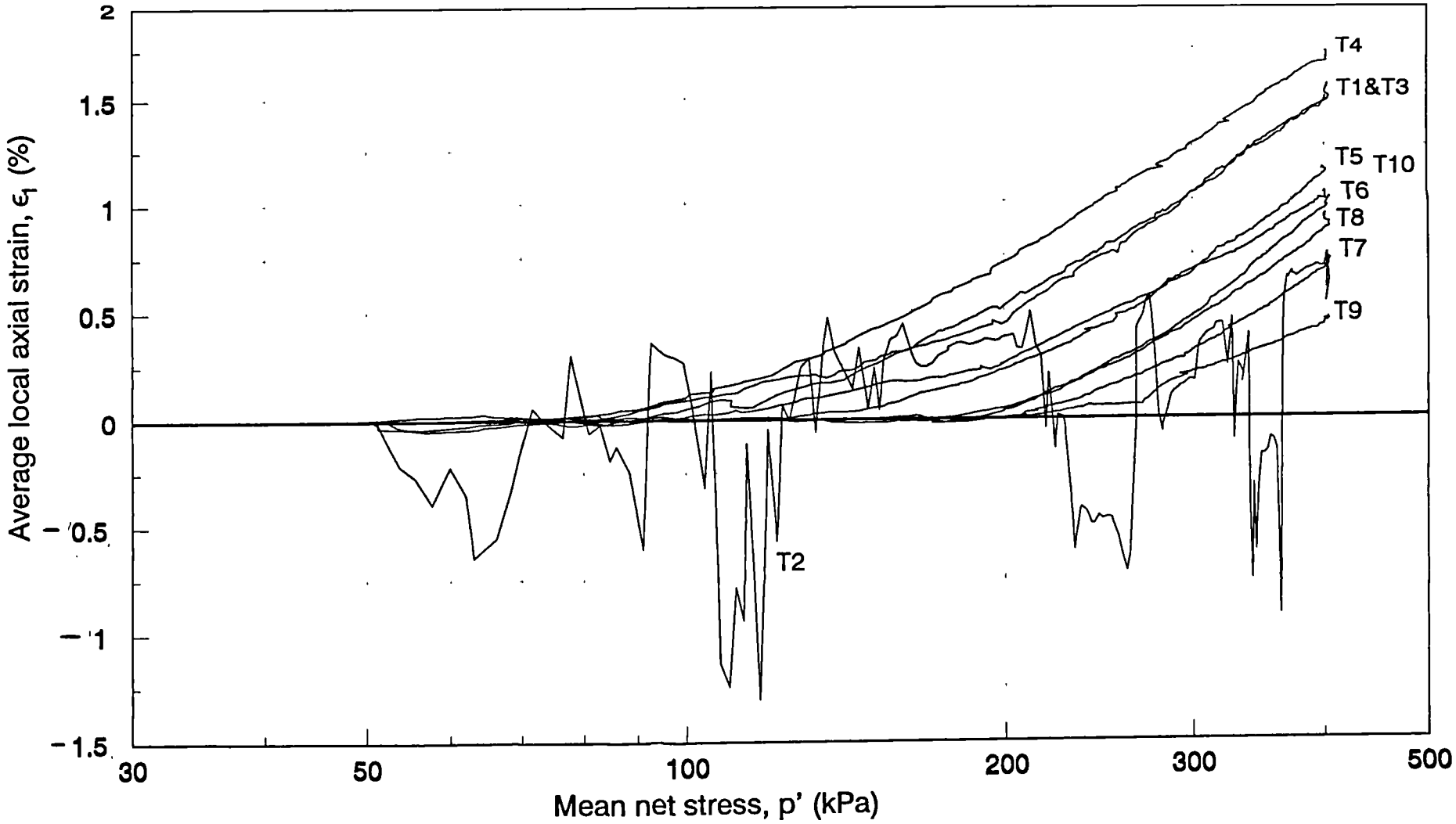

Fig. 6.8 : Variation of local axial strain with mean net stress for all tests during ramped consolidation stage

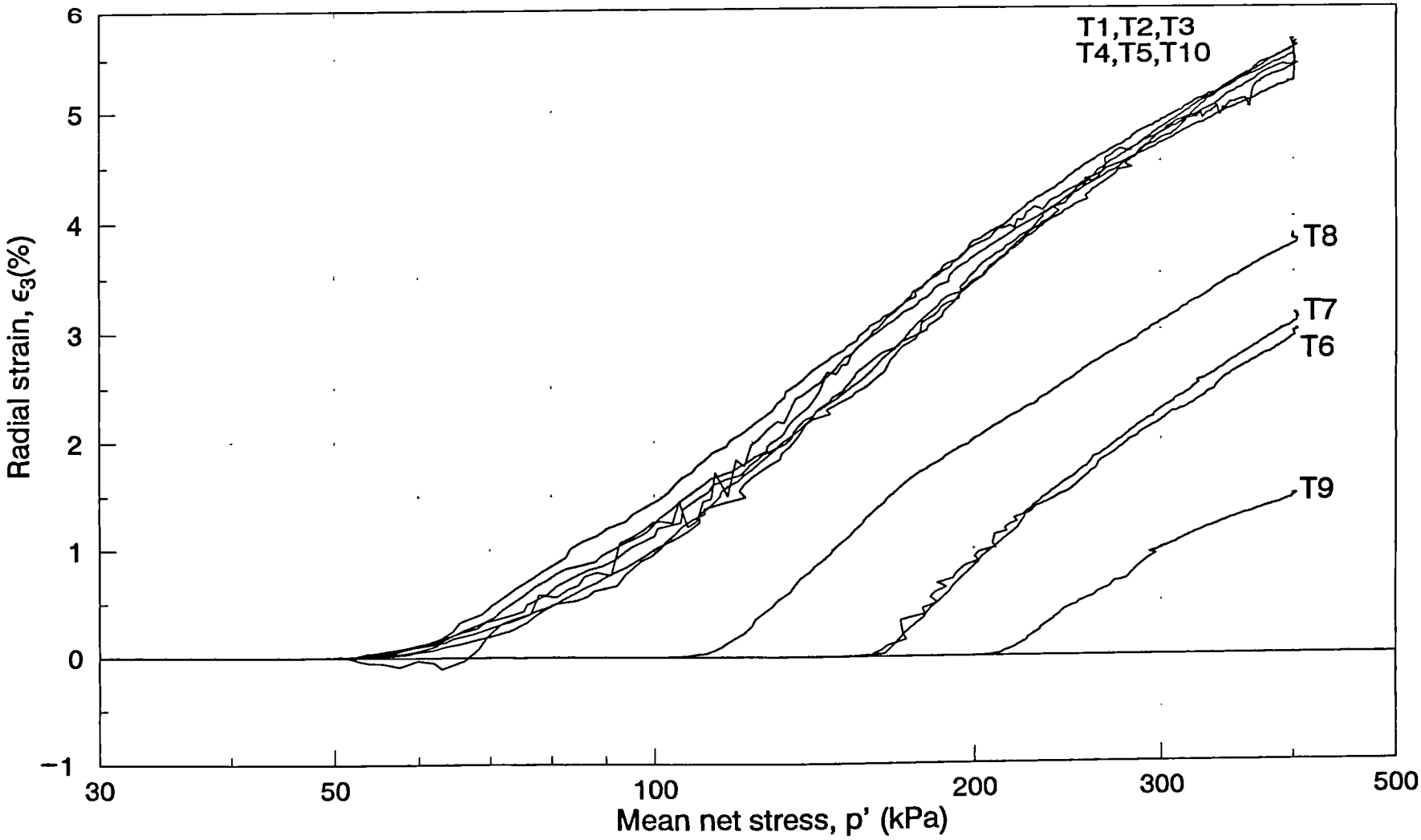

Fig. 6.9 : Variation of radial strain with mean net stress for all tests during ramped consolidation stage

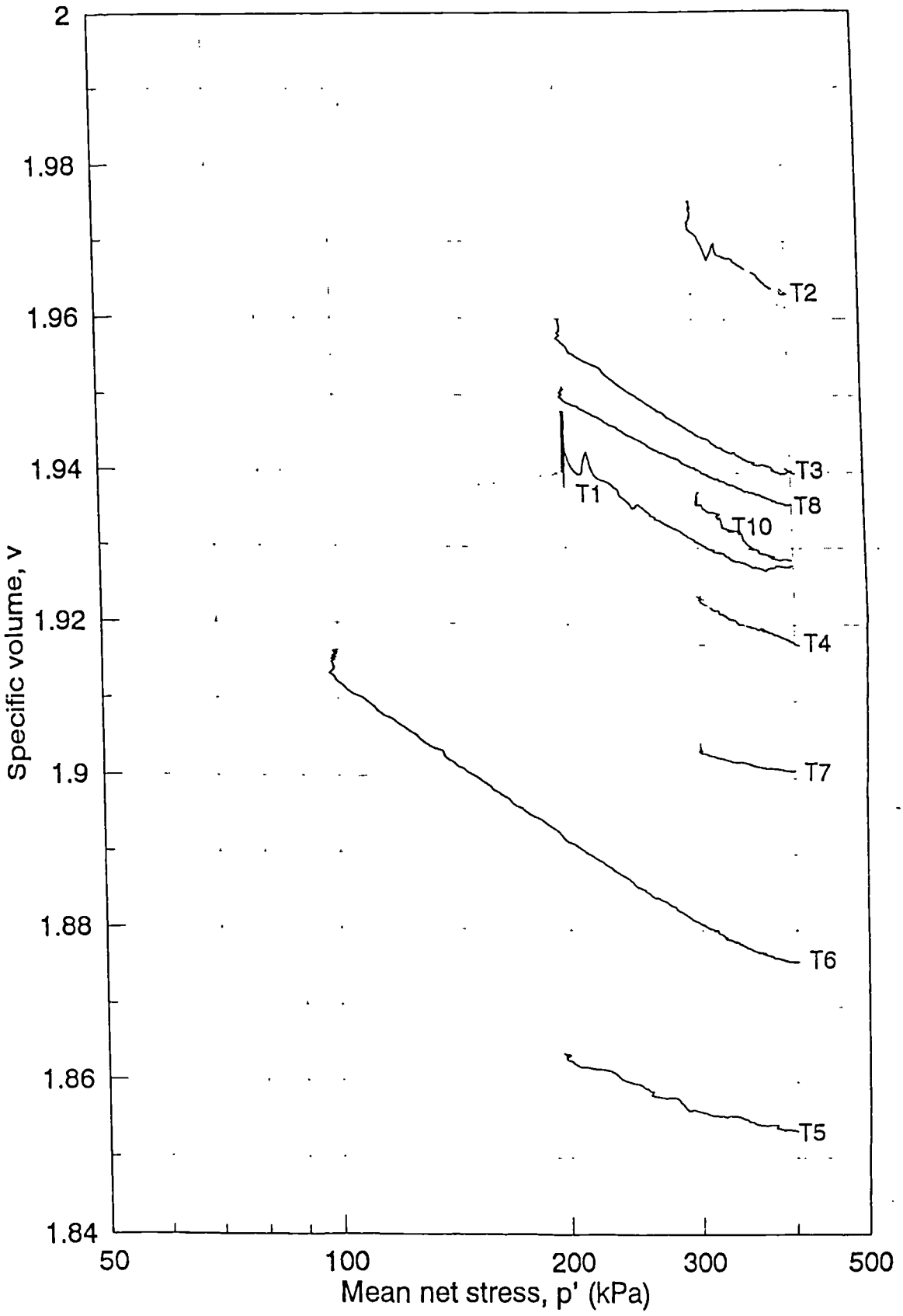

Fig. 6.10 : Variation of specific volume with mean net stress for all tests during swell-back stage

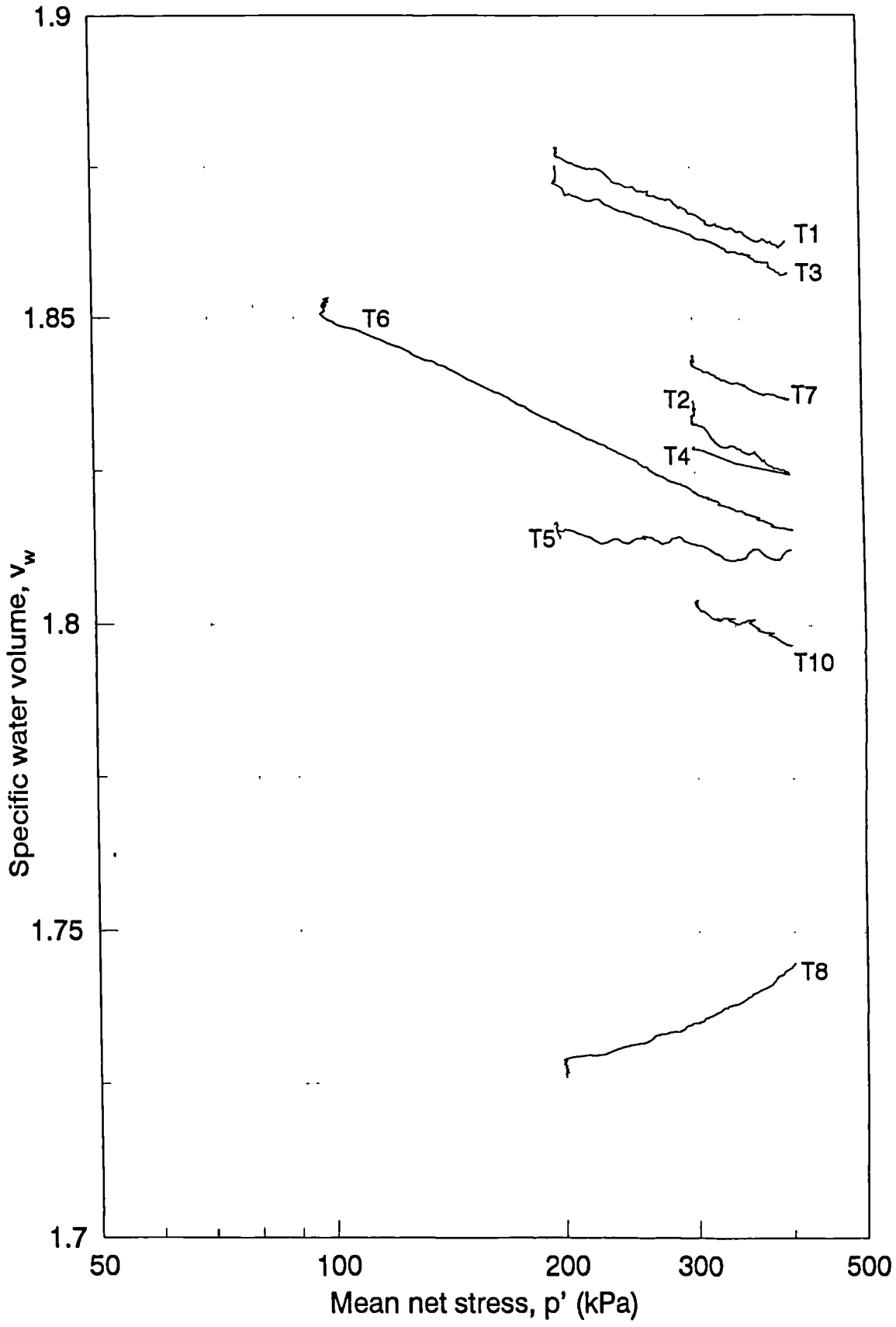

Fig. 6.11 : Variation of specific water volume with mean net stress for all tests during swell-back stage

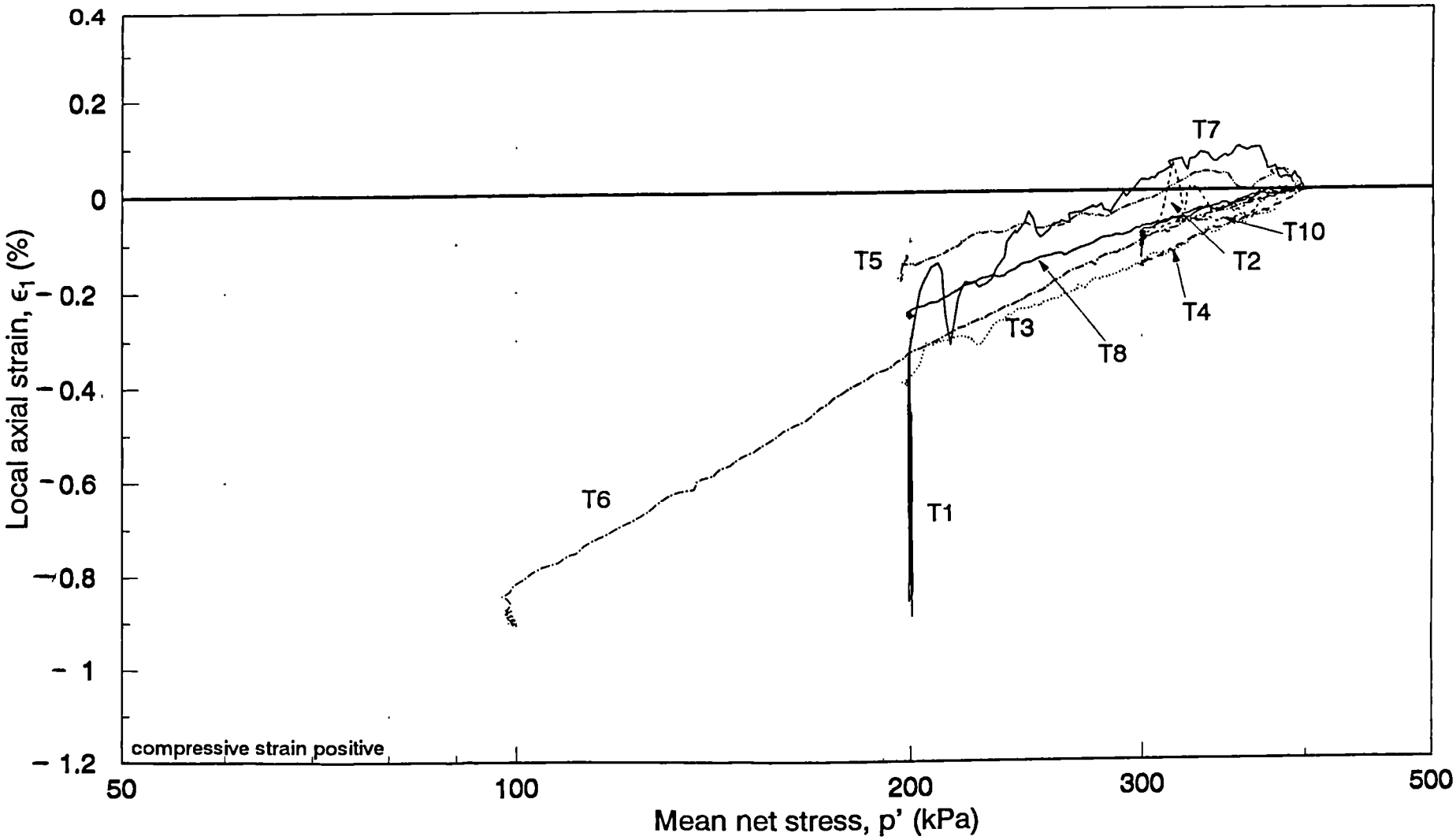

Fig. 6.12 : Variation of axial strain with mean net stress for all tests during swell-back stage

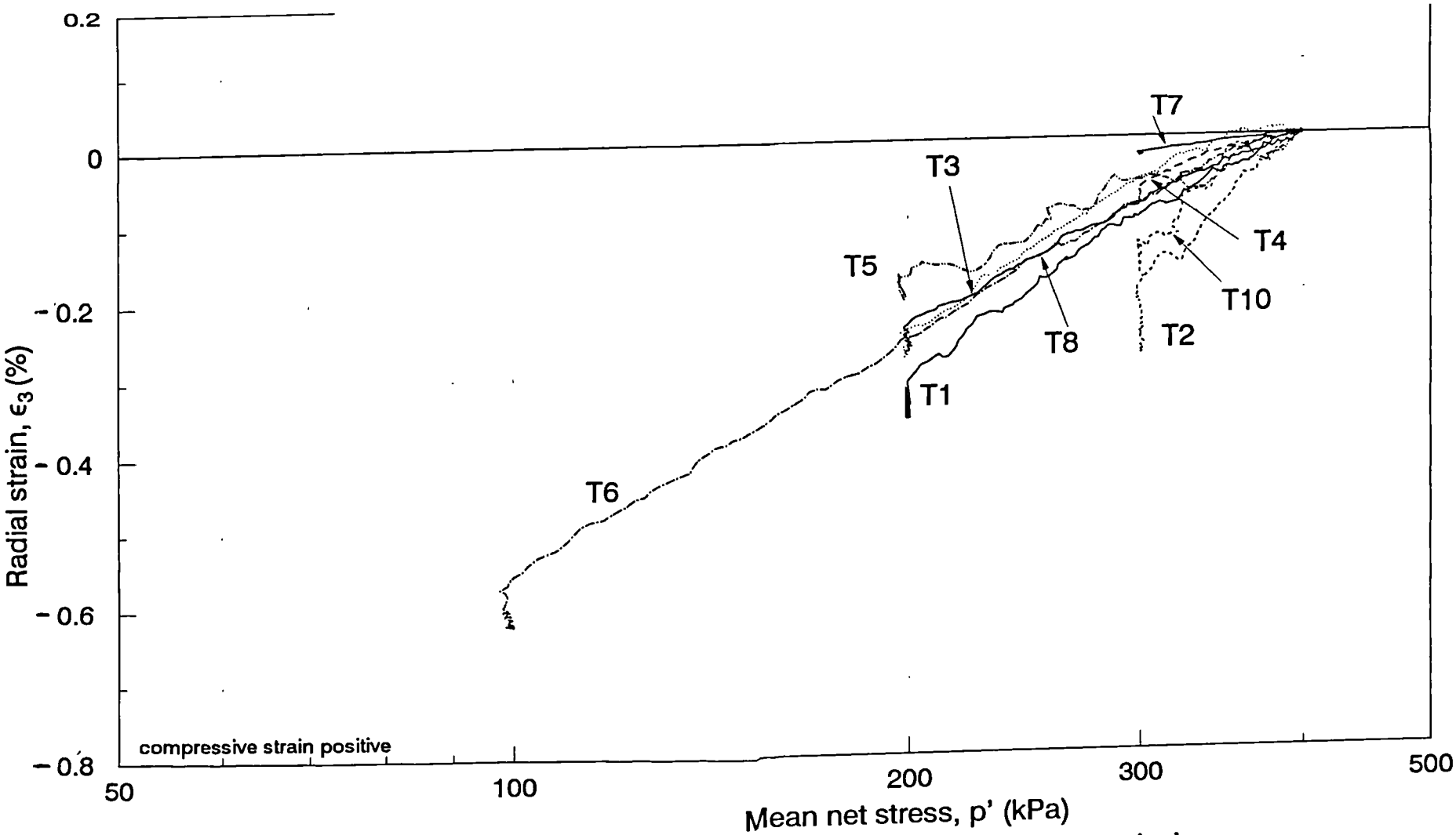

Fig. 6.13 : Variation of radial strain with mean net stress for all tests during swell-back stage

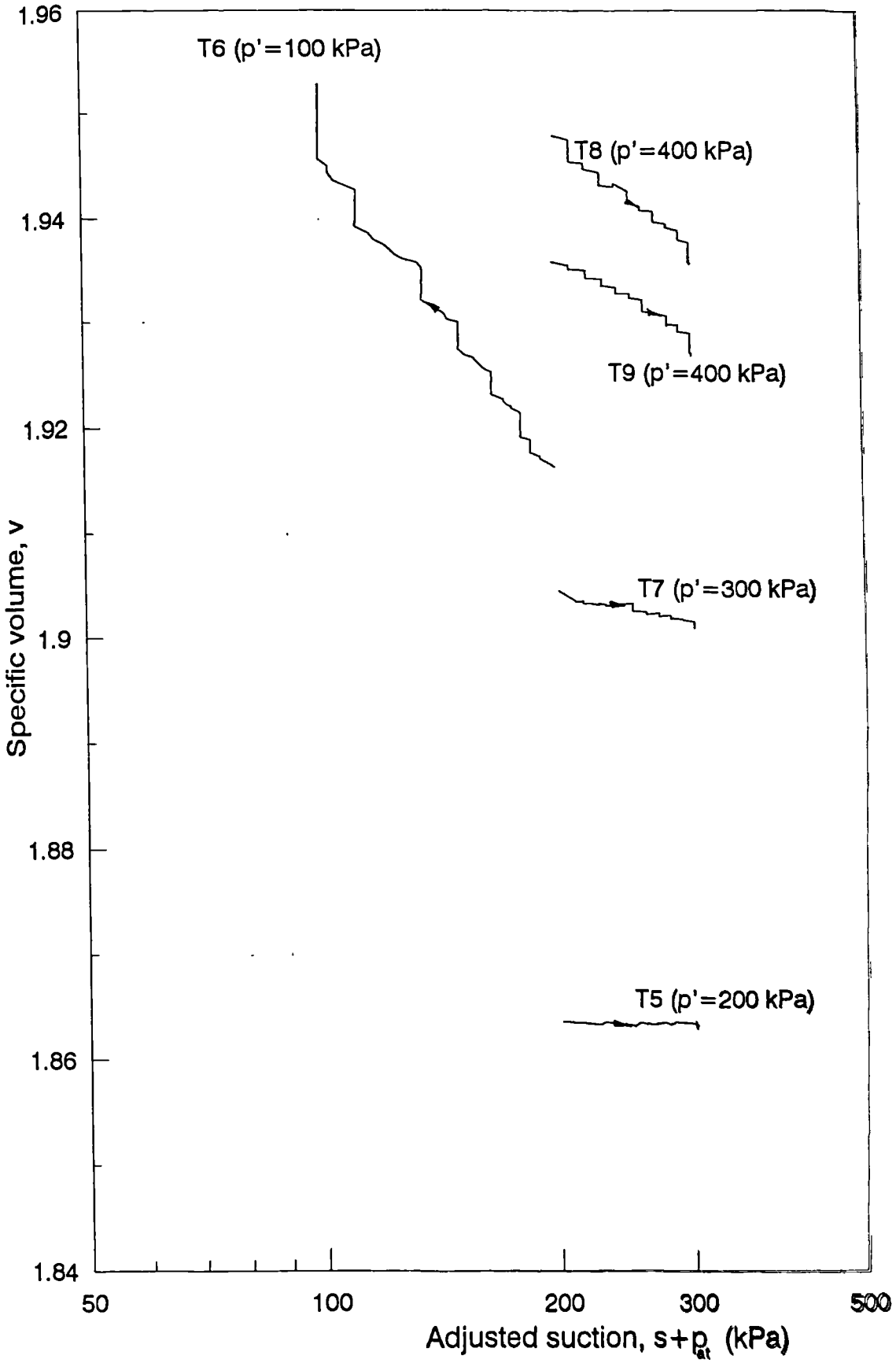

Fig. 6.14 : Variation of specific volume during suction-change stage

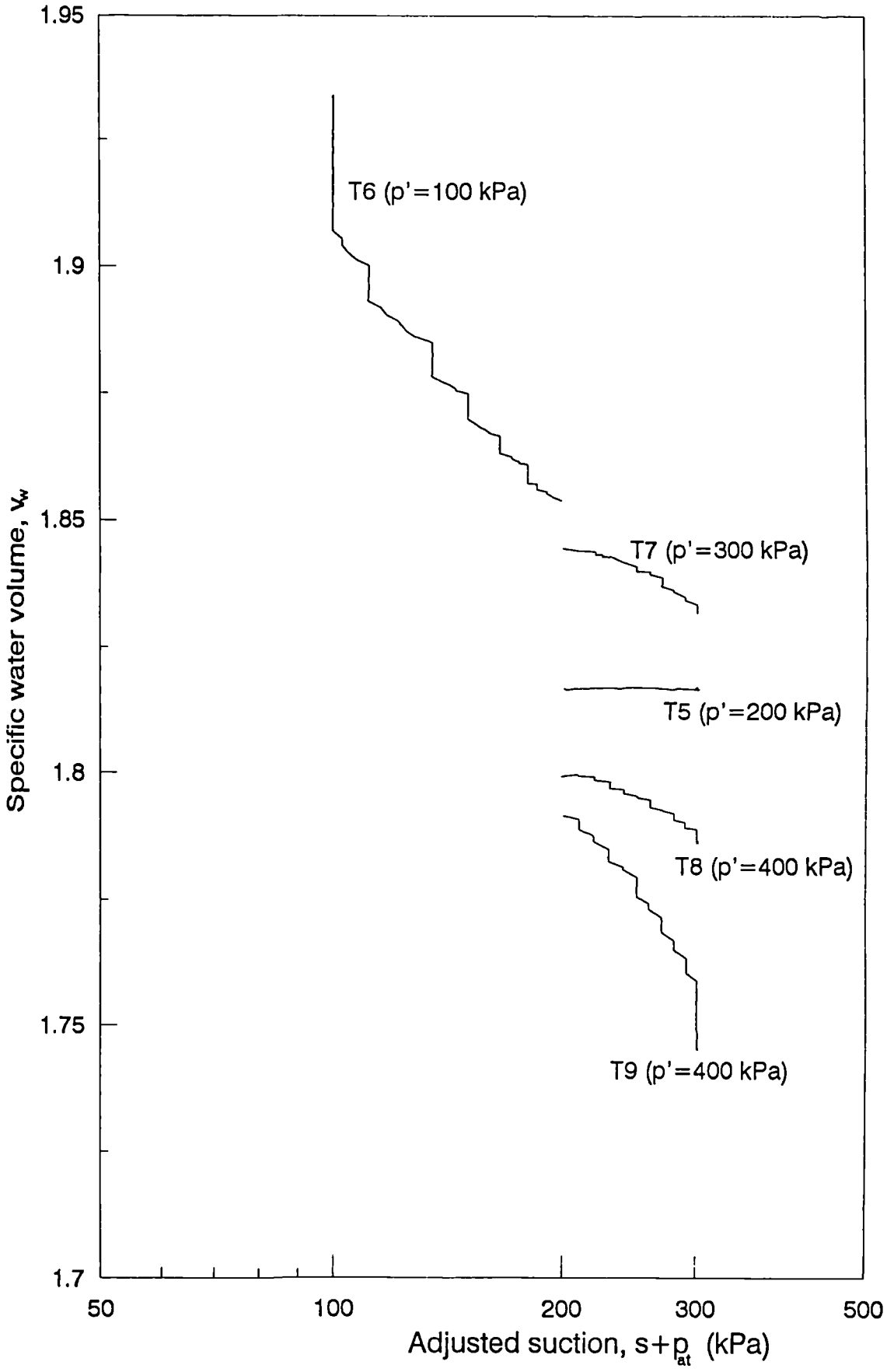

Fig. 6.15 : Variation of specific water volume during suction-change stage

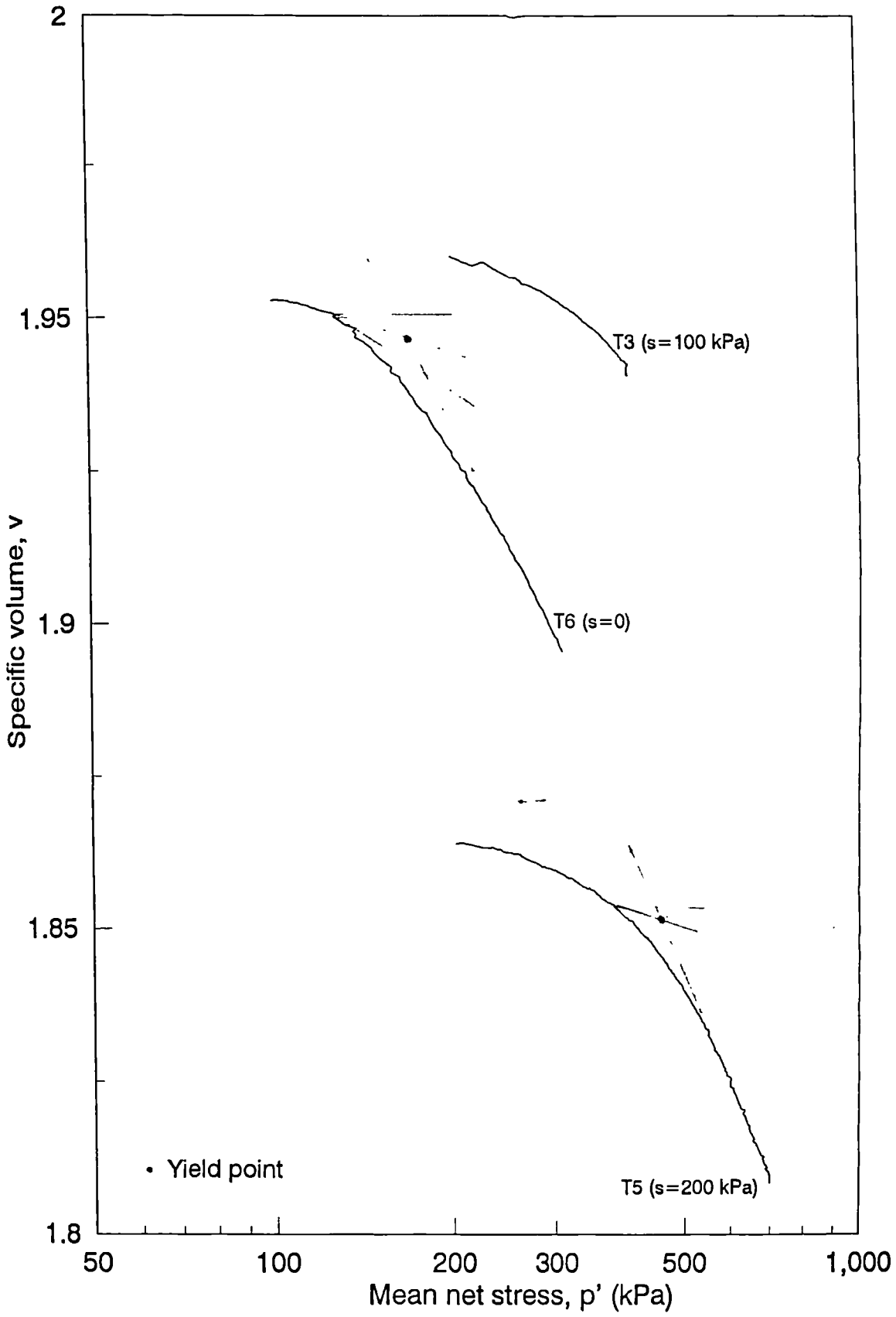

Fig. 6.16 : Variation of specific volume during isotropic re-loading stage

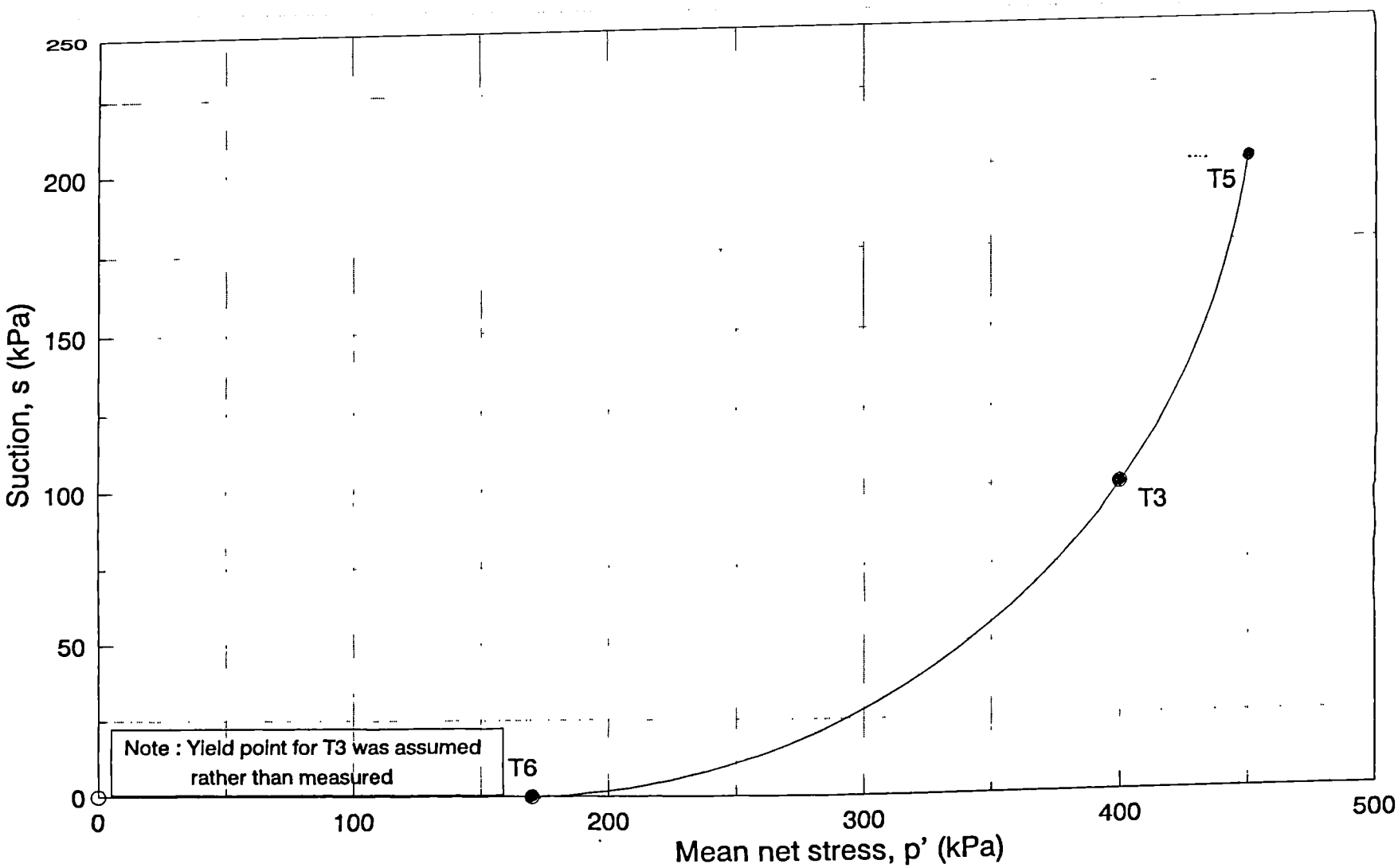

Fig. 6.17 : Position of LC yield curve observed during isotropic re-loading

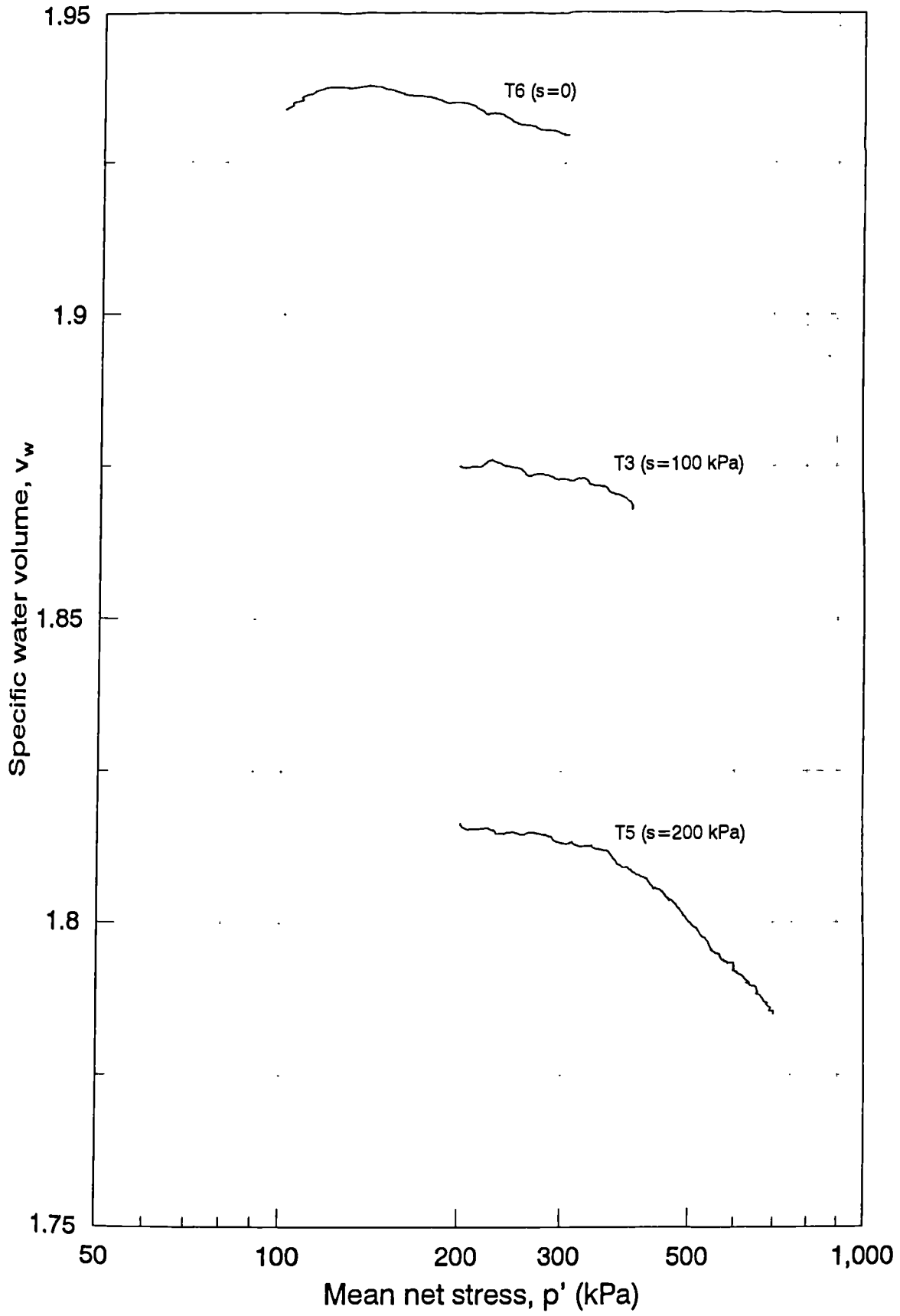

Fig. 6.18 : Variation of specific water volume during isotropic re-loading tests

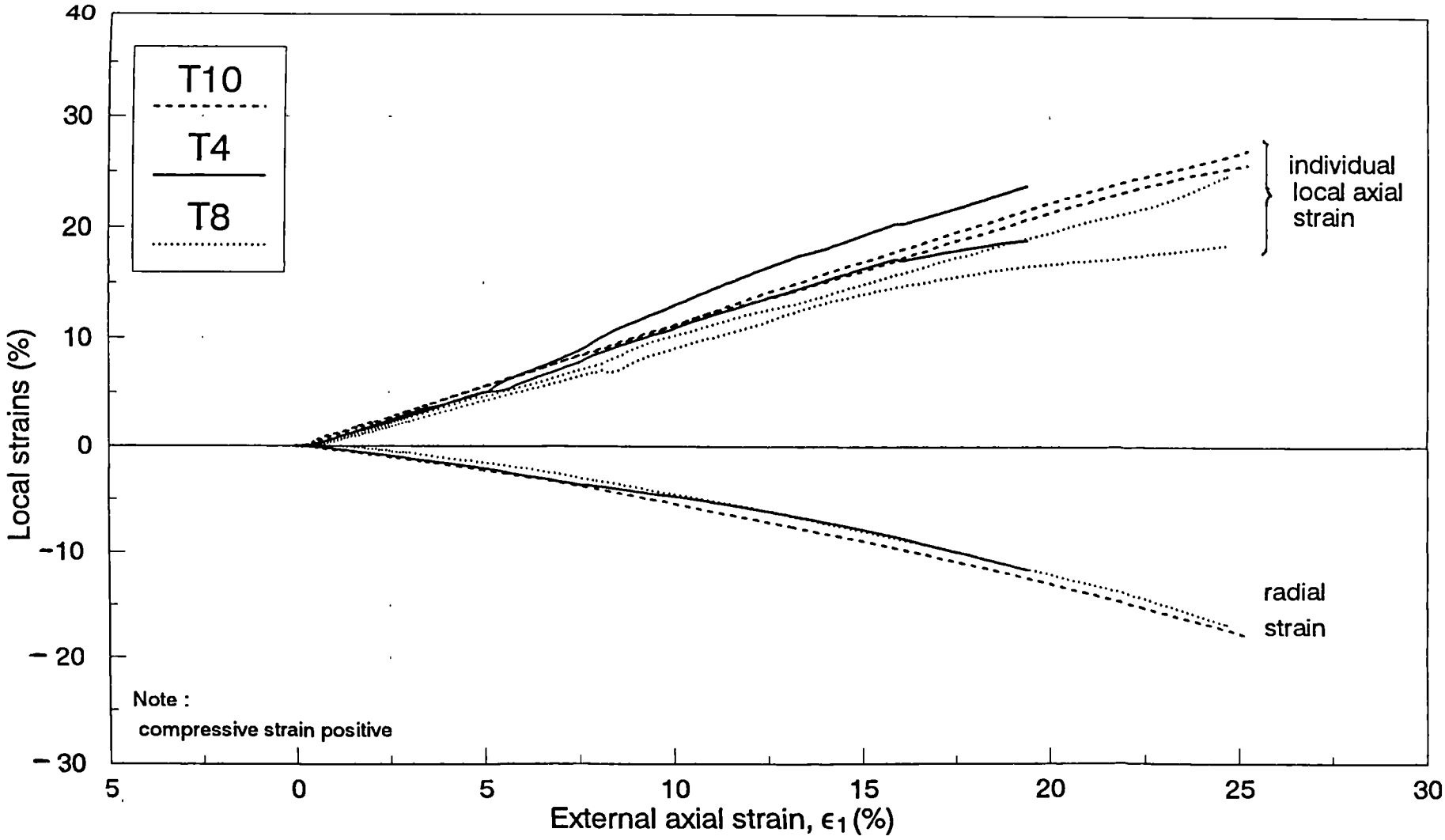

Fig. 6.19 : Performance of local strain gauges in three typical shear tests

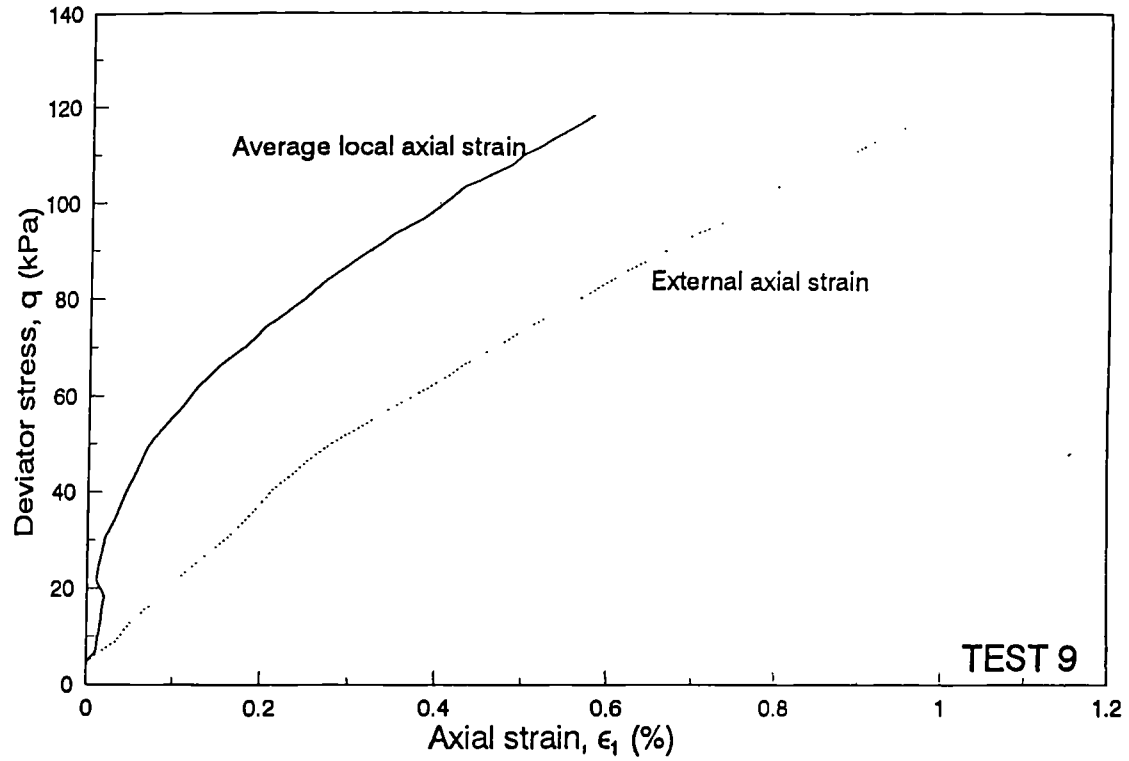

(a) Bedding error during a typical shear test

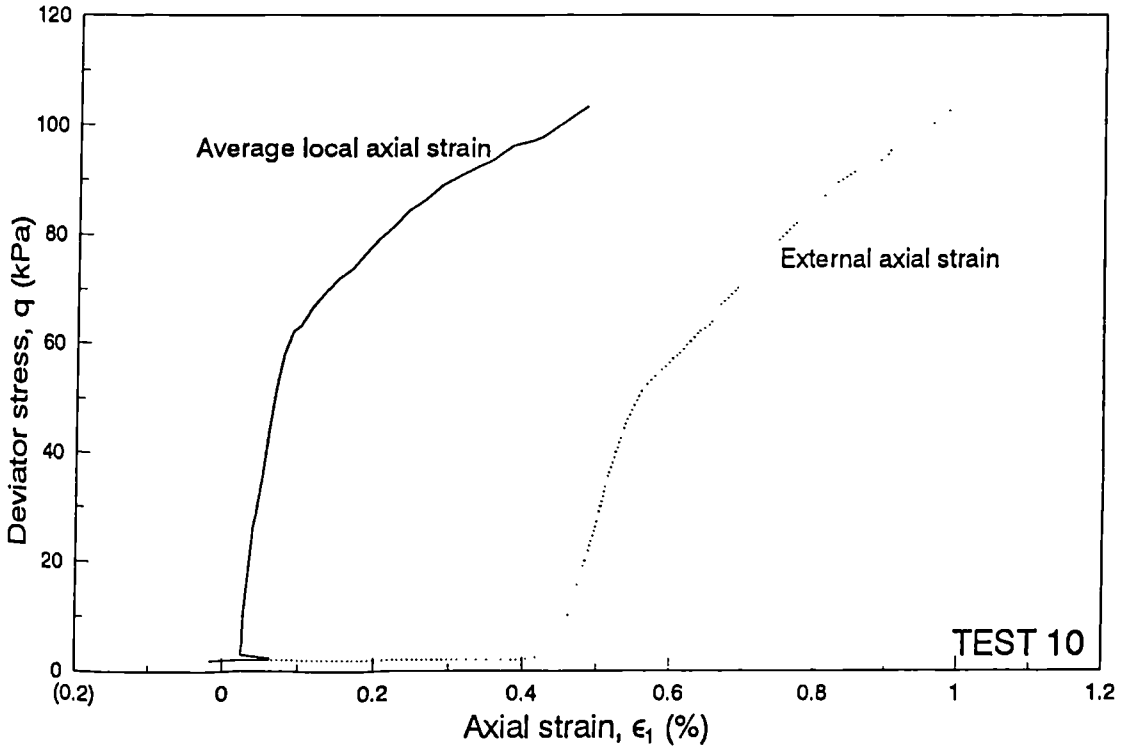

(b) Worst bedding error during shear test

Fig. 6.20 : Bedding errors during two typical shear tests

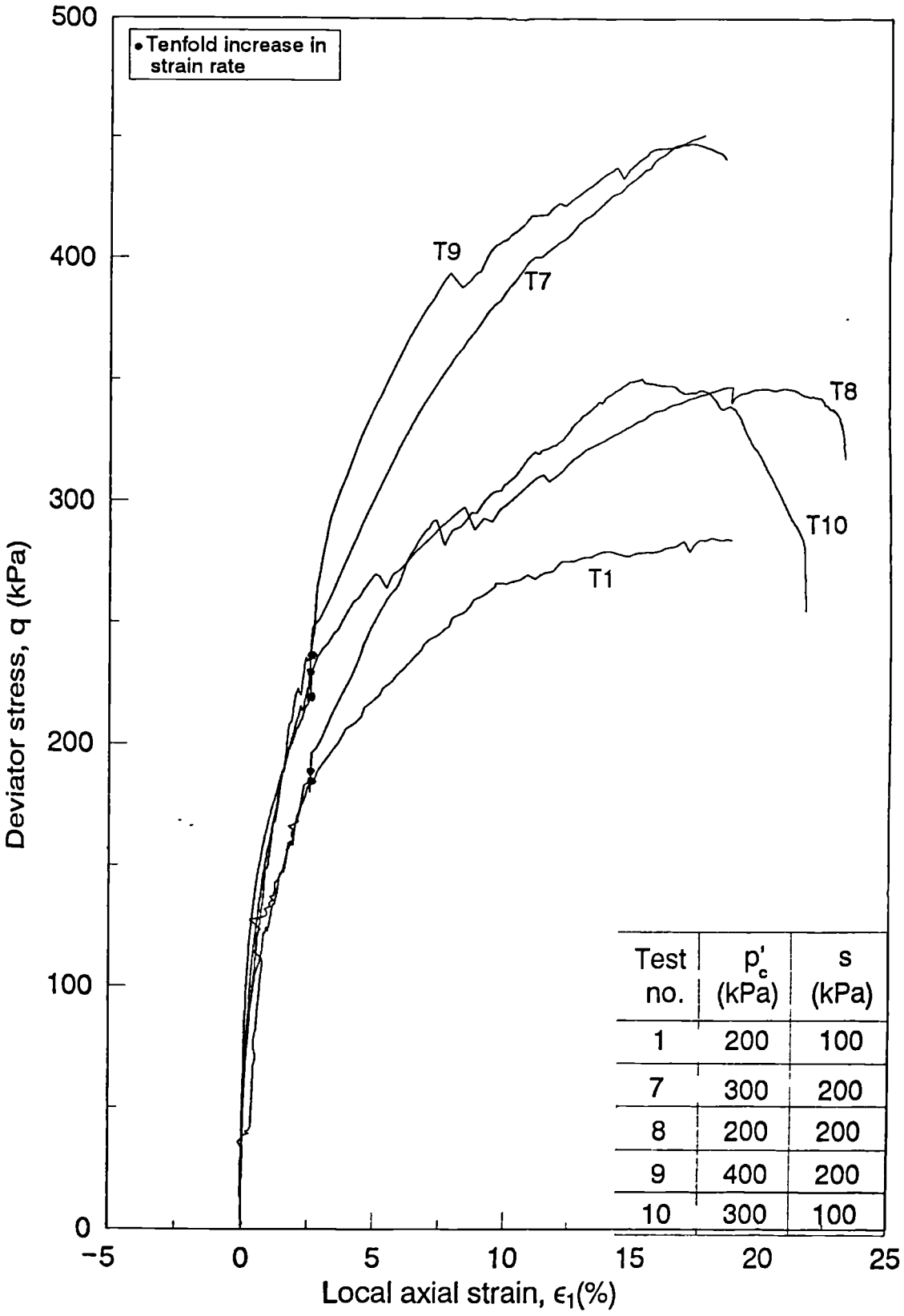

Test no.	p'_c (kPa)	s (kPa)
1	200	100
7	300	200
8	200	200
9	400	200
10	300	100

Fig. 6.21 : Deviator stress versus axial strain for shear tests conducted at constant cell pressure

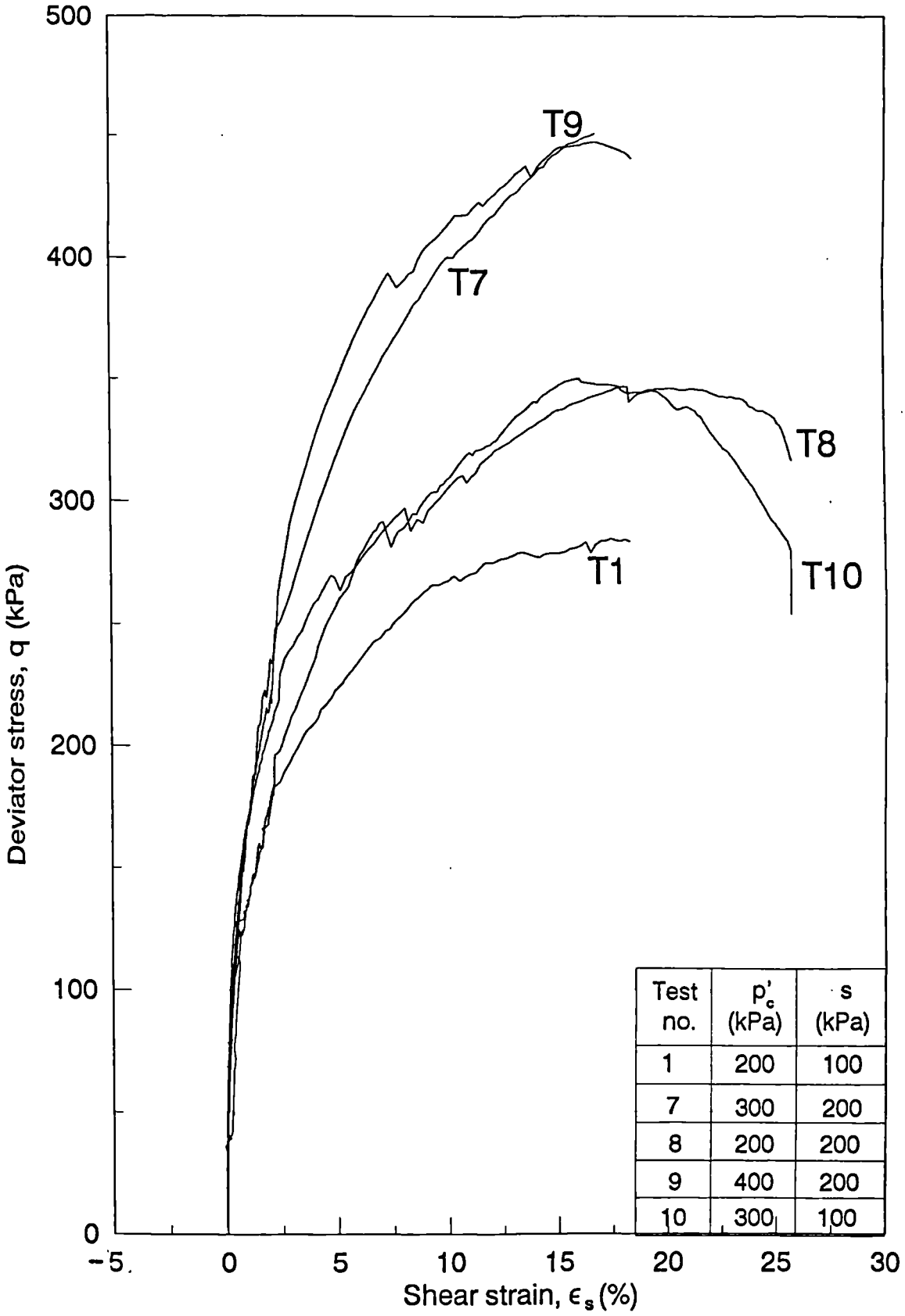

Fig. 6.22 : Deviator stress versus shear strain for shear tests conducted at constant cell pressure

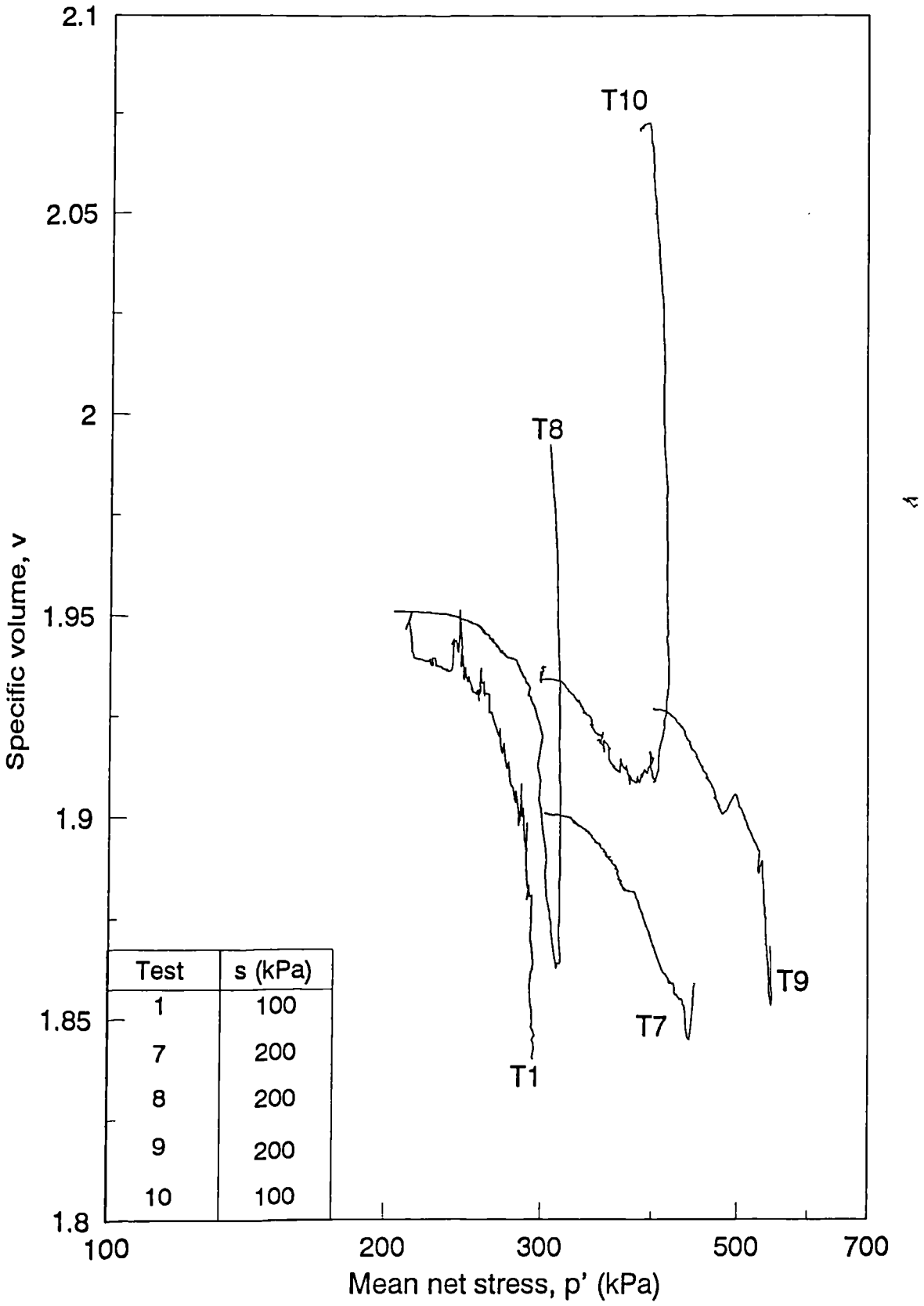

Fig. 6.23 : Variation of specific volume with mean net stress during shear tests conducted at constant cell pressure

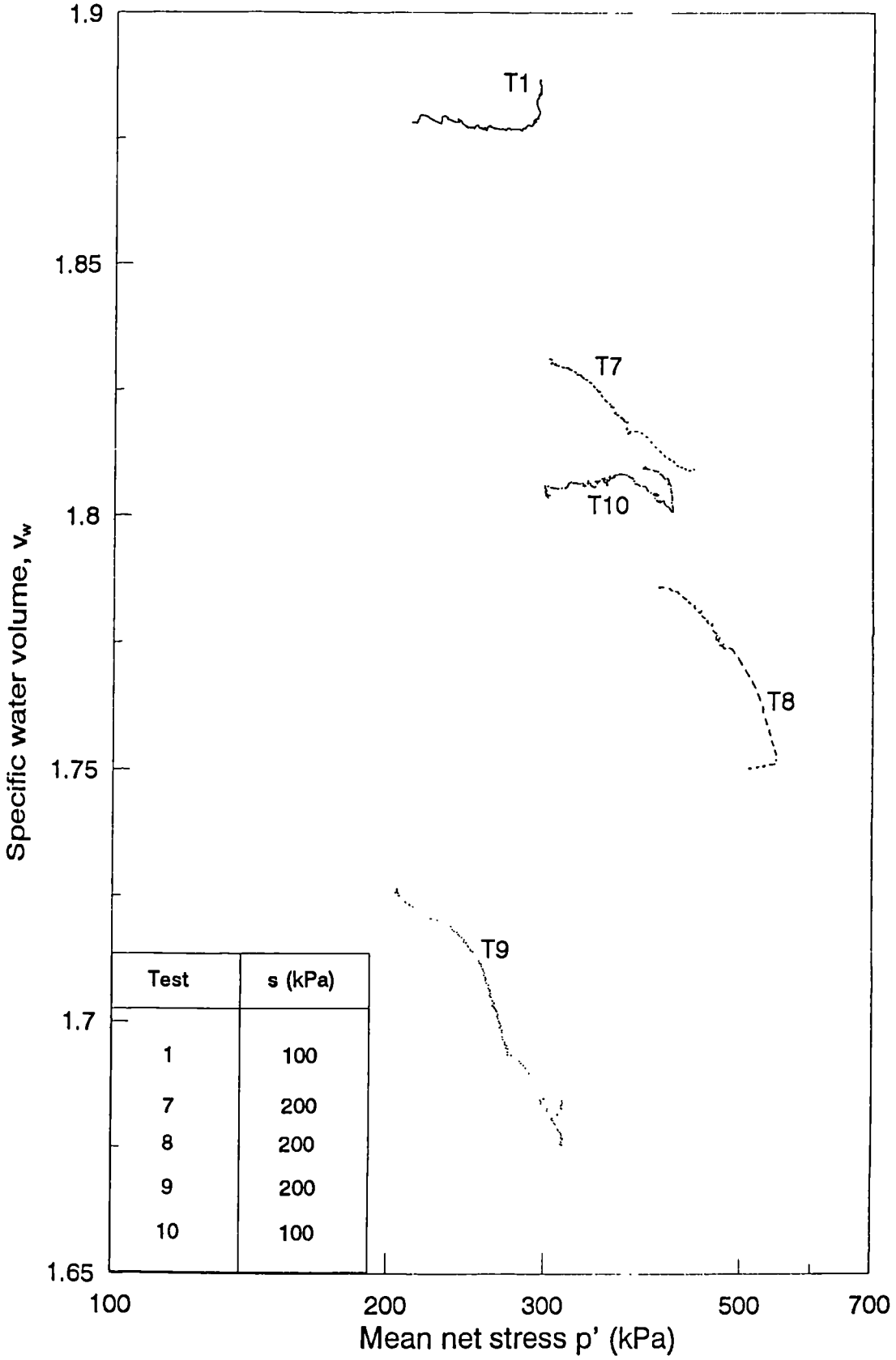

Fig. 6.24 : Variation of specific water volume with mean net stress during shear tests conducted at constant cell pressure

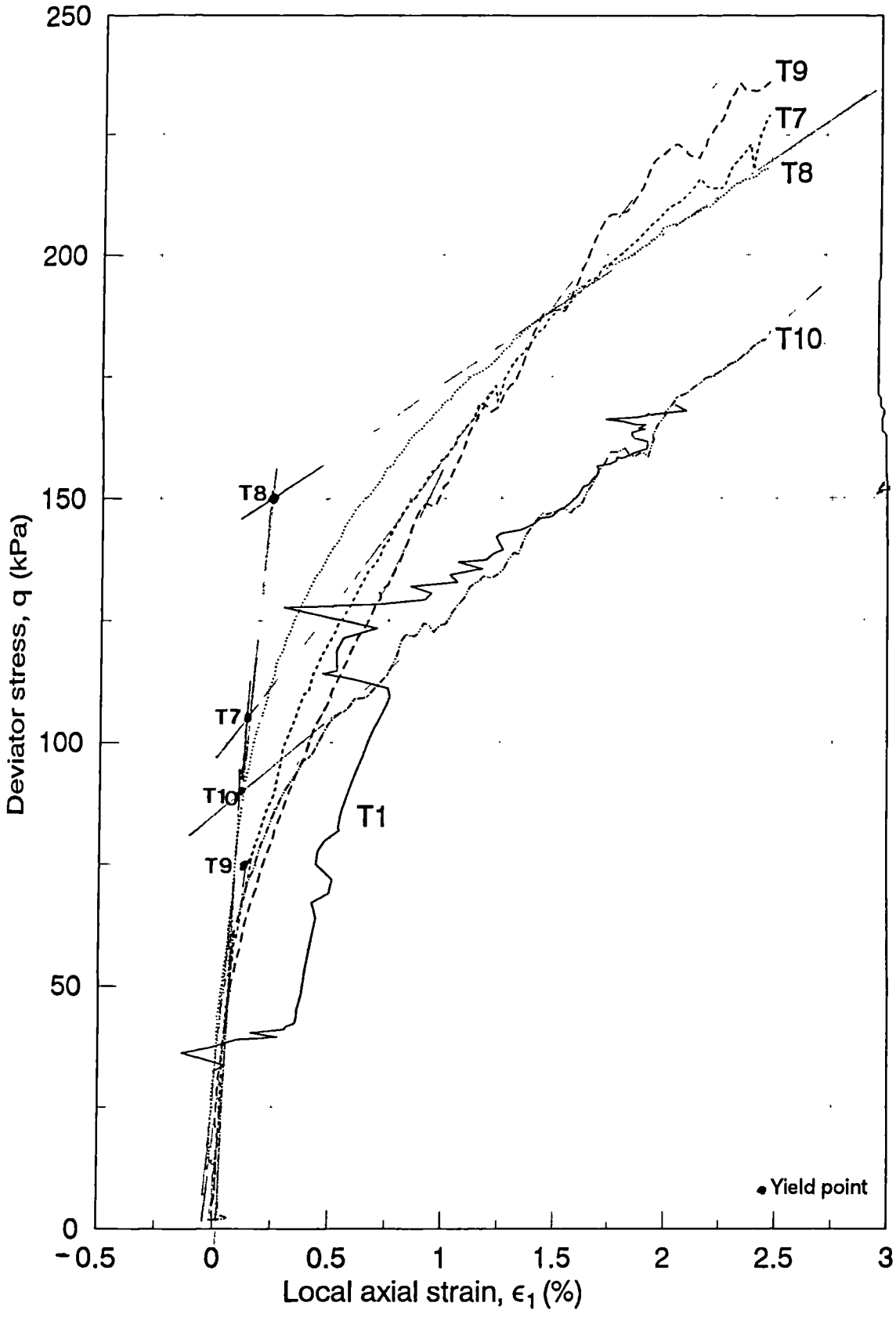

Fig. 6.25 : Enlarged plot of deviator stress versus axial strain for shear tests conducted at constant cell pressure

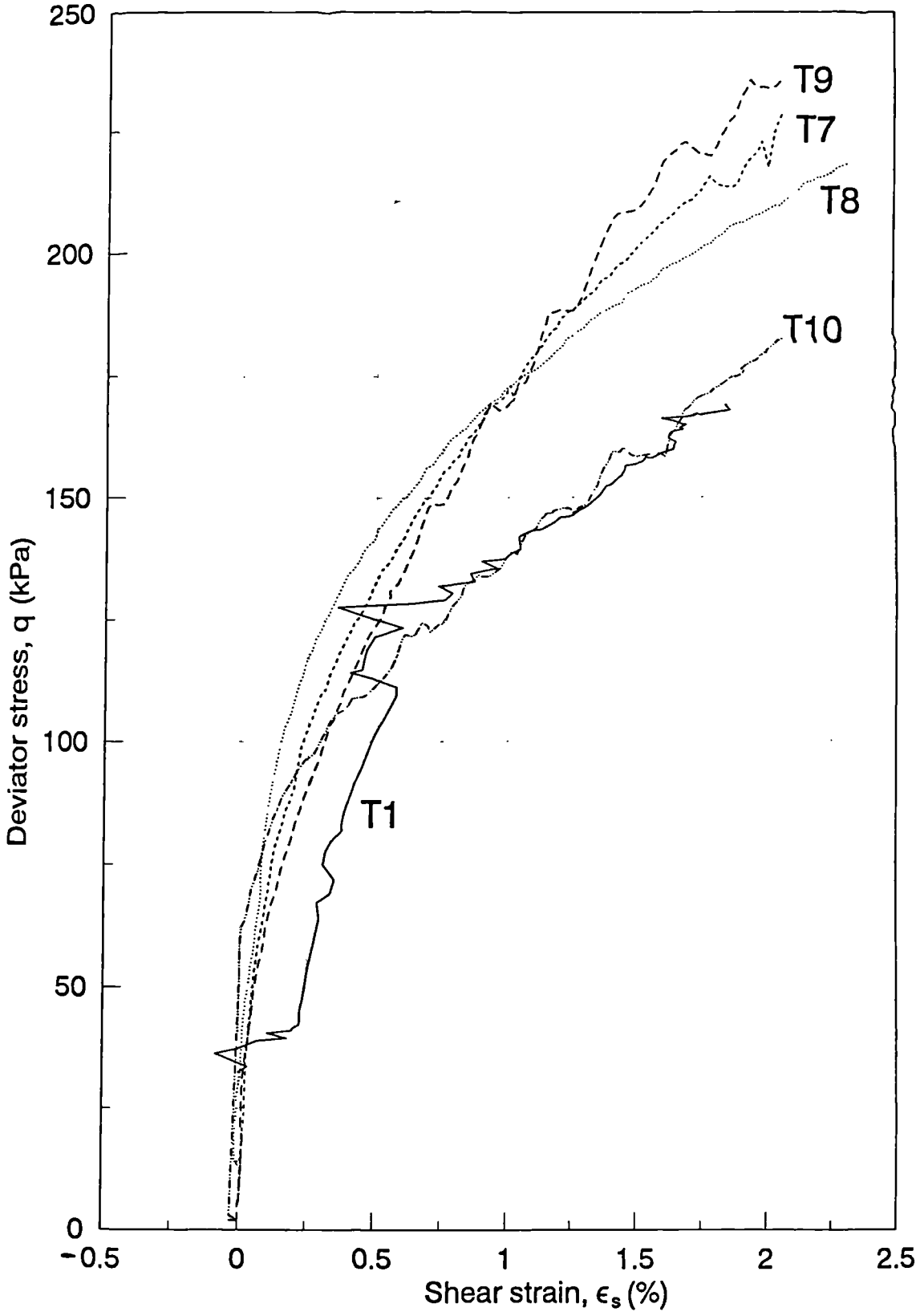

Fig. 6.26 : Enlarged plot of deviator stress versus shear strain for tests conducted at constant cell pressure

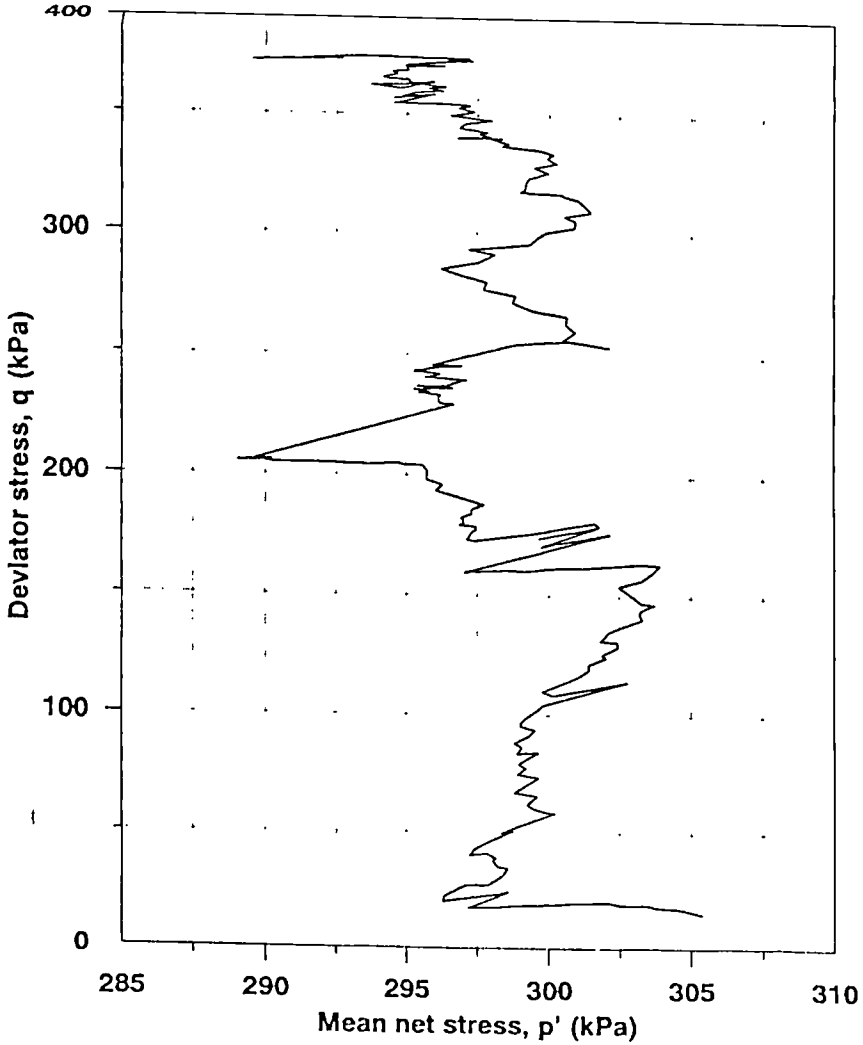

Fig. 6.28 : Stress path during shear stage of Test 4 (constant-p' shearing)

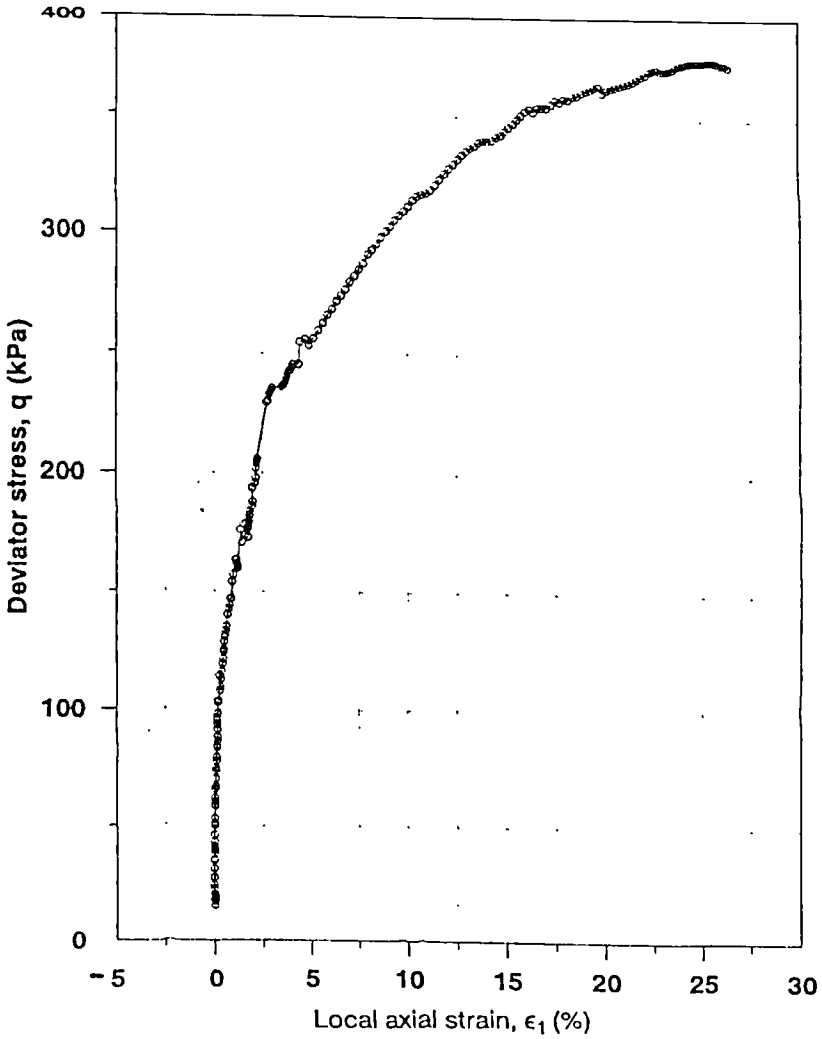

Fig. 6.29 : Deviator stress versus axial strain in Test 4 (constant-p' shearing)

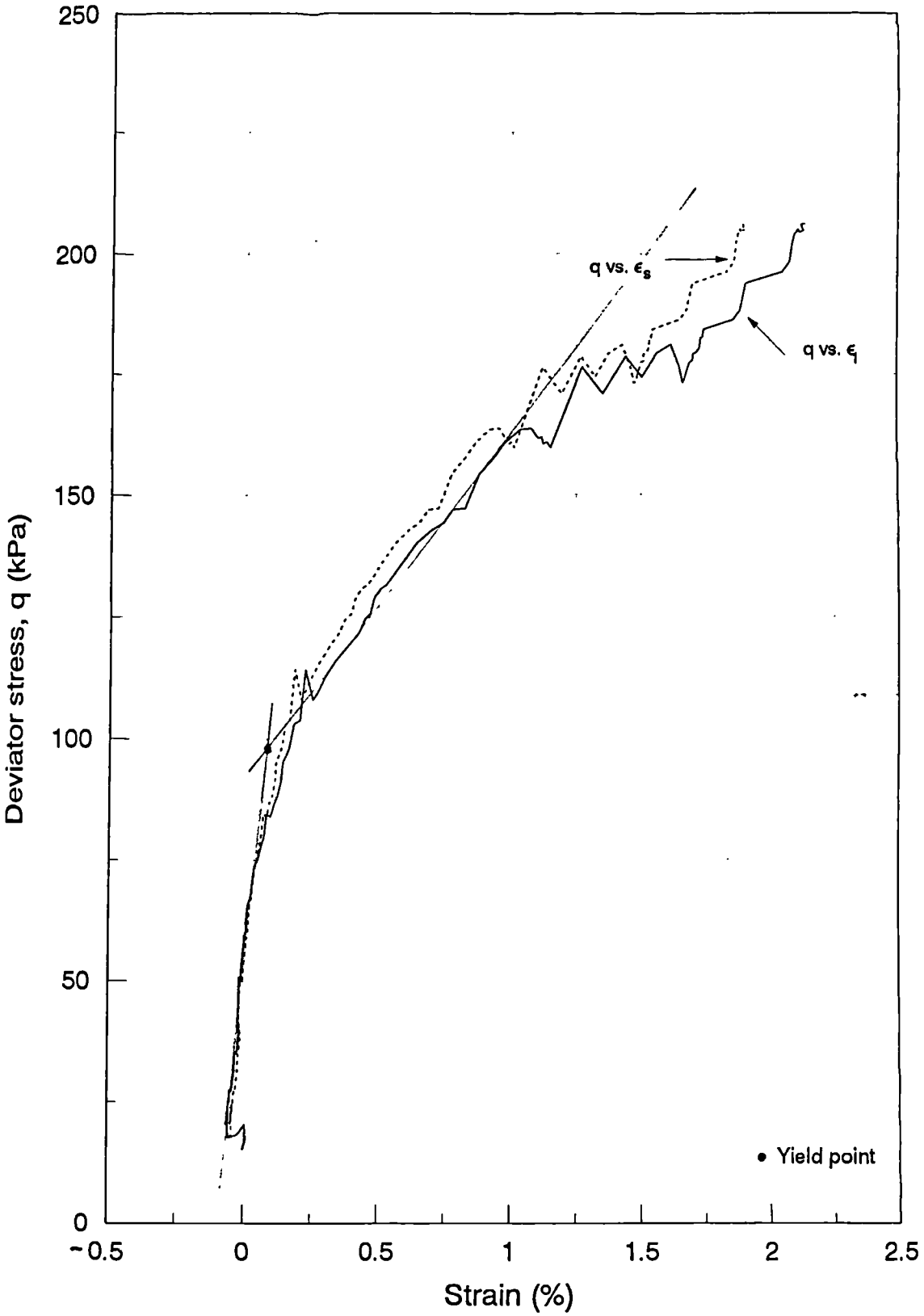

Fig. 6.30 : Enlarged plot of deviator stress versus axial strain and shear strain for Test 4 (constant-p' shearing)

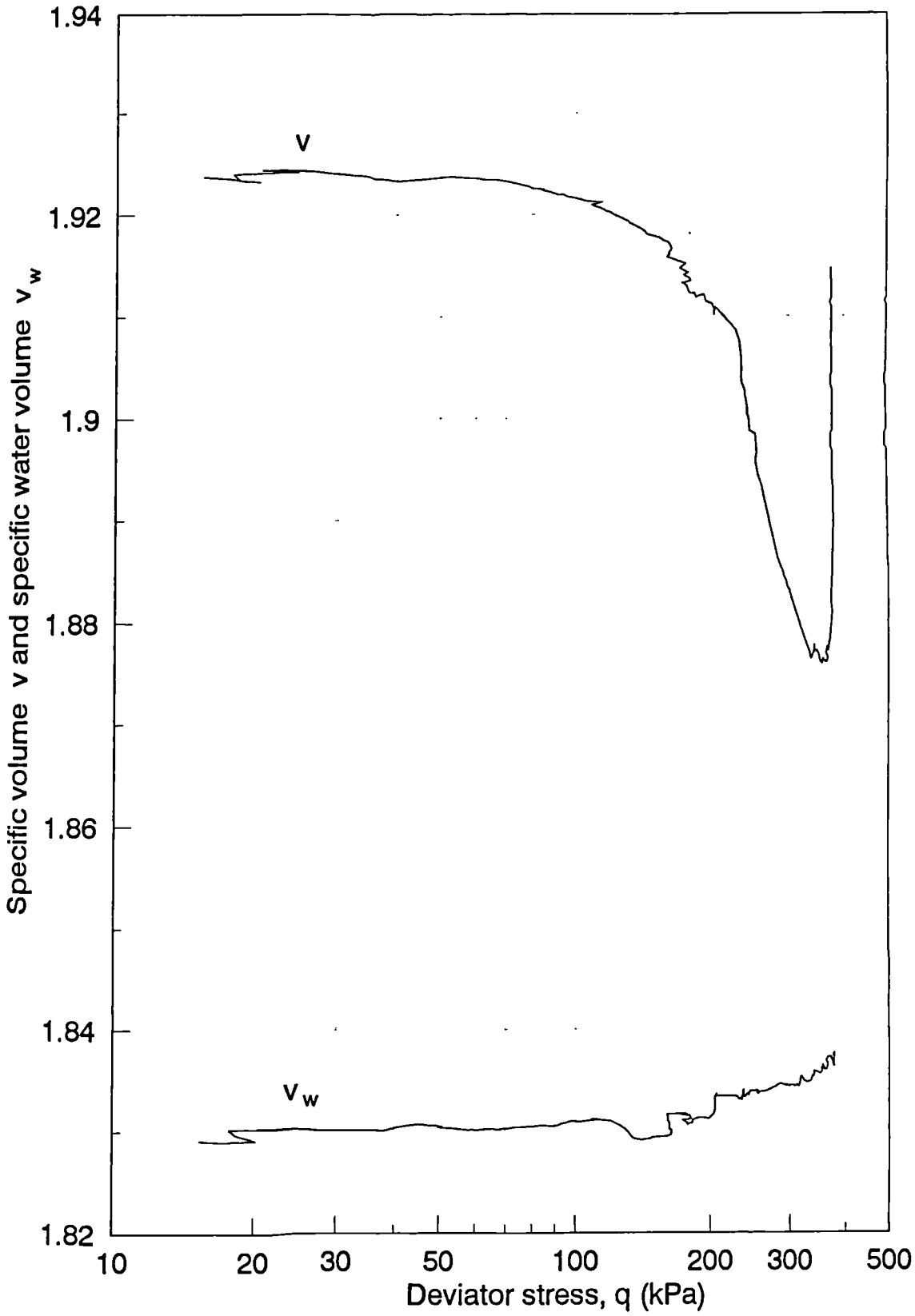

Fig. 6.31 : Variation of v and v_w during shear stage of Test 4 (constant-p' shearing)

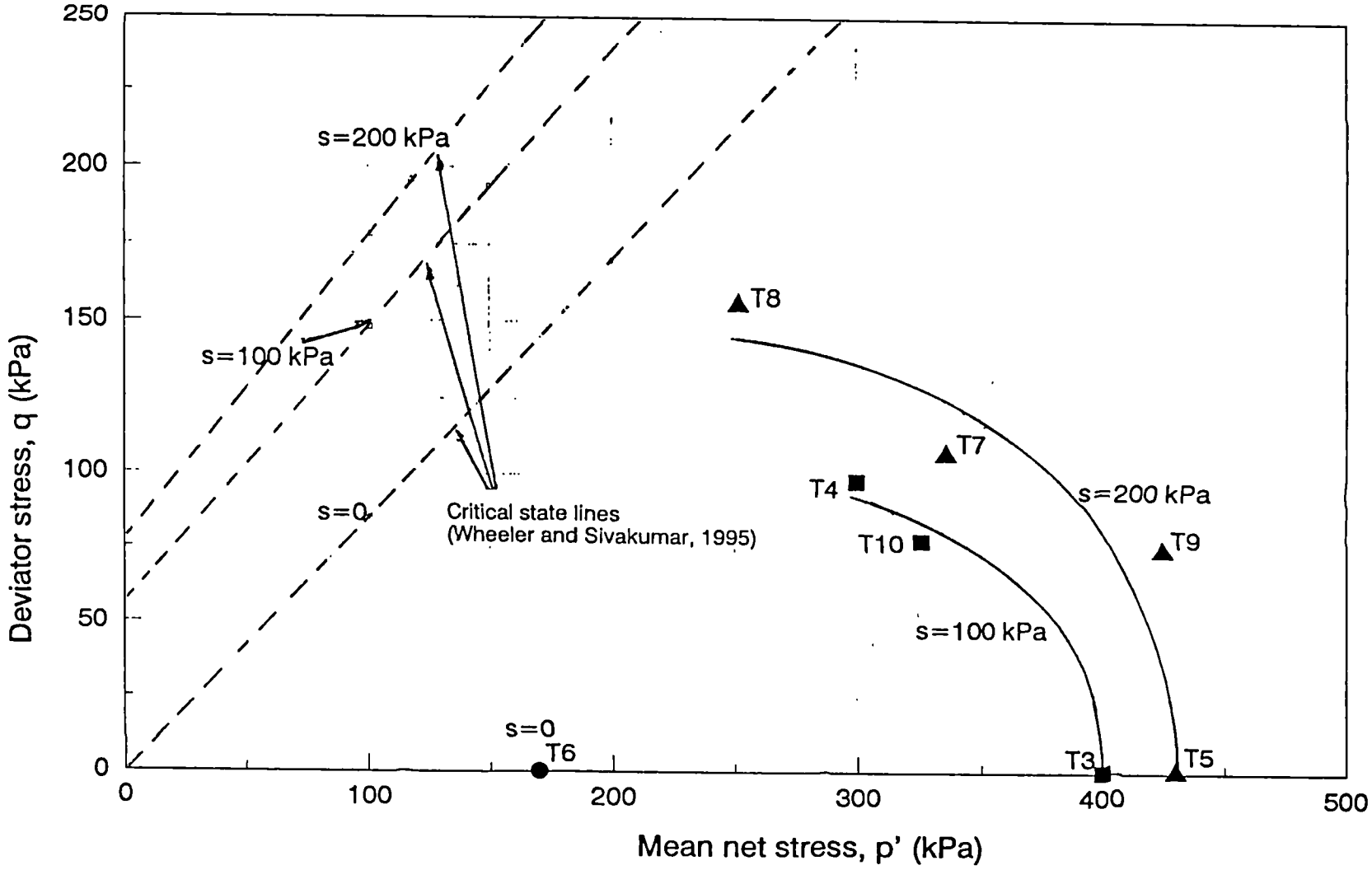

Fig. 6.32 : Yield curves for kaolin at different values of suction

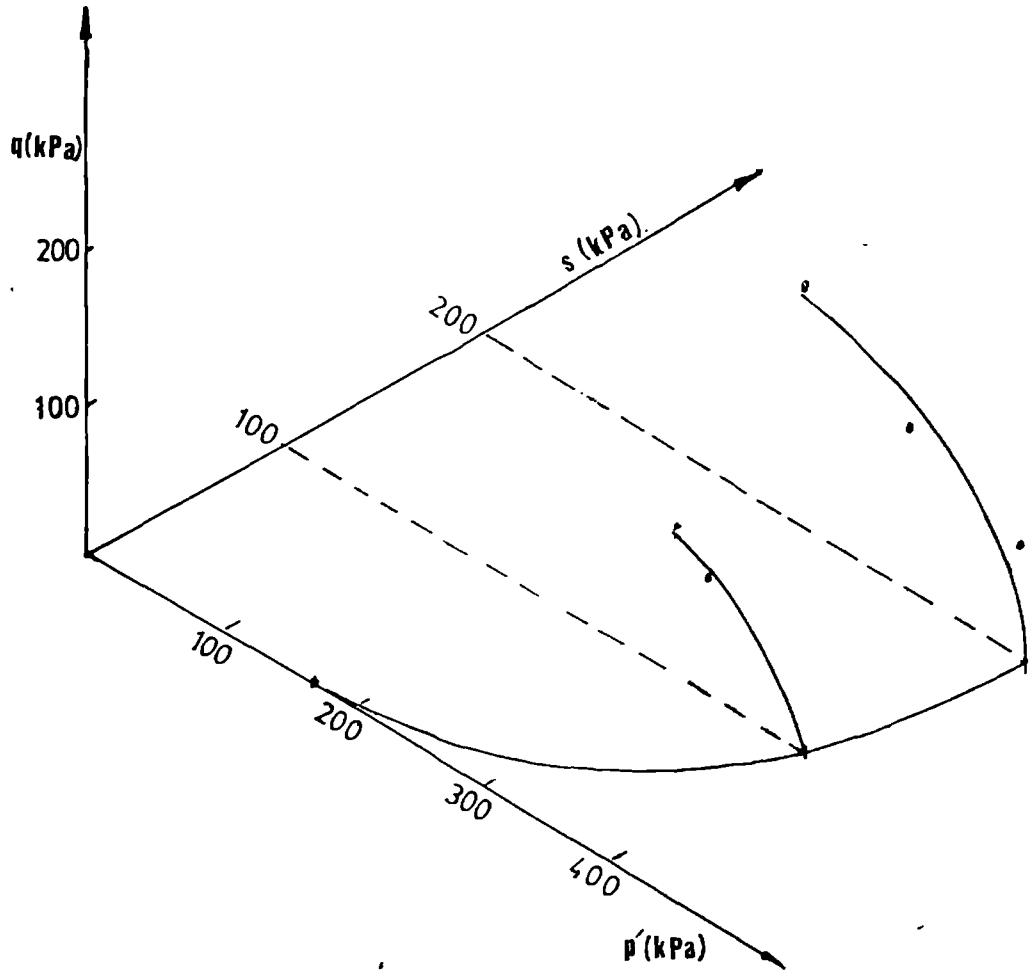

Fig. 6.33 : Yield surface for unsaturated compacted kaolin in p':q:s space (after isotropic consolidation to s_o= 100 kPa, p'_o = 400 kPa)

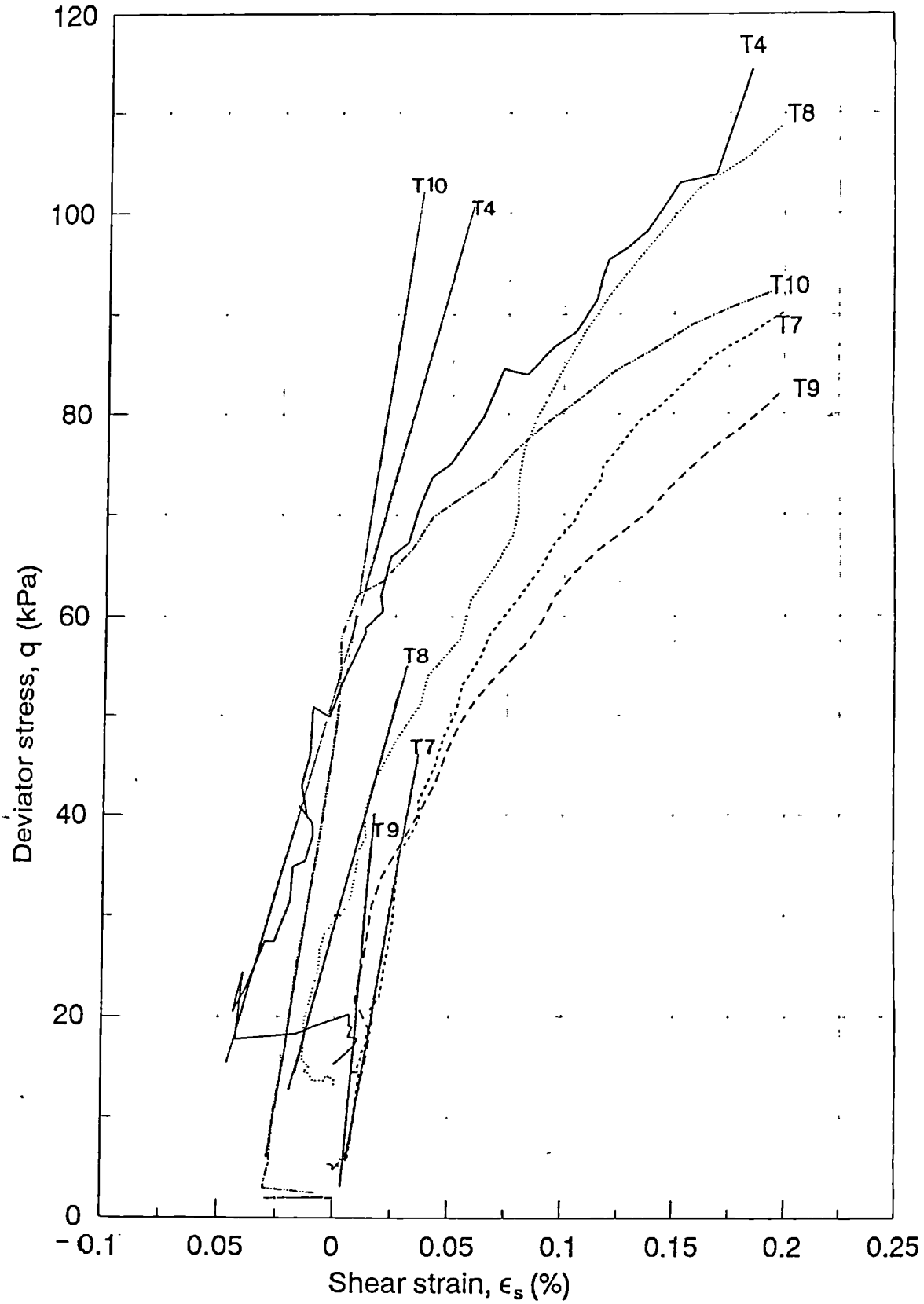

Fig. 6.34 : Enlarged plot of deviator stress versus shear strain for shear tests

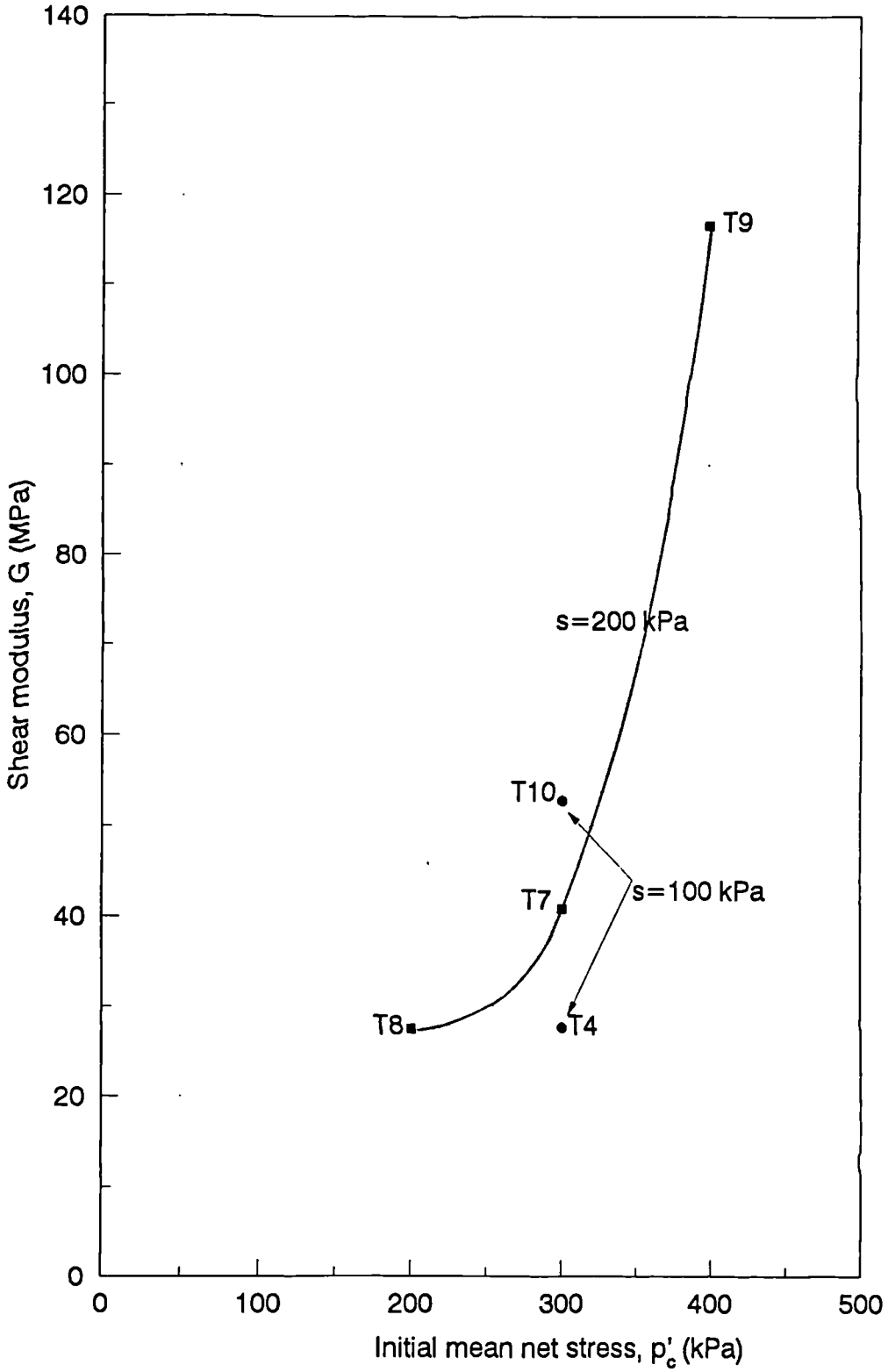

Fig. 6.35 : Variation of shear modulus with mean net stress and suction

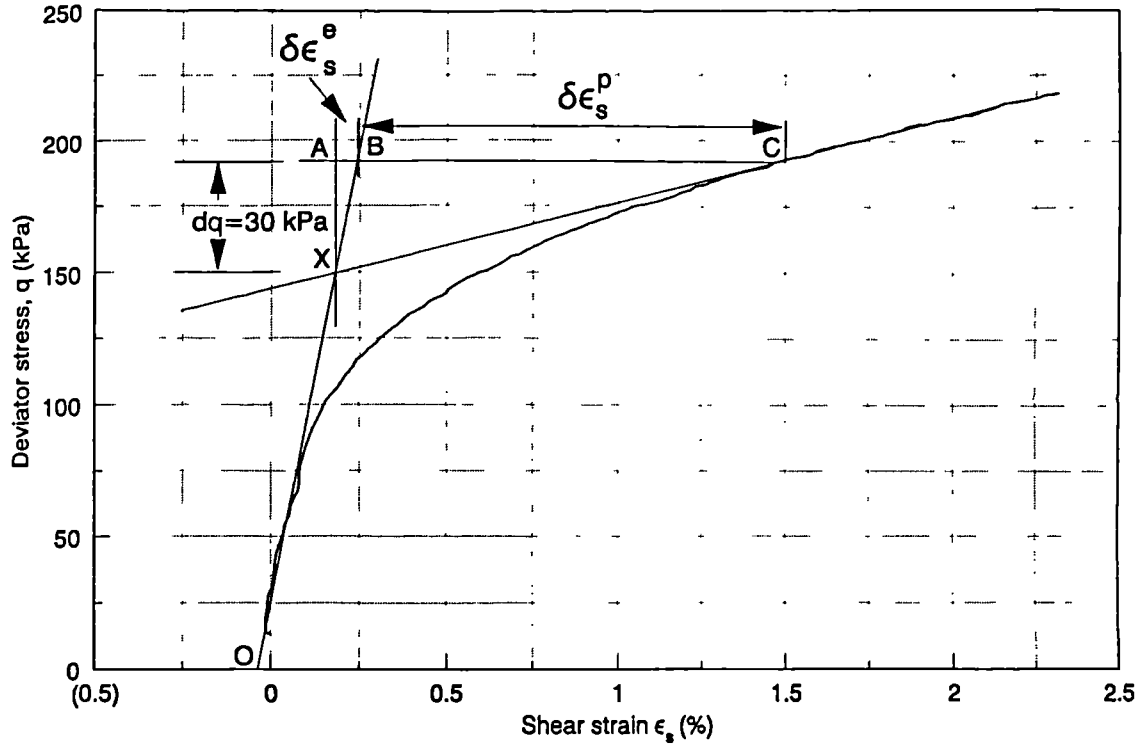

(a) Deviator stress versus shear strain

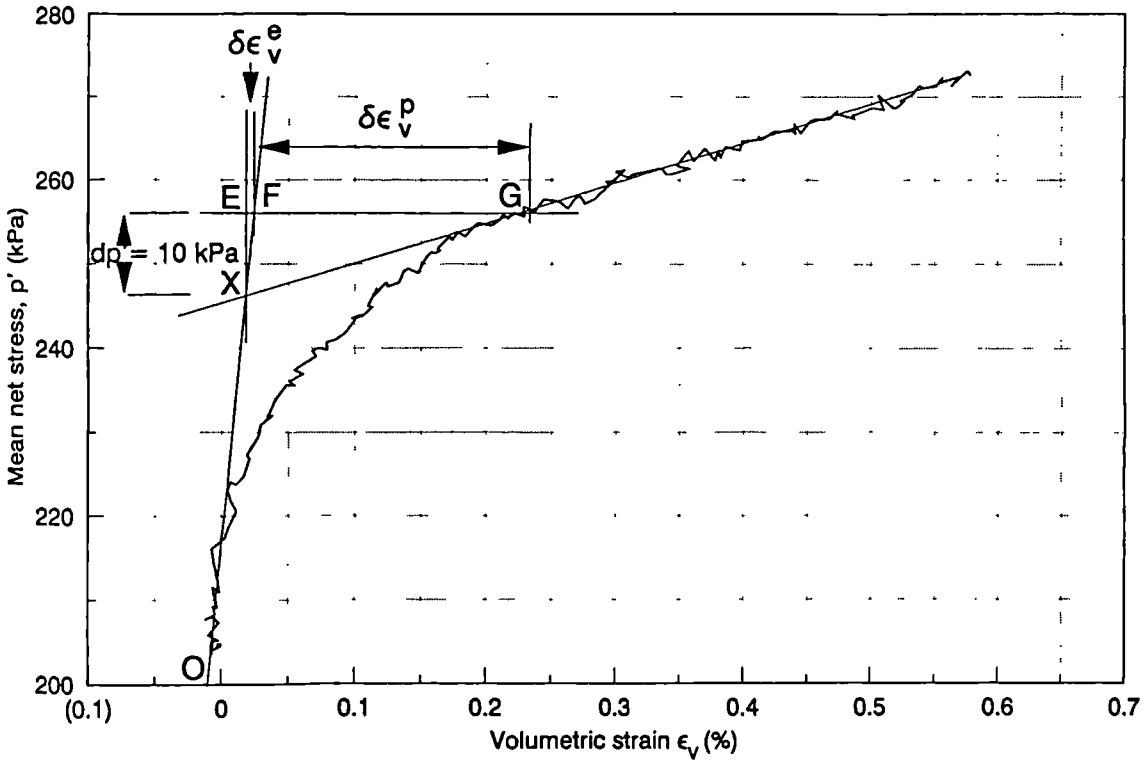

(b) Mean net stress versus volumetric strain

Fig. 6.36 : Calculation of plastic strain increments for Test 8

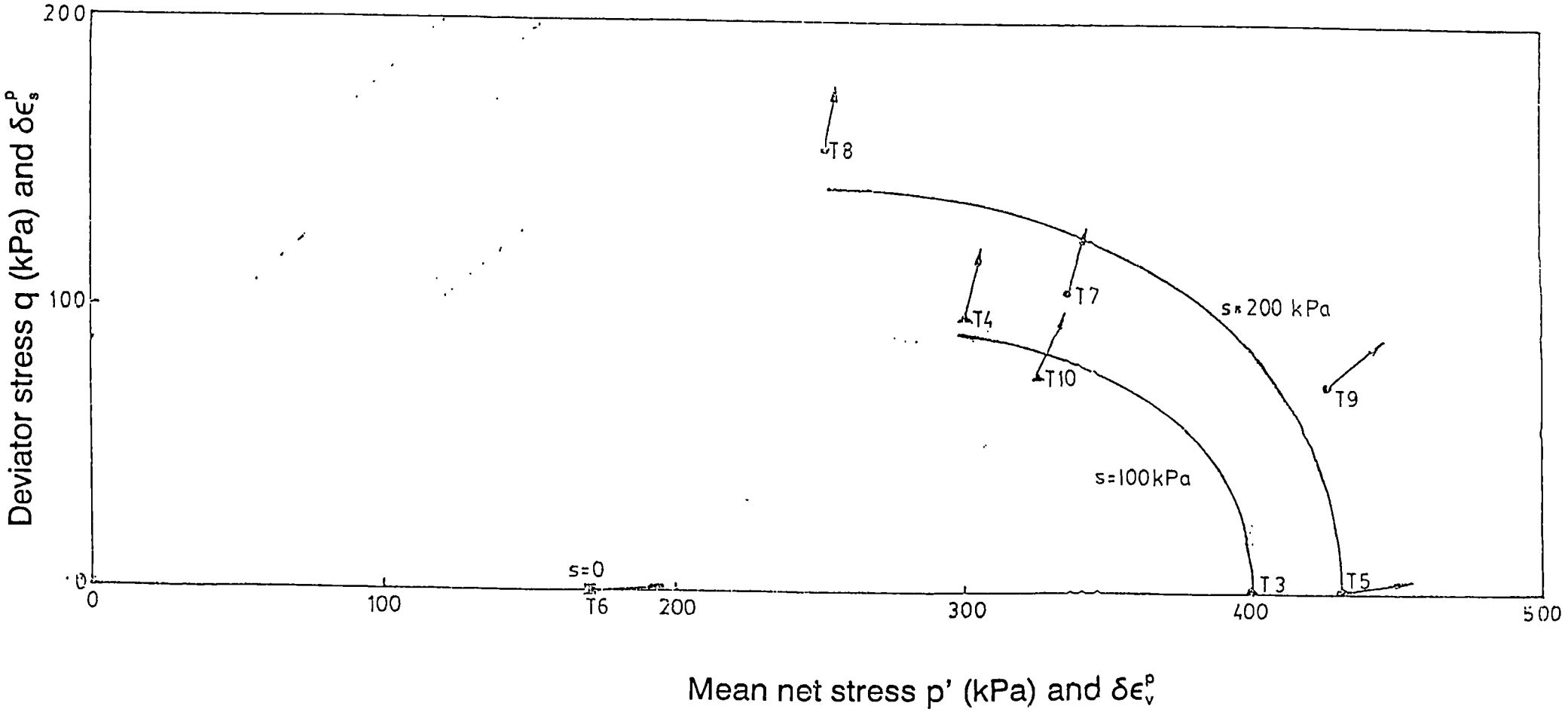

Fig. 6.37 : Plastic strain increment vectors from re-loading/shear stage

Test no.	v	w (%)	S_r (%)	v_w
1	2.159	24.00	54.9	1.636
2	2.146	23.99	55.5	1.636
3	2.176	24.58	55.4	1.651
4	2.135	25.35	59.2	1.672
5	2.098	25.30	61.1	1.671
6	2.137	24.01	55.9	1.636
7	2.149	24.79	57.7	1.663
8	2.153	24.63	56.6	1.653
9	2.118	25.30	59.0	1.671
10	2.123	25.22	59.5	1.668

Table 6.1 : Soil state parameters after compaction

Test no.	p' (kPa)	s (kPa)	v	w (%)	S_r (%)	v_w
1	49.7	100.1	2.155	31.94	73.1	1.846
2	48.3	100.3	2.176	31.40	70.8	1.832
3	50.5	100.1	2.213	31.51	68.8	1.835
4	48.1	100.0	2.150	30.54	70.4	1.809
5	50.0	100.2	2.106	29.44	70.5	1.780
6	152.1	99.9	2.013	31.05	81.2	1.823
7	151.6	99.4	2.041	31.83	81.1	1.844
8	100.0	100.5	2.127	30.52	71.8	1.809
9	198.4	100.6	2.004	30.47	80.5	1.808
10	48.4	101.0	2.131	30.61	71.7	1.811

Table 6. 2 : Soil state parameters at end of equalization stage

Test no.	p' (kPa)	s (kPa)	v	w (%)	S_r (%)	v_w
1	400.6	100.0	1.928	32.57	93.0	1.863
2	400.7	100.2	1.963	31.12	85.6	1.825
3	401.2	99.5	1.940	32.36	91.2	1.858
4	400.1	100.3	1.918	31.12	89.9	1.825
5	399.2	100.1	1.854	30.66	95.2	1.812
6	402.4	99.7	1.876	30.78	93.1	1.816
7	400.8	99.5	1.901	31.58	92.9	1.837
8	398.9	100.4	1.948	29.86	83.5	1.791
9	402.4	98.7	1.936	30.15	85.4	1.800
10	398.6	101.0	1.928	30.07	85.8	1.797

Table 6. 3 : Soil state parameters at end of ramped consolidation stage

Test no	Ramped consolidation				Swell-back		Suction-change		Shearing
	$\lambda(s)$	N(s)	$\alpha(s)$	A(s)	κ	κ_w	κ_s	κ_{sw}	G (MPa)
1	0.133	2.105	-	-	0.023	0.023	-	-	-
2	0.127	2.136	0.018	1.852	0.041	0.041	-	-	-
3	0.169	2.168	-	-	0.029	0.025	-	-	-
4	0.142	2.110	0.006	1.835	0.021	0.015	-	-	28
5	0.148	2.067	-	-	0.015	0.010	0.000	0.000	-
6	0.148	2.082	0.018	1.841	0.029	0.027	0.053	0.116	-
7	0.135	2.106	0.024	1.869	0.010	0.025	0.009	0.031	41
8	0.130	2.131	0.048	1.859	0.022	-0.022	0.030	0.032	27
9	0.102	2.078	0.028	1.838	-	-	0.017	0.117	117
10	0.122	2.097	0.039	1.850	0.034	0.026	-	-	53

Table 6. 4 : Soil constants obtained from all stages of tests

Test no.	p' (kPa)	s (kPa)	v	w (%)	S_r (%)	v_w
1	200.2	99.5	1.948	33.13	92.6	1.878
2	299.7	100.0	1.975	31.56	85.8	1.837
3	199.4	100.4	1.960	33.02	91.2	1.875
4	299.3	100.5	1.924	31.28	89.7	1.829
5	199.3	100.5	1.864	30.81	94.5	1.816
6	100.0	98.4	1.916	32.21	93.1	1.854
7	299.5	99.7	1.905	31.85	93.3	1.844
8	200.9	200.5	1.936	28.11	79.6	1.745
9	No swell-back done in this test					
10	301.5	100.4	1.937	30.34	85.8	1.804

Table 6.5 : Soil state parameters at end of swell-back stage

Test no	p' (kPa)	s (kPa)	v	w (%)	S_r (%)	v_w
1	No suction change done					
2	No suction change done					
3	No suction change done					
4	No suction change done					
5	201.2	198.8	1.864	30.81	94.5	1.817
6	49.8	0.4	1.953	35.24	98.0	1.934
7	300.1	199.5	1.901	31.37	92.3	1.831
8	400.3	200.5	1.951	27.41	76.4	1.726
9	399.3	201.0	1.927	29.66	84.8	1.786
10	No suction change done					

Table 6.6 : Soil state parameters at end of suction-change stage

Test	Suction	From q versus ε_1		From v versus $\ln p'$		Average	
no.	(kPa)	p'_y(kPa)	q_y(kPa)	p'_y(kPa)	q_y(kPa)	p'_y(kPa)	q_y(kPa)
1	100	-	-	-	-	Membrane slippage	
2	100	-	-	-	-	Load cell failure	
3	100	-	-	400	0	400	0
4	100	300	98	-	-	300	98
5	200	-	-	450	0	450	0
6	0	-	-	170	0	170	0
7	200	335	105	336	108	336	107
8	200	250	150	254	162	252	156
9	200	425	75	425	75	425	75
10	100	330	90	322	66	326	78

Table 6.7 : Yield points from re-loading / shear stage

CHAPTER 7
DISCUSSION

7.1 Position of LC yield curve after compaction

The initial position of the LC yield curve, after compaction, identified from the equalization stage of the tests, is sketched again in Fig. 7.1, together with the stress paths employed during the equalization stages. Also shown in Fig. 7.1 is the initial position of the LC yield curve calculated by *Wheeler and Sivakumar* (1995) for the same speswhite kaolin and the same compaction procedure. The yield curve of *Wheeler and Sivakumar* (1995) was based on the theoretical yield curve expression given by Equation 2.39, with the values of the soil parameters λ(s), N(s), κ and κ_s taken from the tests of *Sivakumar* (1993), and the value of the intercept $p_o'(o)$ of the curve with the p' axis selected so as to fit the experimental yield points of *Sivakumar* (1993). From Fig. 7.1 it can be seen that the initial position of LC yield curve obtained from the equalization stage of the current tests was in excellent agreement with the initial position of the yield curve calculated by *Wheeler and Sivakumar* (1995). In fact, the initial position of the yield curve calculated by *Wheeler and Sivakumar* (1995) fits all the experimental observations of the current series of tests (see Section 6.1.2), in that it passes just outside point C but inside points E, G and I, and if extended to higher values of suction it would almost certainly pass outside points B and D but inside points F and H. This excellent agreement on the initial position of the LC yield curve produced by the compaction procedure is very pleasing.

The results from the equalization stage only gave the approximate position of the yield curve. It was possible to say that the yield curve passed outside points B, C and D in Fig. 7.1 and inside points E, F, G, H and I, but it was not possible to locate exactly any points on the yield curve. This was because the reduction of suction

during equalization was achieved by applying a single step change of suction to the sample boundary (see Section 5.3.5). This step change of suction on the sample, boundary resulted in a highly non-uniform distribution of suction within the sample as illustrated in Fig. 7.2. The pore air pressure inside the sample quickly reduced to the air back pressure value applied at the top of the sample, due to the high air permeability, whereas the pore water pressure took much longer to increase to the water back pressure value applied at the base of the sample, because of the relatively low water permeability. During the wetting process the suction reduced most rapidly at a point such as C (Fig. 7.2), close to the base of the sample, and most slowly at a point such as A, at the top of the sample. At intermediate times during wetting, the suction was therefore greatest at A and least at C. This variation of suction throughout the sample meant that it was impossible to identify, on a given wetting stress path, a particular value of suction at which the yield curve was reached and swelling was replaced by collapse.

The yield points during the wetting stage could have been precisely identified by gradually reducing the suction applied to the sample boundary, at a constant rate, rather than reducing it in a single step. A gradual decrease in suction would have required that the water back pressure u_w was increased at a constant rate, slow enough to ensure equalization of suction throughout the sample. This procedure would have been somewhat similar to the ramping of cell pressure during the ramped consolidation stage as described in Section 5.3.3. However this option of gradually reducing the suction was not selected , because of two factors :

a) Lack of time. This method of suction reduction would have taken much longer to perform than a single step reduction of suction, thus reducing the number of tests that could have been performed within the available research time ;

b) Lack of appropriate test apparatus. A gradual reduction of suction would have required automatic control of the water back pressure u_w, via an

additional GDS controller or a computer-controlled stepper motor. This facility was not available for the present research work.

7.2 Normal compression lines

The data from the ramped consolidation stage were used to define the normal compression line for v at a suction of 100 kPa, as described in Section 6.2.1. Fig. 7.3 shows the normal compression line for v from the present tests and also the corresponding data from five tests conducted by *Sivakumar* (1993) at a suction of 100 kPa.

The most obvious difference between the curves from the present tests and those from Sivakumar's tests is the much larger spread in the data from the current tests (covering a range of v of about 0.1 at any given value of p', compared to a range of v of only about 0.02 in Sivakumar's tests). This increased scatter in the data from the current tests could represent either greater variation between samples than occurred in Sivakumar's tests or greater measurement errors than in Sivakumar's tests. Each of these possibilities is now considered.

There is clear evidence of greater variation between samples in the present tests than in Sivakumar's tests, resulting from poorer control of the original compaction procedure. Table 6.1 shows that the compaction water content varied from 23.99% to 25.35% in the present tests (a range of 1.36%), whereas it varied from 24.08% to 24.85% in Sivakumar's tests (a range of only 0.77%). Even more significant, in the present tests the specific volume v after compaction varied from 2.098 to 2.176 (a range of 0.078) and the degree of saturation S_r varied from 54.9% to 61.1% (a range of 6.2%), whereas in Sivakumar's five tests, v varied from 2.195% to 2.213 (a range of only 0.018) and S_r varied from 53.0% to 55.1% (a range of only 2.1%). This suggested that the compactive effort and the compaction procedure, as well as the compaction water content, were much better controlled in

Sivakumar's tests than in the present tests. The reasons for the poorer control of compaction procedure in the present tests are uncertain. Clearly this greater variability between samples may be responsible for much of the increased spread in the data shown in Fig. 7.3.

There is also a suggestion that the values of specific volume v were less accurately measured in the present tests than in Sivakumar's tests. The fundamental difference in the measurement of sample volume change between the present tests and that of Sivakumar's tests was the use of local strain gauges mounted on the samples. Two Imperial College axial displacement gauges and a custom-built radial displacement gauge were used in the present tests to measure the individual axial and radial strains and hence the sample volume change as explained in Section 5.5. In contrast, *Sivakumar* (1993) used a double-walled triaxial cell to measure the sample volume change of the sample (see Section 2.7.4.1). In this method the volume of water leaving or entering the inner cell gave a direct measurement of the sample volume change. The use of the double-walled cell in the measurement of sample volume change was superior to the employment of local strain gauges, because it was accurate at any value of strain and irrespective of the shape of the deformed sample. *Sivakumar* (1993) reported that absolute values of specific volume v were measured to an accuracy of about ± 0.01 and this was borne out by the low level of scatter in his test data in Fig. 7.3 . In contrast, the values of v measured in the present tests were affected by errors arising from any non-uniform deformation of the sample ("barrelling" or "hour-glassing") caused by lateral restraint imposed by friction at the top and bottom platens. Although an attempt was made to correct these errors by adjusting the measured axial and radial strains by using a correction suggested by *Moore* (1966), this correction was imperfect, because it was based on an assumption of elastic behaviour. Any errors caused by non-uniform deformation during the initial equalization stage would, of course, affect the values of v measured at the start of the ramped consolidation stage.

Although the spread of the data was much greater in the present tests than in Sivakumar's tests, inspection of Fig. 7.3 shows that a normal compression line drawn as the average of the present test data would show reasonable agreement with Sivakumar's results. From the present tests the average value of the intercept N(s) of the normal compression line (see Equation 6.1) was 2.108, whereas the corresponding average value from Sivakumar's tests (at a suction of 100 kPa) was 2.122, a difference of only 0.014. The average value of the slope λ(s) of the normal compression line was 0.136 in the present tests and 0.182 in Sivakumar's tests at s = 100 kPa. This difference in the average value of λ(s) seems substantial, but inspection of Fig. 7.3 suggests that much of the apparent difference is due to the higher range of stresses covered in the present tests. The normal compression line of v versus the logarithm of p' is actually gently curved (see Fig. 7.3) and the measured value of λ(s) therefore decreases at higher values of p'.

7.3 Elastic behaviour

The values of the elastic indices $\kappa, \kappa_s, \kappa_w, \kappa_{sw}$ and G are shown, for all tests, in Table 6.4.

7.3.1 Elastic variation of specific volume

Equation 6.3, involving the elastic indices κ and κ_s, was proposed by *Alonso, Gens and Josa* (1990) to represent the elastic variation of v. Values of κ were obtained from the swell-back stage of all tests at s = 100 kPa except in Test 8 where κ was obtained from the swell-back stage at s = 200 kPa and Test 9 where there was no swell-back stage. From the results shown in Table 6.4 the average value of κ was 0.025 and no significant variation of κ with s was apparent (within the limited range of suction values tested) (see Section 6.3.1). This was consistent with the model of *Alonso, Gens and Josa* (1990), where κ was taken as constant and independent of

suction. Although *Alonso, Gens and Josa* (1990) reported that there might be some dependence of κ on s, this aspect of soil behaviour was not considered, so as to keep the model as simple as possible.

Values of κ_s were measured during the suction-increase stage of four tests, and these values of κ_s were found to increase with increasing p' (see Section 6.4.1). For example: in Test 5 (p' = 200 kPa), κ_s = 0.000 ; in Test 7 (p' = 300 kPa), κ_s = 0.009 and in Tests 8 and 9 (p' = 400 kPa), κ_s = 0.023 (average of κ_s values from Tests 8 and 9). This variation of κ_s with p' while κ remained independent of s contradicted the requirement for conservative behaviour in the elastic region (no permanent change of v for a closed stress path remaining inside the elastic region). For conservative behaviour in the elastic region if κ did not vary with s, then κ_s should not vary with p'. This departure from conservative behaviour is illustrated in Fig. 7.4. A closed stress path ABCDE in the $s : p'$ plane is shown in Fig. 7.4 (a), and the corresponding changes of v are shown in Fig. 7.4 (b) if κ is independent of s, but κ_s increases with increasing p' (such that the decrease of v along CD is greater than the increase of v along AB). The end result is a net reduction of v on completing the closed stress path (compare final point E with initial point A in Fig. 7.4 (b)). This lack of conservative behaviour indicates that the soil behaviour may not be truly elastic even for stress paths which remain inside the "yield surface".

For the single test subjected to a suction-decrease stage (Test 6) the value of κ_s was 0.053. This value was considerably higher than any of the κ_s values obtained from the suction-increase stages. This suggests that an additional (plastic) component of swelling may occur on first wetting, and this is not recovered on subsequent drying. Exactly this form of behaviour was proposed in the elasto-plastic constitutive model for highly expansive soils developed by *Gens and Alonso* (1992) (see Section 2.6.4).

7.3.2 Elastic variation of specific water volume

Equation 6.4, involving the elastic indices κ_w and κ_{sw}, was proposed to represent the elastic variation of v_w . This was a new equation, not included in the constitutive models of *Alonso, Gens and Josa* (1990) and *Wheeler and Sivakumar* (1995). Results from the tests (see Table 6.4) showed that the average value of κ_w from the swell-back stages was 0.024 at a suction of 100 kPa. For the single test with swell-back at s = 200 kPa (Test 8) the value of κ_w was -0.022, suggesting that κ_w decreased significantly (from a positive to negative value) with increasing *s*. However at this juncture this finding was rather inconclusive due to insufficient data from a single test.

Values of κ_{sw} were measured during the suction-change stage, and κ_{sw} was found to increase with increasing *p'*. For example : in Test 5 (*p'* = 200 kPa), κ_{sw} = 0.000 : in Test 7 (*p'* = 300 kPa), κ_{sw} = 0.031 and in Tests 8 and 9 (*p'* = 400 kPa), κ_{sw} = 0.074 (average from Tests 8 and 9). A decrease of κ_w with increasing *s* combined with an increase of κ_{sw} with increasing *p'* contravened, once again, the requirement for conservative elastic behaviour(no net change of v_w for a closed stress path). This is illustrated in Fig. 7.4 (c). This lends further support to the suggestion that the soil behaviour is not truly elastic even for stress paths remaining inside the "yield surface".

The value of κ_{sw} from the single suction-decrease stage (Test 6) was, at 0.116, considerably higher than the value that would have been expected at this value of *p'* (100 kPa) from the suction-increase tests. This, again, is consistent with the suggestion of an additional plastic component of deformation on first wetting, as proposed in the model of *Gens and Alonso* (1992).

For tests subjected to isotropic re-loading (see Section 6.5) the value of κ_w from the pre-yield section of the re-loading curve for Test 5 (s = 200 kPa) was 0.007 (see Fig. 6 18). This value was very different to the κ_w value of -0.022 obtained from the swell-back stage of Test 8 (s = 200 kPa). For Test 3, which was subjected to isotropic re-loading at s = 100 kPa, the value of κ_w during the pre-yield section of

the re-loading curve (see Fig. 6.18) was about 0.011. This value was less than half of the average κ_w value of 0.024 obtained from the swell-back stages conducted at s = 100 kPa (see Table 6.4). This all adds further weight to the conclusion that the soil behaviour is not truly elastic even for stress paths remaining inside the "yield surface".

7.3.3 Elastic shear modulus

The variation of shear modulus G with p' and s in the five successful shear tests was shown in Fig. 6.35. At a suction value of 200 kPa, G was found to increase with increasing p'. Any variation of G with suction was difficult to determine, because of the large amount of scatter at s = 100 kPa (see Fig. 6.35). The results shown in Fig. 6.35 can be compared with the results of *Cui* (1993) from suction-controlled triaxial tests on Jossigny silt, shown in Fig. 7.5. *Cui* (1993) found that G increased with increasing p' and with increasing s, despite the scatter in his results. Allowing for the scatter, the variation of G from the present tests, shown in Fig. 6.35, was consistent with Cui's conclusion that G increased with increasing p' and s. Because of the scatter it was not possible to propose an exact form of the variation of G with p' and s.

7.4 Yield surface and flow rule

The yield curves in the q:p' plane, identified from the re-loading/shear stages, were shown in Fig. 6.32 for suctions of 100 and 200 kPa, together with the isotropic yield point at zero suction $p_o^*(o)$. The entire yield surface in q:p':s space was shown in Fig. 6.33. From Fig. 6.32 the constant suction yield curves were approximately elliptical in shape, with one axis of the ellipse coinciding with the p' axis. This supported the suggestion that the samples were isotropic by the time the shear stage was performed; the anisotropic history of the sample induced by the one-dimensional

compaction procedure having been gradually erased by subsequent isotropic consolidation and swell-back. The elliptical shapes of the yield curves fitted well with the constitutive models proposed by *Alonso, Gens and Josa* (1990) and *Wheeler and Sivakumar* (1995).

In contrast, the constant suction yield curves obtained by *Cui* (1993) from his shear tests on unsaturated compacted samples of Jossigny silt were asymmetric and aligned along the K_0-line, as shown in Fig. 7.6. *Yield curves were shown for* suctions of 200, 400, 800 and 1500 kPa. In his tests *Cui* (1993) used a one-dimensional compaction procedure to produce samples which were then sheared, without isotropic consolidation to virgin states and subsequent swell-back. This resulted in highly anisotropic samples during the shear stage. The asymmetric yield curves shown in Fig. 7.6 reflect this anisotropy, and they are of similar shape to those observed for anisotropic saturated soils (see for example, *Ohta and Wroth* (1976), *Tavenas and Leroueil* (1977) and *Graham, Crooks and Lau* (1988)).

The plastic strain increment vectors calculated from the post-yield sections of the re-loading / shear stages of the current tests were shown in Fig. 6.37 superimposed upon the constant suction yield curves. The directions of the plastic strain increment vectors were found to be approximately perpendicular to the yield curves, suggesting that the flow rule was associated. This agreed with the proposal of *Wheeler and Sivakumar* (1995), who adopted an associated flow rule in their elasto-plastic model. In contrast *Alonso, Gens and Josa* (1990) suggested a non-associated flow rule in their model.

Fig. 7.7 shows the plastic strain increment vectors from the shear tests of *Cui* (1993) on unsaturated, compacted Jossigny silt, superimposed on the corresponding yield curve. Results are shown only for a suction of 1500 kPa, but these are typical of all the values of suction tested by *Cui* (1993). The results suggest that, for this material, the flow rule was non-associated, because the direction of the plastic strain increment vectors showed large departures from right angles to the yield curves.

This fundamental difference between Cui's results and those from the present tests was presumably due to the anisotropic nature of the soil samples tested by *Cui* (1993). In the present tests the anisotropy of the soil was gradually erased by subsequent isotropic consolidation and swell-back.

7.5 Overall variation of v and v_w

Figs. 7.8 (a) to 7.8 (j) , show, for each test, the variation of v and v_w with p' (with p' on a logarithmic scale) for the entire test. The variation of v is shown as a solid line whereas the variation of v_w is shown as a dotted line. The complete stress path in p':q: s space for the individual test is shown in the inset. From Figs. 7.8 (a) to 7.8 (j) it can be seen that the changes in v were qualitatively consistent with the predictions of the elasto-plastic models of *Alonso, Gens and Josa* (1990) and *Wheeler and Sivakumar* (1995). Of course these existing models did not predict the variation of v_w . The observed variation of v is qualitatively related to the model predictions in the following sections.

7.5.1 Test 1

During the equalization (wetting) stage AC of Test 1 (at p_e' = 50 kPa) there was initially a small increase in v (see Fig. 7.8 (a)) corresponding to elastic swelling inside the LC yield curve. This was followed by a small reduction in v, corresponding to a small amount of plastic 'collapse' (because there was a small expansion of the yield curve in reaching stress point C).

During the isotropic consolidation stage CD the soil yielded almost immediately (as expected if point C was already on the newly expanded yield curve). The soil then followed the isotropic normal compression line for this value of suction, with a slope of $\lambda(s)$. The resulting large (plastic) reduction of v corresponded to expansion of the yield curve.

During the swell-back stage DE the soil swelled elastically (the stress path coming back inside the yield surface), with an elastic compressibility κ much lower than the plastic value λ(s).

During shear stage EF the results were spiky, due to membrane slippage. Despite this, it can be seen that the initial response of the soil was elastic with the v:$ln\ p'$ plot having a slope κ (identical to that from swell-back stage). The soil then yielded and a much larger plastic reduction of v occurred. Yield occurred on the elliptical yield curve in the q:p' plane, at a value of p' much lower than the value of 400 kPa that would have occurred under isotropic re-loading.

7.5.2 Test 2

Test 2 was badly affected affected by membrane slippage (see Fig. 7.8 (b)). The equalization (wetting) stage AC (conducted at p_e' = 50 kPa) was heavily obscured by slippage. However it can be seen that there was a small net increase in v corresponding to elastic swelling inside the yield curve.

During the isotropic consolidation stage CD there was substantial compression of the soil with the large (plastic) reduction of v corresponding to expansion of the yield curve.

During the swell-back stage DE the sample moved back inside the elastic region, with an elastic compressibility κ much lower than the plastic value λ(s).

The shear stage for Test 2 was unsuccessful due to the failure of load cell.

7.5.3 Test 3

The results for Test 3 are shown in Fig. 7.8 (c). During the equalization (wetting) stage AC (conducted at p_e' = 50 kPa) there was an increase in v,

corresponding to elastic swelling of the soil inside the LC yield curve. No subsequent collapse was observed during the later phase of the stage.

During the isotropic consolidation stage CD there was a slight delay in yielding, indicating that point C was just inside the yield curve. This was then followed by a substantial (plastic) reduction in v, corresponding to expansion of the yield curve. The soil followed the normal compression line with virgin compressibility $\lambda(s)$.

During the swell-back stage DE the stress path moved back elastically inside the yield surface with an elastic constant κ much lower than the plastic value $\lambda(s)$.

During isotropic re-loading, the stage was mistakenly terminated at p' = 400 kPa. The initial response of the soil was elastic, with the κ value during the pre-yield section of the re-loading stage identical to the value of κ during the swell-back stage DE. The sample would presumably have yielded at p' = 400 kPa, because the sample had been subjected to the same value of suction of 100 kPa throughout the entire test and it had previously been consolidated to a p' value of 400 kPa during the earlier consolidation stage.

7.5.4 Test 4

During the equalization stage AC (conducted at p_e' = 50 kPa) there was an increase in v corresponding to elastic swelling of the sample inside the yield curve (see Fig.7.8 (d)).

During the subsequent isotropic consolidation stage CD the soil yielded almost immediately, indicating that point C was on the LC yield curve. The soil then followed the isotropic normal compression line for this value of suction, with a large (plastic) reduction of v corresponding to expansion of the yield curve. Swell-back DE (at s = 100 kPa) occurred with an elastic compressibility κ.

During the shear stage EF, at constant-p', there was initially very little change of v (consistent with elastic behaviour) and there was then a substantial reduction in v corresponding to collapse of the soil sample once the yield surface was reached.

7.5.5 Test 5

During the equalization (wetting) stage AC of Test 5 (conducted at $p_e' = 50$ kPa) there was an increase in v, corresponding to elastic swelling of the soil inside the LC yield curve (see Fig. 7.8 (e)).

During the isotropic consolidation stage CD the soil yielded almost immediately, indicating that point C was on the yield curve. The soil moved along the normal compression line at this value of suction accompanied by a large reduction of v, corresponding to expansion of the yield curve (with virgin compresibility $\lambda(s)$)

During the swell-back stage DE the soil swelled elastically with the stress path moving back inside the yield surface. The elastic compressibility κ was much lower than the plastic value $\lambda(s)$.

In the subsequent suction-increase stage EF there was no measurable change of v, suggesting a κ_s value of zero under these conditions.

During final isotropic re-loading FG the initial response of the soil was elastic with the value of κ from the pre-yield section of the $v : ln\, p'$ plot approximately equal to the value of κ during the swell-back stage. The soil yielded at a value of p' significantly greater than the value of 400 kPa that it had been previously subjected to during the ramped consolidation stage. This indicated the increase in the isotropic yield stress p_o' caused by increasing the suction from 100 kPa to 200 kPa. After yielding the slope $\lambda(s)$ and position of the normal compression line at a suction of 200 kPa differed significantly from the slope and position of the normal compression line at $s = 100$ kPa identified from the earlier consolidation stage CD.

7.5.6 Test 6

During the equalization stage AC (conducted at $p_e^{'}$ = 150 kPa) there was a large reduction of v (collapse) corresponding to expansion of the LC yield curve (see Fig. 7.8 (f)). This showed that point C was well outside the initial position of the LC curve produced by the compaction procedure.

During isotropic consolidation CD the soil yielded immediately, because point C was already on the newly expanded yield curve. The soil then followed the normal compression line for this value of suction with a large (plastic) reduction of v corresponding to expansion of yield curve with plastic compressibility $\lambda(s)$.

During the swell-back stage DE the soil swelled elastically as the stress path moved back inside the yield surface, with an elastic swelling index κ which was much lower than the plastic value of $\lambda(s)$.

During the suction-decrease stage EF there was a significant increase in v, corresponding to swelling of the soil inside the yield curve.

During the isotropic re-loading stage FG at zero suction the soil yielded at a value of p' much less than 400 kPa, showing the reduction of $p_o^{'}$ on decreasing the suction from 100 kPa to zero. The value of elastic compressibility κ for the pre-yield section of the curve on the $v : ln\, p'$ plot was almost identical to the value of κ during the swell-back stage. After yielding, the slope $\lambda(o)$ and position of the normal compression line at zero suction were very different to the slope and position of the normal compression line at s = 100 kPa observed in the earlier consolidation stage CD.

7.5.7 Test 7

During the equalization (wetting) stage AC (conducted at $p_e^{'}$ = 150 kPa) there was a large reduction in v (collapse) corresponding to expansion of the LC yield curve (see Fig. 7.8 (g)).

On subsequent isotropic consolidation CD the soil yielded immediately because point C was already on the newly expanded yield curve. The soil then followed the normal compression line, accompanied by a large reduction in v with plastic compressibility $\lambda(s)$.

During the swell-back stage DE the stress path moved back inside the yield surface with an elastic compressibility κ which was much smaller than the plastic value $\lambda(s)$.

During the suction-increase stage EF there was a very small reduction in v, corresponding to elastic compression of the soil with an elastic constant κ_s.

During the final shear stage FG the initial response of the soil was elastic with the v : $ln\ p'$ plot having a slope κ (identical to the swell-back stage). This was followed by yielding and a much larger (plastic) reduction of v. Yield occurred on the elliptical yield curve in the q : p' plane at a value of p' much lower than the isotropic yield stress for a suction of 200 kPa identified in Test 5.

7.5.8 Test 8

During the equalization (wetting) stage AC of Test 8 (conducted at p_e' = 100 kPa) there was large reduction of v (see Fig. 7.8 (h)), which corresponded to plastic collapse because there was expansion of the LC yield curve from its initial position.

During the isotropic consolidation stage CD the soil yielded almost immediately, because point C was already on the newly expanded yield curve. The soil then followed the normal compression line for this value of suction, accompanied by a large reduction of v corresponding to expansion of the yield curve (virgin compressibility $\lambda(s)$).

During the suction-increase stage DE there was a reduction of v corresponding to elastic compression of the soil via the soil constant κ_s.

On subsequent swell-back EF the soil expanded elastically as the stress path came back inside the yield surface, with an elastic compressibility κ much lower than the plastic value λ(s).

During the final shear stage FG the initial response of the soil was elastic with the initial pre-yield section of the $v : ln\, p'$ plot having a slope κ quite similar to that from the swell-back stage. The soil then yielded, and a much larger plastic reduction of v occurred. Yield occurred on the elliptical yield curve in the $q : p'$ plane at a value of p' much less than the isotropic yield stress at a suction of 200 kPa identified in Test 5. A sudden increase in v during the later part of the shear stage suggested the formation of a shear plane, indicating that the strain readings given by the local strain gauges became unreliable.

7.5.9 Test 9

During the equalization stage AC of Test 9 (conducted at p'_e = 200 kPa) there was a large reduction of v (see Fig. 7.8 (i)), corresponding to plastic collapse produced by expansion of the LC yield curve from its initial position.

During the isotropic consolidation stage CD the soil yielded immediately, because point C was already on the newly expanded yield curve. There was then a large reduction of v, corresponding to the expansion of the yield curve with a virgin compressibility λ(s).

During the suction-increase stage DE there was reduction of v corresponding to elastic shrinkage with a soil constant κ_s.

During the shear stage EF the initial response of the soil was relatively stiff (elastic). The soil yielded on the elliptical yield curve in the $q : p'$ plane at a value of p' similar to the isotropic yield value at s = 200 kPa identified in Test 5 (see Fig. 6.32). The erratic shape of the curve in the $v : ln\, p'$ plot in the later part of the shear

stage was presumably due to the unreliable response of the local strain gauges at high values of strain (see Section 6.6.3).

7.5.10 Test 10

During the equalization (wetting) stage AC of Test 10 (conducted at $p_e^{'}$ = 50 kPa) there was a small increase in v (see Fig. 7.8 (j)), corresponding to elastic swelling inside the LC yield curve. This was followed by a very small amount of plastic 'collapse' (because there was a small expansion of the yield curve in reaching stress point C).

During the isotropic consolidation stage CD the soil yielded almost immediately (because the stress state at point C was already on the newly expanded yield curve). The soil then followed the normal compression line at this value of suction with a large (plastic) reduction of v, corresponding to expansion of the yield curve (virgin compressibility $\lambda(s)$).

During the swell-back stage DE the soil stress state moved back inside the yield surface, with an elastic compressibility κ much lower than the plastic value λ (s).

During the final shear stage EF the initial response of the soil was elastic, with a κ value during the pre-yield section of the curve on the $v : ln\, p'$ plot identical to that from the swell-back stage. Yielding of the soil occurred on the elliptical yield curve at a value of p' much less than the isotropic value of 400 kPa. The apparent sudden increase of v during the later part of the shear stage was presumably due to the formation of a slip plane, which meant that the readings from the local strain gauges became meaningless (see Section 6.6.3)

7.6 Experimental apparatus and procedure

7.6.1 Sample preparation

The variation of the compaction water content and the specific volume and degree of saturation after compaction (see Table 6.1) clearly indicated that the control of the compaction procedure was poorer than achieved by *Sivakumar* (1993) (see Section 7.2). The reasons for this poorer control were uncertain, but the experience clearly highlights the importance of careful attention to the compaction procedure.

7.6.2 Some merits and demerits of the test procedure

a) Membrane slippage. It was observed during the the first two tests that there was slippage between the membrane and the soil sample, as shown in Figs. 6.4 and 7.3. However the problem was overcome in subsequent tests by fitting the footing pads of the axial gauges and the studs supporting the adjusting screws of the radial displacement gauge with small diameter pins, so that the pins fixed the gauges firmly in position and avoided any movement of the footings relative to the soil sample.

b) Tilting of the sample. Slight tilting of the soil sample occurred during some of the tests (see Fig. 6.19). The tilting was measured in the plane containing the two axial gauges mounted on the soil sample diametrically opposite each other. However tilting in a plane perpendicular to the plane containing the axial gauges was not detected. This might affect the accuracy of the axial strain readings.

c) Friction between the sample top cap and the load cell extension. There was a small amount of friction between the inner sides of the load cell extension and the sample top cap during 'docking' prior to the shear stage. This occurred as a result of tilting of the sample during the preceding ramped consolidation and swell-back stages. The initial deviatior stress was

therefore not quite zero at the start of shear stage, resulting in a slight bedding error.

d) Disturbance to the soil sample. The mounting of the local strain gauges (axial and radial) onto the sample inevitably caused some disturbance to the sample. This was unavoidable, because the footing pads of the axial gauges had to be pressed against the membrane so that the pins fixed to the footing pads pierced through the membrane and deep into the soil sample. This operation was important to ensure proper contact between the sample and the footing pads of the axial gauges.

e) Technique for suction-change. In the present tests, suction reduction during the equalization stage and suction-increase or suction-decrease during the suction-change stage were carried out by manually changing the value of the water back pressure in a step-loading manner. This procedure could have been improved if facilities had been available to ramp the water back pressure in a continous fashion.

7.6.3 Measurement of v

One of the important aspects of testing unsaturated soil samples in the triaxial apparatus is the measurement of sample volume change during all stages of the test. The double-walled cell was successfully used by *Wheeler* (1986) and *Sham* (1989) in the testing of soil samples containing gas bubbles and later by *Sivakumar* (1993) in the testing of unsaturated compacted kaolin samples. The principle of the double-walled cell is simple in that the volume change of the sample is given directly by the volume of water entering or leaving the inner cell (see Fig. 2.37 and Section 2.7.4.1). The method was accurate at any value of strain and irrespective of the shape of the deformed sample. *Sivakumar* (1993) reported that the absolute values of v were measured to an accuracy of 0.01.

In the present tests two Imperial College axial displacement gauges and a custom-built radial displacement gauge were mounted onto the soil sample to measure the individual axial and radial strains during all stages of the tests. The volumetric strains of the sample and hence the sample volume change were calculated from the individual axial and radial strains as described in Sections 5.5.4 and 5.5.5. Unfortunately the accuracy of this procedure is affected by any non-uniform deformation of the sample.

If the relative merits of both methods of measuring the sample volume change are compared then the double-walled cell seems to give more accurate measurements of sample volume change. However local axial and radial gauges are also useful if accurate measurements of shear strain are required at small strain levels (where external measurements of axial strain are affected by bedding errors and system compliance). So if accurate values of both shear strain ε_s and volumetric strain ε_v were needed, the best solution would be to have a double-walled cell fitted with local strain gauges (if cost was immaterial).

7.6.4 Logging and Control

The logging facilities used in the current tests did not include a feedback control program, such as required for conducting stress path tests. Therefore the only available options for conducting the final re-loading shear stages were to either re-load isotropically ($\Delta q/\Delta p' = 0$) or to shear at constant cell pressure ($\Delta q/\Delta p' = 3$). To capitalise on the available experimental equipment and to enhance the testing techniques, some improvements could be incorporated into the existing logging and control facilities such as :

a) Use of feedback control on the existing hydraulic triaxial cell, to allow stress path control and testing of soil samples at different inclinations of the stress path ($\Delta q/\Delta p'$).

b) Use of a stepper motor and a computer programme to control the suction variation during wetting and drying stages. This would mean that the suction within the sample would be continously variable (as achieved by *Sivakumar* (1993)).

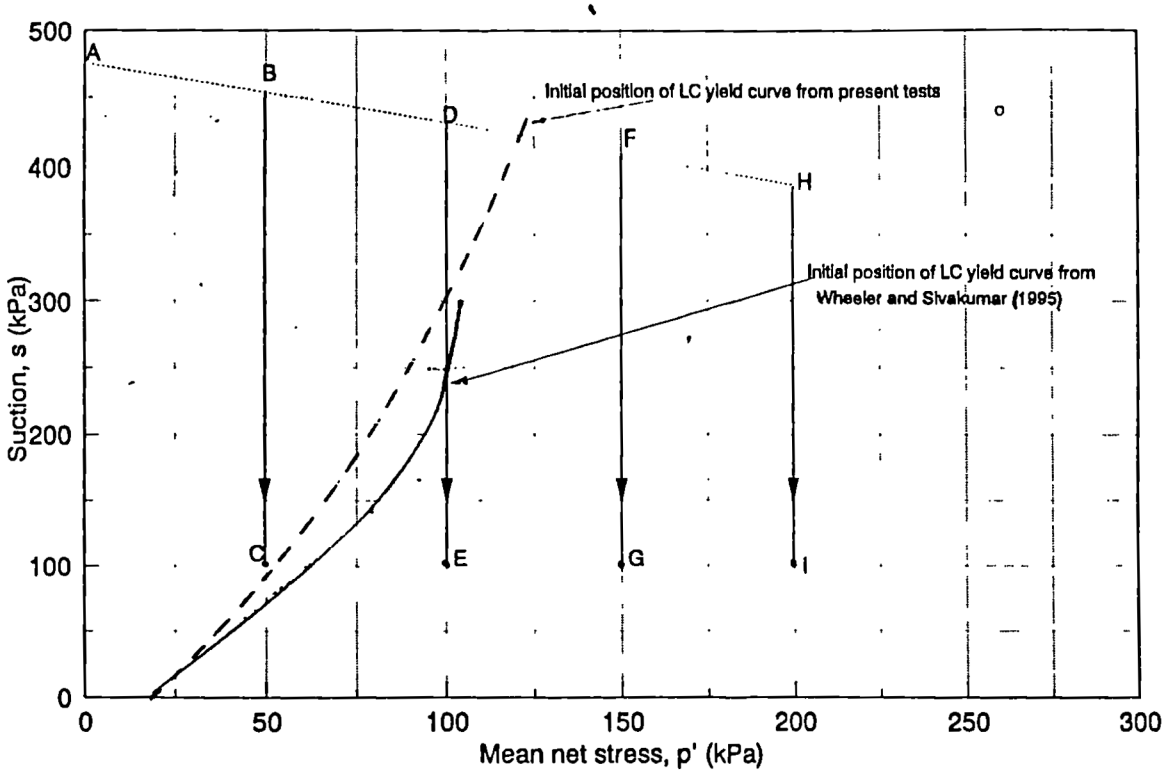

Fig. 7.1 : Initial position of LC yield curve

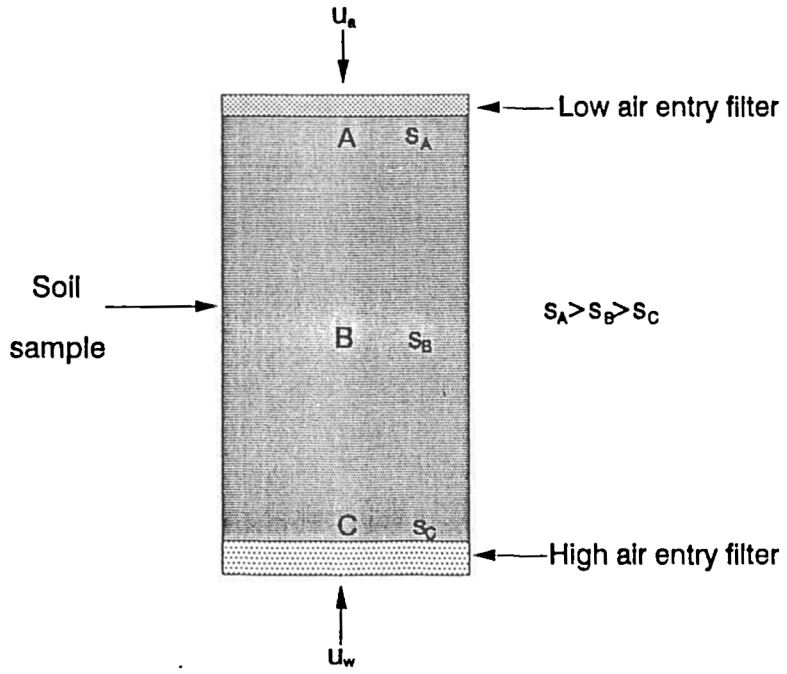

Fig. 7.2 : Non-equalization of suction throughout soil sample during the wetting phase of the equalization stage

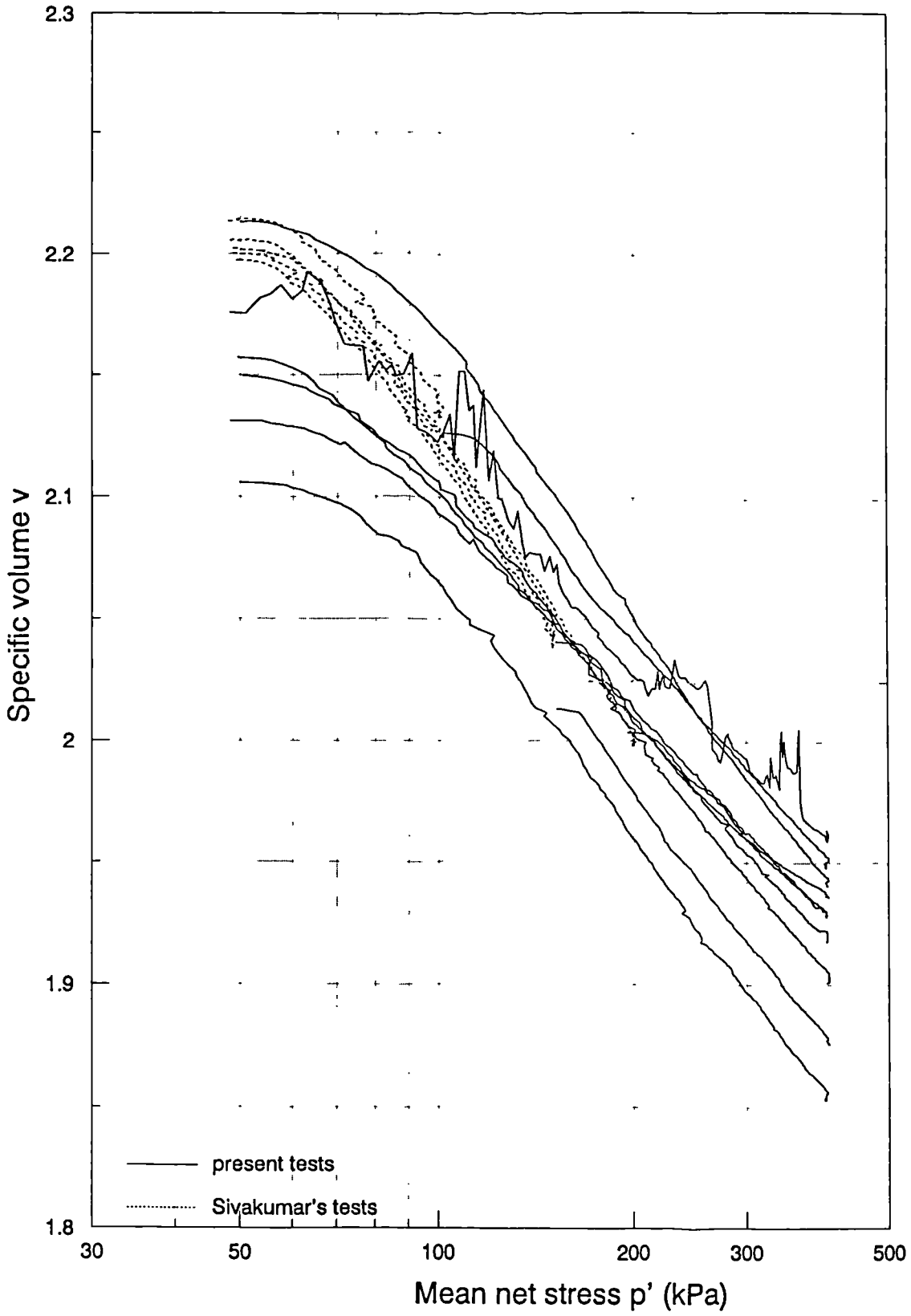

Fig. 7.3 : Variation of specific volume with mean net stress during ramped consolidation from the present tests and from Sivakumar's tests at s = 100 kPa

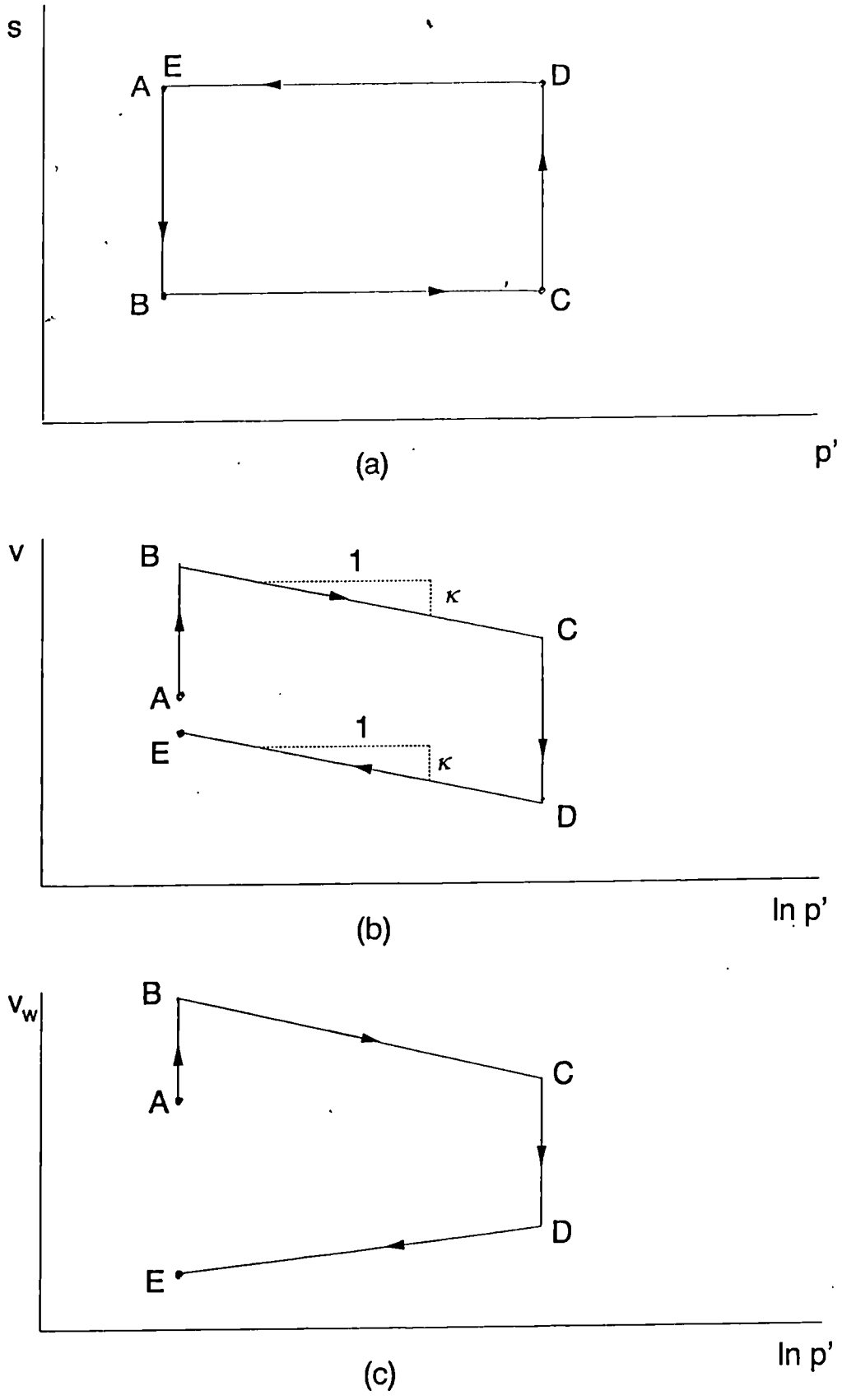

Fig. 7.4 : Variation of v and v_w during closed elastic stress path

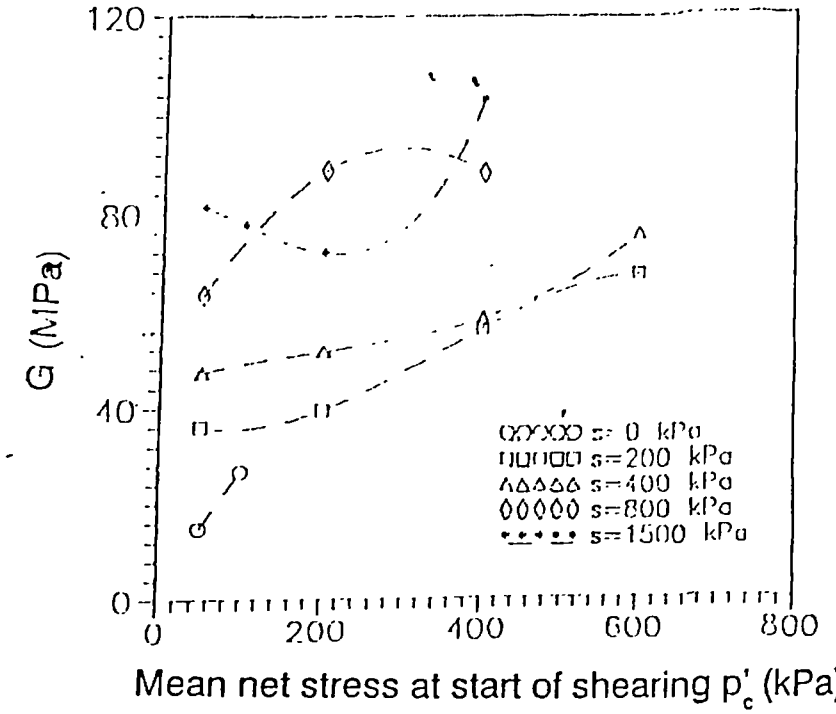

Fig. 7.5 : Variation of G with p' and s from shear tests on unsaturated, compacted Jossigny silt (Cui, 1993)

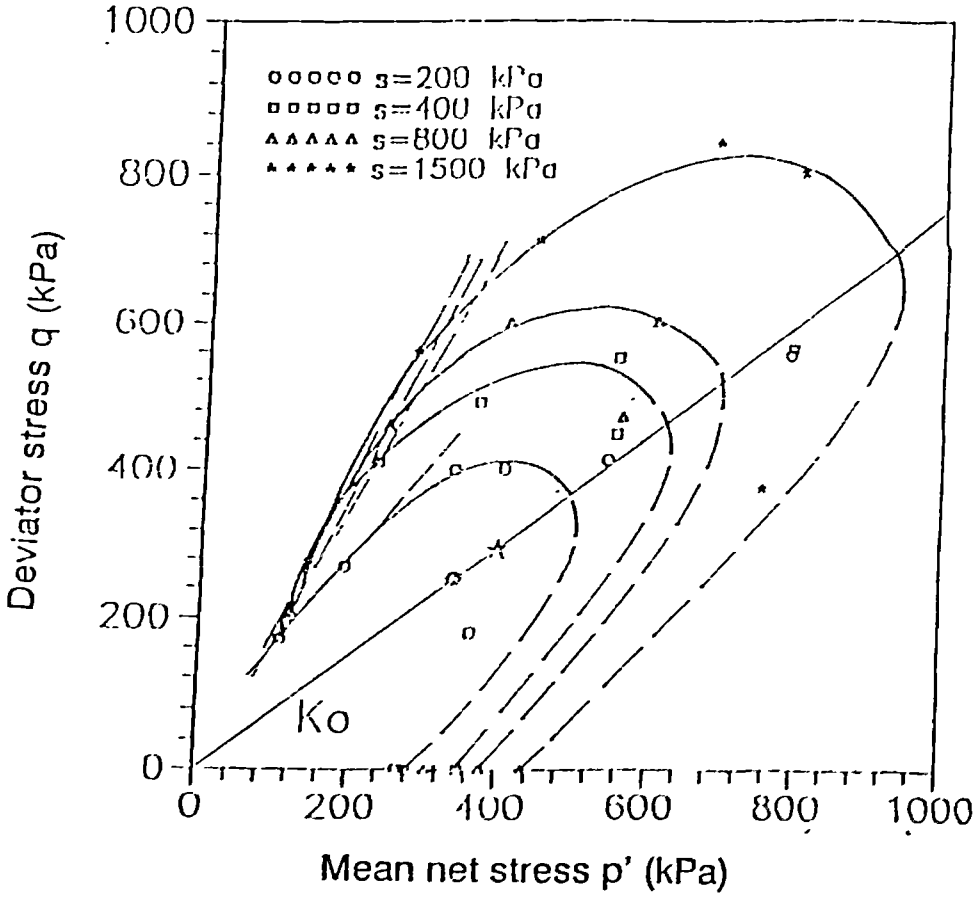

Fig. 7.6 : Yield curves for unsaturated compacted samples of Jossigny silt (Cui, 1993)

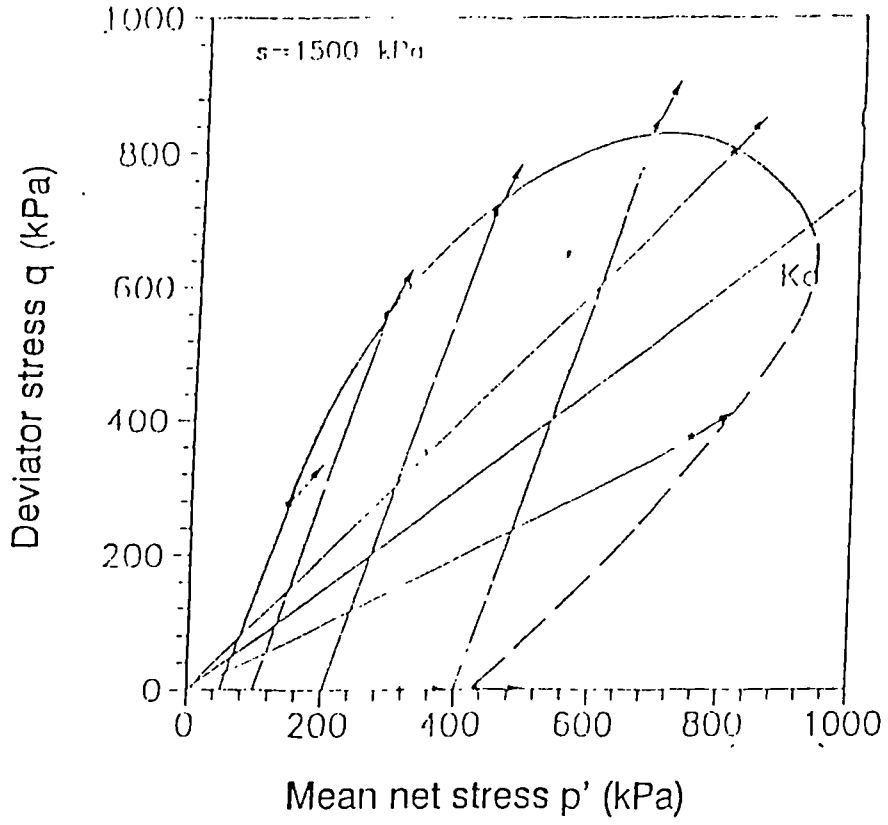

Fig. 7.7 : Plastic strain increment vectors for unsaturated compacted Jossigny silt (Cui, 1993)

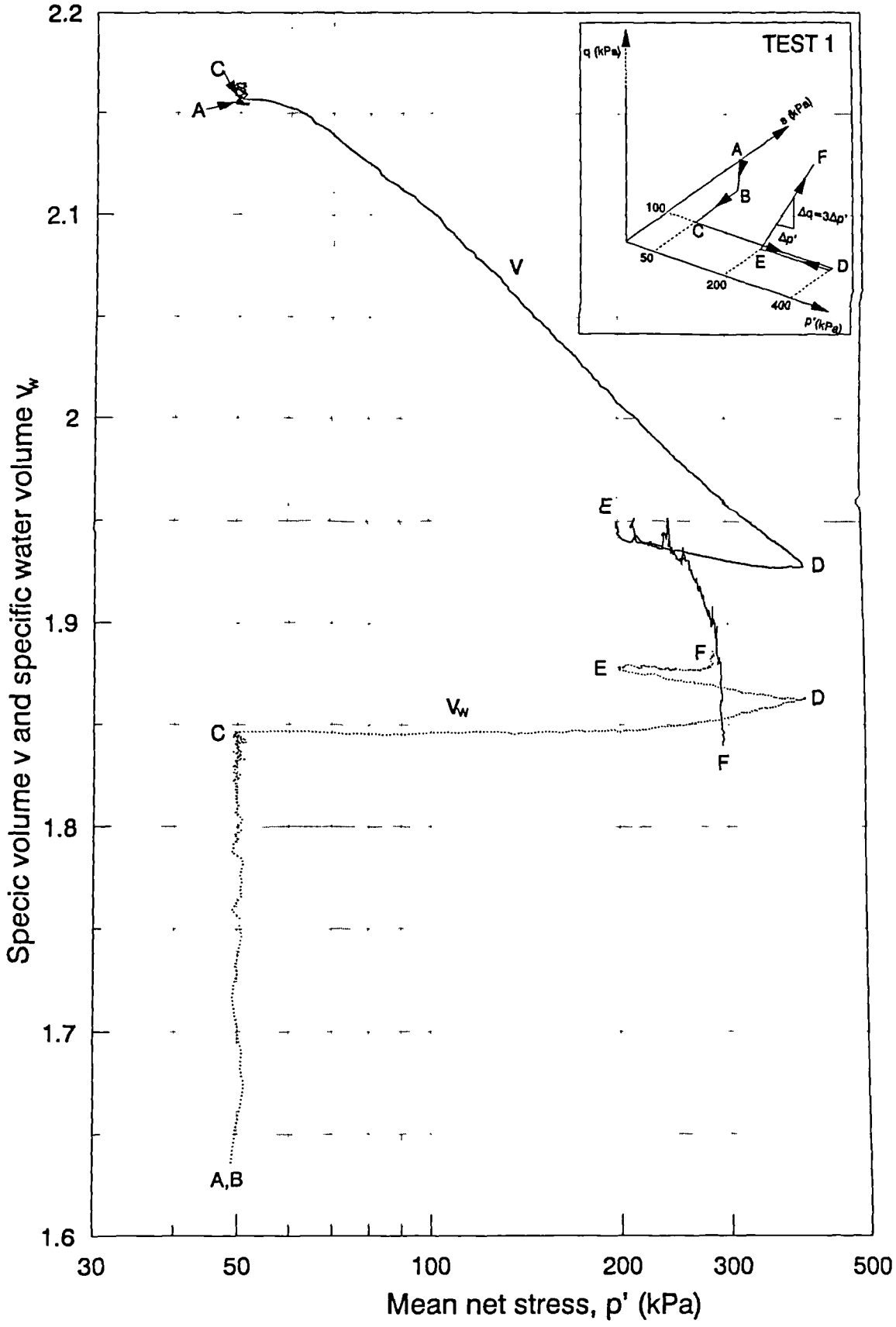

Fig. 7.8 (a) : Variation of specific volume and specific water volume with mean net stress for all stages of Test 1

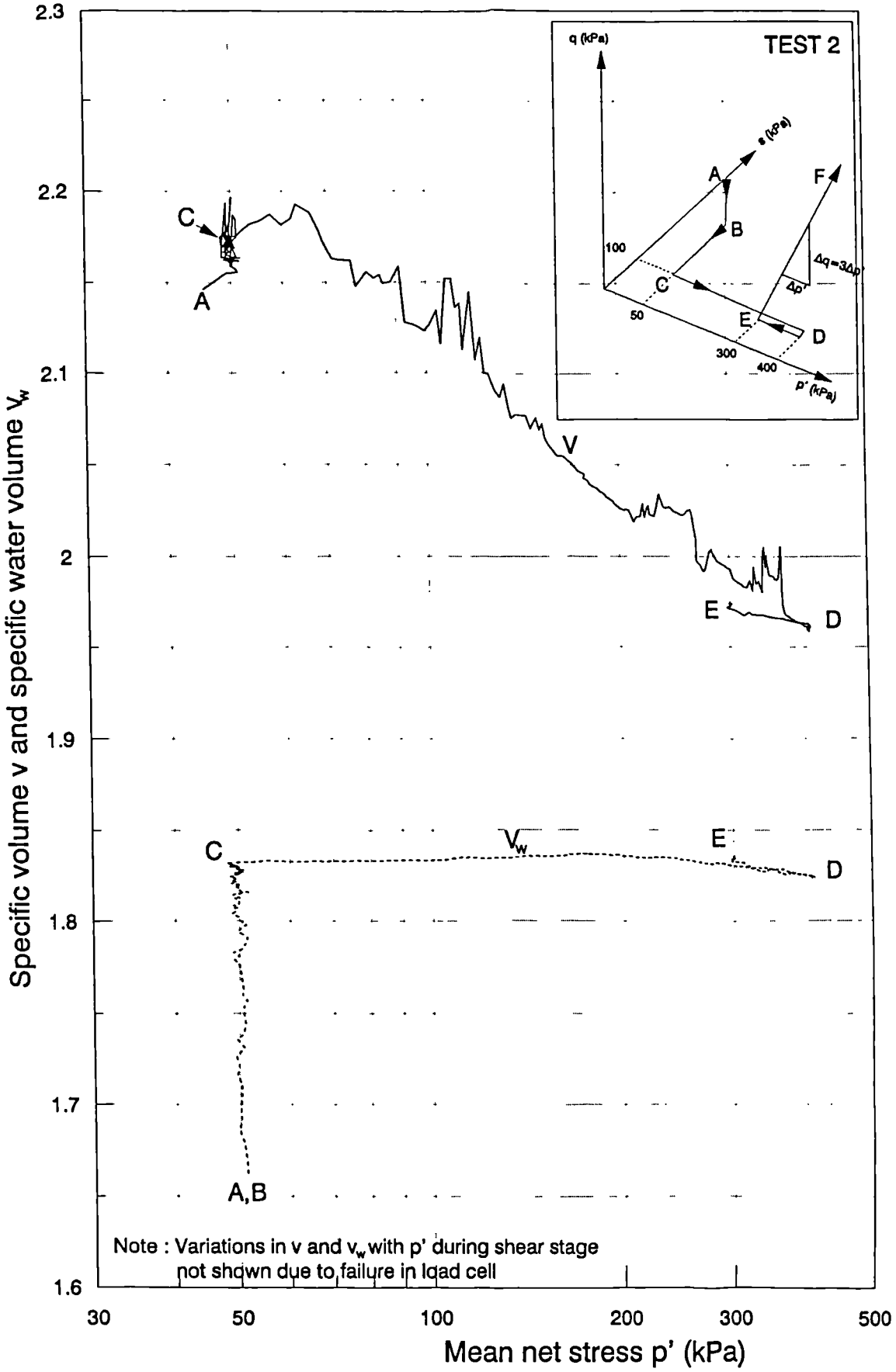

Fig. 7.8 (b) : Variation of specific volume and specific water volume with mean net stress for all stages of Test 2

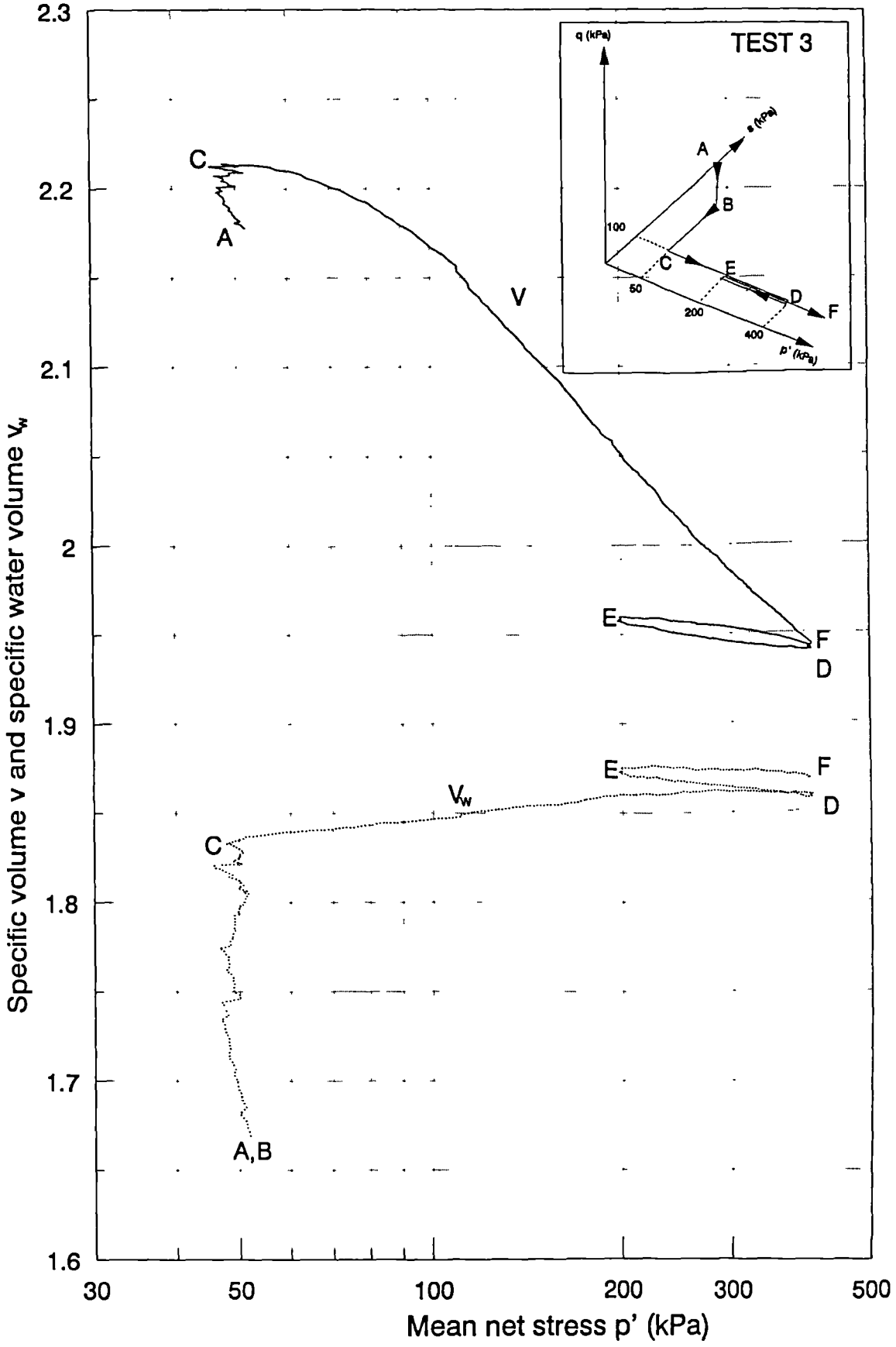

Fig. 7.8 (c) : Variation of specific volume and specific water volume with mean net stress for all stages of Test 3

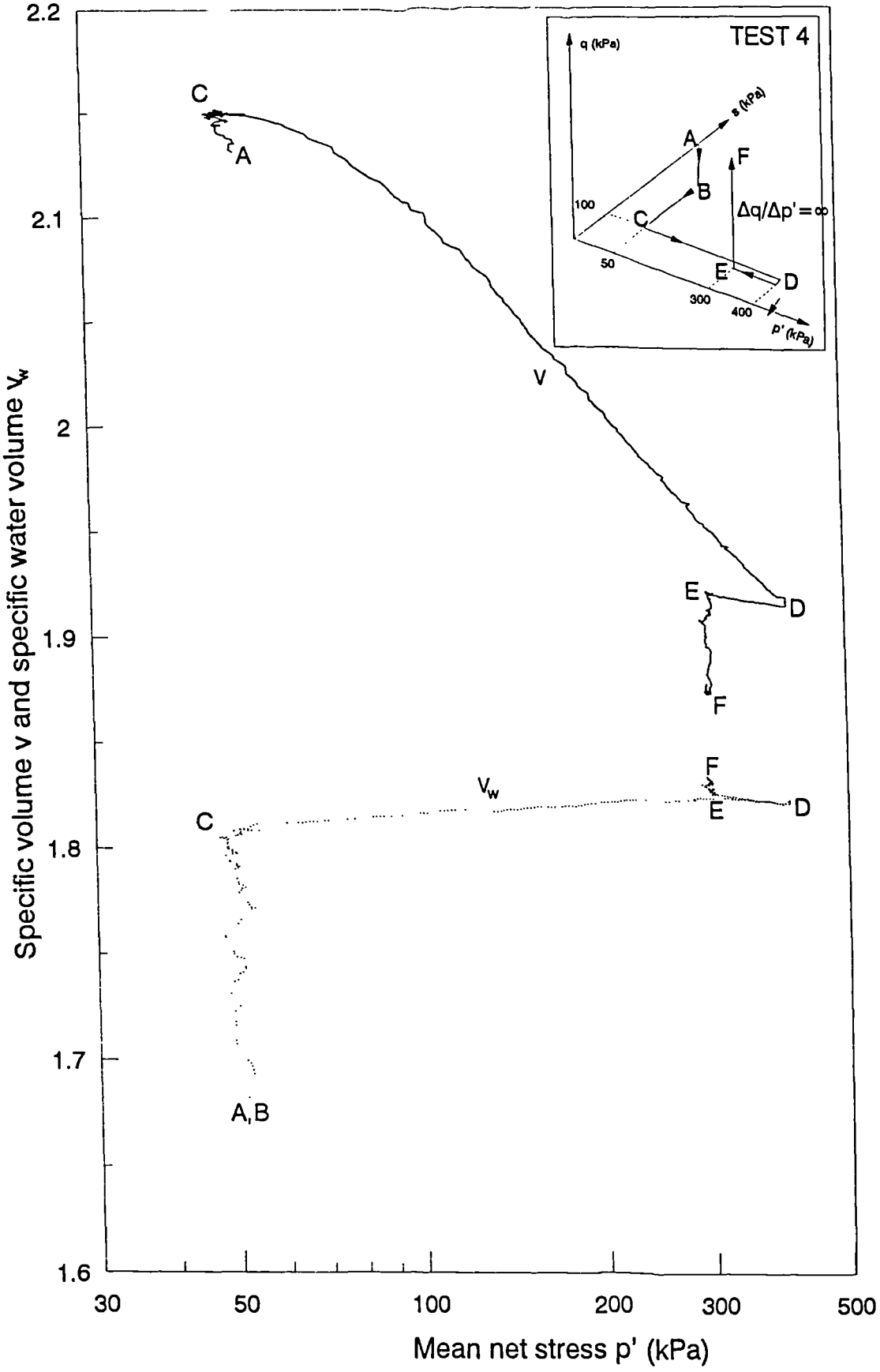

Fig. 7.8 (d) : Variation of specific volume and specific water volume with mean net stress for all stages of Test 4

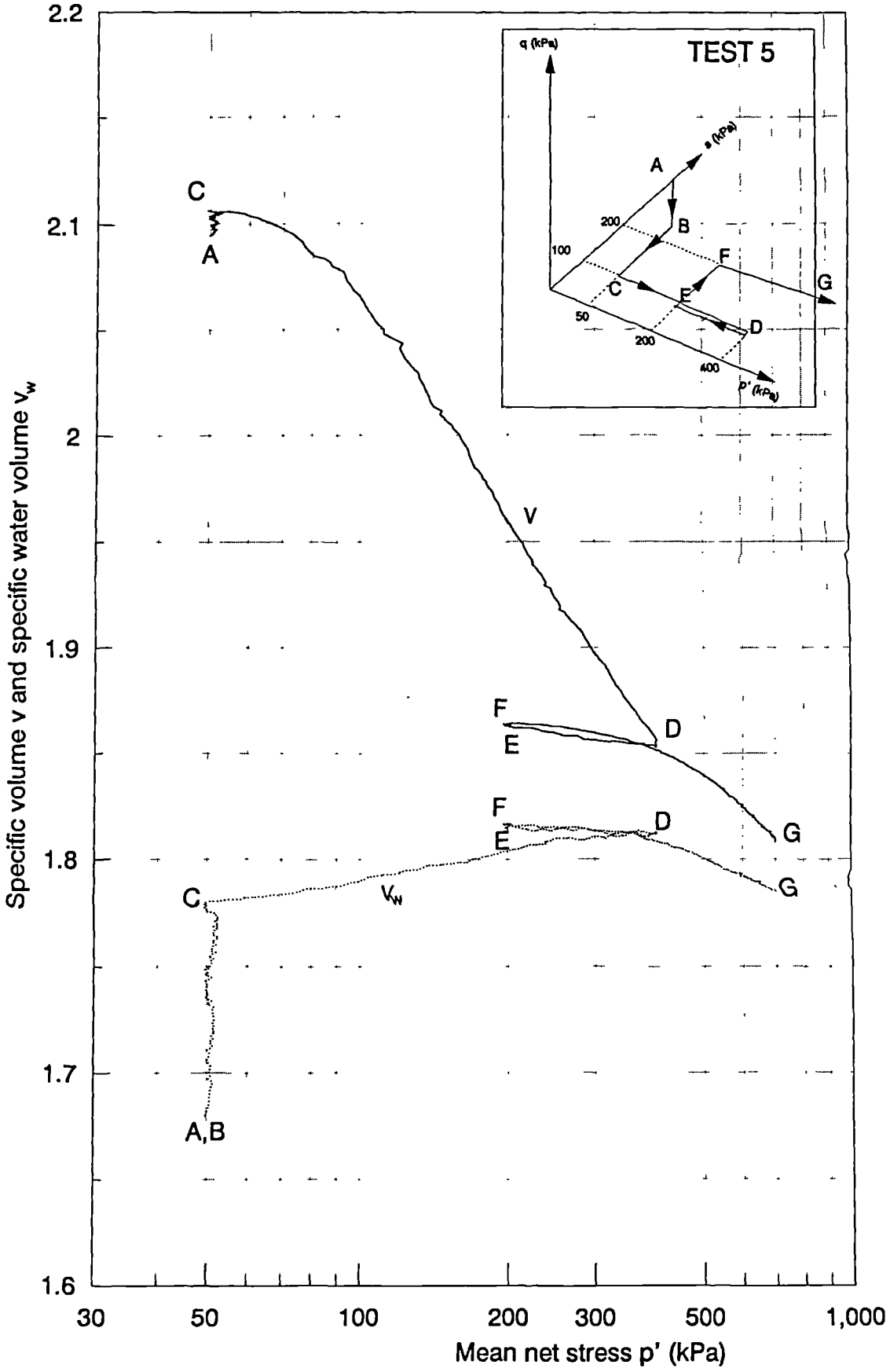

Fig. 7.8 (e) : Variation of specific volume and specific water volume with mean net stress for all stages of Test 5

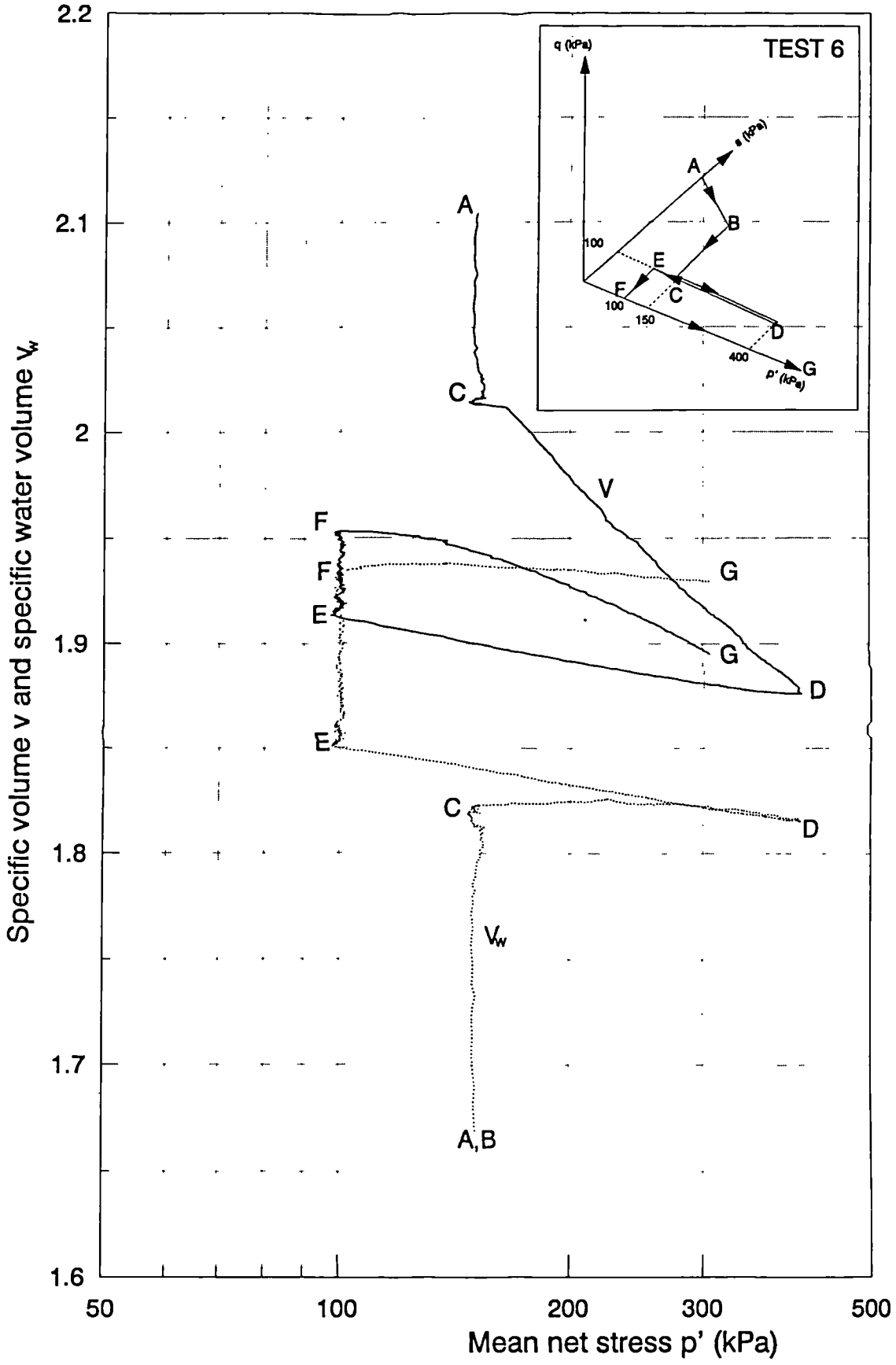

Fig. 7.8 (f) : Variation of specific volume and specific water volume with mean net stress for all stages of Test 6

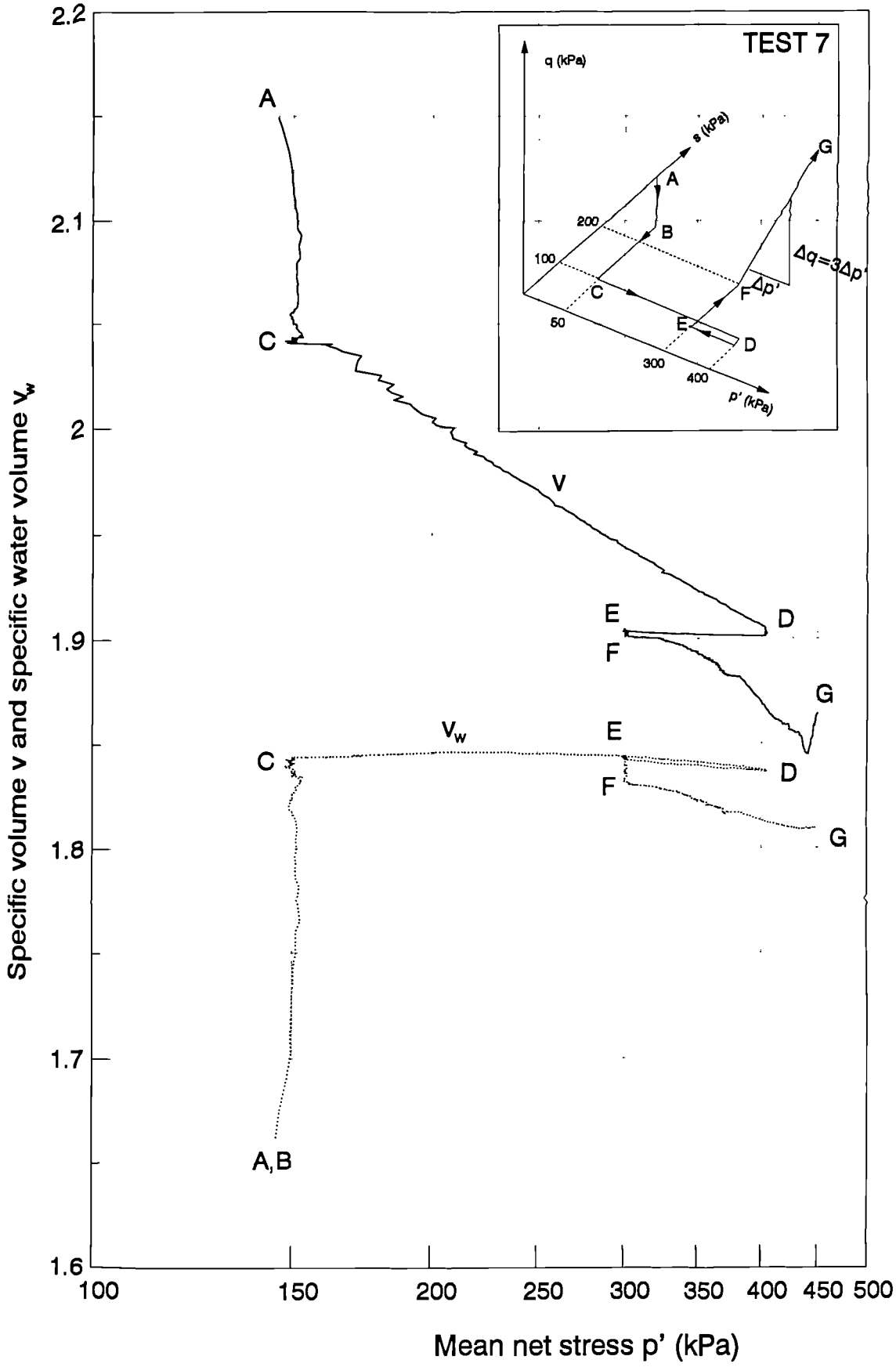

Fig.7.8(g) : Variation of specific volume and specific water volume with mean net stress for all stages of Test 7

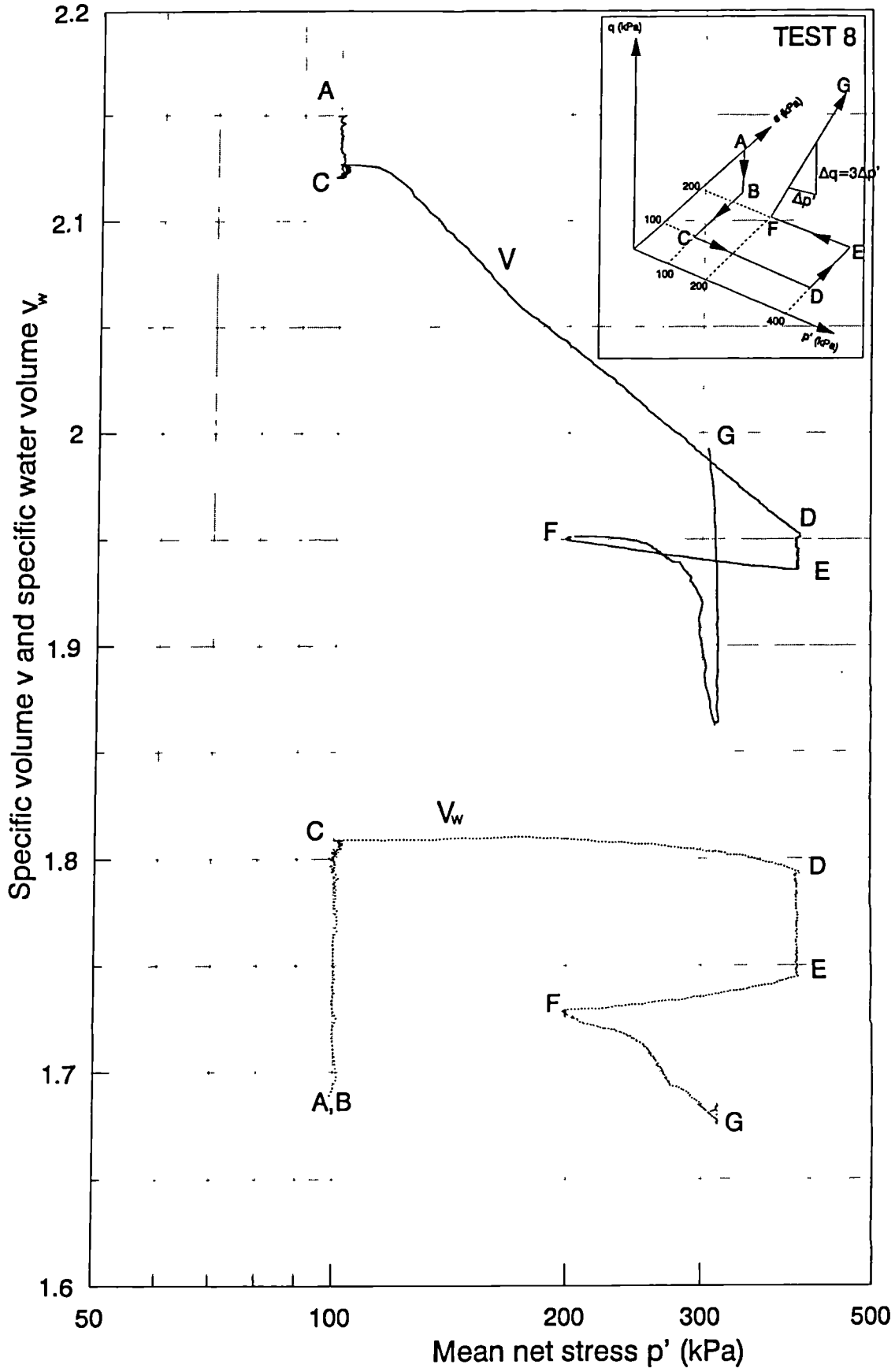

Fig. 7.8 (h) : Variation of specific volume and specific water volume with mean net stress for all stages of Test 8

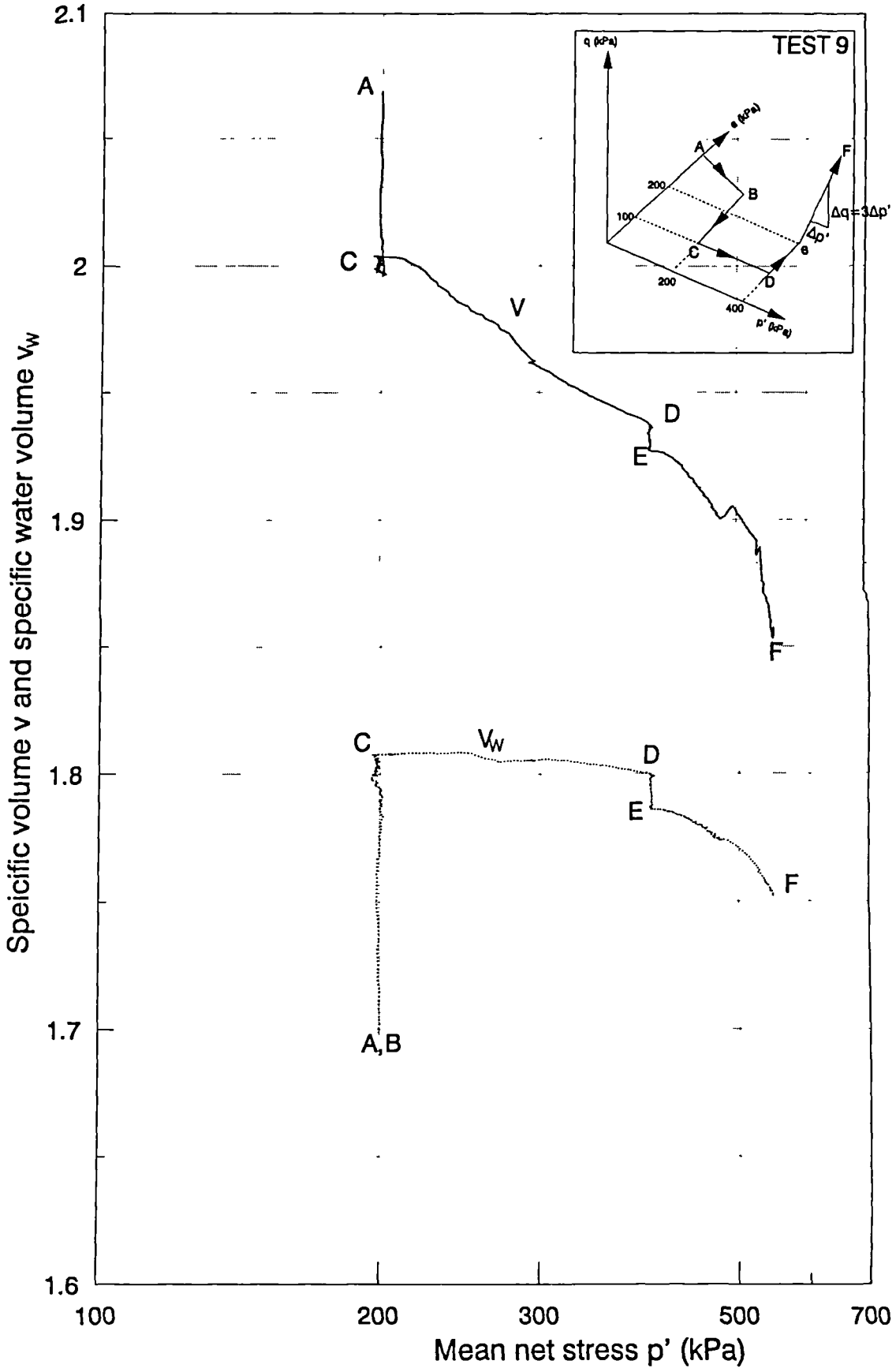

Fig. 7.8 (i) : Variation of specific volume and specific water volume with mean net stress for all stages of Test 9

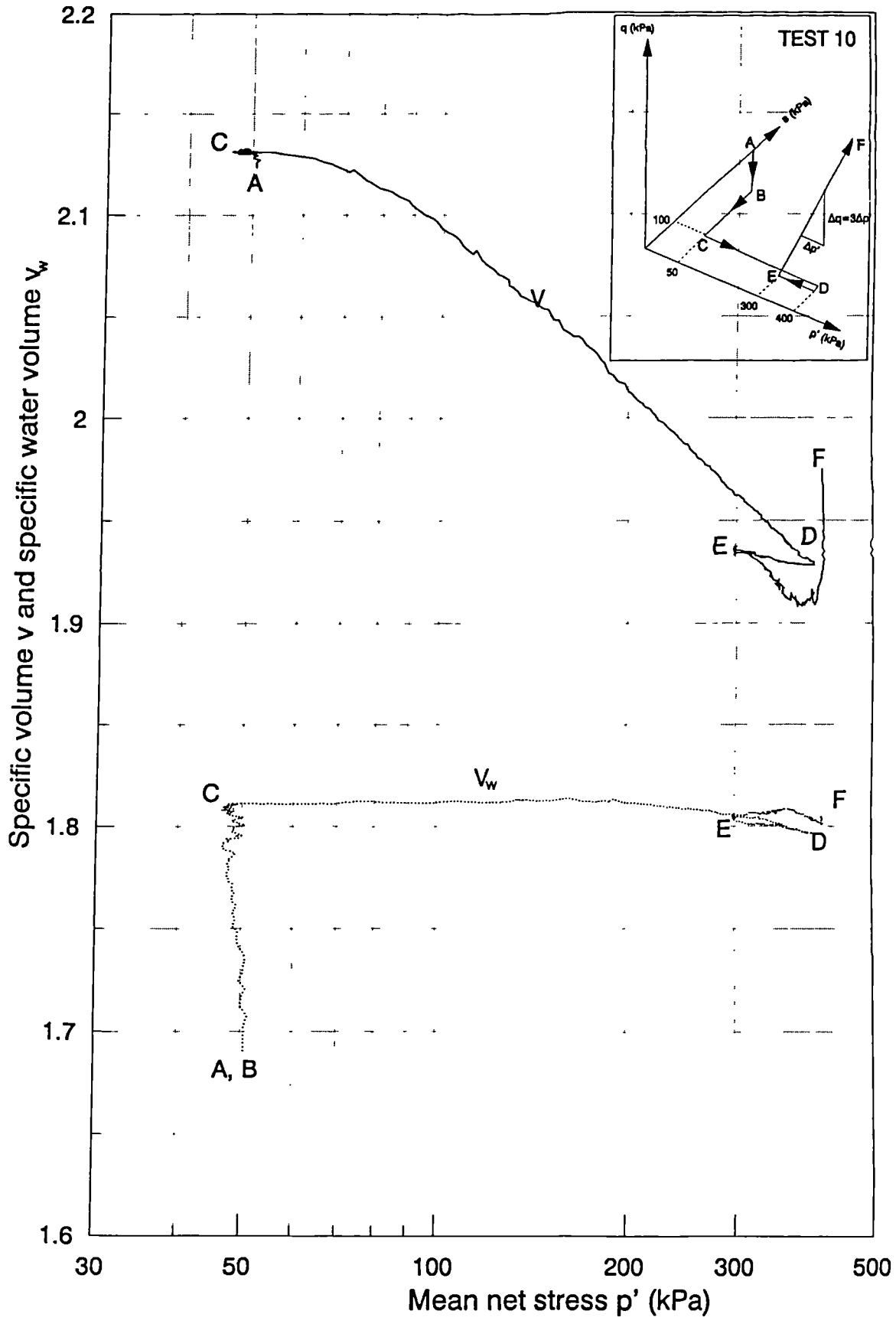

Fig. 7.8 (j) : Variation of specific volume and specific water volume with mean net stress for all stages of Test 10

CHAPTER 8

CONCLUSIONS AND FURTHER WORK

A programme of suction-controlled triaxial tests was performed to investigate aspects of the mechanical behaviour of unsaturated compacted kaolin. A total of ten tests, with an average duration of 48 days, were conducted within the project. This final chapter summarizes the main findings that have been drawn from the experimental work. The chapter is divided into three main sections. Firstly it concludes on the merits and demerits of the experimental equipment and test methodology, including sample preparation and testing techniques. Secondly the chapter briefly summarizes the main conclusions that have been drawn from the work concerning the mechanical behaviour of unsaturated compacted kaolin and its interpretation within an elasto-plastic critical state constitutive model. Finally recommendations for further work are made, which highlight some aspects of unsaturated soil behaviour which require further investigation.

8.1 Experimental equipment and test methodology

Tests on unsaturated soil were carried out on 50mm diameter kaolin soil samples. The soil samples were directly compacted in a specially built compaction mould at a compaction water content of about 25% (4% below optimum as determined by the standard Proctor compaction tests). Each sample was compacted in 9 layers, with each layer being compressed at a displacement rate of 1.5 mm/minute to a vertical pressure of 400 kPa in a compression machine. The variation of water content after compaction between samples was 1.36%, the variation of the degree of saturation was about 6.2% between samples while the variation of specific volume between samples was 3.6 %. This indicated that the compaction procedure

was not as well controlled as in the earlier tests of *Sivakumar* (1993) on the same material. The reasons for this poorer level of compaction control were unclear.

The tests were conducted in a Bishop-Wesley hydraulic triaxial cell, with a wide body to accommodate local strain gauges. The cell pressure and lower chamber pressure were provided by GDS digital pressure/volume controllers, whereas the pore air pressure and pore water pressure were manually controlled by regulators operating on a compressed air supply. Pore air pressure was controlled at the top of the sample, via a dry low air entry filter, whereas pore water pressure was controlled at the bottom of the sample, via a saturated high air entry filter. The cell pressure, pore air pressure and pore water presure were measured by pressure transducers. The deviator load on the sample was measured by an internal load cell fixed to the cell top plate. The volume of water draining from the sample was measured with an Imperial College volume gauge which was connected to the water back pressure line. The measurement of sample volume change was by means of two axial gauges and a radial displacement gauge mounted directly on the soil sample. The axial gauges and the radial gauge measured the axial and radial strains independently and hence the sample volume change. Two external LVDTs attached to the cross-arm of the triaxial cell were used to complement the measurement of axial displacements of the sample during shearing.

The use of local strain gauges in the measurement of sample volume change appeared to result in poorer accuracy in the measurement of specific volume than was achieved by *Sivakumar* (1993). This was, presumably, the result of the non-uniform deformation of the sample during testing. The use of double-walled cell as a means of measuring the sample volume change would have been superior to the use of local strain gauges.

Data from all transducers and gauges were logged into disks during the tests using Quicklog PC™ software. The software was only able to log and save data into disks without performing any calculation while the tests were in progress. On

completion of a test the data was transferred to a spreadsheet for subsequent processing. The software was solely for logging ; no feedback control capability was available. As a result only two types of stress path were available for the final re-loading/shear stages of tests ($\Delta q/\Delta p' = 0$ and 3).

Each sample was initially subjected to an undrained application of net stress of 50 to 200 kPa. This was followed by an equalization (wetting) stage, in which the mean net stress was held constant at 50 to 200 kPa while the suction was reduced in a single step to 100 kPa. The subsequent stage involved ramped consolidation at a constant suction of 100 kPa to a mean net stress p_o' of 400 kPa. When consolidation was complete the samples were subjected to a swell-back stage. Four samples were swelled back to p_c' = 300 kPa, four samples were swelled back to p_c' = 200 kPa, one sample was swelled to p_c' = 100 kPa while another one was not subjected to a swell-back stage.

In some tests a suction-change stage was conducted after the swell-back stage (in one test the suction change was performed before reduction of p'). Four samples were subjected to suction increase stage to s = 200 kPa while one sample was subjected to suction decrease stage to s = 0. In the final re-loading/shear stage three samples were subjected to isotropic re-loading (at suctions of zero, 100 and 200 kPa respectively). Six tests involved a shear stage with the stress path inclined at $\Delta q/\Delta p'$ = 3 (three of these tests were conducted at a suction of 100 kPa while another three were conducted at a suction of 200 kPa). An attempt was made to carry out a single shear test with p' held constant, but this was not entirely successful (because of the lack of a feedback control system for performing stress path testing).

8.2 Observed behaviour

The experimental work described in this thesis confirmed some of the behaviour of unsaturated soil as predicted by the elasto-plastic critical state models of

Alonso, Gens and Josa (1990) and *Wheeler and Sivakumar* (1995), but the observed behaviour differed from the model predictions in several points of detail. Some of the main conclusions drawn from the experimental work are as follow :

a) Initial position and shape of the LC yield curve. The behaviour observed during the initial undrained application of net stress and the subsequent equalization (wetting) stage was consistent with the existence of a LC yield curve in the $s : p'$ plane, as proposed by *Alonso, Gens and Josa* (1990) and *Wheeler and Sivakumar* (1995). The initial position and shape of the yield curve, produced by the compaction procedure, showed good agreement with the model of *Wheeler and Sivakumar* (1995) and was similar to that observed by *Sivakumar* (1993) in his tests on kaolin samples compacted in the same manner as the samples in the current project.

b) Normal compression lines. On isotropic loading to virgin states at a suction of 100 kPa, in the ramped consolidation stage, the values of v fell on a unique isotropic normal compression line in $v : p'$ space. The values of the slope $\lambda(s)$ and intercept N(s) of the normal compression line (at a suction of 100 kPa) obtained from the current tests were lower than the corresponding values of *Sivakumar* (1993). This was partly due to slight curvature of the normal compression line and the fact that the present tests covered a higher range of mean net stress than Sivakumar's tests. There was also considerably greater scatter in the values of $\lambda(s)$ and N(s) than was present in Sivakumar's tests. This was attributed to poorer compaction control and lower accuracy in the measurement of sample volume change (because of the use of local strain gauges instead of a double-walled cell).

c) Elastic behaviour. The swell-back and suction change stages provided information on the elastic indices κ and κ_s. The value of κ was found to be essentially independent of suction (over the limited range of suction tested) whereas the value of κ_s was found to increase with increasing p'. This

suggested a net change in v for a closed stress path in the $s : p'$ plane, contravening the requirement of conservative behaviour for elastic stress paths. This suggested that the soil behaviour was not truly elastic even for stress paths remaining inside the "yield curve". The shear modulus G, measured in the early part of the final shear stage was also found to increase with increasing p' (and possibly with increasing s), although it was not possible to propose an exact form for the relationship between G, p' and s, due to large scatter in the data.

d) Yield surface. The yield point was generally identified as the point of intersection of two straight lines drawn on the $v : \ln p$ plot. It was often very difficult to define a precise yield point and the suggestion of a very distinct yield point by the models is not entirely correct. The volumetric behaviour of the soil normally gave better indication of the yield point than the shear behaviour. Constant suction cross-sections of the yield surface (yield curves in the $q : p'$ plane) were found to be elliptical in shape. This general shape was consistent with the models of *Alonso, Gens and Josa* (1990) and *Wheeler and Sivakumar* (1995). The shape of yield curves was also consistent with an isotropic soil, in contrast with the results of *Cui* (1993) from tests on Jossigny silt with a strongly anisotropic stress history.

e) Flow rule. The plastic strain increment vectors were approximately perpendicular to the yield curves in the $q : p'$ plane, suggesting an associated flow rule. This form of flow rule was consistent with an isotropic soil, in contrast with the non-associated flow rule suggested by *Cui* (1993) on the basis of his tests on samples with anisotropic stress history.

f) Variation of specific water volume. The values of the slope $\alpha(s)$ and intercept A(s) of the normal compression line for v_w (at a suction of 100 kPa) obtained from the current tests were higher than the corresponding values of *Sivakumar* (1993). This was probably due to the incomplete

equalization of pore water pressure during the early part of the test (equalization stage), which affected the subsequent *ramped consolidation* stage. The value of the elastic parameter κ_w was found to be basically independent of suction (over the limited range of suction tested) whereas the value of κ_{sw} was found to increase with increasing p' (in suction-increase tests). This suggested a net change in v_w for a closed stress path in the $s : p'$ plane, contravening the requirement of conservative behaviour for elastic stress paths. This lent further support to the suggestion that the soil behaviour was not truly elastic even for stress paths remaining inside the "yield curve".

8.3 Recommendations for further work

The experimental research work described in this thesis has highlighted some aspects of the mechanical behaviour of unsaturated compacted kaolin. Most of the observed behaviour was consistent with the predictions of the elasto-plastic critical state constitutive models of *Alonso, Gens and Josa* (1990) and *Wheeler and Sivakumar* (1995). However certain features of the observed behaviour were not predicted by these constitutive models, for example the suggestion of an irrecoverable component of swelling on first wetting. In view of the limited number of tests possible in the curent experimental programme there is room for further investigation of unsaturated soil behaviour, such as :

a) The final re-loading / shear stage in the tests involved only two different inclinations of stress path ($\Delta q/\Delta p'$ = 0 or 3) (see Section 5.3.6). Further work could therefore include a feed-back system incorporated into the triaxial apparatus so that any desired stress paths on the soil could be conducted. Automatic control of the pore water pressure would also be desirable, so that the suction could be varied in a controlled and continous fashion.

b) In the experimental work tests on soil samples commenced with an initially high value of suction (although unknown) and the LC yield curve was expanded by reducing s or increasing p'. No direct investigation was carried out on the existence of Suction Increase (SI) yield curve, as proposed by *Alonso, Gens and Josa* (1990). This was because in the tests the suction was never increased above the high initial value produced by the compaction procedure. Further experimental work could investigate this aspect of the model.

c) The behaviour of unsaturated soil observed in the current research work was based on one particular type of soil fabric produced by a particular method of compaction (see Section 5.2). It has been shown by many investigators that the behaviour of unsaturated soil is highly influenced by the soil fabric (see Section 2.1), whether naturally occurring or man-made. Thus further work could be done on kaolin samples by employing different types of compaction (varying the compaction water content, the compactive effort and the method of compaction (static or dynamic)).

d) The unsaturated soil behaviour investigated in the current tests was based on kaolin samples. A wide variety of different unsaturated soil types occur in practice, and the behaviour of kaolin may not be representative of all these soils. For example, compacted laterite soils (a form of residual soil) found in the tropics are known to be highly expansive (*Lee*, 1993). There is therefore a lot of scope for study of different types of unsaturated soil.

e) A great deal of work on unsaturated soil behaviour has concentrated on compacted soil samples. The behaviour of unsaturated compacted soil might not represent the behaviour of unsaturated natural soil, because of the differences in soil fabric between compacted and naturally occurring unsaturated soils. This would warrant further investigation of the mechanical behaviour of unsaturated natural soils. This is a major challenge, because of

the difficulty of taking undisturbed samples of naturally occurring unsaturated soils.

f). Experimental results showed that the stress-strain curves in most tests were non-linear during the early part of the shear stage. Yielding was simplified to a single point determined by the intersection of two straight portions of the relevant stress-strain plots. This was not necessarily true (yield was actually a gradual process) but as the constitutive modelling of unsaturated soil is less highly developed than that for saturated soil, this approach served a first step towards the understanding of unsaturated soil behaviour. Thus future work on unsaturated soil behaviour should investigate the use of a multi-surface kinematic yield model, as described in Section 2.8 for saturated soil.

LIST OF REFERENCES

1. Ackerley, S.K., Hellings, J.E. and Jardine, R.J. (1987). A new device for measuring local axial strains on triaxial specimens. Discussion, Geotechnique, Vol 37, pp 414 - 415.

2. Aitchinson, G.D. (1961). Relationship of moisture stress and effective stress functions in unsaturated soils. Proc. Conf. on Pore Pressure and Suction in Soil, Butterworth, London.

3. Aitchison, G.D and Woodburn, J.A. (1960). Soil suction in foundation design. Proc. 7th. ICSMFE, Mexico, Vol. 2, pp 1 -8.

4. Alonso, E.E., Gens, A. and Hight, D.W. (1987). General Report : Problem Soils. 9th. ECSMFE, Dublin, Vol. 3, pp 1087 - 1146.

5. Alonso, E.E., Gens, A. and Josa, A. (1990). A constitutive model for partially saturated soil. Geotechnique Vol. 40, No. 3, pp 405 - 430.

6. Baracos, A., Graham, J. and Domaschuk, L. (1980). Yielding and rupture in a lacustrine clay. Canadian Geotechnical Journal, Vol. 17, No. 4, pp 559 - 573.

7. Barden, L., Madedor, A.O. and Sides, G.R (1960). Volume change characteristics of unsaturated clay. Journal of the SMFE, Proc. ASCE, Vol. 95, No. SM1, pp 33 - 51.

8. Balasubramaniam, A.S. (1974). A critical study of the uniqueness of state boundary surface for saturated specimens of kaolin. Geotechnical Engineering, South East Asian Geotechnical Society, Vol. 5, No.1, pp 21 - 38.

9. Bishop, A.W. (1959). The principle of effective stress. Teknik Ukeblad, Vol. 39, pp 859 - 863.

10. Bishop, A.W., Alpan, I., Blight, G.E. and Donald, I.B. (1960). Factors controlling the effective strength of partly saturated cohesive soils. Research Conference on Shear Strength of Cohesive Soils, Colorado, USA, pp 503 - 532.

11. Bishop, A.W. and Blight, G.E. (1963), Some aspects of effective stress in saturated and partly saturated soils. Geotechnique, Vol. 13, No. 3 , pp 177 - 197.

12. Bishop, A.W. and Donald, I.B. (1961), The experimantal study of partly saturated soil in the triaxial apparatus. 5th. ICSMFE, Paris Vol 1, pp 13 - 21.

13. Bishop, A.W. and Henkel, D.J. (1962), The measurement of soil properties in the triaxial apparatus, 2nd. Edition, Edward Arnold, London.

14. Brackley, I.J.A. (1971), Partial collapse in unsaturated expansive clay. 5th. Regional Conf. SMFE for Africa, Luanda, Vol. 1, pp 1 - 8.

15. Brand, E.W. (1988). Some aspects of field measurements for slopes in residual soils. Proc. 2nd. Int. Conf. on Field Measurements in Geomechanics. pp 531 - 545.

16. Burland, J.B (1965). Some aspects of the mechanical behaviour of partly saturated soils. Symposium on Moisture Equilibria and Moisture Changes in Soils Beneath Covered Areas, CSIRO, Australia, pp 270 - 278.

17. Burland, J.B. and Symes, M.J. (1982), A simple axial displacement gauge for use in the triaxial apparatus. Technical Note, Geotechnique Vol. 32, No. 1, pp 62 - 65.

18. Chandler, R.J. and Gutierrez, C.I. (1986). The filter paper method of suction measurement. Technical Note, Geotechnique Vol. 36, No. 2, pp 265 - 268.

19. Clayton, C.R.I. and Khatrush, S.A. (1987). A new device for measuring local axial strains on triaxial specimen. Discussion, Geotechnique Vol. 37, No. 3, pp 413 - 417.

20. Coleman, J.D. (1962). Stress/strain relations for partially saturated soil. Correspondence, Geotechnique Vol. 12, No. 4, pp 348 - 350.

21. Costa-Filho, L. de M. (1985). Measurement of axial strains in triaxial tests on London clay. Geotechnical Testing Journal, ASCE, Vol. 8, No. 1, pp 3 -13.

22. Cui, Y.J. (1993). Etude du comportement d'un limon compacte non sature et de sa modelisation dans un cadre ealsto-plastique. PhD thesis, CERMES, Ecole Nationale des Ponts et Chaussees, Paris.

23. Cui, Y.J. and Delage, P. (1993). On the elasto-plastic behaviour of an unsaturated silt. ACSE National Convention on Unsaturated Soil, Dallas, Texas, USA, pp 1 - 12.

24. Delage, P., Suraj de Silva, G.P.R. and De Laure, E. (1987). Un nouvel appareil triaxial les sols non satures. Proc. 9th. ECSMFE, Vol. 1, pp 26 - 28.

25. Delage, P., Suraj de Silva, G.P.R and Vicol, T. (1992). Suction-controlled testing of non-saturated soils with an osmotic consolidometer, 7th. Int. Conf. on Expansive Soils, Dallas, Texas, USA.

26. Edil, T.B., Motan, S.E. and Toha, F.X. (1981). Mechanical behaviour and testing methods of unsaturated soils. Laboratory Shear Strength of Soil, ASTM, STP 740, pp 114 - 129.

27. Escario, V. and Juca, J.F.T. (1989). Strength and deformation of partly saturated soils. 12th. ICSMFE, Rio de Janerio, Vol. 1, pp 43 - 46.

28. Escario, V. and Saez, J. (1986). The shear strength of partly saturated soils. Technical Note, Geotechnique Vol. 36, No. 3. pp 453 - 456.

29. Fredlund, D.G. (1975). A diffused air volume indicator for unsaturated soils. Canadian Geotechnical Journal, Vol. 12, No. 4, pp 533 - 539.

30. Fredlund, D.G. (1979). Appropriate concept and technology for unsaturated soils. Canadian Geotechnical Journal, Vol. 16, No. 1, pp 121 - 139.

31. Fredlund, D.G . and Morgenstern, N.R. (1976). Constitutive relations for volume change in unsaturated soils. Canadian Geotechnical Journal, Vol. 13, No. 261, pp 261 - 276.

32. Fredlund, D.G. and Morgenstern, N.R. (1977). Stress state variables for unsaturated soils. Journal of the Geotecnical Engineering, Proc. ASCE, Vol. 103, No. GT5, pp 447 - 465.

33. Fredlund, D.G., Morgenstern, N.R. and Widger, R.A. (1978). The shear strength of unsaturated soils. Canadian Geotechnical Journal, Vol. 1, No. 3, pp 313 - 321.

34. Fredlund, D.G. and Rahardjo, H. (1988). State of development in the measurement of soil suction. Proc. Int. Conf. on Engineering Problems in Regional Soils, Beijing, China, pp 582 - 588.

35. Fredlund, D.G., Rahardjo, H. and Gan, J.K.M. (1987). Non-linearity of strength envelope for unsaturated soils. Proc. 6th. Int. Conf. on Expansive Soils, New Delhi, India, pp 49 - 54.

36. Fredlund, D.G and Wong, D.K.H. (1989). Calibration of thermal conductivity sensors for measuring soil suction. Geotechnical Testing Journal, ASTM, Vol. 12, No. 3, pp 188 - 194.

37. Gan, J.K.M., Fredlund, D.G. and Rahardjo, H. (1988). Determination of the shear strength parameters of an unsaturated soil using the direct shear test. Canadian Geotechnical Journal, Vol. 25, pp 500 - 510.

38. Gens, A. and Alonso, E.E. (1992). A framework for the behaviour of unsaturated expansive clays. Canadian Geotechnical Journal, Vol. 29, No. 6, pp 1013 - 1032.

39. Graham, J., Crooks, J.H.A and Lau, S.L.K. (1988). Yield envelopes : identification and geometric properties. Geotechnique, Vol. 38, No. 1, pp 125 - 134.

40. Graham, J., Noonan, M.L. and Lew, K.V. (1988). Yield states and stress-strain relationship in a natural plastic clay. Canadian Geotechnical Journal, Vol. 20, No. 3, pp 502 - 516.

41. Gulhati, S.K. and Satija, B.S. (1989). Shear strength of partially saturated soils. 10th. ICSMFE, Vol. 1, pp 609 - 612.

42. Hilf, J.W. (1956). An investigation of pore pressures in compacted cohesive soils. Technical Memorandum No. 654, Bureau of Reclamation, USDI, Denver, Colorado, USA.

43. Hird, C.C and Yung, C.Y. (1989). The use of proximity transducers for local strain measurements in triaxial tests. Technical Note, Geotechnical Testing Journal, ASTM, Vol. 12, No. 4, pp 292 - 296.

44. Ho, Y.F. and Fredlund D.G. (1982). A multi-stage triaxial tests for unsaturated soils. Geotechnical Testing Journal, Vol. 5, No. 1/2, pp 18 - 25.

45. Holtz, W.G. and Hilf, J.W. (1961). Settlement of soil foundations due to saturation. Proc. 5th. ICSMFE, Paris, Vol. 1, pp 673 - 679.

46. Jardine, R.J. and Pott, D.M. (1988). Hutton tension leg platform foundations : prediction of driven pile behaviour. Geotechnique, Vol 38, No. 2, pp 231- 252.

47. Jardine, R.J., Symes, M.J. and Burland, J.B. (1984). The measurement of soil stiffness in the triaxial apparatus. Geotechnique, Vol. 34, No. 3, pp 323 - 340.

48. Jennings, J.E. (1961). A revised effective stress law for use in the prediction of the behaviour of unsaturated soil. Proc. Pore Pressure and Suction in Soils, Butterworth, London.

49. Jennings, J.E. and Burland, J.B (1962). Limitations to the use of effective stresses in partly saturated soils. Geotechnique, Vol.12, No. 2, pp 125 - 144.

50. Josa, A., Balmaceda, A., Gens, A., and Alonso, E.E. (1992). An elasto-plastic model for partially saturated soils exhibiting a maximum of collapse. Int. Conf. on Computational Plasticity, Barcelona, Spain, Pineridge Press, Swansea UK.

51. Krahn, J., Fredlund, D.G and Klassen, M.J (1989). Effect of soil suction on slope stability at Notch Hill. Canadian Geotechnical Journal, Vol. 26, pp 269 - 278.

52. Lee, E.C. (1993). Experimental Studies of Inflitration in Compacted Residual Soil, MPhil thesis, University of Sheffield.

53. Lloret, A. and Alonso, E.E. (1985). State surfaces for partially saturated soils. 11th. ICSMFE, San Francisco, pp 557 - 562.

54. Manheim, F.T. (1960). A hydraulic sqeezer for obtaining interstitial water from consolidated and unconsolidated sediment. US Geological Survey Proceedings, Paper 550-C, pp 256 - 261.

55. Marshall, T.J. (1959). Relationship between water and soil. Com. Bureau Soils Technical Comm. No. 50.

56. Matyas, E.L. and Radhakrishna, H.S. (1968). Volume change characteristics of partially saturated soils. Geotechnique, Vol. 18, No. 4, pp 432 - 448.

57. Moore, W.M. (1966). Effect of variation in Poisson's ratio on soil triaxial testing. Highway Research Record, Vol. 108, pp 19 - 30.

58. Ohta, H. and Wroth, C.P. (1976). Anisotropy and stress orientation in clay under load. Proc. 2nd. Int. Conf. in Numerical Methods in Geomechanics ASCE, pp 319 - 328.

59. Parry, R.H.G and Nadarajah, V. (1973). A volumetric yield locus for lightly over-consolidated clay. Geotechnique, Vol. 23, No. 3, pp 450 - 453.

60. Ridley, A.M. and Burland, J.B. (1994). A new instrument for the measurement of soil moisture suction. Technical Note, Geotechnique, Vol. 43. No. 2, pp 321 - 324.

61. Roscoe, K.H. and Burland, J.B. (1968). On the generalised stress-strain behaviour of 'wet' clay. In Engineering Plasticity (Editors : J. Heyman and F.A. Leckie), Cambridge University Press.

62. Schofield, A.N. and Wroth, C.P. (1968). Critical State Soil Mechanics, McGraw Hill, London.

63. Seed, H.B. and Chan, C.K. (1959). Structure and strength characteristics of compacted clays. Proc. ASCE, No. SM5, pp 87 - 127.

64. Sham, W.K. (1989). The undrained shear strength of soil containing large gas bubbles, Phd thesis, Queens University of Belfast.

65. Sivakumar, V. (1993). A critical state framework for unsaturated soil, PhD thesis, University of Sheffield.

66. Sivakumar, V. and Wheeler, S.J. (1993). Elasto-plastic volume change of unsaturated compacted clay. ASCE National Convention on Unsaturated Soils, Dallas, Texas, USA.

67. Skempton, A.W. (1960). Effective stresses in soils, concrete and rocks. Proc. Conf. on Pore Pressure and Suction in Soils, Butterworth, London.

68. Smith, P.R., Jardine, R.J. and Hight, D.W. (1992). The yielding of Bothkennar clay. Geotechnique, Vol. 42, No. 2, pp 257-274.

69. Stallebrass, S.E. (1990). Modelling small strains for analysis in geotechnical engineering. Groung Engineering, Jan/Feb 1990, pp 26-29.

70. Tavenas, F. and Leroueil, S. (1977). Effects of stresses and time on yielding of clay. 9th. ICSMFE, Tokyo, Vol. 1, pp 319 - 358.

71. Tavenas, F., Des Rossiers, J.P., Leroueil, S., Rochelle, P. and Roy, M.(1979). The use of strain energy as a yield and creep criterion for lightly over-consolidated clays. Geotechnique, Vol .29, No. 3, pp 285 - 303.

72.. Terzaghi, K. (1936). The shearing resistance of saturated soils and the angle between the planes of shear. Proc. 1st. ICSMFE, Cambridge, Mass.

73. Thomas, H.R. and Rees, S.W. (1994). Seasonal ground movement in unsaturated clay : an examination of field behaviour. Technical Note, Geotechnique, Vol. 44, No. 2, pp 353 - 358.

74. Thomas, S.D. (1987). The consolidation behaviour of gassy soils, DPhil thesis, University of Oxford, U.K.

75. Toll, D.G. (1990). A framework for unsaturated soil behaviour. Geotechnique, Vol. 40, No. 1, pp 31 - 44.

76. Wheeler, S.J. (1986). The stress-strain behaviour of soils containing gas bubbles. DPhil thesis, University of Oxford.

77. Wheeler, S.J. (1988a). A conceptual model for soils containing large gas bubbles. Geotechnique, Vol. 38, No. 3, pp 389 - 397.

78. Wheeler, S.J. (1988b). The undrained shear strength of soils containing large gas bubbles. Geotechnique, Vol. 38, No. 3, pp 399 - 413.

79. Wheeler, S.J. (1991). An alternative framework for unsaturated soil behaviour. Discussion, Geotechnique, Vol. 41, No. 2, pp 257 - 261.

80. Wheeler, S.J. and Sivakumar, V. (1993a). Development and application of a critical state model for unsaturated soil. Proc. Wroth Memorial Symposium on Predictive Soil Mechanics, Oxford.

81. Wheeler, S.J. and Sivakumar, V. (1993b). A state boundary for unsaturated soil. Int. Conf. on Engineered Fills, Newcastle-Upon-Tyne, UK, pp 1 - 12.

82. Wheeler, S.J. and Sivakumar, V. (1995). An elasto-palstic critical state framework for unsaturated soil. Geotechnique, Vol. 45, No. 1.

83. Wood, D.M. (1990). Soil behaviour and critical state soil mechanics, Cambridge University Press.

84. Wroth, C.P and Houslby, G.T. (1985). Soil mechanics : property characterization and analysis procedure. Proc. 11th. ICSMFE, San Francisco, Vol. 1, pp 1 - 55.